The Effect of Nitrite on Pitting and Stress Corrosion Cracking of Corrosion Resistant Alloys (CRA) under Oil Field Conditions.

A thesis submitted to the University of Manchester for the degree of PhD
in the Faculty of Engineering and Physical Sciences.

2011

Akinyemi O. Okeremi

School of Materials

LIST OF CONTENT

LIST OF TABLES

LIST OF FIGURES

ABSTRACT

The need to inject treated seawater to enhance reservoir pressure and secondary oil recovery is increasing in the oil field, so also is the reservoir souring potential caused by the activities of Sulphate Reducing Bacteria (SRB) generating H_2S in the reservoir. The total cost of SRB mediated corrosion in the United States alone is estimated to be 1-2 billion US dollars per year. In the last few years, a number of potential souring mitigation and prevention tools have been studied. These include: sulphate-reduction using membranes, biocide injection and nitrate injection. Out of all the various methods used for the mitigation and prevention of reservoir souring, the use of nitrate injection in conjunction with waterflood projects is becoming more popular because of its economic benefits and least environmental impact. However, nitrate injection is still widely considered as an emergent technology because there are still many unknowns. One of the major unknowns, of great concern is the susceptibility of subsea hardware components to nitrite, which is a by-product of nitrate anti-souring treatment. Any detrimental effect can compromise the technical integrity of subsea installations.

The objective of this research is to study the corrosion susceptibility of CRA (13Cr- Martensitic, 22Cr, and 25Cr super duplex stainless steel) to pitting and stress corrosion cracking in the presence of nitrite. Research hitherto, has investigated corrosion susceptibility of carbon steel to nitrite and found out that nitrite causes pitting in carbon steel. This research work built on previous studies and extensively investigated the effect of nitrite on CRA materials in terms of pitting and stress corrosion cracking. Using electrochemistry techniques in conjunction with C-ring test and slow strain rate test, with variables such as temperature, and nitrite concentration all under anaerobic conditions. Metallographic examination and further evaluation using scanning electron microscopy confirmed pitting and intergranular stress corrosion cracking of 13Cr-L80 and 25Cr due to presence of nitrite.

Test data confirmed that sodium nitrite is an anodic inhibitor; it shifts the corrosion potentials to more noble potential and also shifts the anodic curve to lower current, given a net reduction in corrosion rate. A critical concentration of 400ppm is required for inhibition to be effective on 13Cr-L80 and 25Cr. However, below the critical concentration, nitrite significantly increases the corrosion rate. The experimental data generated from this research work provides very valuable information that will tremendously assist the materials selection process for subsea and subsurface hardware components and also serve as a guide in the corrosion management process in existing systems.

University of Manchester
Akinyemi O. Okeremi
PhD

The Effect of Nitrite on Pitting and Stress Corrosion Cracking of Corrosion Resistant Alloys (CRA) under Oil Field Conditions.
2011.

DECLARATION

I declare that no portion of the work referred to in the thesis has been submitted in support of an application for another degree or qualification of this or any other university or other institute of learning

09/26/2011

Akinyemi O. Okeremi

CERTIFICATION

I certify that Akinyemi O. Okeremi, a postgraduate student of the Faculty of Engineering and Physical Sciences, School of Materials, The University of Manchester did this report under my supervision in pursuit of his PhD degree.

Prof. David Scantlebury

COPYRIGHT STATEMENT

i. The author of this thesis (including any appendices and/or schedules to this thesis) owns certain copyright or related rights in it (the “Copyright”) and s/he has given The University of Manchester certain rights to use such Copyright, including for administrative purposes.

ii. Copies of this thesis, either in full or in extracts and whether in hard or electronic copy, may be made **only** in accordance with the Copyright, Designs and Patents Act 1988 (as amended) and regulations issued under it or, where appropriate, in accordance with licensing agreements which the University has from time to time. This page must form part of any such copies made.

iii. The ownership of certain Copyright, patents, designs, trademarks and other intellectual property (the “Intellectual Property”) and any reproductions of copyright works in the thesis, for example graphs and tables (“Reproductions”), which may be described in this thesis, may not be owned by the author and may be owned by third parties. Such Intellectual Property and Reproductions cannot and must not be made available for use without the prior written permission of the owner(s) of the relevant Intellectual Property and/or Reproductions.

iv. Further information on the conditions under which disclosure, publication and commercialisation of this thesis, the Copyright and any Intellectual Property and/or Reproductions described in it may take place is available in the University IP Policy (see http://www.campus.manchester.ac.uk/medialibrary/policies/intellectual-property.pdf), in any relevant Thesis restriction declarations deposited in the University Library, The University Library’s regulations (see http://www.manchester.ac.uk/library/aboutus/regulations) and in The University’s policy on presentation of Theses.

DEDICATION

I do not count myself to have apprehended but one thing I do, forgetting those things, which are behind and reaching forward to those things, which are ahead. I trust in the Lord with all my heart leaning not unto my own understanding but in all my ways acknowledge God and He shall direct my path and prosper me.

This work is dedicated to God almighty; I thank Him for giving me the enablement and for His steadfast love that never ceases nor His mercies come to an end. They are new every morning. Great is your faithfulness O LORD. Now, unto the King eternal, immortal, invisible, the only wise God, be honour and glory forever and ever, Amen.

This work is also dedicated to my family both immediate and extended. They have all been a source of encouragement and inspiration. I love and appreciate you all.

ACKNOWLEDGEMENT

All the glory must be to the LORD for He is worthy of our praise! It has always been my desire to have a PhD, but there had been obstacles (mostly financial). Ideally, I should have done this over a decade ago but I thank God for He makes all things beautiful in His time. In most cases, if a desire is not accomplished it eventually leads to discouragement, desperation and despair (the 3 D's to failure), but I thank God that I never lost focus, not for a single day! Over the years I have come to realise that only those who keep at it get to the expected end and that when the going gets tough, the tough get going. God's thoughts towards me are thoughts of peace and not of evil, to give me a hope and a future, to take me to the expected end!

It is quite amazing that three years have gone by. As I write this final report, I give God the glory for He that started the good work in me shall surely take me to the expected end. Working full time while studying part-time and at the same time raising a family could be quite hectic, but I thank God for giving me the strength, courage, knowledge and perfect health all year round. It is indeed the Lord's doing and it is marvellous in our eyes.

A lot happened within the three years. On the 29th of December 2008, my father-in-law, Late Chief Moses Adeniyi Adesiyun passed on to glory at the age of 74 after a very brief illness. It was his first and last admission in the hospital. Indeed there is never a convenient time to lose a loved one! He was the best father-in-law in the world and one of the greatest men I ever met, so great, yet so simple, humble and selfless (never wanted to bother anyone and always willing to sacrifice all to make others comfortable and happy), a man of peace, a peacemaker, a gentleman to the core, a rare gem, man of integrity and honour, an honest and upright man of God. He was always prepared, even for death. He had written instructions for his funeral few years before he passed. He left a big legacy; he often talked about 3-H's and 1-P to success, honesty, humility, hard work and prayers. He deeply touched everybody he met, his demise came as a shock, and my wife was 39 weeks pregnant. He fought a good fight; he finished his race and now is laid before him a crown of righteousness. The beatitudes states that "Blessed are the pure in heart for

they shall see God". Indeed I know he has seen God. This is my consolation and hope that we are parting now only to meet to part no more eventually. I discussed with him freely without any reservation and often took counsel from him. I miss him; he was indeed a good father. May his gentle soul, rest in peace.

Eight days after my father-in-law's demise, we had a new addition to the family, a bouncing baby boy. Number 8 symbolises new beginning. Indeed his birth was a new beginning. We named him Oluwajoba (God enthroned king), Moses (in honour of my late father-in-law. He is indeed our joy and blessing just as our other 3 children. We now have 2 girls and 2 boys, equation balanced and we can practice true democracy in the house. I almost got tempted to name the baby Ebenezer because indeed; thus far has the Lord helped us. We look forward to nieces, nephews and grandchildren. As for my wife and I, we are through with having children.

Job wise, I have been very busy despite the ongoing recession. Had first oil of two of my projects; BC-10, Brazil in July 2008 and Perdido (GoM, South Texas) in May 2010. Top of the news, I was appointed the Materials and Corrosion Lead Engineer for one of the largest projects Shell ever embarked on, the Prelude project to be located in offshore Australia. Subea engineering, fabrication and integration will be done in Kuala Lumpur, Malaysia. It's the first Shell project to combine upstream and downstream. It has a huge gas reserve and would be the first floating LNG. I am excited to be a part of this project. It will surely look good on my resume and career. I have always wanted to be involved with downstream operations. In August 2010, my entire family relocated from Houston Texas, USA to Kuala Lumpur, Malaysia. It was a big move and actually delayed completion of this research work by almost 4 months. I am glad we are now fully settled in Kuala Lumpur. One year has gone by just like that!

I would like to express my sincere gratitude to my wife, Yetunde Oluwayemisi Okeremi and our children, Oluwadara, Oluwatise, Oluwapamilerin and Oluwajoba Okeremi for their love, encouragement and support. In the course of this work I have had to work long hours and stay in the office till very late. They have all been very supportive. My wife is indeed a real gem and very

precious to me. I love her very much. She is the best! The Bible declares the he who finds a good wife finds a good thing and obtains favour from the Lord. I am indeed favoured. The Bible also declares that *children are the heritage of the Lord and the fruit of the womb its reward; happy is a man who has his quiver full of them.* Our children are really wonderful children and they have made us glad. They are our joy and blessing from God.

I would also like to express my sincere gratitude to my parents, Rt. Rev and Mrs. R.M. Okeremi and my mother–in-law, Mrs. Kofo Adesiyun. They have made it their lives worth educating people and I am really happy to be one of them. They have constantly reminded me of my goal and desire to have a PhD and have also been a source of encouragement. May I also seize this opportunity to congratulate my parents on their recent retirement as the pioneer Bishop of Ife-East Diocese, Anglican Communion, Church of Nigeria, Modakeke, Ife, Osun State, Nigeria. I pray that you will live long and in good health to enjoy the fruits of your labour in Jesus name, Amen.

I also appreciate my brothers, sisters, brothers-in-law, sisters-in-law, nieces and nephews for their support and prayers.

I cannot but acknowledge the Corrosion and Protection Centre for giving me the privilege and opportunity to come back to my alma mater in pursuit of a doctorate program over a decade after I finished my Masters program. It's really exciting to be back at the Centre with almost all my former Lecturers now Senior Professors; really great! Recently, the school name was changed from UMIST to University of Manchester. I am especially grateful to God for two of my Lecturers, Prof. David Scantlebury and Prof. Peter Skeldon. Dave was diagnosed with cancer a couple of years ago. We were all very devastated, but he took it in good faith and never lost his sense of humour for a day. He went through the entire treatment in good spirit and I am really glad he is fully recovered. He is now very healthy and strong. Praise God. Even in the midst of uncertainty and medical situation, he agreed to be my Supervisor and I am really delighted God preserved his life and it gives me special joy every time I see him. He has been of tremendous assistance to me; showing a lot of interest and enthusiasm in the research and has tremendously motivated me. I also thank God for Peter who recently survived a heart attack.

He was more than a Lecturer to me during my Masters program. I thank him for his fatherly love and advice and I am really glad he is hale and hearty.

I cannot but express my sincere appreciation to my internal examiner, Prof Bob Cottis for once again taking me on board as one of his students. Anytime I think about him, the first thing that comes to mind is the fact that he is an I.T "guru" and very sophisticated with his noise impedance models. It has always been a pleasure to see him over the years at the NACE conference. He has shown so must interest and given necessary support throughout the course of my research. He gave me a lot of very useful leads in the course of this research work and made very viable contributions while I was finalising this thesis. I am also privileged to be one of the last set of students before he retires. I wish his a happy retirement. I also acknowledge Prof. Bob Akid, my external examiner for agreeing to examine my research work and for his detailed review of my thesis.

Special thanks to the leadership team in Shell International Exploration and Production, Inc. Americas and Shell Global Solution for their support. I cannot but mention the following people for the contributions and impact they have made in my life: Robert Patterson, Jay Smith, Doug Peart, Steve Balint, Bob Helmkamp, Kunle Allen, Frank Pattee, Wendy Dominguez, Bill Coit, Eric Gerberding, Jim Seaver, Paul Pickering, Willem Van Gestel, Maimunah Ismail, Adam Badri, Maarten Simon-Thomas, Manuel Gonzalez, Deyuan Fan, Bruce Miglin, Raghu Damodaran, Vidish Rao, Bosun Oni, Posi Fadahunsi, Gbenga Odusami, Susan Lorimer, Kola Fagbayi and several others. They have shown so much interest in me and have supported every effort to progress my career. Some of them are retired now, and I wish them a happy retirement. I acknowledge Shell Global Solutions GSEI/4 Houston for allowing me to run my experiments at their facility. I also thank Bill Grimes and Yue Chen for sharing their laboratory with me and for all their assistance. They are very resourceful and always willing to assist. I learnt a lot of experimental skills from them. Special thanks to Lonnie Wheaton, Bob Beilke, Dick Rothengass and Jacque Jackson laboratory technicians at Shell Global Solutions for their immeasurable assistance. I appreciate Robbie Leitch and

Najua Samsuri for setting up an extranet site that enabled me to transmit data in a secure way to my professors. Lastly, I appreciate all my colleagues.

I am very grateful to Shell International Exploration and Production Inc. EP Technical, for being my co-sponsor through the Educational Reimbursement Programme. With Shell's support and my personal resources, I have been able to fund this entire research work without taking a loan. I also thank the D6 lab of the Corrosion and Protection Centre, University of Manchester, UK for providing research grant for all the research work done at the Centre.

I acknowledge RathGibson and Sandvik Materials Technology for supplying the instrument tubing that was used for the tests. I would like to thank Prof. A.A. Afonja and Prof. O.O. Adewoye, my Professors at Obafemi Awolowo University, Ile-Ife, Nigeria (now retired) for their encouragement and interest. I was always reminded of the "unfinished business" (PhD program) whenever we had a discussion. About 3 years ago, Prof. Afonja and his wife visited us in Houston and we discussed at length. I made a promise that I would do the program pretty soon. I am grateful for the opportunity to fulfil that promise.

I appreciate the support of my brothers and sisters; Mr. Akinyele and Mrs. Ibironke Okeremi, Mr. Akinwumi and Mrs. Moyosola Okeremi, Mr. Akintunde and Mrs. Atinuke Okeremi, Dr. Oluseyi and Mrs. Oluleye Malomo, Mr. Adetayo and Mrs. Modupe Adesiyun, Mr. Adedeji and Mrs. Oluwakemi Adesiyun, and Dr. Adewole and Mrs. Ola Adesiyun. I cannot but acknowledge my nieces and nephews; Mofoluke, Moyosore, Mofinfoluwa, Oluwaferanmi, Oluwabukunmi, and Oluwafeyifunmi Okeremi; Oluwayimika, Oluwabukunmi, Oluwasemilore, Mogbekeloluwa, Moboluwarin, Mofeyisope, Daniel and Debora Adesiyun. Also the new arrival, Ireoluwatomide Malomo, he was born just as I was rounding up this thesis. I congratulate Landlord and his wife as we earnestly wait for the arrival of the twins, our expectation will not be cut short in Jesus name, Amen.

Lastly I would like to thank friends, pastors and other family members for their support and prayers.

God bless you all, Amen.

PREFACE

Right from my childhood days, I had always been curious. Whenever I stumbled into any mechanical or electrical device that had a fault, I was curious to identify what the problem was and tried to fix it. In the process, I had fixed several things but, also caused more damage to other things. As I grew older, there was less of the latter. My parents were very supportive; they redirected and encouraged me appropriately. My mum always calls me the "problem solver". I was less than 10 years old when I crept to the back of our broken refrigerator that was faulty; found the problem to be a loose contact, reconnected it and got the fridge working. I had no doubt I was going to be an engineer. In fact, I was still in the elementary school when my uncle's wife, Mrs. Toyese-Akintunde gave me the nickname, "my engineer". With that vision, I did pure sciences with Additional Mathematics (sometimes referred to as Further Maths) in high school after which I proceeded to Obafemi Awolowo University, Ile-Ife, Nigeria for my Bachelors in Engineering. I had always wanted to study Electrical and Electronics Engineering but by divine orchestration I found myself in the department of Metallurgical and Materials Engineering. No regrets. As compensation, I am married to an Electrical and Electronics Engineer.

In my 2nd year in High School, my father had a national conference in Port-Harcourt, Nigeria. I pleaded with him to take me along, which he did. While in Port-Harcourt, we visited one of his friends who worked for Shell and lived in the Shell residential area (Shell RA) Port-Harcourt. I was inspired by the serene atmosphere. In the course of our discussions, I found out that corrosion was a major challenge for the oil industry. So I figured that the best way to be a Shell employee is to have a solution to their problems! I was further inspired and challenged by my professors (Prof A.A. Afonja, first Professor of Metallurgy in Africa and Prof O.O. Adewoye); who were both trained in Britain. When it was time to select a final year project, I did failure analysis on a gas pipeline from one of Shell's flow stations in the western part of Nigeria. After the successful completion of my Bachelors of Science, I was recommended by Prof. Afonja and Prof. Adewoye for a master's program in

Corrosion Science and Engineering at the Corrosion and Protection Centre in UMIST, Manchester UK (now University of Manchester), which I successfully completed in 1996. I was immediately offered admission to progress my master's dissertation into a PhD research work. I however did not see the practical application of the research work in the industry and did not want to do a PhD that was only good on paper. Unfortunately, since I was not in position to fully fund my research work, I had little influence on the proposed research; hence I opted out to get a job instead.

In 1996, the price of crude oil crashed like a pack of cards with virtually all the oil companies downsizing and definitely not hiring. I was disappointed to find out that I had narrowed my scope to corrosion in the oil industry that was not ready to hire me. In an effort to broaden my scope, I proceeded to Columbia University, New York, USA where I completed another master's degree in Materials Science and Engineering in 2000. I was actually admitted into Columbia for a master's program leading to PhD. I passed the qualifying exam for the PhD program, but unfortunately could not get any financial support for the research. Disappointed, I opted out the second time (again because of financial constraint) to join the work force. In 2002, I got my dream job as a Subsea Engineer with Shell International Exploration and Production Inc, EP Project Houston. My career in Shell has been very successful, I work as a Materials and Corrosion Engineer but have always felt a vacuum as a result of the uncompleted task; my PhD program. As mentioned in my acknowledgement, often my parents and professors had reminded me of the "unfinished project". After working for about 5 years, I was financially buoyant to fund my PhD program; hence I decided to give it a go then or never.

Doing this research work has been quite interesting and challenging. Challenging because I had to combine it with my full time job and also keep my family engaged. I would summarise my experience using 4-P's: patience, persistence, perseverance and prudence. I learnt a lot and saw the benefit of applying my work experience in the course of the research work. I probably would not have learnt this much if I had done this immediately after my master's program. Indeed, all things work together for good to them that love God and are called according to His purpose.

LIST OF ABBREVATIONS

API: American Petroleum Institute
ASTM: American Society for Testing and Materials
BCC: Body Centred Cubic
CCT: Critical Crevice Temperature
CPP: Cyclic Potentiodynamic Polarisation
CPT: Critical Pitting Temperature
CR: Corrosion Rate
CRA: Corrosion Resistant Alloys
DAC: Differential Aeration Cell
DF: Damage Functions
DFA: Damage Function Analysis
DNA: Deoxyribose Nucleic Acid
DOC: Dissolved Oxygen Content
FCC: Face Centred Cubic
FEA: Finite Element Analysis
HOI: Hemisphere of Influence
HSE: Health, Safety and Environment
ID: Inside Diameter
LPR: Linear Polarisation Resistance
MIC: Microbial Induced Corrosion/ Microbiologically Influenced Corrosion
MOC: Management of Change
MPY: Mil per Year
MTR: Materials Test Results
NACE: National Association of Corrosion Engineers
NRB: Nitrate Reducing Bacteria
NRSOB: Nitrate Reducing Sulphide Oxidizing Bacteria
OCP: Open Circuit Potential
OD: Outside Diameter
OSPAR: Oslo/Paris Convention for the Protection of the Marine Environment
OVAT: One Variable At a Time
PDM: Point Defect Model

PIPB: Photo Inhibition of Passivity Breakdown

PLONOR: Pose Little or No Risk

PPB: Parts per Billion

PPM: Parts per Million

PR: Polarisation Resistance

PRE_N: Pitting Resistance Equivalent Number

PWRI: Produced Water Re-Injection

RBI: Risk Based Inspection

SCC: Stress Corrosion Cracking

SCE: Saturated Calomel Electrode

SIF: Stress Intensity Factor

SEM: Scanning Electron Microscope

SRB: Sulphate Reducing Bacteria

SSR: Slow Strain Rate

SVIM: Solute-Vacancy Interaction Model

THPS: Tetrakis, Hydroxymethyl-Phosphonium Sulphate

TSA: Thermal Sprayed Aluminium

TTF: Time to Failure

TOC: Total Organic Carbon

UTS: Ultimate Tensile Strength

VFA: Volatile Fatty Acids

WRT: With Respect To

1 INTRODUCTION

Oil companies are injecting seawater into reservoirs to enhance reservoir pressure and secondary oil recovery. Although seawater injection has been found to be a successful option for secondary oil recovery, it presents a major problem for the oil industry because it promotes reservoir souring caused by the growth of Sulphate Reducing Bacteria (SRB). Biogenic reservoir souring occurs when an oilfield turns sour (featuring H_2S) due to uncontrolled activity of reservoir resident micro organisms, Sulphate Reducing Bacteria (SRB) that are capable of reducing sulphate to sulphide. This occurs in all anaerobic subsurface habitats that are conducive to SRB growth, usually after injecting extraneous water, like seawater provided the four essential ingredients listed below are present:

1. Sulphate (electron acceptor)
2. Carbon energy source (e.g. Volatile Fatty Acids)
3. Nutrient for reproduction (e.g. Phosphorus, nitrogen, trace element)
4. Suitable temperature regime (typically 35 to 120^{o}C)

In an anaerobic environment where sulphate ions are present, SRB metabolise carbon energy source to reduce sulphate, using nutrients for reproduction. They form biofilm and colonise part of the reservoir that is conducive for their growth. The most plausible cause of reservoir souring is the activity and growth of SRB in the zone where seawater mixes with formation water. In the mixing zone, electron donors such as organic compounds or hydrogen, electron acceptor such as sulphate and other essential nutrients like nitrogen and phosphate all take part in the souring process. The anaerobic respiration of SRB can be illustrated using the following chemical reaction

$$\text{Carbon Source} + SO_4^{2-} \rightarrow CO_2 + H_2S + \text{Energy}$$

Volatile Fatty Acids (VFA: $C_nH_{2n+1}COOH$ where n is an integer and n=1 for acetate) and crude oil are very common sources of carbon. Once H_2S is generated, it will distribute over water/oil/gas, and migrate to producers, usually following the flood front. The effect of souring typically becomes noticeable when traces of H_2S start appearing in produced gas, or closely

behind the breakthrough front of injected seawater. Figure 1 illustrates a conducive environment for reservoir souring in a cartoon form[1].

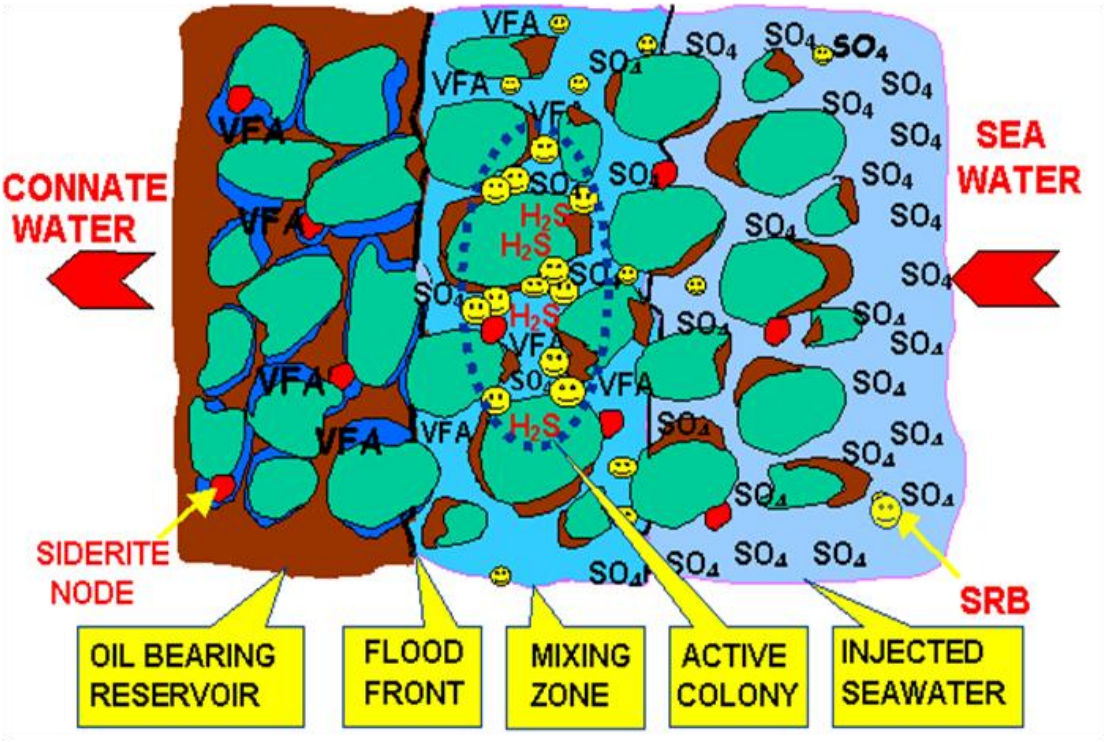

Figure 1: Cartoon illustrating a conducive environment for reservoir souring[1]

H_2S production is a threat to the technical integrity of the system. It compromises the quality of sales product thereby decreasing its value. Presence of H_2S also increases refining costs and poses HSE risks to human.

The activities of SRB has long been a major concern in oilfield water systems because they cause unplanned increase in H_2S concentration in produced fluids (reservoir souring) and microbial induced corrosion of pipe work and associated facilities for water injection systems. The total cost of SRB mediated corrosion in the United State alone is estimated to be 1-2 billion US dollars per year[2]. With the cost of handling biogenic hydrogen sulphide (H_2S) production from petroleum reservoirs running into hundreds of millions of dollars yearly, the drive to control such a costly and hazardous problem has become a priority.

A number of selective chemical inhibitors of microbial growth are being promoted that are claimed to specifically prevent the detrimental activity of

SRB colonies and prevent souring. In particular, nitrate anti-souring treatment appears to be gaining popularity over the conventional biocide treatment or the sulphate removal. The nitrate anti-souring treatment occurs via various mechanisms[3]. The first of which is the suppression of sulphide generation by the selective manipulation of indigenous bacteria through nutrient addition such that the NRB are nourished to enhance their proliferation, thereby suppressing the activities of the SRB. NRB generally out-compete SRB for common carbon and energy sources such as acetate and longer chained fatty acids. This shifts the flow of electrons in the energy-generating metabolism of bacteria away from sulphate reduction towards nitrate reduction. It is also believed that some SRB may shift to nitrate respiration thereby reducing nitrate to nitrogen. The nitrate reduction from the activities of the NRB can be expressed by the following chemical reaction:

$$\text{Carbon Source} + NO_3^- \rightarrow CO_2 + N_2 + \text{Energy}$$

The second mechanism is biological oxidation that involves the activity of the nitrate-reducing sulphate-oxidising bacteria (NRSOB) that consumes the already produced H_2S.

$$H_2S + NO_3^- \rightarrow N_2 + SO_4^{2-}$$

The reactions inherent in NRB activity can shift the redox potential of the reservoir causing the reduction of nitrate by NRB to nitrite, which will act to inhibit SRB activity and favour the further proliferation of NRB. This forms the basis for the third mechanism, which is the inhibition of SRB.

$$NRB + NO_3^- \rightarrow NO_2$$

There is an increase in the number of operators using nitrate to combat reservoir souring and suppress SRB, probably because the biological anti-souring treatment is environmentally friendly for offshore application and the fact that it is comparatively inexpensive. Although the mechanism is well known and there is field data to demonstrate nitrate injection as a means of preventing reservoir souring. There is however no data available on the effect of the by-products of nitrate-based package on the corrosion susceptibility of CRA materials used for injector and producer down-hole components and other subsea hardware. Of particular concern is the intermittent generation of

low concentrations of nitrite. Figure 2 shows the down-hole components of a typical water injection well, which indicates use of corrosion resistant alloys.

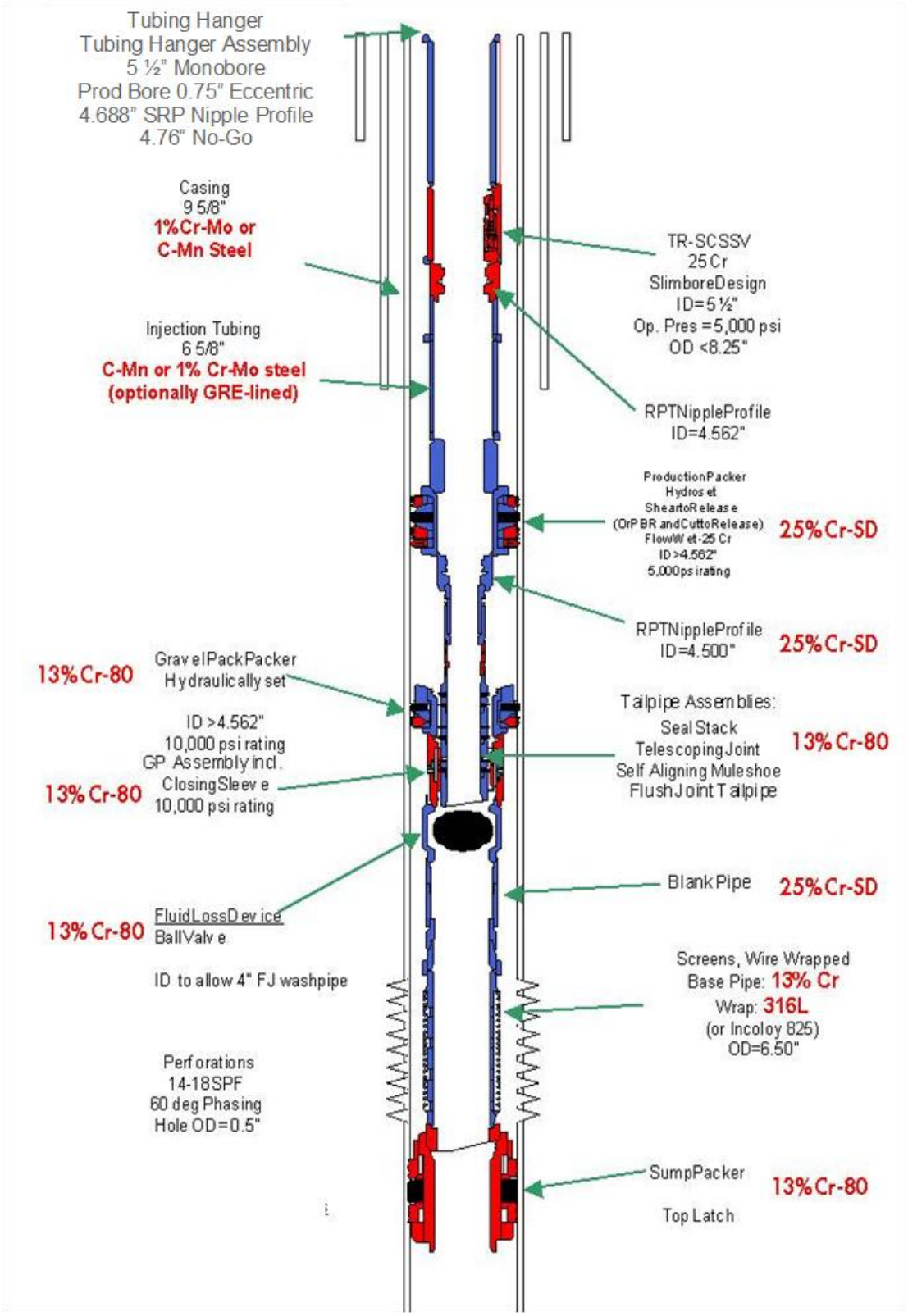

Figure 2: Typical Water Injector wells Downhole Components[5]

Recent studies have shown that generated nitrite could either exist in transient form in some systems or continuous low concentrations in other systems. Generated nitrite is a strong oxidant and at very high concentrations can act as an anodic inhibitor. Nevertheless at low continuous concentrations, nitrite may increase the tendency for general and pitting corrosion of carbon steel down-hole components in injection and producing wells.

Nitrite is often applied as a corrosion inhibitor for carbon steel with injection rate in excess of 100ppm. Nitrite inhibition mechanism on carbon steel is passivation due to the formation of ferric oxide film. However, there is concern that at levels slightly below what is sufficient for passivation; nitrite can promote corrosion on the imperfectly passivated metal substrate. Also in the presence of sulphide (iron sulphide in this case), nitrite being a very strong oxidant will oxidise sulphide leading to possible production of elemental sulphur causing perforation of the steel in sections where iron sulphide was present[4]. The extent of this phenomenon is highly dependent upon environmental conditions and to date no testing has been conducted with corrosion-resistant alloys (CRA).

Furthermore, in the presence of denitrification bacteria, organic matter and anaerobic conditions, nitrate acts as the electron acceptor and may be reduced to species such as NO, N_2O, or N_2O_2 which have greater potential to induce corrosion.

The use of nitrate injection treatment in conjunction with waterflood projects appears to be increasingly popular for the mitigation and prevention of reservoir souring because of its economic benefits and least environmental impact. However, nitrate injection is still widely considered as an emergent technology because there are still many gaps to be filled. Based on experience as a Corrosion/Material Engineer in the oil industry, one of the key areas where design engineers struggle is the selection of suitable CRA for down-hole and subsea components such as casing, tubular, tubing hangers, jumpers, manifold, flowlines and risers in fields where nitrate injection is used for mitigating reservoir souring because the mitigating effect of nitrite (in terms of pitting and stress corrosion cracking) on CRA materials typically used in these areas is still not completely understood. Shell Global Solution

conducted preliminary work to assess the corrosion of carbon steel and Sumitomo Super 13Cr-110ksi[6] in the presence of nitrite. However, there are still lots of uncertainties on the susceptibility of nitrate/nitrite of CRA materials to pitting and stress corrosion cracking in this environment. These uncertainties require further research work to eliminate such unknowns. This is a known gap in the industry.

The objective of this research is to study the effect of nitrite on both the general and localised corrosion rate of Corrosion Resistant Alloys (13Cr-martensitic stainless steel, 22Cr duplex and 25Cr super duplex stainless steel). In the course of this investigation, the effect of nitrite in the oil environment on corrosion resistant alloys in terms of pitting and stress corrosion cracking shall be determined.

Findings from this research shall provide good contribution to knowledge; it would give Material Engineers more confidence in selecting CRA materials for subsea and down-hole components especially in areas where corrosion resistance is required for oil and gas fields; where nitrate injection is used as an anti souring agent. Findings would also provide guidance on how to ultimately improve the life cycle performance of CRA materials used for down-hole completions and other subsea hardware in terms of operating criteria to ensure the components are operated within a safe zone, such that technical integrity is maintained for the life of the asset.

This research was run under the Individual Split-Site PhD Student Program (formerly known as External PhD), which is one of the programs offered at the University of Manchester. The University of Manchester shall award the PhD; however a significant part of the research work was done at Shell Global Solution Research Centre at West Hollow, Houston Texas, USA over a period of 3 years from September 1, 2007 to proposed end date of September 30, 2010 as indicated in the roadmap shown in Figure 3. However, the end date slipped by almost a year.

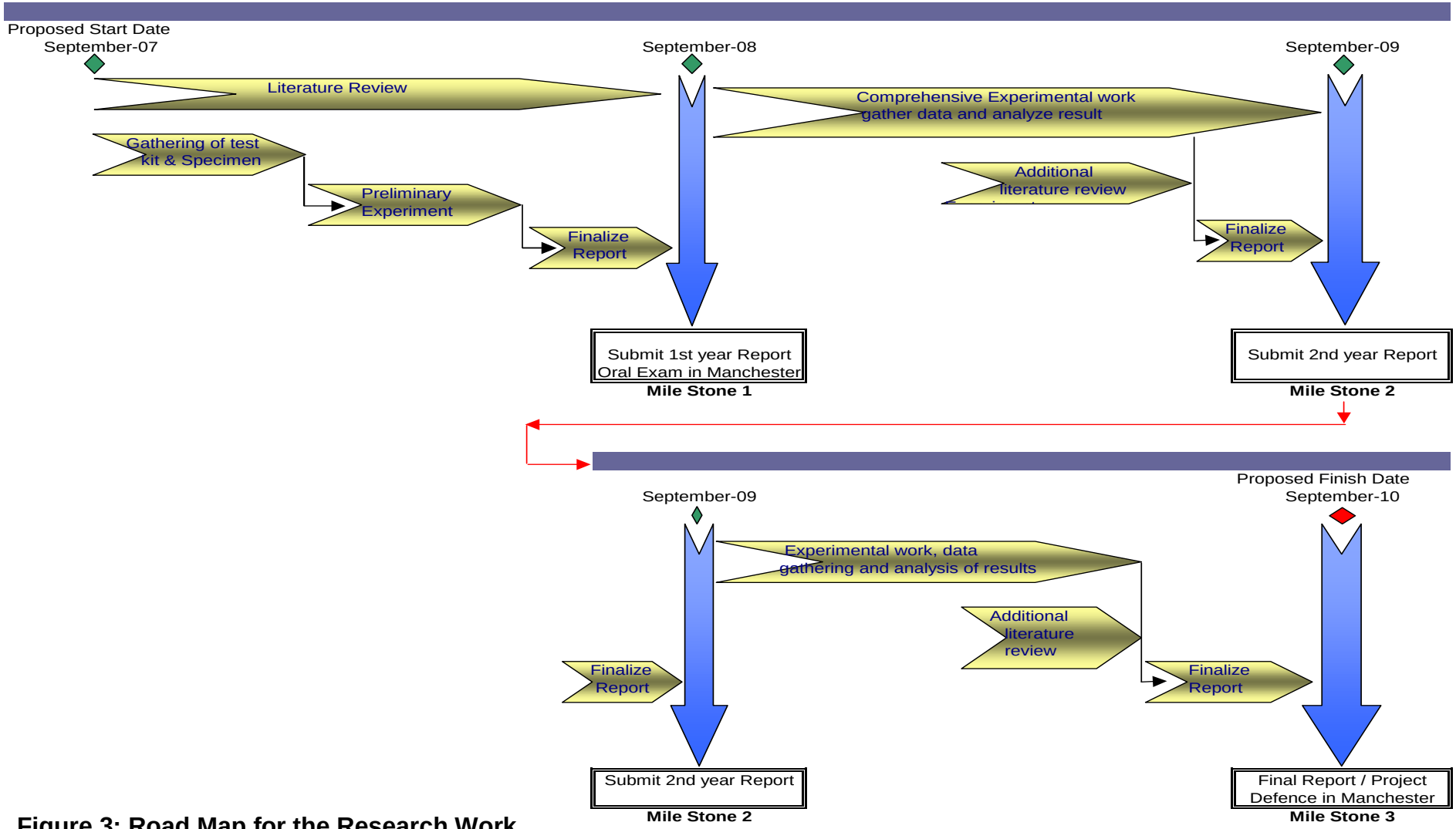

Figure 3: Road Map for the Research Work

There were three milestones; each milestone marked the end of the year and the beginning of the subsequent year except for milestone 3, which is the end of the program. The submission of the first year report and oral examination at the University of Manchester marked the end of the first milestone while submission of the second year report and oral examination at the University of Manchester marked the end of the second milestone. The submission of the thesis and oral examination marks the end of the final milestone and completion of the program.

This research work is a continuation of the preliminary work done by Shell Global Solution in Houston to investigate the resistance of CRA materials to pitting and Stress corrosion cracking; hence the methodology is very similar at the earlier stage of the research work in order to validate past results, clarify any ambiguity and then build on it.

The objective of this research work was achieved in two stages; comprehensive literature review and experimental work. A comprehensive literature review of what has been done so far in the area of interest, to ensure there were no duplications, validate the gap that was intended to be filled by this research work, address key issues and identify any potential gap not originally proposed that could be filled. Also the synergy of evaluation techniques used shall be explored.

The literature review covered mechanism and biological aspects of nitrate anti-souring treatment, the effect of concurrent presence of nitrate and nitrite, the potential consequence of nitrate/nitrite with respect to corrosion processes and fundamental chemistry on the nitrite oxidation behaviour, study of passive film formed on CRA, mechanism and kinetics of passive film breakdown.

Electrochemical techniques such as open potential measurements, cyclic potentiodynamic polarisation and potentiostatic Polarisation were used to further understand corrosion behaviour of CRA in nitrate/nitrite environment and also identify susceptibility regimes. As base case, C-ring exposure testing was used to further investigate environmentally assisted cracking phenomenon. However, for test materials that exhibit active/passive

behaviour and the passive protective layer cannot be damaged in a C-Ring test, an appropriate test method such as slow strain rate test that guarantees the passive layer is broken was used.

The chemical analyses, hardness test and tensile test results were obtained from the materials test results (MTR) and other engineering supporting document provided by the supply vendors of the various test samples. Information supplied by the vendors was assumed to be correct and did not require further validation. This assumption was based on the fact that all the test samples were supplied by reputable companies that have existing alliance with Shell. As part of the alliance agreement, routine audits are carried out by Shell to validate information supplied by the vendors. All metal samples were traced all the way to the mill.

Three grades of CRA materials were initially tested namely; 13Cr-L80 martensitic stainless steel, standard 22-Cr duplex stainless steel and the 25-Cr super duplex stainless steel. Later, the testing was narrowed down to 13Cr-L80 martensitic stainless steel and 25-Cr Super Duplex stainless steel. None of the tests was carried out with live bugs; rather reduction of sodium nitrate to sodium nitrite by nitrate reducing bacteria was simulated using sodium nitrite solution. Also synthetic seawater was prepared using ready mixed synthetic seawater salt prepared in accordance with ASTM D1141, standard practice for the preparation of substitute ocean water[7] as substitute for seawater.

Dilute solution of sodium hydroxide and hydrochloric acid were used to adjust the pH of the synthetic seawater solution to the desired pH of 8.2 at the beginning of all the tests carried out. Nitrogen gas (with very low oxygen content) was bubbled through the test solutions to remove dissolved oxygen in the test solution to about 5-17ppb (depending on temperature of test solution) in order to obtain anaerobic condition. Test solutions were heated as required to maintain the desired temperature. All tests were carried out in airtight glassware with backpressure maintained by continuously bubbling nitrogen and expelled gas bubbled into a water column for the duration of the test to prevent oxygen ingress (i.e. closed system, under anaerobic conditions).

The variables for all the tests were:

1. Material: 13Cr, 22Cr and 25Cr (3 variables)
2. Temperature: 25^{o}C, and 80^{o}C (2 variables)
3. Nitrite concentrations
4. Nitrate Concentration
5. Applied potential (for potentiostatic tests)

Tests were carried out in duplicate or triplicate to ensure repeatability/ reliability of test data and also for proper validation.

Having identified gap that would be good addition to knowledge, clear objectives and pragmatic methodologies were postulated to ensure the objectives of this research work are achieved.

The following hypotheses were made:

a. Typical of anodic inhibitors, nitrite requires a critical concentration for effective inhibition.
b. Although nitrite acts as anodic inhibitor however, below the critical dosage or in excessive concentrations (above 8,000ppm):
    i. Nitrite increases the corrosion rate of corrosion resistant alloys.
    ii. Nitrite makes corrosion resistant alloys specifically (13Cr, 22Cr and 25Cr) susceptible to pitting and stress corrosion cracking. The susceptibility increases with temperature but decreases with increasing alloying of Cr, Mo, N and Ni.

2 LITERATURE REVIEW

2.1 Reservoir Souring due to Water Injection

For a long time, the activities of SRB have been a major concern in oilfield water systems because they drastically increase the H_2S concentration in produced fluids (reservoir souring) beyond what is planned. They also aid localised microbial induced corrosion (MIC) of pipe works and associated hardware in water injection and produced water systems.

Sulphate-reducing bacteria (SRB) often thrive when seawater is injected into oilfields in order to increase reservoir pressure and drive more oil out (secondary recovery). SRB are responsible for H_2S production, which causes 'souring' of the crude oil; microbiologically influenced corrosion (MIC); increased solids loading in water injection systems (iron sulphides, etc.); and can cause plugging of injection wells as a result of sulphide or biofilm proliferation. In order to prevent SRB growth, each year the industry spends millions of dollars on chemicals such as biocides.

Under anaerobic conditions SRB reduce sulphate and simultaneously oxidise a limited range of organic compounds. Oil reservoirs contain volatile fatty acids (VFA), which are used as carbon and energy source by different types of SRB widely distributed in oilfield waters. This activity leads to H_2S generation which cause reservoir souring.

Traditionally, seawater injection systems have been treated with biocide to inhibit the growth of SRB and reduce microbial induced corrosion. The most commonly used biocides are Glutaraldehyde and Tetrakis hydroxymethyl phosphonium sulphate (THPS). Biocides are toxic; therefore represent health risk for platform personnel during handling. Biocides are also toxic to the marine environment.

2.2 Nitrate Injection to control Reservoir Souring

A novel treatment that utilises nitrate has recently been used under certain circumstances to control reservoir souring. The objective of nitrate treatment is to suppress sulphide generation by the selective manipulation of indigenous bacteria through nutrient addition. Nitrate is regarded as "pose little" or no risk (PLONOR) to the marine environment on the OSPAR list[8], and is considered

as a natural ingredient in seawater. Thus, nitrate is non-hazardous to personnel working on the platform and also the marine environment. Hence, the change from biocide to nitrate treatment should consequently result in a considerably better working environment including reduced possibility of occupational injuries but unfortunately this has not been the case because most nitrate treatments still require supplementary biocide treatment especially for the topside facilities.

According to Thorstenson et al[9], "*laboratory experiments have shown that nitrate treatment can be an effective alternative to biocide treatment to reduce the number and activity of SRB"*. Based on their experimental results, the decision was made to implement nitrate treatment into water injection on the Veslefrikk oil platform in the North Sea. This was a bold step considering the fact that nitrate treatment is still a novel technology with several unknowns. Veslefrikk platform is situated 145km west of Bergen in West Norway. The field started producing in 1989. A maximum daily production of 12000Sm^3/d (423,776 MSCF/D) was achieved but the production rate later dropped to approximately 7000Sm^3/d (247,202 MSCF/D). For reservoir pressure support, produced gas and seawater were injected into the reservoir. Production systems were located on two different platforms, a wellhead platform and a floating unit, which also hosts the seawater injection treatment plant. Water is transferred via two 8" flexible hoses to the water injection manifold situated at the wellhead platform before injection into the reservoir. The capacity of the seawater injection is approximately 17000Sm^3/d (600,000 MSCF/D) at pump discharge pressure of 20-22.5MPa (200-225bar). Seawater is drawn at a water depth of 27m, filtered to 80micron, deoxygenated using a vacuum deaerator to less than 20ppb and batched treated with biocide using glutaraldehyde (but no chlorination) from field start up in 1989. Ten years later, batched biocide treatment was replaced with continuous nitrate injection. After about 4 months of continuous nitrate injection, there was a drastic reduction in the activity of SRB in biofilm samples in the seawater injection. After 32 months of nitrate treatment, SRB numbers were reduced 20,000 fold and SRB activity 50 fold with a concomitant enrichment of NRB. Also corrosion measurements taken from weight loss measurements of metal

coupons decreased from 0.7mm/y to 0.2mm/y. Field data from the Veslefrikk platform indicates that nitrate treatment can efficiently inhibit growth of SRB in seawater injection systems. Also, test results from a laboratory experiment conducted with oil reservoir model column confirmed that nitrate injection inhibits sulphide production[10]. Nitrate injection promotes the growth of nitrate-reducing bacteria (NRB) at the detriment of sulphate-reducing bacteria (SRB).

2.2.1 Mechanisms of Nitrate Inhibition of Reservoir Souring

There are several potential mechanisms through which nitrate inhibits reservoir souring but, the mechanisms are often not fully understood[11]. Nevertheless, the thermodynamic aspect of the reduction process is an important factor that must be considered irrespective of the mechanism that dominates. The microbiological reduction of nitrate provides approximately three times more energy to bacteria than the reduction of sulphate. Therefore, when both nitrate and sulphate are present, nitrate becomes the preferred electron acceptor and bacteria capable of proliferating on nitrate dominate[12].

Based on findings from literature on nitrate treatment to inhibit reservoir souring, the most popular inhibition mechanism is by competing for carbon sources. When competing for the same carbon source, NRB in theory, out competes SRB because nitrate is a stronger oxidant than sulphate therefore nitrate provides a competitive advantage to NRB during competition for available carbon sources as such, NRB are capable of much faster growth than SRB. Another school of thought states that NRB generally out-compete SRB for common carbon and energy sources, such as acetate and longer chained fatty acids thereby, shifts the flow of electrons in the energy generating metabolism of bacteria away from sulphate reduction towards nitrate reduction as illustrated by the following equations[4];

$$SO_4^{2-} + 8e^- + 10H^+ \rightarrow H_2S + 4H_2O + \text{energy}$$

$$2NO_3^- + 10e^- + 12H^+ \rightarrow N_2 + 6H_2O + \text{energy}$$

Ideally, nitrate reduction process generates nitrogen gas as the end product but sometimes it also results in the production of nitrite ions as illustrated by the following equation;

$$NO_3^- + 2e^- + 2H^+ \rightarrow NO_2^- + H_2O + \text{energy}$$

According to Rizk[4], "*NRB may also produce traces of nitrogen oxides that are capable of raising the oxidation-reduction (redox) potential of the environment. This shifts the flow of electrons in energy generating metabolism of bacteria away from sulphate reduction towards nitrate reduction, thereby increasing the proliferation of NRB at the expense of SRB"*.

In produced water re-injection systems where the nutrient levels (e.g. carbon and phosphate sources.) are high, rapid growth of NRBs as a result of nitrate injection can result in larger biomass production whereas in the case of seawater injection systems with limited nutrients, nitrate injection is not expected to increase the overall cell numbers and biomass[9].

As part of the tests conducted in the Veslefrikk field, population growth of SRB and NRB were verified on carbon sources such as lactate, acetate, palmitate and benzoate. It was observed that both SRB and NRB present in the seawater injection system were able to utilise the same carbon sources.

Prior to nitrate injection, sulphate respiration was more favourable in seawater injection system because seawater contains 28mM sulphate and only traces of nitrate. Nitrate injection led to the establishment of a dominating NRB population and a decline in number and activity of SRB, showing that only a small amount of nitrate was sufficient to shift the microbial activity from sulphate to nitrate respiration.

The fact that NRB dominated the bacterial community and the number of SRB dropped drastically in the Veslefrikk field, suggests that competition for carbon may be a major contributor to the inhibition of SRB. However, this argument is only valid in a carbon-limited system, which is the case for Veslefrikk, where oxygen is removed using vacuum deaerator and no organic water injection additives used. The nitrate concentration used at the Veslefrikk field is very low, however, other oil fields, with different water treatment units such as the deaeration tower and Minox, and Seajet that introduce other organic additives, may require higher concentrations of nitrate in order to achieve similar results.

Another popular mechanism by which nitrate inhibits souring is through a process where SRB utilise nitrate as an alternative to sulphate (as the

electron acceptor) in their energy-generating metabolism, thereby preventing sulphide generation while SRB remains active. This is possible because some SRB are able to survive nitrate application by switching from sulphate respiration to nitrate/nitrite[13]. Evidence in the literature suggests that some SRB can use nitrate as a terminal electron acceptor[13-15]. This mechanism was validated in a laboratory study on strains of SRB identified as Desulfovibrio gracilis, recovered during backflows of Halfdan water injectors, an oil field located in the Danish sector of the North Sea where water injection is used for reservoir pressure maintenance and line sweep. Results from previous laboratory studies show that at very low sulphate concentrations when both nitrate and sulphate are present, nitrate can serve as an electron acceptor instead of sulphate and, therefore, prevents sulphide production whilst the SRB remain active[16-17]. However, the study on Halfdan shows that Desulfovibrio gracilis can preferentially use nitrate even in the presence of high sulphate concentrations. As a result, H_2S was no longer produced and nitrate achieves the desired effect.

The third common mechanism that suppresses SRB activity is the inhibitory action of nitrite (NO_2^-), which is formed as a nitrogen intermediate by the activity of NRB i.e. NRB may produce compounds such as nitrite that are toxic to SRB, thereby exterminating the SRB colonies[11, 18, 19].

$$NO_3^- + 2e^- + 2H^+ \rightarrow NO_2^- + H_2O$$

According to another school of thought, SRB may also be inhibited by toxic reduction products from the reduction of nitrate. It has been reported that toxic products formed as a result of the reduction of nitrate to N_2, NO_2, NO and N_20 inhibit bacteria growth[20, 21]. Also NO_2 can oxidise sulphide already produced by SRB (in the system in the form of iron sulphide) and form toxic products[22]. It has also been reported that one SRB strain possessed nitrite-reductase genes that proliferates when the organism was exposed to nitrate. It was hypothesised that this may act as a detoxification mechanism to remove damaging nitrite from the cell[23]. In addition, nitrite can act as a chemical H_2S scavenger by producing compounds capable of raising the redox potential of the environment to a level that inhibits SRB activity [11, 18, 19].

$$12H_2S + 12HS^- + 16NO_2^- + 28H^+ \rightarrow 3S_8 + 8N_2 + 32H_2O$$

The shift towards a more positive redox potential is enhanced by the chemical oxidation of sulphide by nitrite. Another report which is in agreement with this thought suggests that nitrate souring control mechanism is such that nitrate impacts on SRB activity and biofilm redox potential, as a result of which corrosion due to SRB activity will be reduced[9], souring inhibited and previously formed sulphide removed[24, 25].

Another mechanism of nitrate inhibition of souring is through the action of Nitrate Reducing Sulphide Oxidizing Bacteria (NRSOB) which is a special group of NRB that are capable of reducing nitrate, whilst simultaneously oxidizing sulphide, thereby providing a curative process for H_2S already present in the system[26]. In this case the production of sulphide would not be inhibited, but the use of sulphide by nitrate-reducing bacteria would prevent its accumulation. This mechanism has been found to play an important role in, the Skjold field located in the Danish Sector of the North Sea where seawater injection was introduced after about 3 years of production to maintain reservoir pressure. The field has 20 producers and 8 water injectors all completed in the water zone except one. However, due to the fractured nature of the reservoir, injection water breakthrough occurred shortly after injection commenced. In a particular instance, water breakthrough from injector Skjold-7 occurred in producer Skjold-12 only a few hours after injection commenced. Less than 6 months after seawater injection commenced, the field recorded the first H_2S production of 1.8ppm in the gas phase. H_2S production steadily increased over the years with the wellhead H_2S concentration in the produced gas varying between 10ppm and 1000ppm. In 1994, regular biocide, THPS injection into the oil production systems was introduced. This reduced the H_2S production from the Skjold reservoir by about 40% compared to no THPS injection[27]. In addition, biocide treatment of the injection water with THPS resulted in other benefits such as dissolution of iron sulphide deposits and reduction in the biofouling of the water injection system, thus helping to minimize the potential for microbial influenced corrosion[28].

Sand pack and core-flood laboratory experiments were performed in order to suggest conditions to be used in a field trial, results of the studies showed that

the addition of nitrate to an active mixed population of oil field bacteria results in a marked decrease in sulphide generation[18, 19]. Hence 2 pilot nitrate injection tests were conducted in Q2 and Q3 of 2000 on two injection wells and a field-wide trial started in November, 2000. Injecting sodium nitrate product (40 % w/w), corresponding to an average injection rate of 173 mg/l. Nitrate injection was stopped in February, 2001 just 3 months after. There was a significant increase in the populations of mesophilic NRB and mesophilic NRSOB, especially after the field wide trial.

Also nitrite build up was observed which, demonstrates that there is a microbiological mechanism at work, with NRB reducing nitrate to nitrite, along with co-oxidation of sulphide. Conclusions from the microbiological monitoring conducted during the trials confirmed that NRB were stimulated by the nitrate treatment and the dominant mechanism was either inhibition of SRB due to nitrite build-up or biological oxidation of sulphide due the activity of NRSOB[25].

The fact that some oilfield SRB can use nitrate, in the presence of sulphate from seawater, further confirms the preferential use of nitrate by SRB instead of sulphate as the electron acceptor in their energy-generating metabolism (i.e. SRB acting as NRB). This could be of great benefit because even when competition between SRB and NRB does not give the desired result, inhibition of reservoir souring is still achieved by virtue of SRB utilising nitrate instead of sulphate. However, if nitrate dosing is stopped for a long period, these SRB may return to sulphate reduction, thereby producing H_2S.

NRSOB reduce nitrate to nitrite, nitrous oxide, nitrogen or ammonium whilst the sulphide is oxidised to either sulphur or sulphate[29, 30].

$$5HS^- + 8NO_3^- + 3H^+ \rightarrow 5SO_4^{2-} + 4N_2 + 4H_2O$$

The stoichiometry of the reaction depends on the ratio of sulphide to nitrate. With excess sulphide, the main products are sulphur and nitrogen, while with excess nitrate; the main products are sulphate and nitrite[29]. Both NRB and some SRB may show NRSOB activity[31].

A special denitrifying microorganism known as Thiobacillus denitrificans classified as NRSOB can simultaneously reduce nitrate and oxidise pre-

existing sulphide thereby preventing build up of sulphide concentration as follows:

$$CO_2 + NO_3^- + \text{Reduced sulphur compounds} \rightarrow \text{Cells} + N_2 + SO_4^{2-} + H^+$$

According to Jenneman, and Gevertz[32] "[NRSOB is described as another category of microorganism characterised with] *similar biologically mediated sulphide oxidation by heterotrophic (i.e. organic carbon-utilising) NRB that are indigenous in oil field brines and utilise similar organic substrates to SRB and give rise to elemental sulphur"*. Also according to Rizk[4], "*nitrite can chemically scavenge pre-existing sulphide at a rate that could be dependent on pH. The reaction results in the production of elemental sulphur or sulphate"*. The generation of elemental sulphur may have detrimental consequence with respect to corrosion in certain instances since the sulphide can react with cations such as Fe^{2+} and Fe^{3+} to generate iron sulphide.

According to an introductory review work on the simulation of NRB in oilfield to control reservoir souring conducted by the Energy Institute, London in 2003, it was suggested that inhibition of SRB is due to the formation of nitrite from nitrate injection[33]. This school of thought is probably due to the toxic nature of nitrite. However, recent research work has confirmed that the same nitrogen concentration in the form of either nitrate or nitrite would be required to suppress SRB activity[4], it is however not clear from published work if other N-O compounds biologically generated by NRB could inhibit SRB activity or whether nitrate reduction to nitrite results in only the transitory presence of nitrite or a build up in nitrite concentration. Investigating these issues is however not in the scope of this research work.

As earlier stated, nitrate can control souring by several different mechanisms, depending on the circumstance; the various mechanisms may all work at the same time, which makes the use of nitrate potentially very versatile. It is therefore very important to understand the controlling mechanism during nitrate injection in order to provide adequate corrosion control.

2.2.2 Field Application of Nitrate Injection to Control Reservoir Souring

Despite the limited understanding of the souring control mechanism, nitrate treatment is increasingly used for selective control of SRB and associated biogenic generation of hydrogen sulphide in petroleum reservoirs and oilfield water handling systems. The treatment has generally proven to be very effective for souring control compared to more conventional anti-microbial agents[33] and has the potential to supplant biocides for the mitigation of petroleum reservoir souring and microbial induced corrosion. Several field tests have demonstrated the potential usefulness of nitrate for controlling souring[9, 12, 25, 34-36].

Field tests have identified significant numbers of SRB growing in and around some water injectors, even where nitrate is being dosed to the injected water. However, conventional knowledge suggests that NRB populations, which are also high in number, out-compete SRB for the available carbon source. Hypothesis for how SRB are able to survive nitrate application is that some species are able to switch from sulphate respiration to nitrate/nitrite respiration. Evidence in the literature suggests that some SRB can use nitrate as a terminal electron acceptor[14]. However, in the case of certain strains this has only been observed at very low sulphate concentrations[16]. According to Seitz and Cypionka[15], *"for other species, when both sulphate and nitrate are present in non-limiting concentrations, sulphate reduction is suppressed in favour of nitrate reduction"*. The rationale for this conclusion was later given from thermodynamic perspective by Larsen, Rod and Zwolle[12] who stated that "*the reduction of nitrate provides approximately three times more energy to bacteria than the reduction of sulphate"*. Hence, when both nitrate and sulphate are present, nitrate automatically becomes the preferred electron acceptor and bacteria capable of growing on nitrate dominate. According to another school of thought, if significant proportion of SRB is able to use nitrate, then some SRB could compete successfully with specialised NRB.

There are various conceptual views on the likely location of SRB activity leading to souring in majority of seawater-flooded reservoirs. One view states that SRB activity could happen deep within the reservoir at the advancing flood front, which would require the activity of thermophilic SRB. An

alternative view states that most of the SRB activity is in the region of the injection well bore. Nitrate injection at the injection well bore would be simpler than deep reservoir injection while on the other hand; high sulphate concentrations in the vicinity of the injection well bore could affect the demand on nitrate. In a situation where the SRB activity is in the well bore area, a larger mixed species biomass may result in the near well bore area of a reservoir. It is then possible that cessation of nitrate treatment may lead to worsened souring by the larger bacterial population.

Whereas biocides exert control by elimination of bacteria, in the case of nitrate, its control mechanism relies on a population of NRB being present in the system, or on a surface. The MIC potential of such NRB biofilm in topside equipment is not well documented. This is a potential drawback for nitrate application. It has also been suggestions that nitrite, produced by some NRB, can be corrosive under certain conditions.

Most published data on the effect of nitrate treatment are commercially orientated and there is concern that the selective release of data may jeopardize the surge of interest in this promising technology and greatly undermine its potential widespread application hence there is limited literature on nitrate injection. There is a very high likelihood that the concentration of utilisable organic carbon is important in determining the nitrate or nitrite concentrations required for souring control as both SRB and denitrifying bacteria compete for the same organic substrates. The reduction of nitrate, like the reduction of sulphate by SRB, is an example of respiratory metabolism under anaerobic conditions, using nitrate as a terminal electron acceptor and many types of bacteria containing nitrate reductase enzymes to facilitate the reaction:

$$NO_3^- + 2e^- + 2H^+ \rightarrow NO_2^- + H_2O$$

Growth by this reaction is limited, because the amount of energy released is relatively small and the end product, nitrite is toxic. Under appropriate conditions, nitrite may be excreted and further reduced via hydroxylamine to ammonia; this process is called nitrate ammonification. A few bacteria (principally Pseudomonas and Bacillus species) can reduce nitrate beyond

the level of nitrite to molecular nitrogen through a process known as denitrification:

$$2NO_3^- + 10e^- + 12H^+ \rightarrow N_2 + 6H_2O$$

In such conditions, nitrate serves as an extremely effective electron acceptor. The reduction of nitrate to either nitrite or nitrogen requires the corresponding oxidation of an organic substance acting as the energy source thereby, leading to competition for the available organic substrates between SRB and NRB. When the NRB out-competes the SRB for organic nutrients with the proliferation of NRB at the expense of SRB, the process is known as bio-competitive elimination, which is one of the mechanisms by which nitrate injection prevents reservoir souring. Over the years, the use of nitrate to prevent reservoir souring is becoming rampant in the oil industry. Several field tests have demonstrated the potential usefulness of nitrate for controlling souring[9, 12, 25, 34-36]. In 2003 the Institute of Petroleum (now the Energy Institute) in the United Kingdom published a useful introductory overview about use of nitrate treatments to control SRB, MIC and reservoir souring[33]. However there is very little knowledge on how to control the detrimental consequence with respect to corrosion caused by the introduction of nitrate/nitrite into the system. Available organic substrate, NRB, SRB, presence of other bacteria capable of further reducing nitrite and several other factors all play an important role in understanding the detrimental effects of nitrate/nitrite injection.

Acetate is an example of oxidation of the electron donor as illustrated in the following reaction:

$$2H_2O + CH_3COO^- \rightarrow 2CO_2 + 7H^+ + 8e^-$$

This reaction illustrates the importance of organic carbon availability on the nitrate treatment; it generates the electrons required for the NRB to reduce nitrate to nitrite and other N-O compounds.

A very interesting NACE paper on corrosion by SRB that utilize nitrate confirms that SRB can utilise nitrate as an electron acceptor. In the course of the work, 16S rRNA gene sequencing and phylogenetic analysis[37] were used to isolate SRB from a Danish North Sea oilfield water injection system. Large fragments of the genes were further amplified and sequenced with DNA tools.

The isolated species was cultivated, purified and subsequently identified as being strain OP102 which is more than 97% similar to desulfovibrio gracilis. By isolating and sequencing a SRB species of interest, other mechanisms by which nitrate can act that were not of interest were eliminated and they were able to zero in on one particle mechanism of interest. According to Dunsmore et al[13], "[strain OP102, like some other desulfovibrio species of SRB], *"can reduce nitrate as an electron acceptor and produce ammonia in the absence of sulphate"*.

Furthermore, according to work done by Dalsgaard and Baks[17] on nitrate reduction in sulphate reducing bacterium, desulfovibrio desulphuricans, isolated from a rice paddy soil have been reported to reduce nitrate to ammonia. Also in the presence of sulphate, when nitrate was dosed at 100mg/l, nitrate was reduced by OP102, with some ammonium production.

In static tests, the influence of desulfovibrio on corrosion was assessed using carbon steel coupons, in the presence of sulphate only and also in the presence of sulphate with 100mg/l nitrate. Nitrate, nitrite and ammonium were measured using a Palin test to determine the rate of nitrate reduction (as the sole electron acceptor) and the rate of by-product generation while sulphide was measured using the methylene blue method. Test results confirmed that OP102 was able to respire using nitrate. Consequently nitrate concentration reduced from 600mg/l to almost 0mg/l over the course of two weeks. After a lag period (perhaps related to pH changes in the system), ammonium was seen to increase from approximately 5mg/l to over 120mg/l in both tests. Stoichiometrically, assuming 100% conversion (which is rarely feasible in a biological system), 3g of nitrate can produce 1g of ammonium. However, in this experiment the stoichiometry ratio was 5:1, which suggests that a large proportion of the nitrate reduced was converted to ammonium. A small concentration of nitrite was also produced (maximum 3mg/l). However, this was transient and most measurements over the two weeks recorded nothing more than a trace. Sulphide generation followed a similar trend for test bottle with different nitrate concentrations (0, 5, 20 and 60 mg/l). Sulphide increased quickly to approximately 150mg/l on day 9, before the rate of sulphide production slowed considerably reaching a maximum concentration of

205mg/l. However, the bottle dosed with 100mg/l of nitrate produced significantly less sulphide, after day 7. The rate of sulphide production was considerably slower than what was recorded in other bottles reaching a maximum sulphide concentration of 162mg/l. Since these were pure OP102 species tests, many of the usual mechanisms, by which nitrate can act, were precluded. Since no nitrite was measured, the authors concluded that the only possible mechanism that led to nitrate reduction was that the SRB utilised the nitrate as an electron acceptor and this affected sulphide generation, when nitrate was present in relatively high concentrations.

Dunsmore et al[13] also stated that, "*the use of nitrate as an electron acceptor occurred in the presence of normal, seawater-strength concentrations of sulphate (2800mg/l)"*. It has been reported that one SRB strain possessed nitrite-reductase genes and that these were up regulated when the organism was exposed to nitrate. It has also been hypothesised that this may act as a detoxification mechanism to remove damaging nitrite from the cell[23].

2.2.3 Effect of Nitrate/Nitrite on Corrosion Rate

According to test result reported by Dunsmore et al[13], the average corrosion rates measured when coupons were incubated in medium with sulphate, as the only electron acceptor was 0.3mpy and 1.15mpy when coupons were incubated in medium with sulphate and nitrate as the electron acceptors. From these results corrosion appeared to be worse in the test systems where nitrate was present. The increase in corrosion rate could be attributed to the generation of sulphide in the system. However, corrosion rates were less than 1.5mpy in both cases hence considered low for this system. Iron sulphide is soluble however in this case, being a non-flowing system, this film was not disturbed and as such was able to protect the underlying metal, had it been a flowing system, the corrosion rate would probably be higher. Furthermore, detailed SEM analysis showed that the occurrence of pitting corrosion was fairly low in all the tests, both with and without nitrate[13]. It was suggested that the presence of strain OP102 that reduced nitrate to ammonia eliminated production of nitrite and invariably minimised the occurrence of localised corrosion. Some small pits of up to 10μm in diameter, (which could be the result of MIC) were found. These initial pits could eventually propagate and

compromise the technical integrity of the carbon steel system. It should however, be noted that this individual characterisation of pitting, by one species, under defined conditions in no way precludes the need for further work on this subject. Further work within the scope of this research would be carried out to investigate pitting corrosion resulting from nitrate/nitrite injection. It is however important to mention that findings from the work done by Dunsmore et al further support Rizk and Stott's school of thought that nitrite, a by-product of intense NRB activity, is the likely agent of enhanced general and/or localised corrosion in nitrate-treated systems[3].

Another very interesting finding from this NACE paper is the fact that desulfovibrio are reported to be non-acetate oxidisers and may in fact generate acetate[13]. According to Dunsmore et al[13], *"the ability for desulfovibrio to grow chemolithotrophically (can use inorganic electron donors) and autotrophically (can use an inorganic carbon source, namely CO_2) makes them unique among other species of SRBs"*. This means that some desulfovibrio species can use H_2 as electron donor, sulphate as electron acceptor and CO_2 as the sole carbon source[38]. During this process H_2 is oxidised to H_2O, sulphate is reduced to sulphide and the CO_2 is used to produce sugars, which are then incorporated into the cells as biomass. As previously discussed, production of iron sulphide may have detrimental consequence with respect to corrosion because of its solubility in water. On the other hand, the process consumes CO_2 to produce organic compound thereby reducing the detrimental effect of CO_2 corrosion.

Experimental work done by Thorstenson and others on biocide replacement by nitrate in seawater injection systems, indicate the *removal of SRB from the biofilm lead to reduced corrosion[9]*. *According to* Widdel[39], *"SRB are known to play a key role in anaerobic MIC by several mechanisms. They remove molecular hydrogen from the metal surface by oxidation with sulphate as electron acceptor (cathodic depolarisation), resulting in a net oxidation of the metal. Desulfovibro are known to be very effective depolarisers due to their high affinity to hydrogen. At the anode, where iron is oxidised and goes into solution, Fe^{2+} reacts with H_2S to form solid FeS. Ferrous sulphide in contact with iron acts as a cathode and facilitates the depolarisation significantly.*

[Hence]*, when SRB are removed from the biofilm at the metal surface, and replaced with microbes that are not H_2S producers, reduced corrosion should be expected".* Typically, in water injection systems, the velocity of water have predominantly been less than 5.5m/s; at this rate the water velocity does not influence the corrosion rate[9].

In 2003, Rizk, Stott and Robertson[40] conducted an independent evaluation of nitrate anti-souring reservoir treatment on carbon steel with the objective to provide clear guidelines with regard to nitrate application and its effect on corrosion processes. For the first phase of their work, static vessels were used to investigate why some produced water system give rise to much greater nitrite production as a by-product of nitrate treatment than others, pH and organic carbon concentration were identified as two important factors[3]. Worst-case nitrite production was found to occur in high CO_2 loading systems especially those with pH < 6. It was also observed that the presence of nitrite was strongly associated with enhanced corrosion.

For the second phase of the work, continuously flowing cells were used to evaluate the effects of nitrite production on corrosion in a mixture of produced water and seawater[4]. Continuous flow cells were specifically used to overcome the objection that static tests bring about gradual build-up of nitrite, which would not occur in a flowing pipeline where there is a shorter residence time. The flow cell tests included continuous, interrupted and delayed nitrate treatments, together with nitrate free control tests. It was concluded that nitrate treatment at 60mg/l gave rise to enhanced general corrosion of up to 0.42mm/y, compared to less than 0.1mm/y typically expected for untreated water. It was also observed that nitrate treatment increased both the density and depth of pits on carbon steel. However, the effect of nitrite (formed from nitrate) on corrosion was relatively small compared to the risk of much higher corrosion rates that can be caused by untreated SRB growth. Also based on test results, it was confirmed that nitrate treatment is effective in suppressing H_2S generation in laboratory test cells. It was also observed that the effect of nitrate on corrosion was strongly influenced by the specific environment. Comparing the corrosion effect of nitrate on seawater and PWRI, little or no enhanced corrosion effects were observed in the case of seawater. However,

in some PWRI cases, enhanced corrosion associated with nitrate dosing was observed. Although the enhanced corrosion rates were high enough to cause concern, the corrosion rates were not 'catastrophic' and were certainly lower than the rates of corrosion of up to 2mm/y that could be experienced in the presence of uncontrolled long-term SRB activity. This is a very strong argument to support nitrate treatment as a means of preventing reservoir souring. It is also consistent with Norsk Hydro conclusions[41]. It was clear from the results of the study that enhanced corrosion was strongly associated with the generation of nitrite and that nitrate treatment of produced water for re-injection is a much more complex and capricious scenario than seawater treatment with nitrate. Significant pitting corrosion was observed on carbon steel specimens from a test cell in which nitrate was reintroduced compared to a pre-soured system.

Different conclusions have been drawn from corrosion monitoring data in real systems. This is often due to the fact that the corrosion monitoring programmes have been inadequate to provide a valid assessment. However, in situations where more ample monitoring had been carried out on seawater injection systems, the results generally show a decrease in corrosion after nitrate treatment. Based on field data from Gullfaks field where nitrate injection has been used to inhibit H_2S generation, it has been suggested that decrease in corrosion after nitrate treatment is probably due to better control of SRB in the injection pipe work[34]. This suggestion is consistent with other literatures, although there is slight increase in the general corrosion due to nitrate dosing; the tremendous reduction in corrosion rate due to uncontrolled SRB activities makes the enhanced corrosion due to nitrate injection insignificant and a net reduction in the overall corrosion rate.

Further work on corrosion inhibition of carbon steel in PWRI systems that use nitrate treatment to control SRB activities and reservoir souring conducted by Stott, and others was presented during 2008 NACE conference in New Orleans. The paper states that increase in corrosion rate of carbon steel has not been observed with the use of nitrate in seawater injection. Rather, there is evidence that nitrate may actually reduce corrosion. However, laboratory and field reports have identified that nitrate treatment can give rise to

increased general and localised corrosion in certain PWRI systems[42]. The authors went further to state that the influence of nitrate on corrosion rate in PWRI systems is unpredictable[42]. This is consistent with previous publications. There is concern that the use of nitrate as a highly effective and environmentally favourable alternative to conventional biocide treatments could in the case of certain PWRI applications be undermined by the side effect of enhanced corrosion hence, Stott, and others went further to investigate the possibility of using corrosion inhibitors to prevent potential corrosion problems associated with nitrate injection. Laboratory test program was conducted to evaluate 6 different corrosion inhibitors. The general and pitting corrosion rates were measured in the presence of biofilm containing high NRB population. The increased general corrosion rate and pitting penetration rates that were observed during nitrate treatment were substantially reduced by the best performing inhibitors.

Further preliminary test result from Rizk and Stott[3] speculate that nitrite inhibition mechanism on carbon steel is by passivation due to formation of a very thin ferric oxide film. In the absence of sulphide, insufficient nitrite could promote the formation of a partially protective layer of the corrosion product. Depending on the properties of the corrosion product, slight corrosion may occur. In the presence of aggressive ions, slight insufficiencies of nitrite promote pitting. If nitrite predominates over aggressive ions such as chloride and sulphate it acts as an inhibitor, however at high aggressive ion to nitrite ratios (as with nitrate treatment of seawater) general corrosion is expected. This indicates that a critical amount of nitrite is required. The critical nitrite concentration depends on the chloride concentration. This is in agreement with Macdonald[43] postulation on point defect model later described in this report. It is not surprising that further findings indicate that optimal nitrate treatment and its corresponding effect are highly field specific[3] since the chloride concentration and other factors earlier mentioned such as available organic substrate, NRB, SRB, presence of other bacteria capable of further reducing nitrite vary from one field to the other. It appears that oxygen reduction is the main cathodic reaction supporting corrosion in nitrite/chloride solutions hence, it is expected that the rate of localised corrosion would be

reduced but not eliminated by removal of oxygen. The by-products of the process such as nitrite and possibly N_2O can cause corrosion problems. As earlier mentioned, it is also possible for nitrite to oxidise sulphides into elemental sulphur. Sulphur is soluble in water, hence sulphur in the sections where iron sulphide was oxidised could easily dissolve thereby causing perforation of steel. Since nitrate is rapidly reduced to nitrite in the reservoir, then the addition of nitrate is expected to have a similar consequence. Also with pre-existing sulphide films, nitrite may induce localised corrosion of defects in the films.

Preliminary investigation work done by Rizk and his colleagues at CAPCIS showed that the presence of biologically generated nitrite may depend on the water chemistry[3, 4]. Presence of nitrite was transient in some systems while low concentration of nitrite was continuously observed in other systems.

The continuous presence of low concentration of nitrite and possibly other strong oxidants such as N_2O as by-products of nitrate injection is of considerable concern due to their potentially undesirable corrosion processes which pose the biggest threat to the wide spread implementation of nitrate injection as a means to control reservoir souring. Findings from the literature indicate the following as possible corrosion risks associated with nitrate injection:

1. Prolonged biological generation of nitrite that might induce pitting corrosion.
2. Oxidising action of the additive or NRB by-products, i.e. negating the effect of de-aeration of the injected water.
3. Formation of semi protective oxide film which might lead to pitting if the entire surface is not adequately protected.
4. Partial passivation in seawater which might also lead to localised corrosion.
5. In a situation where produced water is re-injected and nitrate injection is in the order of thousands of mg/l, there is the possibility of nitrate stress corrosion cracking at temperatures of 60-80^{o}C[4].
6. Reaction product such as sulphur or thiosulphate could cause corrosion issues in certain circumstances.

7. Microbial influenced corrosion under nitrate reducing biofilms.
8. By-product of NRB may be used for SRB recovery leading to enhanced corrosion due to the emergence of H_2S
9. Production of ammonia could affect the pH and induce stress corrosion of copper and copper based alloys

Although the interaction of various mechanisms that cause the corrosion risks is not well know, but it is clear that the sulphur and nitrogen cycles are closely linked, the interrelationships are finely balanced and the end result (sulphate-reduction, nitrate-reduction, inhibitory effects) will be controlled by several factors such as microbial species present, sulphate, organic acid, nitrate and physio-chemical environment as a whole. Most likely, various mechanisms could be operating simultaneously and to a varying degree in different regions of the reservoir, it would however be difficult to distinguish between them. There are indications that the persistent presence of low concentrations of biologically generated nitrite could be well correlated to increase in corrosion rates, this is of particular interest to this research work.

Nitrite is suggested to be an anodic corrosion inhibitor for carbon steel and cast iron generally at pH above 5 and sufficiently high concentration when it predominates over aggressive ions such as chloride, sulphate and nitrate. As earlier mentioned, its protective mechanism is the formation of an extremely thin protective ferric oxide passive film without necessarily increasing the solubility of ferrous iron salt that could cause localised corrosion. Any ferrous ion that emerges undergoes redox reaction with nitrite producing black or dark brown solid such as magnetite that suppresses corrosion. However, inhibition by nitrite is not considered a safe process as it can cause localised corrosion when the nitrite concentration is insufficient to cause complete passivation. A possible explanation for this phenomenon is that when the nitrite concentration is not sufficient to produce the protective ferric oxide passive film on the entire metal surface, the unprotected surface become anodic with respect to the protected surface and goes into dissolution. This case is similar to that of differential oxygen exposure. This would certainly be the case for saline water injection; hence the tendency for nitrite to increase localised corrosion when the nitrite concentration is insufficient to cause complete

passivation is a concern for nitrate injection as an application to prevent reservoir souring. This is in agreement with another school of thought which states that in the absence of nitrate or nitrite, when carbon steel is exposed to deaerated seawater, its corrosivity is minimal because the corrosion rate is limited by the transportation of low parts per billion (ppb) concentrations of residual oxygen to the carbon steel surface. Even at high flow conditions, the corrosion rate is in the order of 0.01mm/year or less with no tendency for pitting provided there is no residual chlorine or bromine in the seawater[42]. In contrast, produced water is often able to cause significant corrosion in the absence of oxygen (CO_2 corrosion) mainly because the cathodic reaction in this case is hydrogen evolution as a result of low pH due to the presence of CO_2. Hence the corrosion rate is not limited by the transportation of low concentration of residual oxygen. The exact corrosion rate will depend on factors such as the pH, presence of H_2S, temperature and presence of corrosion inhibitor and other chemicals. Some combination of these factors could lead to localised corrosion.

According to the classic corrosion program conducted at the National Physical Laboratory, United Kingdom in the 1960's[44 - 50], chloride, sulphate and nitrate are classed together as non-oxidising. However, some evidence of nitrate electro-reduction was noted, but only in high concentrated solutions[44] and may be more prominent at higher temperatures. In contrast to nitrate, nitrite is classed as both inhibiting and oxidising. The oxidising effect of nitrite is evident when steel is exposed to pure sodium nitrite solution in the absence of dissolved oxygen, passivation of the metal occurs[50]. Also nitrite is a better oxidant towards bare steel than nitrate, this is probably due to the kinetics of nitrate reduction being slow unless the temperature and nitrate concentration are high or the pH is low. NRB reduce nitrate far more rapidly than what can be achieved on a metal surface. Reaction of nitrate with ferrous ions is also extremely slow unless the concentration of both the nitrate and ferrous ions in aqueous solution are high[50]. As a result, ferrous nitrate is not a stable solid. Therefore nitrite is much more liable than nitrate in dilute solution and it is readily reduced to variety of products such as nitrogen and ammonium ions.

According to Scott et al[42], "*inhibition by nitrite is not a safe process, as it can cause localised corrosion when the nitrite concentration is insufficient to cause complete passivation, as it certainly would be the case of saline water injection"*. This claim was illustrated in tests conducted with aerated 1 Molar NaCl Solution containing 460mg/l of nitrite. However it was not possible to determine whether this type of corrosion will proceed in the absence of oxygen. Most likely, oxygen reduction is the main cathodic reaction supporting corrosion in nitrite/chloride solutions. Hence it is logical to expect that the rate of localised corrosion would be reduced but not eliminated by oxygen removal. Other publications also iterate the detrimental effects of nitrite on corrosion of steel in the presences of aggressive ions such as chloride, sulphate and nitrate[44, 45]. However hitherto, there is no conclusive research work to investigate the detrimental effect of nitrite on CRA.

In a deoxygenated mixture of sodium chloride and sodium nitrite, nitrite acts as a strong oxidant passivating the steel surface. However there is likelihood that a soluble salt, ferrous chloride, will form in the system. Hence at any flaw or breakdown of the passive film, the redox reaction between ferrous ion and nitrite competes with the dissolution of ferrous ions generated by chloride as counter ions leading to pitting which propagates rapidly due to the galvanic action in which the passive metal acts as large cathode coupled to a small anode which is the pit. This theory further supports and emphasises the importance of the chloride/nitrite ion ratio.

In 1990, Mercer[50] reviewed the work done at the National Physical Laboratory and found out the work gives no indication that nitrate could introduce a specific corrosion mechanism in the presence of a large excess of a more aggressive anion such as chloride. However, a series of papers by a Spanish group in the late 1980's[51-53] claimed that nitrate plays an important factor in increasing the estuarine corrosion rate of steel in the presence of dissolved oxygen. Analysing their raw data indicates a doubling of the corrosion rate in the presence of 25mg/l of nitrate. The authors went further to state that nitrate is an oxidant (depolarizer) of the cathodic reaction, or alternatively a catalyst for oxygen reduction. These observations relate to processes (such as cathodic reactions on well-developed rust layers) that do not apply to

anaerobic conditions and are consistent with other publications. Also, the doubling in corrosion rate does agree with Norsk Hydro[41] observations, despite the differences in flow and oxygen content, which may suggest that some direct nitrate reduction occurred in both cases. It is important to note that even though the corrosion rate doubled it was still low and acceptable. The impression that nitrate itself may be chemically reduced on scaled steel surfaces without necessarily giving rise to a distinct corrosion problem is in accord with Norsk Hydro[41] data, which showed a small increase in corrosion rate with 25mg/l nitrate added to deoxygenated seawater and a larger increase with 150mg/l nitrate (under flowing conditions with velocity of 4m/s), but all the corrosion rates were below 0.1mm/y which is less than corrosion rates as a result of the addition of 0.5ppm chlorine to the same seawater.

In contrast to nitrate, it is well known that nitrite is both electro-active and redox-active; for example, it passivates steel in de-aerated solution, and reacts rapidly with ferrous ions or H_2S. Therefore, in the absence of H_2S, it seems that traces of nitrite, which is a by-product of intense NRB activity, is the likely agent of enhanced general and/or localised corrosion in nitrate-treated PWRI systems. Experimental work carried out by Rizk confirmed a strong correlation between the presence of nitrite (typically at concentrations of less than 10mg/l) and enhanced corrosion[3]. The challenge however is the fact that the phenomenon of microbiological nitrite generation from nitrate is extremely unpredictable and system specific. No doubt, it depends on the water chemistry, specific microflora and other factors.

From some field stimulation tests conducted by Rizk, it was observed that nitrite was generated from nitrate injection and that nitrite stimulated pitting corrosion of carbon steel in one field while in other field stimulation tests nitrite production did not cause any problem[3]. In an effort to understand the reason behind this contradicting results from field stimulation tests and also to gain better understanding of possible corrosion risk scenarios that might be associated with nitrate treatment, Rizk and Co progressed the research work further to assess the corrosion risks associated with nitrate injection by means of materials exposure tests on carbon steel and electrochemical corrosion studies under both static and flowing conditions. The study was funded by

Reservoir Microbiology Forum of the Energy Institute with the aim of achieving the following:

1. Investigate the interlinked issues associated with nitrate treatment
2. Study the biological aspects and effectiveness of nitrate treatment as an anti-souring agent
3. Identify conditions influencing the effectiveness of nitrate injection
4. Examine the effect of pH and nutritional variation on nitrite generation from nitrate anti-souring treatment
5. Understand the possible side effect of nitrate treatment and its by-products on corrosion processes of injector/producer tubular.

For the study, 95% seawater (from CAPCIS coastal site at Anglesey) and 5% produced water (from Shell Haewane Brim, a gas injection field) was used as test solution with addition of 300mg/l of yeast extract, acetate and propionate as nutrient supplements to promote bacteria growth and 60mg/l nitrate concentration. The test was conducted under laboratory conditions. Indigenous species of bacteria, microflora were inoculated into the cell. Adjustment of pH was achieved by injection of CO_2 gas and addition of sodium bicarbonate $NaHCO_3$ to stimulate typical reservoir conditions. For optimal growth of microflora, an operating temperature of 40^oC was maintained using a water bath. As is typical for laboratory tests, nitrate was found to be effective in stifling H_2S generation. Early blackening was observed in all the high nutrient cells within the first few days of the test indicating SRB activity however, the cells cleared off as the test progressed, indicating that nitrate was able to suppress SRB activities from sulphate reduction. Nitrite production was low in seawater alone but significantly increased when comingled with produced water. Maximum nitrite production occurred at lower pH values and moderate produced water admixture. Nitrate addition efficiently curtailed sulphide production by SRB under all test conditions and no detection of sulphide despite early blackening in all high nutrient cells[33].

Test results indicate that the addition of nitrate to a solution with seawater only has no significant effect on the corrosion of mild steel. However, when nitrate was added to a produced water re-injection system of pH 5.5 and low - medium carbon availability (below 100mg/l of acetate equivalent), several

corrosion issues were observed[33]. Iterated below is a summary of observations and postulations from the tests:

1. Both general and pitting corrosion rates of mild steel were increased
2. The corrosion rate induced by nitrate is more consistent compared to the corrosion effect of sulphide which is unpredictable
3. Treatment produced a porous, discontinued and non uniform biofilm
4. Nitrite and other possible N-O compounds and elemental sulphur might have been generated
5. Nitrate does not completely cease SRB activity but shift from sulphate reduction to nitrate reduction
6. Nitrate treatment gives higher redox potential than that of a biogenic sour system which could be crucial for the control of SRB
7. In nitrate treatment, is highly dependent on the pH of the system. Nitrite production increased greatly at low pH of around 5.5 compared to pH 6.5 and 7.5

These observations are consistent with findings from literature and previous experiments. The experimental results also confirm an earlier school of thought that nitrite production is a function of the concentration of the carbon source[3], hence it is not surprising that the result of test conducted by Tony Rizk and others indicates significant corrosion issues during nitrate treatment with Produced Water Re-Injection (PWRI). The PWRI is the source of organic carbon which is an important component required for the biogenic reduction of nitrate to nitrite. A reasonable conclusion is that corrosion was as a result of nitrite corrosion, with nitrite possibly generated through the second mechanic earlier discussed. In which case, the reduction of nitrate to nitrite by NRB shifted the Redox potential of the reservoir, thereby favouring further proliferation of NRB and inhibition SRB activities.

$$NRB + NO_3^- \rightarrow NO_2^-$$

Evaluating the chemistry and thermodynamics involved in the reduction of nitrate to nitrite as indicated by the chemical reaction below:

$$NO_3^- + 2e^- + 2H^+ \rightarrow NO_2^- + H_2O$$

$$\Delta G = \Delta G^0 - 4.6RT\left(Log\frac{\left[NO_2^-\right]}{\left[NO_3^-\right]} - 2pH \right) \quad (1)$$

Where ΔG is the Gibbs free energy for the reaction, ΔG^0 is the Standard Gibbs free energy for the reaction, R is the gas constant and T is the temperature (K).

Hence, it is not surprising that the reduction reaction is a function of pH. Also as indicated in equation 1, the Gibbs free energy for nitrate reduction to nitrite increases with decrease in pH therefore, the rate increases as pH decreases. Another point to note is that the thermodynamics of nitrate being reduced to nitrite is a function of the $[NO_2^-]/[NO_3^-]$ ratio.

A survey of standard equilibrium potential (E^o) values for a variety of reactions indicates that under neutral conditions, nitrate, nitrite and some of the intermediates (N-O) between nitrite and nitrogen are all thermodynamically capable of oxidising Fe to (Fe^{2+})[54]. Kinetic factors tied to activation energies may be the reason for these reactions to proceed normally at low rates.

Visual and microscopic examination of carbon steel test samples showed that nitrite stimulated pitting corrosion of carbon steel but Stress corrosion cracking of carbon steel was unlikely in nitrate solution. Nitrate treatment led to greater density of pitting with penetration rates up to 0.43mm/y compared to 0.2mm/y with negligible pitting observed in conventional biocide treatment[33]. While the results indicate a relatively small increase in corrosion rate caused by nitrate, there may be variation in its effect depending on the specific operating conditions. However, compared with untreated seawater system with SRB growth, the measured corrosion rate was up to 4.5mm/y, which indicates the increase in corrosion rate as a result of nitrate treatment, is relatively small compared to the corrosion rate of untreated system.

On the other hand, results from the PWRI pilot test conducted by Norkse Shell in the Draugen field showed that addition of nitrate to produced water was efficient to control near well reservoir souring however the corrosion rates increased logarithmically[55]. Also, few parts per million (ppm) of nitrite was observed in the nitrate treated produced water. Upon biocide treatment, there was instantaneous decrease in nitrite and corrosion rate decreased to the

background level. This result led to another school of thought that bacterial activity resulting from the addition of nitrate is the primary reason for the increase in corrosion rate. During the test, corrosion inhibitor was injected to control CO_2 corrosion and the redox potential measured. There was no clear difference in the redox potential between injected water, treated with nitrate and water without nitrate. Also the efficiency of the corrosion inhibitor was tested after a period of produced water injection without nitrate. When corrosion inhibitor was added to the system the corrosion rate decreased from 0.12mm/y to 0.01mm/y and the rate immediately increased when the corrosion inhibitor injection was stopped. This clearly indicates that the corrosion inhibitor effectively controlled CO_2 corrosion in produced water without nitrate. The fact that the corrosion rate and nitrite concentration decreased immediately biocide was injected into the system indicates that microorganism caused the corrosion. Hence it was concluded that the increase in corrosion rates was most likely due to microbial induced corrosion (MIC). Similar results have been obtained in other studies[56-58]. One of the metabolites in nitrate reduction by NRB is nitrite[56].

Examination of the corrosion coupons showed yellow deposits presumed to be elemental sulphur or polysulphides. The yellow deposit turned white on exposure to air. These are characteristic signs of the presence of elemental sulphide, which as previously discussed is highly corrosive due to its ability to react with cation such as Fe^{2+} to produce iron sulphide which is very solubility in water. The presence of elemental sulphur gives an indication of the nitrate reduction process. As mentioned earlier, certain species of NRB known as Nitrate Reducing, Sulphide Oxidising Bacteria (NRSOB) are capable of partly reducing nitrate to nitrite (or nitrogen oxides) and simultaneously oxidise existing H_2S sulphide. Reaction between nitrite/nitrogen oxides and sulphide ion (S^{2-}) can result in the formation of elemental sulphur or polysulphides. The presence of few ppm of nitrite and simultaneous exponential increase in corrosion rates further confirms NRSOB activity. Using electrochemical probes to monitor corrosion in a system PWRI[59]; test results showed thick biofilm formation and an increase in corrosion rate. It is however necessary to exercise caution and not jump to conclusion without further verification

because redox reactions within thick biofilms may mimic corrosion. Hence, verification by weight loss is required. Test results of work done by Dunsmore and Co.[13] concluded that in the presence of SRB, which reduce nitrate in preference to sulphate, corrosion rates were low after nitrate treatment and gave no cause for concern.

In another research work conducted by CAPCIS Ltd on behalf of Shell EP Research and Development in 2009, to study the effect of nitrate anti-souring treatment on corrosion of mild steel in Astokh seawater and seawater mixed with produced water. Two set of tests were carried out at ambient temperatures using two ratios of seawater to formation water (100% seawater and brine comprised 25% produced water, 75% real seawater mixture with 50mg/l of yeast extract and trace of ferrous iron) purged with a gas mix containing 2% CO_2, and 98% nitrogen to maintain field specific anaerobic conditions. The first set of tests were carried out using chemically untreated seawater while the second set of tests were carried out using seawater chemically treated with nitrate concentration of 50mg/I (active nitrate ion). Weight loss and linear polarisation resistance (LPR) tests were carried out in accordance with ASTM G1 using A709 steel. LPR test results of the cells gave an average general corrosion rate of 0.03mm/y before nitrate treatment. Once nitrate treatment was introduced, corrosion rates rose to about 0.2mm/y, after an initial delay, for all treated cells[60]. The initial delay was probably due to the time taken for the nitrate to reach the cells and accumulate to a 'critical' value required for NRB metabolism. It is generally accepted theory that corrosion, especially pitting, was not caused directly by nitrate ions, rather it was caused by the by-products of NRB metabolism, most commonly nitrite ions. The corrosion rates determined by weight loss and LPR exhibited very similar trends. In both cases, the corrosion rates are modestly elevated under a nitrate treatment regime. Corrosion rates determined by weight loss and LPR technique do not differentiate between pitting and general corrosion but only relates to general corrosion. However, evaluation of the weight loss coupons using standard light microscopy and SEM revealed pitting on all the coupons that were exposed to nitrate treatment with the deepest pits having pit depth of 20 to 30μm. Hence, the elevated corrosion

rates determined by LPR and weight loss coupons were most likely caused by the pitting process, which cannot be extrapolated directly from weight loss and LPR measurements. Summation of the general corrosion rate and pitting rate for each condition gives the maximum total penetration rate. The total penetration rate for test samples exposed to seawater treated with nitrate was 0.25mm/y while those exposed to seawater and produced water mix treated with nitrate was 0.24mm/y. The total penetration rates for the untreated conditions (i.e. seawater only, seawater and produced water mix) were both below 0.1mm/y. This indicates that just by treating either seawater or seawater and produced water mix with nitrate, the total penetration rate at least doubled. This is consistent with most literature, however the key finding from this work is acknowledging the fact that nitrate treatment did not affect the general corrosion rate but localised corrosion (which was mainly pitting) and the fact that pitting, is not caused directly by nitrate ions but rather caused by the by-products of NRB metabolism, most commonly nitrite ions. Nitrite, unlike nitrate, is electro-active and promotes localised corrosion when it is present in insufficient concentration to counter balance the aggressive ions that are present in the system causing partial passivation in the system, leading to localised corrosion. This statement also supports the theory that a critical nitrite concentration is required before nitrite can be effectively used as an anodic inhibitor and that the critical nitrite concentration is a function of the aggressive ions present in the system. In the case of seawater sample from Astokh, a couple of peculiarities were noted:

Firstly, the metabolic activity of bacteria was relatively low, compared to many other injection waters, because of the low dissolved organic carbon (mainly acetate) content of the Astokh seawater. This leads to limited nitrite by-product generation by NRB metabolism.

Secondly, the dissolved CO_2 concentration in the re-injected Astokh seawater was low compared to many produced waters; therefore, the intrinsic corrosivity of the injection water was comparably less than that of systems containing higher content of dissolved CO_2.

Thirdly, the system was not sour. This makes a huge difference because in the presence of H_2S, nitrite reacts directly with H_2S to produce a variety of

sulphur compounds including, in some cases, elemental sulphur and complex corrosion phenomena might result. The corrosion phenomena in PWRI systems are difficult to predict and vary widely, depending on the nature of the products (sulphur, thiosulphate, polythionic acids, etc.); however, where elemental sulphur is produced, it may give rise to seriously elevated rates of general and pitting corrosion.

Finally, the temperature of the PWRI system was considerably lower than many other systems. This might have led to the lower rate of microbiological metabolism, compared to higher temperature environments (i.e. lower rate of production of corrosive by-products, such as nitrite) and also it directly lowers the rate of the resultant chemical corrosion reactions[60].

During the Reservoir Microbiology, Energy Institute joint meeting in 2004, Beeder[61] presented his work on corrosion problems associated with nitrate. He described the operational problems experienced in a mixture of aquifer water and produced water, with high CO_2 content. He stated that serious pitting corrosion was observed with nitrate injection. Tests were performed both in the field and in the laboratory, with the highest corrosion rates being experienced in the case of the laboratory tests. He stated that the phenomenon is still not fully understood, but inferred that the corrosion resulted from NRB, which caused depolarisation of the metal surfaces and were able to oxidise ferrous iron. He also suggested that high corrosion results were most likely as a result of the formation of elemental sulphur[42]. He however categorically stated that it was unclear whether the high corrosion rate was as a result of sulphur produced from the microbiological action of NRSOB or from accidental oxygen ingress.

Another school of thought by Stott and others states that when carbon steel is exposed to deaerated seawater and oxygen-free produced water in the absence of nitrate/nitrite, the seawater is non-corrosive, the corrosion rate is being limited by transport of residual oxygen at ppb level to the surface of the steel surface hence even under high flow conditions, the corrosion rate will be less than 0.01mm/y with no pitting provided there is no residual chlorine or bromine in the seawater. In contrast, in the absence of oxygen but substantial amount of CO_2, produced water is able to cause significant corrosion (CO_2

corrosion) because the cathodic reaction in this case is hydrogen evolution since CO_2 is capable of lowering the pH. The exact corrosion rate will depend on the usual factors such as pH, presence of H_2S, temperature and presence of corrosion inhibitor. Combination of any of these factors may lead to localised corrosion[42].

Nitrate is grouped with chloride and sulphate as aggressive and non-oxidising in low concentrations however, nitrate is significantly less aggressive than chloride and sulphate[62]. Nitrate electro-reduction was noted in highly concentrated solution and more prominent at higher temperature. On the other hand, nitrite is classed as both inhibiting and oxidising. When nitrite is added to distilled water in the absence of dissolved oxygen, nitrite can passivate steel, however when the concentration of nitrite is insufficient to cause complete passivation, nitrite can cause localised corrosion.

According to Sturman, et al[63], "*in the presence of H_2S, nitrite and nitrate behave very differently. Nitrite can react directly with H_2S, whereas nitrate does so indirectly via the growth of NRB. A variety of sulphur compounds may be produced by these reactions, and some new corrosion phenomena may be expected".*

Also according to Mc Inerney et al[64], "*H_2S may be oxidised all the way to sulphate, which would be the ideal case in practice. However, in cases where elemental sulphur is produced, that could give rise to seriously elevated rates of corrosion"*. The corrosion phenomenon will vary widely depending on the exact products (sulphur, thiosulphate, polythionic acids, etc.), temperature, pH etc. The paper pointed out a very interesting distinction between the interaction of H_2S with nitrate and nitrite. The interaction of nitrite and H_2S is basically an inorganic chemical reaction while the interaction of nitrate and H_2S is through a microbial influenced reaction. Several literatures have confirmed the ability of NRB to reduce nitrate to nitrite, some also suggest that nitrite is seen as a transient product in nitrate reduction process. It is therefore reasonable to infer that the chemical reaction of nitrite with existing H_2S is a possible explanation for the consumption of nitrite in the nitrate anti-souring process. It would be interesting to determine the limiting condition between

the chemical reaction of nitrite with H_2S and further reduction of nitrite by NRB to other N-O compounds. This is however not within the scope of this work.

The fact that nitrate and nitrate behave differently in the presence of H_2S also suggest a possible reason for wide difference in the corrosion rates obtained from a nitrate treatment of chemically simulated souring condition in the laboratory and a test in which live bugs are used. Consideration would be given to this point while analysing test results in the course of this research work.

At the Hanford tank reservation, the tanks contain approximately 50 million gallons of liquid legacy radioactive waste from cold war weapons production, stored in 177 double-shelled carbon steel underground storage tanks. When the vitrification plant construction is finalised and the waste processing operations is eventually completed, the waste will be vitrified and the resulting waste glass logs disposed at the Yucca Mountain Repository. In the interim, storage tanks are used for storage. These tanks are maintained to ensure technical integrity is not compromised. Generally, all of the wastes tend to be highly alkaline in nature, typically with pH > 10 and hydroxide concentrations in excess of 6M. However, the waste chemistry tends to change over time due to various chemical reactions taking place inside the tanks. As a result, the chemistries for some of the waste tanks are no longer to specification with respect to corrosion (e.g., operational specification requires the pH to be maintained at a level greater than 13 whereas some of the tanks have their pH between 11 and 12). Hence, there is concern that tank integrity could potentially be compromised because of these changes in chemistry. Therefore, there is an urgent need to define mitigation procedures to ensure the integrity of the tanks is not compromised. One of such effort is the work of Gui and Co[65] to study the effect of complex mixture of nitrate, nitrite, organic compounds (e.g. acetate, oxalate, ethylene-di-amine-tetra-acetate and glycolate), hydroxide and chloride on the anodic behaviour of carbon steel tanks at the United States Department of Energy's Hanford nuclear waste reservation. The study evaluated the effect of pH, nitrite concentration, nitrite/nitrate concentration ratios, total organic carbon and the chloride concentration on the open circuit potential, pitting potential and repassivation

potential. Previous investigation showed that localised corrosion and stress corrosion cracking (SCC) were unlikely in the existing and expected composition of the waste however, since these wastes are a complex mixture of nitrate, nitrite, organic compounds, hydroxide, chloride, and other species, the influence of each of these on possible tank performance is unclear. When separately present in other systems, most of these constituents have been studied individually to address their effects on localised corrosion of various materials[66-69]. However, their effects on localised corrosion of carbon steel in a complex mixture of radioactive waste are still unknown. There had been previous work done on related issues on nuclear waste but they did not systematically address the effect of the constituents of the complex mixture on the localised corrosion of carbon steel[70, 71]. Hence, the objective of Gui and his co-authors was to determine the range of conditions where the tank steel is susceptible to localised corrosion and also provide insights to define possible corrosion mitigation strategies. They particularly studied the effects of pH, nitrite concentration, organic compounds (i.e., the total organic carbon level) on the electrochemical polarisation behaviour, characterised by open circuit potential, pitting potential and repassivation potential. Their findings indicate that adjusting pH is capable of returning the tank chemistry back to specification, but it did not significantly reduce the corrosivity of the stimulant[65].

For aqueous solutions, the typical cathodic reactions are oxygen reduction, hydrogen evolution, metal reduction or metal deposition as illustrated by the following reactions;

$$O_2 + 4H^+ + 4e^- \rightarrow 2H_2O \quad \text{(For acid solutions)}$$

$$O_2 + 2H_2O + 4e^- \rightarrow 4OH^- \quad \text{(For neutral or basic solutions)}$$

$$2H^+ + 2e^- \rightarrow H^{\uparrow}_{2(g)} \quad \text{(Hydrogen Evolution)}$$

$$M^{n+} + e^- \rightarrow M^{(n-1)+} \quad \text{(Metal ion reduction)}$$

$$M^{n+} + ne^- \rightarrow M_{(s)} \quad \text{(Metal Deposition)}$$

Where n is the oxidation number. Oxygen reduction is a very common cathodic reaction, since oxygen is present in the atmosphere and in solutions exposed to the atmosphere. Hydrogen evolution or hydrogen ion reduction is

the cathodic reaction that occurs during corrosion in acids. Metal ion reduction and metal deposition are not common but can cause severe corrosion problems in special situations. One particular case worth mentioning here is the plating of copper ions, produced upstream in a water circuit, on the internal aluminium surface of a radiator. The plated nodules, which may form even at very low concentrations of copper ions, tend to be dispersed and are thus good catalysts for the subsequent reduction of dissolved oxygen. A good example of metal reduction is the reduction of Fe^{3+} to Fe^{2+}. In neutral waters the anodic corrosion of some very reactive metals like aluminium, zinc, or magnesium, develops enough energy to split water directly as illustrated in the following reaction as the cathodic reaction;

$$2H_2O_{(l)} + 2e^- \rightarrow H^{\uparrow}_{2\,(g)} + 2OH^-$$

In cases where the solution is neutral or basic (such as the case of the nuclear waste tanks), oxygen reduction is expected to dominate the cathodic reaction. Using the Nernst equation, the half-cell reduction potential can be expressed as;

$$E_{red} = E^o_{red} - \frac{RT}{nF} In \frac{a_{red}}{a_{oxid}} \quad (2)$$

Where E_{red} is the half-cell reduction potential (v), E^o_{red} is the standard half-cell reduction potential (v), R is the universal gas constant (R = 8.314472 J K^{-1} mol^{-1}), T is the absolute temperature (K) i.e. T = T°C + 273.15, F is the Faraday constant, the number of coulombs per mole of electrons (F = 9.6485309 ×10^4 C mol^{-1}), n is the number of electrons transferred in the half-reaction, a is the chemical activity for the relevant species.

$a_x = \gamma[X]$ (3)

where γ is the activity coefficient of species X. However since activity coefficients tend to unity at low concentrations, activities in the Nernst equation are frequently replaced by simple concentrations.

At room temperature (25°C), (RT/F) may be treated like a constant and replaced by 0.025679V or 25.679mV. The Nernst equation is frequently expressed in terms of common logarithms rather than natural logarithms, in which case the Nernst equation is written, for a half-cell reduction at 25 °C as:

$$E = E^0 - \frac{0.0591}{n}\log_{10}\frac{a_{red}}{a_{oxid}} \quad (4)$$

Hence for the oxygen reduction in a neutral or basic solution, the activity of H_2O and pure gas is taken to be 1; the electrochemical half cell potential can be expressed as:

$$E = E^0 - 0.0591\log_{10}[OH^-] \quad (5)$$

Since

$$pOH = -\log_{10}[OH^-] \quad (6)$$

Then,

$$E = E^0 + 0.0591pOH \quad (7)$$

Given that the ionisation constant K_w for water is 10^{-14}, then:

$$pOH = 14 - pH \quad (8)$$

$$\therefore E = E^o + 0.8274 - 0.0591pH \quad (9)$$

Based on the relationship between the reduction potential and pH, it is generally expected that the open circuit potential will decrease with an increase of pH since the equilibrium potentials of the chemicals that have dominated cathodic reactions shift in the negative direction with an increase in pH. Thus, the open circuit potential will shift towards the negative direction according to mixed potential theory, assuming the pH shift did not have a significant impact on the anodic reaction. It is therefore not surprising that test result from the work of Gui and Co. shows that the open circuit potential (E_{ocp}) decreased with increase in pH from 7 to 13.5

In an environment with complex solution chemistry such as the nuclear waste tanks, high concentrations of nitrate and nitrite allow for other range of possible cathodic reactions involving nitrogen-containing species[72]. Possible cathodic reactions include reduction of nitrate to nitrite, reduction of nitrite to ammonia or nitrous oxide or nitrogen (I) oxide, which is commonly known as laughing gas.

$$NO_3^- + H_2O + 2e^- \rightarrow NO_2^- + 2OH^-$$

$$\boldsymbol{E_{red}\,(NO_3^-/NO_2^-) = E^0 - 0.0591pH + 0.0295log\frac{[NO_3^-]}{[NO_2^-]}} \quad (10)$$

$$NO_2^- + 5H_2O + 6e^- \rightarrow NH_3^{\uparrow} + 7OH^-$$

$$\boldsymbol{E_{red}\,(NO_2^-/NH_3) = E^0 - 0.069pH + 0.0098log[NO_2^-]} \quad (11)$$

$$2NO_2^- + 3H_2O + 4e^- \rightarrow N_2O + 6OH^-$$

$$E_{red}\,(NO_2^- / N_2O) = E^o - 0.0866\,pH + 0.0296\log[NO_2^-] \quad (12)$$

In equations 10, 11 and 12, the activity of NH_3 and the partial pressure of N_2O were assumed to be unity. Although the cathodic reactions in the tank were likely more complex than those illustrated above and might have several intermediary steps, these equations illustrate the possible cathodic reactions. The relationship of the reduction potential and pH for the three reactions are similar to that of oxygen reduction. Hence the expectation that the open circuit potential will decrease with an increase of pH still holds.

Comparing the reduction potential for the three possible nitrate reduction reactions listed above and the open circuit potential as a function of nitrite concentration shows that nitrite concentration has no significant effect on all three reduction potentials[73]. Test results from the work of Gui and Co. also show that the open circuit potential measured in the simulant solutions were more negative than any of the individual reversal potentials at any given nitrite concentration. This indicates there is the possibility that all the three reactions contributed to the cathodic reaction at open circuit potential. Therefore Gui and his co-authors concluded that, the role of nitrite might be pH buffer resulting from its reduction to either ammonia or nitrous oxide and thus reduced the corrosivity in the pits.

Although the authors did not perform direct measurement or confirmation of these reactions, these reactions do represent thermodynamically plausible reaction pathways that might explain the beneficial influence of nitrite. Their conclusion that nitrite concentration had no significant effect on all three reduction potentials is consistent with experimental results from this research work in section 4.2.1 which showed that nitrite concentration had no effect on the cathodic reactions.

Gui and his co-authors also observed that the pitting potential (E_{pit}) generally decreased with increasing pH whereas the repassivation potential decreased

from pH 7 to 9, then dramatically increased from pH 9 to 11 and again decreased as the pH was further increased from 11. From the standpoint of pit initiation, the most important parameter is the difference between the repassivation potential (E_{rp}) and the open circuit potential ($E_{rp} – E_{ocp}$), as well as the difference between the pitting potential (E_{pit}) and the repassivation potential (E_{rp}) i.e. ($E_{pit} – E_{rp}$). As a rule of thumb, ($E_{rp} – E_{ocp}$) > 200mV is taken as a good safety margin. This is extremely important since larger margins usually imply that the propensity and risk for localised corrosion is lower. The authors compared the potential difference between pitting potential and repassivation potential ($E_{pit} - E_{rp}$) and that of repassivation potential and open circuit potential ($E_{rp} – E_{ocp}$) as a function of pH. They clearly observed that, the differences were positive and relatively high for pH values above 10, indicating that pit initiation is relatively unlikely to occur above pH of 10. Not only were the differences high, they did not change significantly above pH 11 with further increases in pH. Hence the authors inferred that although the current chemistry was out of specification with respect to pH (pH 11 rather than pH 13 specified), from the perspective of pitting corrosion the environment of interest appears to have no significant difference on corrosivity to carbon steel at pH 11 to pH 13 or higher. Thus the authors concluded that, pH adjustment towards more alkaline conditions might not provide further benefits in terms of optimising operation conditions of the tanks. The authors also observed that the repassivation potential was extremely close to open circuit potential at pH 7, indicating that pit initiation is much more likely to occur at this pH in the nuclear waste tanks[73].

Gui and his colleagues also considered the effect of nitrite and the nitrite/nitrate ratio. Nitrite was found to be a potent inhibitor for carbon steel. A critical concentration of approximately 1.2M appeared to be beneficial to increase the difference of repassivation potential and open circuit potential considerably and thus prevent pitting corrosion from occurring[65], further increase in nitrite concentration above the critical concentration showed no further benefit. This result is consistent with Yang and Mcdonald's observation[74] and previous hypothesis that at fairly high concentrations, nitrite acts as a corrosion inhibitor for carbon steel. However, nitrite is also identified

as a dangerous inhibitor because it has the tendency to promote localised corrosion when insufficient amount is added to counter balance aggressive ions that are present. This effect is often seen in nitrite inhibited oxygenated cooling water when nitrate is slightly under dosed (i.e. less than the chloride level). Typically this system contains less than 200ppm chloride depending on the source of water however, if seawater is used, the chloride content is about 18000ppm and could even be a lot more if produced water is used. Their research clearly identified the critical nitrate concentration for carbon steel exposed to the nuclear waste stimulant as 1.2M. No extra benefit with respect to improving the pitting and repassivation potentials was gained with further increases in the nitrite concentration above 3.5M. This probably explains why most field applications that use nitrate injection to mitigate reservoir souring inject around to 80mg/l (1.16M) active sodium nitrate. Also their test results indicate the repassivation potentials were closer to the pitting potentials at higher nitrite concentrations. The smaller difference between E_{rp} and E_{pit} indicates better pitting corrosion resistance, which supports their claim that nitrite appears to be a potent inhibitor for carbon steel. The authors recommended further investigation to establish a link between the repassivation potential and the critical nitrite concentration. As part of the scope of this work, the critical concentration and relationship with the repassivation potential on CRA materials will be investigated.

The authors observed that pitting corrosion was less severe at higher nitrite concentration when specimen appearance was compared. Their observation is consistent with the school of thought that considers nitrite as a good inhibitor and that its protection mechanism is by the formation of a protective passive film. They also observed that the standard simulant contains 1.2M of nitrite and 3.7M of nitrate initially but in the endpoint solution, the nitrite increased to 2.3M while nitrate reduced to 2.4M. Therefore, the concentration ratio as well as the absolute concentrations of nitrite and nitrate was predicted to change with time. They were however not sure whether the positive movements in the pitting potential and the repassivation potential were function of the absolute nitrite concentration or the ratio of nitrite to nitrate. To investigate this, they performed CPP tests in AN107 solutions with different

nitrite/nitrate ratios as well as with approximately the same nitrite to nitrate ratio but with different absolute nitrite and nitrate concentrations. The changes of E_{ocp}, E_{pit} and E_{rp} at different nitrite/nitrate ratios are plotted. Surprisingly, the trend was very similar to the changes of E_{ocp}, E_{pit} and E_{rp} at different nitrite concentrations, except when the ratio was 0.5 because the solution at this nitrite/nitrate ratio also had a different nitrate concentration (1.5M). They considered this reasonable because for most tests shown, the nitrate concentration was maintained at 3.7M and thus nitrite concentration was the only variable. They plotted the change of E_{pit}, E_{rp} and E_{ocp} as a function of nitrite concentration when the ratio of nitrite to nitrate concentration was approximately one. They observed that when the nitrite concentration was increasing from 1.5M to 3.5M, the values of E_{rp} and E_{pit} remained relatively constant and no significant change in any of the three-electrochemical parameters. The authors therefore concluded that from a localised corrosion perspective, when the nitrate concentration is fixed, it is beneficial to increase the absolute nitrite concentration however when both nitrite and nitrate concentrations are variable, it could be beneficial to maintaining a ratio of nitrite to nitrate concentration above 0.5[73].

Gui and others also performed tests with different total organic carbon concentrations with and without nitrite to investigate whether the organic carbon compounds function as inhibitors just like nitrite. In the absence of nitrite, total organic carbon was found to be a minor inhibitor. The open circuit potential, pitting potential and repassivation potential increased slightly with increased total organic carbon concentrations but the magnitude of the change was very minor. The repassivation potential remained to be more negative than open circuit potential, indicating that pit initiation was possible. However, in the presence of nitrite, increase in the total organic carbon concentration had a mixed influence on localised corrosion. It had no significant effect on open circuit potential, but resulted in some increase in the pitting potential, which is considered beneficial. However, an increase in total organic carbon concentration also generally resulted in a decrease in the repassivation potential thereby moving the repassivation potential closer to the open circuit potential, which is detrimental for localised corrosion

resistance. According to F. Gui et al[73], "[the conclusion was that] *it may not be beneficial to include a high total organic carbon concentration and nitrite at the same time as these two might compete against each other and reduce the inhibition effect that can be obtained from either"*. This observation further supports the conclusion made by Rafaey[75], that at high concentrations some organic compounds could have detrimental effect to pitting corrosion even though they were relatively efficient inhibitors at low concentrations.

It is generally accepted that carbon steel will tend to be passive in alkaline environments; chloride is detrimental to passive materials and promotes pitting corrosion. Tests were performed to investigate the effect of chloride on the polarisation behaviour of carbon steel in AN107 solution. Test results showed that change in chloride concentration from 0.05M up to 0.2M had no significant impact on both the pitting potential and the repassivation potentials. This observation is not fully aligned with the general agreement that increase in chloride concentration would decrease the pitting potential but usually has no effect on repassivation potential[76].

Shademan and Co[6] conducted corrosion assessment of carbon steel and Sumitomo super 13Cr-110Ksi material during nitrate anti-souring reservoir treatment in laboratory conditions at Shell Global Solution in Houston, USA. In the course of their study, the effect of nitrite on the general corrosion rate of carbon steel and super 13Cr martensitic was investigated. Also preliminary work was done to test the susceptibility of super 13Cr martensitic to localised corrosion in the presence of nitrite. Weight loss test results for both carbon steel and super 13Cr martensitic in deaerated 15% NaCl solution with 20mg/l of $NaNO_2$ at 71^{o}C showed general corrosion rate of 0.3 - 0.4mpy for carbon steel and 0.1mpy for super 13Cr. C-ring autoclave test results for super 13Cr martensitic in deaerated 15% NaCl solution with nitrite concentration up to 100mg/l at 71^{o}C showed no cracking but pitting observed on the surfaces. Also cyclic Polarisation curve for 13Cr martensitic in the same environment without nitrite and with nitrite concentration up to 100mg/l both showed similar electrochemical behaviour for super 13Cr martensitic. The polarisation curves did not show any significant shift in the free corrosion potential as the nitrite concentration was increased from 0mg/l to 100mg/l. The curve showed noisy

passive current density, which is an indication of the semi protective nature of the passive film in that environment. The repassivation potential was below the free corrosion potential, which indicates that pitting is not likely to occur in this condition. To further investigate the effect of nitrite on super 13Cr martensitic, cathodic polarisation tests were performed in identical environment as the cyclic polarisation curves. Also the test result did not show any effect of nitrite on the current densities hence they concluded that nitrite is not an oxidiser, and has no effect on the general corrosion rate of carbon steel and super 13Cr martensitic.

Although super 13Cr was found to be susceptible to pitting, however its susceptibility to pitting does not increase with increase in nitrite concentrations up to 100mg/l nor was it susceptible to stress corrosion cracking in 20mg/l nitrite solution at 71^{o}C. The conclusion that nitrite has no effect on the general corrosion rate of carbon steel is contrary to conclusion from previous work. Their conclusion was rather premature. However, it is worth noting that the test was only conducted at nitrite concentration up to 100mg/I, test results from this work show unstable conditions for nitrite concentration within this range. This research work and some other studies have indicated that above a critical nitrite concentration, nitrite works as an anodic corrosion inhibitor.

Data obtained at Teddington for turned mild steel surface exposed to conductivity water flowing at 0.2m/s at 25^{o}C, showed that 10^{-5} M sodium nitrite is adequate for inhibition[77]. Also Pryor and Cohen investigated the adverse effect caused by insufficient quantity of anodic inhibitor. Their curves show the effect of sodium nitrite solution at inhibitor concentrations which indicates addition of an insufficient quantity actually increases the corrosion rate but that the corrosion rate drops suddenly when a critical concentration (normality of 10^{-5}) is passed[78]. They stated that corrosion rate depends mainly on the oxygen supply to the cathodic area. When the inhibitor is present in amount slightly less than the critical amount and a large part of the specimen is uninhibited, this area is available for the cathodic reaction, hence that the anodic attack will become more rapid because corrosion is concentrated on the small anodic area instead of being spread over large area (as in the absence of inhibitor), the intensity of corrosion (corrosion per unit area of the

part affected) is increased even more than the total corrosion[79]. This explanation is in agreement with Mayne and Menter's explanation that even if no point peculiarly favourable to the cathodic reaction exists, covering a part of the surface reduces the area available for the cathodic reaction hence a given current represents a greater current density and an increased polarisation which invariably leads to intensified corrosion attack on the uninhibited area[80, 81]. The intensification of corrosion attack after insufficient addition of inhibitor had been shown in the Cambridge researches of 1925 and 1927. Some of Mears' measurements in 1935 had indicated that in certain cases even the corrosion rate can be increased[82]. The Pryor-Cohen curves showed that the increase in total corrosion is a common phenomenon that is anticipated. However the situation was more severe than anticipated due to the fact that the attack which started upon a single area continues there in preference to other areas thereby causing rapid penetration into the metal. For example, a blister formed over the site of attack, prevents the inhibitor from getting to the place where it is needed to stop the corrosion. To avoid this phenomenon, an inhibitor that does not produce corrosion product in form of membrane must be selected. It is therefore very important to understand the inhibition mechanism of nitrite.

Anodic inhibitors usually produce thin invisible films on the surface of the metal. Under slightly alkaline and sometimes neutral condition, it is reasonable to expect more soluble oxidising agents to be effective if the inhibitive power of oxygen when stirred is due to replenishment of oxygen at sensitive spots. Nitrite is an oxidising agent much used as a corrosion inhibitor however, it seems fairly certain that the inhibitive properties of nitrite are not directly dependent on its oxidising power. As shown by Robertson, molybdates and tungstates act as inhibitors[83], but as shown by Pryor and Cohen, air must be present[78]. Nitrite inhibits whether or not air is present but the concentration of nitrite required for inhibition is lowered if oxygen is present[79]. This key information emphasises the influence of oxygen on the critical concentration required for inhibition. The influence of oxygen will be further explored in the course of this research work. Sherwood also stated that nitrites can prevent corrosion even when chlorides are present, provided

sufficient amount is added, the amount required increases with the chloride content[84]. When insufficient amount is added, pitting occurs.

Nitrites although sometimes regarded as reducing agents especially at low concentration possess oxidizing properties and tend to render iron passive thereby stopping corrosion in weakly alkaline solution. According to Evans[85], *"nitrite is considered to act like chromates, converting any ferrous salts formed at susceptible points to ferric hydroxide at the place of origin so that the attack is stifled"*. In this condition, nitrite promotes anodic polarisation, which facilitates the formation of protective films and causes the metal to assume a passive state. Upon onset of the passive state (the initial anode process) the passive film formed retards oxidation of the metal into the ionic condition; hence the anode potential becomes more positive. The potential shift for iron electrode may exceed 1V[86].

According to work done by Brossia et al[87] on the inhibition of stress corrosion cracking of carbon steel storage tanks at Hanford, it was reported that nitrite is a very effective inhibitor of SCC in nitrate-based waste simulants. Subsequent work done by Brossia and some other people confirmed that the nitrite/nitrate concentration ratio and applied potential have pronounced influence on SCC susceptibility[88]. Experimental data from their work shows that SCC susceptibility is strongly dependent on potential. In a carbon steel system, at potentials below -50mV (SCE), SCC was only observed in solutions with no nitrate. Also SCC could be eliminated at potentials higher than -50 mV (SCE) provided sufficient amount of nitrite was present. The nitrite/nitrate ratio required to eliminate SCC increased as the potential increased. It was found that at any given potential, SCC can be mitigated by increasing the nitrite/nitrate ratio. It was also identified that at a constant nitrite/nitrate ratio the susceptibility for SCC decreases with decreasing potential. As the nitrite/nitrate ratio increases, the difference between open circuit potential and the cracking potential widens thereby decreasing the risk for SCC. This is particularly the case since the open circuit potential has been observed to also decrease with decreasing nitrite/nitrate ratios[89]. This is not surprising, general believe is that crack initiation typically occurs at pits or other metal defects. From CPP tests performed in the course of this research work, it was

evident that the nitrite concentration and the applied potential substantially influenced pitting corrosion which invariably influences the susceptibility of the material to SCC.

Crack inhibition in carbon steel exposed to nitrite systems was also observed by Ondrejcin[90] and others[91- 93] but the magnitude of nitrite inhibition was not noted in their work nor was there any discussion on the possible nitrite inhibition mechanism. The mechanism by which nitrite inhibits SCC in carbon steel is still unknown. However, under the investigated conditions, nitrite could reduce to either nitrous oxide also known as "laughing gas" or ammonia according to the following reactions:

$$2NO_2^- + 3H_2O + 4e^- \rightarrow N_2O + 6OH^-$$

$$NO_2^- + 5H_2O + 6e^- \rightarrow NH_3 + 7OH^-$$

These reactions result in the production of hydroxide which increases the pH of the solution thereby providing additional buffering capacity at the crack tip and possibly promoting passivity or repassivation. This might have more significant effect on CRA than carbon steel.

However, the nitrate-based waste simulants used by Brossia and his co authors also contained significant concentrations of aluminate (> 0.2M) which was found to be a weak inhibitor with respect to localised corrosion[89]. In the absence of aluminate, the estimated crack growth rate was approximately twice that observed in the presence of aluminate. This seems to demonstrate that aluminate was beneficial to the crack growth reduction in the test environments. However, contrary to what was observed by Brossia, report from the alumina process industry states that aluminate has the tendency to increase the susceptibility of materials to SCC because the passive film formed in the presence of aluminate is easy to crack under stress[94, 95].

According to Brossia et al[87], "*this may suggest that the passive film formed in the simulant is different from that in the caustic aluminate solution in the process industry and aluminate in the simulant does provide some inhibition for both localised corrosion and SCC".*

Based on literature search performed, the chemistry of nitrite and /or nitrate was better understood. Also the effect of nitrite/nitrate on the susceptibility of

carbon steel to SCC was better understood. Hence the focus of this research work would be to validate some of the findings and further investigate the effect of nitrite on CRA as contribution to knowledge since most of the work done to date was on carbon steel. The main difference between carbon steel and CRA is the ability to form a passive protective layer on CRA. Hence the failure mechanism is typically the breakdown of the passive layer followed by localised corrosion in the area where there was passive film breakdown whereas; carbon steel typically suffers from general metal loss. It could be inferred from Brossia's paper that nature of passive film formed by nitrite has a major effect on its susceptibility to SCC. Therefore, to effectively study the effect of nitrite on CRA, it is of paramount importance to acquire better understanding of the effect of nitrite on passivity, kinetics of passivation on CRA and the mechanism of passivity breakdown in the presence of nitrite/nitrate.

2.3 Passivity of Metals

The phenomenon of metallic passivity has always fascinated engineers and scientists. There are several arguments as to when metals were first used by mankind, it is likely that some native metals; that were found in nature in their metallic form, such as copper, silver, and gold were used several tens of thousands of years before human history was recorded. Much later, human learned to smelt ores and formulate alloys (the "Bronze Age", 4000 to 2000 BC), including the smelting of iron (the "iron age", starting more than 2000 years ago) resulting in unprecedented technological transformation of the society. The mastering of iron and steel production resulted in the development of machines, which in turn led to the industrial revolution. Later, more highly reactive metals that possess particular properties (e.g. low densities), principally aluminium, magnesium, titanium and zirconium, were obtained using electrochemical methods. These metals and their alloys ushered in technologies and systems as diverse as high performance aircrafts and nuclear power.

According to Macdonald[96], "*along with fire, the wheel, and the derivation of language, the development of metals and alloys has been a cornerstone in the evolution of the human experience. Mankind has been able to develop a*

metals-based civilization primarily because the reactive metals (Fe, Ni, Cr, Al, Ti, Zr, Pb, Mg, U, W, etc.) which react spontaneously with oxygen or water under terrestrial environmental conditions, exhibit extraordinary kinetic stabilities in oxide form. In nature, the reactive metals occurred in oxidized form and must have been recovered by reduction".

Reactive metals are used in many applications because of the formation of thin reaction product layers (`passive films') on the surface that effectively protect the underlying metal from the corrosive environment. In 1790, Keir tried to define the phenomenon of 'passivity' however because of the complex nature and specific conditions under which passivity occurs, it was difficult for him to properly define the phenomenon. Passivity is best defined as the ability for an actively corroding metal to essentially becoming inert due to loss of chemical reactivity by certain metals and alloys under particular conditions. 40 years later, Schonbein and Faraday extensively explored the phenomenon of passivity. Schonbein apparently coined the word 'passivity', but it was Faraday who brought the phenomenon to the forefront of electrochemistry[97] on the basis of his famous iron-in-nitric acid experiment, in which iron was found to be immune from attack in concentrated nitric acid but not in dilute nitric. This observation was not fully understood until the development of the electrochemical thermodynamic diagrams by Pourbaix in the 1960s[98] and it is still misinterpreted by many people. From the time of Schonbein and Faraday (1830s), the reason for the stability of iron in concentrated nitric acid has been attributed to the existence of a thin film on the metal (or alloy) surface that effectively isolates the metal from the corrosive environment.

The phenomenon of passivity is best illustrated, in modern form, using the potential-current polarisation curve of a metal such as iron in phosphoric acid/phosphate buffer solutions as shown in Figure 4. Upon increasing the potential (i.e. oxidising power) in the positive direction from the open circuit potential, the current (corrosion rate) at first increased more-or-less exponentially in the 'active' region, where the predominant reaction is metal dissolution hence slight increase in the oxidising power of the solution caused a rapid increase in the corrosion rate. At a sufficiently high potential, after passing through a maximum current, at the active-passive transition, further

increase in the oxidising power, led to sudden decrease in corrosion rate, the corrosion rate decreased to a plateau that defines the passive state.

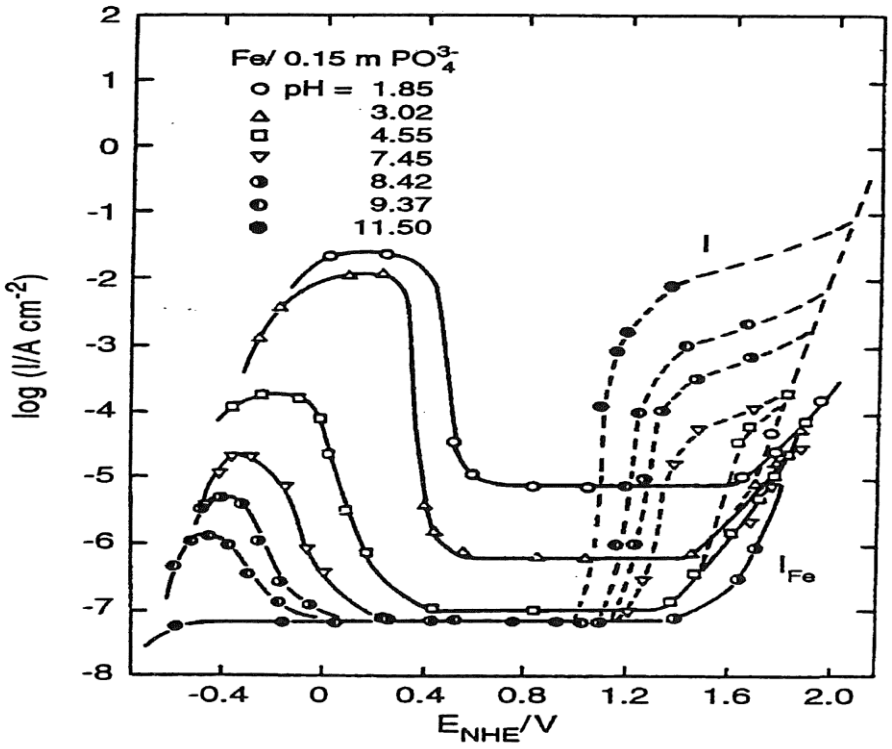

Figure 4: Anodic polarisation curves for iron in 0.15M Na_3PO_4/NaOH solutions of different pH values showing the dissolution current, I_{Fe} (solid curves) and the total current, I (dashed curves) after 1h in the steady state[99]

During the transition from the active to the passive region, a 10^3 to 10^6 reduction in corrosion rate is usually observed[100]. The precise cause for the unusual active-passive-transpassive transition is not completely understood. It is a special case of activation polarisation due to the formation of a surface film or protective barrier that is stable over a considerable range of oxidising power and is eventually destroyed in strong oxidising solutions. Hence metals that exhibit active-passive transition become passive or very corrosion resistant in moderate/strong oxidising environments however, under extremely strong oxidising conditions, these metals or alloys lose their corrosion resistance. For iron in phosphoric acid/phosphate buffer solutions, the passive state exists over a voltage range of about 1V, which may be compared with the voltage range of 1.23V for the thermodynamic stability of water (P_{H_2} = P_{O_2} = 1atm) at 25°C[100]. In the passive region, further increase in

the oxidising power produces little or no change in the corrosion rate until the transition from passive to transpassive region is reached, at which point, further increase in the oxidising power, increases the corrosion rate due to oxygen evolution. Experimental data reveals that oxygen evolution becomes increasingly prevalent at lower voltages as the pH increases. This effect primarily reflects the shift in the equilibrium potential for the oxygen electrode reaction.

It is worth noting that the dissolution current remains constant well into the oxygen evolution region, but it ultimately increases at a sufficiently high potential. There are several arguments on the mechanism of transpassive 'dissolution', one school of thought states that it is due to breakdown of the passive film over extended regions of the surface, rather than at localised points as in the case of pitting[101]. Breakdown of the passive film is expected to occur when cation ejection from the barrier layer involves a change in the oxidation state of the ion for example;

$$Fe^{2+} \rightarrow Fe^{3+} + V_{Fe} + e^{-}$$

Thereby generating cation vacancies (V_{Fe}) in a charge transfer process. If the potential is sufficiently high, the rate of generation of cation vacancies at the barrier layer/outer layer interface, and hence the flux of cation vacancies across the barrier layer, becomes insensitive to local structural variations. Under these circumstances, cation vacancy condensation will occur over extended regions. Regardless of the exact mechanism, transpassive dissolution marks the upper boundary of the passive state.

As stated by Macdonald[96], 'the nature of passivity and the structure of passive layer have been subjects of intense curiosity for almost two centuries. However, it was not until the development of scanning electron microscopy (SEM), transmission electron microscopy (TEM), and in situ techniques, such as ellipsometry and more recently Scanning Tunnelling Microscopy (STM) and Atomic Force Microscopy (AFM), that researchers have been able to construct physical/morphological models".

Figure 5 shows the schematic of processes that led to the formation of bilayer passive films on metal surface. The general picture that has emerged is that

the passive film forms as a bilayer structure comprising a defective oxide layer (the 'primary' passive film) that forms directly from the metal and a precipitated outer layer that forms via the hydrolysis of cations ejected from the inner layer. Solution phase species may be incorporated in the outer layer, but not in the inner layer, whereas alloying elements from the substrate alloy may be incorporated into both layers.

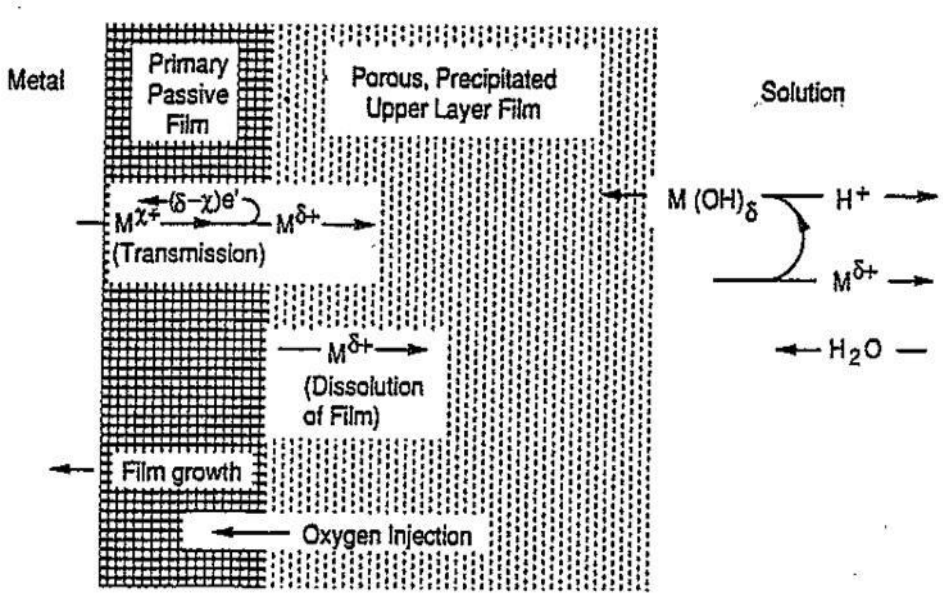

Figure 5: Schematic of processes that lead to the formation of bilayer passive films on metal surface[96]

For systems were the outer layers do not form, or where the outer layer presents little impediment to transport of species to the barrier layer/outer layer interface, the specific impedance in the absence of redox couples is very high (e.g. ~10^6 - $10^7 \Omega$ cm^2 for NiO on Ni) but in the presence of a redox couple [e.g. $Fe(CN)_6^{3-/4-}$] the impedance is often low[101]. This demonstrates that the barrier layer may be good electronic conductor but generally it is a poor ionic conductor.

In 1836 before the concept of pH, Faraday reported the outcome of his iron-in-nitric acid experiment stating that iron freely corrodes in dilute nitric acid with the evolution of a gas (hydrogen). However, in concentrated nitric acid, apparently no reaction occurred, in spite of the greater acidity of the medium[97, 102]. However, if the iron surface was scratched in situ, a burst of corrosion activity occurred along the scratch, but then quickly died away. Hence, Faraday correctly surmised that the surface had become 'oxidized',

however, the oxide film was too thin (order of a few nanometres) to be detected by the naked eye (thicker films would have produced interference patterns, the physics of which were more or less known since the time of Newton and Huygens). Faraday was however unable to answer the intriguing question as to why the surface became 'passive' in concentrated nitric acid (which is a more aggressive environment), contrary to the expectations at the time of the experiment. The answer to this paradox did not evolve until the 1960s when electrochemistry underwent a profound transformation with the introduction of potential-pH diagrams by Marcel Pourbaix[98].

In Pourbaix atlas of electrochemical equilibria, he summarized the electrochemical thermodynamic behaviours of most of the elements in the periodic table. Figure 6 Show the schematic Pourbaix diagram for the iron-water system which illustrates the resolution of Faraday's paradox.

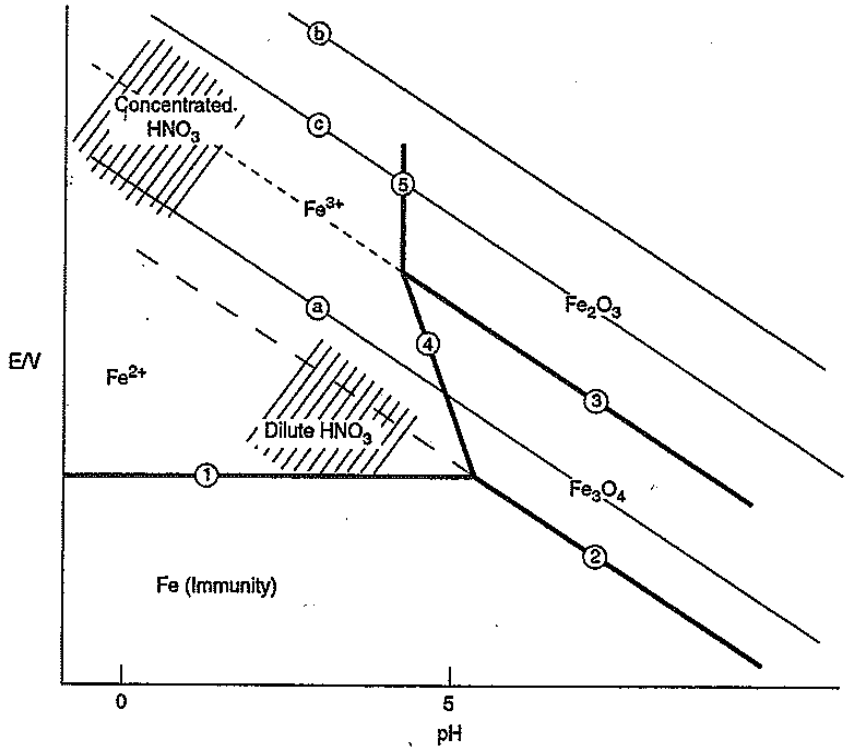

Lines (a), (b), and (c) correspond to the following eqilibria:

$H^+ + e^- \leftrightharpoons \frac{1}{2}H_2$ (a)

$O_2 + 4H^+ + 4e^- \leftrightharpoons 2H_2O$ (b)

$NO_3^- + 3H^+ + 2e^- \leftrightharpoons HNO_2 + H_2O$ (c)

Figure 6: Schematic Pourbaix diagram for iron illustrating the resolution of the Faraday paradox in the corrosion of iron in nitric acid[96]

Pourbaix noted that for spontaneity, the second law of thermodynamics requires that

$(E-E^o)\ I \geq 0$ (13)

where E is the potential, E^o is the equilibrium potential and I is the cell current. For oxidation reaction the current, I, is defined as being positive while for reduction reaction it is defined as being negative. The corrosion potential must satisfy the relationship $E_a^o < E_{cor} < E_c^o$ where E_a^o and E_c^o are the equilibrium potentials for the partial anodic and cathodic reactions, respectively. Hence, iron in deaerated acid solution, the partial anodic reaction is oxidation of iron as represented in line 1 of Figure 6 by the following reaction:

$$Fe \rightarrow Fe^{2+} + 2e^-$$

While the cathodic reaction is hydrogen evolution represented by line a, will adopt a corrosion potential that lies between lines 1 and a, with the value of E_{cor} being determined by the relative values of the kinetic parameters of the two partial processes. In oxygenated (aerated) solutions, E_{cor} will possibly be between lines 1 and b, because oxygen reduction is the likely cathodic reaction. In the days of Faraday, Pourbaix diagrams did not exist neither were there reference electrodes nor high impedance voltmeter hence he could not have known where on Pourbaix diagram for iron the corrosion potentials for iron in dilute nitric acid and in concentrated nitric acid would be.

However, based on collective knowledge and experience in electrochemistry over the years, it is possible to speculate the potential-pH that existed in Faradays experiment. Dilute nitric acid is a weak oxidising agent, so the principal cathodic reaction was most likely hydrogen evolution hence the corrosion potential is expected to lie between Lines 1 and a at relatively high pH, as indicated in Figure 6. On the other hand, concentrated nitric acid is a strong oxidising agent, so the principal cathodic reaction was most likely nitrate reduction to nitrite as indicated by equilibrium for line c. Hence at low pH, the corrosion potential, E_{cor}, could be anywhere between Lines 1 and c. Oxidation reaction of iron (Fe/Fe^{2+}) is relatively fast compared with hydrogen reduction (hydrogen evolution) on iron, this results in a mixed potential. Hence, the corrosion potential is expected to be below the extension of line 2 (Fe/Fe_3O_4) into the Fe^{2+} stability region, but, of course, above line 1, in the

case of dilute HNO_3. Under these conditions, Fe_3O_4 cannot form on the surface, even as a metastable phase. Iron is very active and will freely corrode in this medium. However, in the case of concentrated HNO_3, nitrate reduction to nitrite is likely to be fast due to the high concentration of NO_3^- hence the corrosion potential will be high and certainly more positive than the extension of line 2 (Fe/Fe_3O_4) into the stability region for Fe^{2+} at low pH. Therefore, Fe_3O_4 can form as a metastable phase, thus giving rise to passivity, giving the rationale behind kinetic inactivity of iron observed by Faraday in his experiment.

Removal of the film by scratching leads to drop of the local potential due to dissolution of iron, thereby rendering hydrogen evolution a viable cathodic reaction. However, depletion of H^+ at the scratched site would eventually cause the potential to shift in the positive direction and lead to the reformation of Fe_3O_4 as a metastable, passive film. If the potential becomes sufficiently positive, it may even be above the extension of line 3 (Fe_3O_4/Fe_2O_3). In this scenario, Fe_2O_3 may form on Fe_3O_4 as an additional metastable phase, resulting in the bilayer structure that is commonly observed[100]. However, because Fe_3O_4 is metastable (in the case of concentrated HNO_3), its existence on the surface depends upon a balance between the rate of formation and the rate of removal. If one or both of these processes depends upon the thickness of the Fe_3O_4 layer, then a steady state in the thickness (and in the current) will be observed.

Although thermodynamics alone is sufficient to resolve Faraday's paradox, a satisfactory theory of the passive state requires a detailed description of the kinetics of growth of the passive film and in particular of the processes that occur at the metal/film and film/solution interfaces. Although the passive oxide films greatly reduce the dissolution rate of metals, they do not completely protect the surfaces from corrosion. In particular, passive surfaces are susceptible to various forms of localised corrosion, including pitting corrosion, stress corrosion cracking, corrosion fatigue, and crevice corrosion. The occurrence of any of these phenomena requires the initial breakdown of passivity, in which the barrier layer is ruptured and the underlying metal is exposed to the aggressive environment. Ideally, breakdown in passive film is

repaired through a self healing progress. However, in the event that the breakdown of the passive film survives, propagation requires continued separation of the anode and the cathode, such that an aggressive environment is maintained within the developing crevice. This implies that the crevice may repassivate if separation of the anode and the cathode cannot be maintained, or the underlying mechanism is interrupted by changes in the external environment. The probability of survival of the broken passive film is determined by the kinetics of repassivation, which depends on the chemical composition of the environment, the nature of the breakdown sites, and the electrochemical properties of the system. For type 304 stainless steel in chloride-containing solution, the probability of survival is about one in one hundred to ten thousand[103].

Two fundamentally different repassivation phenomena have been identified. The first one is the 'Prompt' repassivation of the post breakdown event, in which case the nucleus fails to achieve the threshold conditions necessary for survival[103-105] while the second is the 'delayed' repassivation, in which case competition for the limited resources on the external surfaces (e.g. oxygen reduction) allows only the fittest pits to survive.

2.4 Passivity Breakdown

Passivity breakdown is a dynamic phenomenon, in which transient breakdown/repassivation events occur over the large population of potential breakdown sites that exist on a real surface (metastable pitting). The statistical characteristics are quasi-Poissonian, leading many to conclude that passivity breakdown is a stochastic (random) process[103-105]. However, certain sites on a surface are more prone to breakdown than others. Passivity breakdown is fundamentally a deterministic process, with the outcome of the breakdown being predictable on the basis of known physical laws. Numerous theories and models have been proposed for passivity breakdown. One of the earliest models for the growth of passive films was by Cabrera and Mott[106]. Their model assumed the following:

i. Film grows by the transport of cations across the film to the film/solution interface where they react with electrolyte,

ii. Strength of the electric field is constant throughout the film and is equal to Φ_f/L, where Φ_f is the total potential drop across the film and L is the film thickness Penetration of cations through the film is assisted by high electric field,

iii. The rate limiting step for the growth of passive film is the emission of metal cations from the metal into the film.

In the energy-distance diagram shown in Figure 7, the energy barrier for the initial entry of cations into the film is greater than that for subsequent movement through the film.

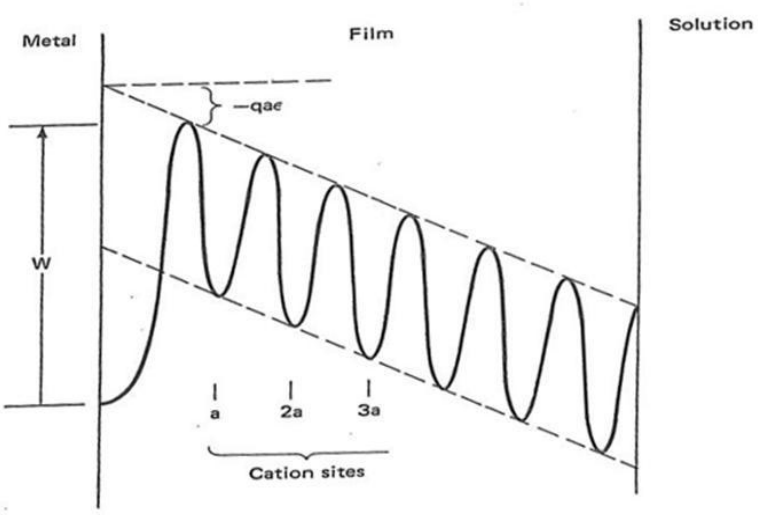

Figure 7: Potential energy diagram for the movement of cation through an oxide film assuming that cation injection from the metal is rate-limiting[99]

Based on the assumptions given above, Cabrera and Mott gave the following expression for the differential film growth rate[106]:

$$\frac{dL}{dt} = N\Omega v \, exp\left[\left(-w + \frac{qa\emptyset_f}{2L}\right)/KT\right] \quad (14)$$

Where N is the number of mobile cations per unit surface area, Ω is the molecular volume per cation, v is the vibrational frequency, w is the activation energy for the entry of cations into the film, q is the charge on the cation, a is the jump distance, and KT is the thermal energy. Integrating equation 14 yields an inverse logarithmic rate law:

$$\frac{1}{L} = C - DIn\, t \quad (15)$$

Where,

$$\boldsymbol{C} = \frac{\mathbf{2}}{\boldsymbol{qa\emptyset_f}}\left\{\boldsymbol{w} - \boldsymbol{KT\ In}\left[\frac{\mathbf{2}(\boldsymbol{w}-\mathbf{39}\boldsymbol{KT})^{\mathbf{2}}\boldsymbol{N\Omega v}}{\boldsymbol{\emptyset_f qaKT}}\right]\right\} \quad (16)$$

and

$$\boldsymbol{D} = \frac{\boldsymbol{2KT}}{\boldsymbol{qa\emptyset_f}} \quad (17)$$

The Cabrera-Mott model has been extensively applied to interpret the growth of oxide films on metal surfaces but the model tends to yield unrealistic values for the jump distance, a. Contrary to the assumptions of Cabrera and Mott, later discovery indicates passive films tend to grow via the movement of anions through the film to the metal-film interface, where they react with the metal.

In 1970, Fehlner and Mott[107] worked together to modify the original model. They made the following new assumptions:

i. Diffusion is responsible for film growth,
ii. The rate limiting step is the emission of an anion from the environment into the film at the film/solution interface, and
iii. The activation energy for the rate limiting step increases with thickness and can be expressed as follows;

$$w = w^o + \mu L \quad (18)$$

Based on their assumptions, the differential rate law was expressed as[107]:

$$\frac{\boldsymbol{dL}}{\boldsymbol{dt}} = \boldsymbol{N\Omega v\ exp}\left[\left(-\boldsymbol{W^o} - \boldsymbol{\mu L} + \frac{\boldsymbol{qa\emptyset_f}}{\boldsymbol{2L}}\right)/\boldsymbol{KT}\right] \quad (19)$$

Integrating equation 19 yields the logarithmic growth rate law given as:

$$\boldsymbol{L} = \frac{\boldsymbol{KT}}{\boldsymbol{\mu}}\left\{\left[\boldsymbol{In}\left(\frac{\boldsymbol{\mu}}{\boldsymbol{KT}}\right) + \boldsymbol{In}(\boldsymbol{N\Omega v}) - \frac{\boldsymbol{w^o}}{\boldsymbol{KT}} + \frac{\boldsymbol{qa\varepsilon}}{\boldsymbol{2KT}}\right] + \boldsymbol{In}(\boldsymbol{t} + \boldsymbol{t^o})\right\} \quad (20)$$

where

$$\boldsymbol{\varepsilon} = \frac{\boldsymbol{\emptyset_f}}{\boldsymbol{L}} \quad (21)$$

However, the main objection to this model is the fact that experimental evidence indicate that the interfacial reaction given below is fast (i.e. equilibrium is established rapidly) hence emission of an anion from the environment into the film is unlikely to be the rate determining step contrary to the assumption made by Fehlner and Mott[107].

$$O_{(oxide)} + 2H^+ + 2e^- \leftrightharpoons H_2O$$

Based on experimental work on the growth of passive films on iron in borate buffer solutions by Sato and Cohen[108], the place exchange mechanism illustrated in Figure 8 was proposed to explain the empirical rate law:

$$\boldsymbol{i = K' \exp\left(mV_{app} - Q_t/n\right)} \quad (22)$$

where i is the current, V_{app} is the applied voltage, Q_t is the accumulated charge (proportional to L), K', m, and n are constants.

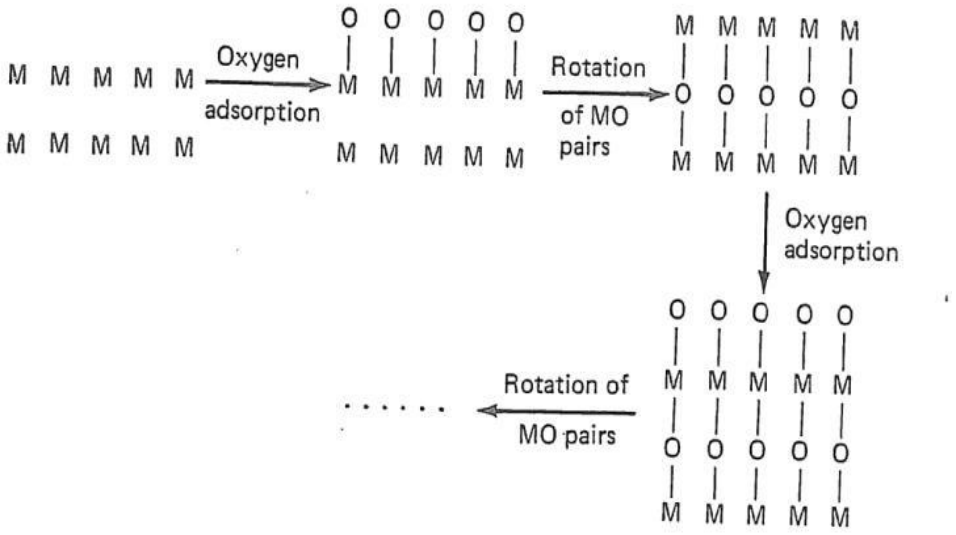

Figure 8: Schematic diagram of place exchange mechanism for the growth of oxide films on metal surface[99]

Under potentiostatic conditions, Sato and Notoya integrated equation 22 to yield a logarithmic law expressed given as[109]:

$$L = A + B \ln(t + t_o) \quad (23)$$

where A and B are functions of various fundamental parameters given by as:

$$\boldsymbol{A = \frac{l_v RT}{w_o}\left[In\frac{w_o \beta T}{l_v RT} + \frac{\sigma}{T}\right] + \frac{l_v F V_{app}}{2w_o}} \quad (24)$$

and

$$\boldsymbol{B = \frac{l_v RT}{w_o}} \quad (25)$$

This model requires the cooperative rotation of MO pairs, probability of this happening reduces as the film thickness increases. Fromhold[110] developed the model further and argued that the place exchange mechanism is viable even for relatively thick films. Out of all the numerous models that were proposed for passivity breakdown, only three of them systematically yield

analytical relationships between measurable parameters and various independent variables that can be tested experimentally[101]. Lei et al[111] and Milosev et al[112] evaluated various theories and models and concluded that only the PDM is consistent with the experimental data for the systems investigated.

The Point Defect Model (PDM) was initially developed by Lin, Chao, and Macdonald[113] in 1981 and later modified by Ellerbrock and Macdonald[114]. The Halide Nucleus Model (HNM) by Okada[115] provides analytical expressions for the critical breakdown potential (V_c) and induction time for passivity (t_{ind}) while the PDM accounts for the distributions in V_c and t_{ind}, for alloying effects, photo-inhibition of passivity breakdown, and the evolution of localised corrosion damage[101]. The basis of the PDM is that films are considered to be highly defective structures with the principal defect being cation vacancies ($V_M^{X'}$), anion vacancies ($V_O^{\bullet\bullet}$), electrons (e^-), and holes (h^o). The various reactions involving these species at the metal/film and film/solution interfaces are assumed to be in quasi-equilibrium as shown in Figure 9.

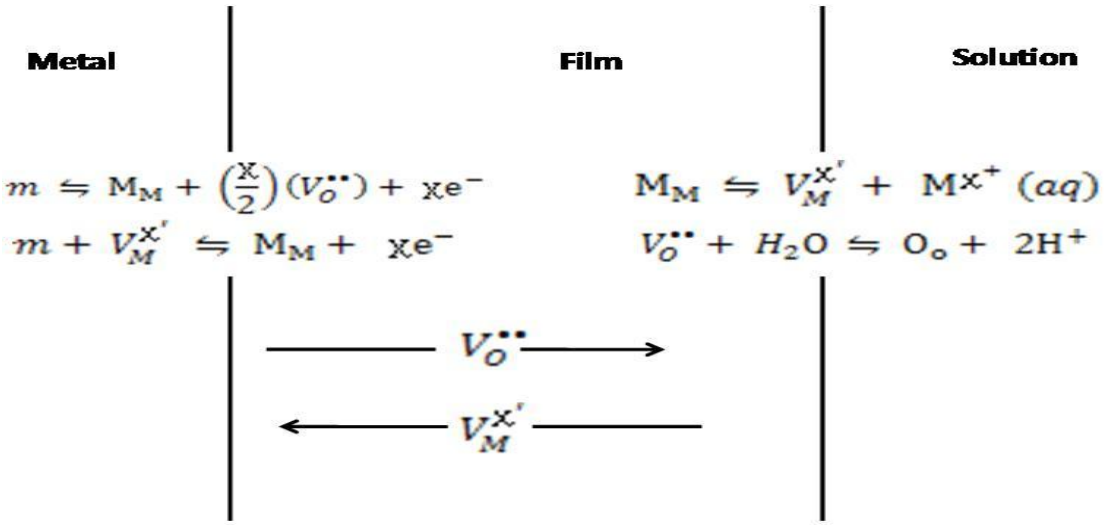

Figure 9: Processes assumed to occur during the anodic growth of passive films according to PDM. M = metal atom, M_M = metal cation site and O_o = oxygen ion in anion site, $V_M^{x'}$ = cation vacancy and $V_O^{\bullet\bullet}$ = anion vacancy[99]

As such during film growth, anion vacancies are created at the metal/film and consumed at the film/solution interfaces. On the other hand, cation vacancies are created at the film/solution interface and consumed at the metal/film

interface. The net effect of the movement of anion vacancies from the metal/film interface to the film/solution interface (or anions in the reversed direction) is film growth (square brackets).

$$\frac{2}{\mathrm{X}}m + H_2O \rightarrow \left[\frac{2}{\mathrm{X}}M_M + O_O\right] + 2H^+ + 2e^-$$

Whereas movement of cations from the film/solution interface inwards towards the metal only leads to metal dissolution:

$$m \rightarrow M^{\mathrm{X}^+}(aq) + \mathrm{X}e^-$$

Thus, it was concluded that film growth occurs inwards into the metal phase via movement of anions through the film. The PDM postulates that passivity breakdown occurs as a result of cation vacancy condensation at the metal/barrier layer interface at sites in the passive film that are characterised by high cation vacancy fluxes, due to the aggressive anion induced, autocatalytic generation of cation vacancies at the barrier layer/solution interface. The excess vacancies then condense to form a two -dimensional vacancy condensate beneath the “weak points” in the barrier layer that are characterised by high cation vacancy diffusivity. Vacancy condensation effectively causes local separation between the barrier layer and the metal. These sites correspond to regions of structural discontinuity, such as (but not limited to) ghost grain boundaries, emergent dislocations, and the points of intersection between the barrier layer and precipitates (e.g. Al_2Cu in Al), inclusions (e.g. MnS in stainless steels), and other second phase particles[96].

The essential concept is that, if the enhanced flux of cation vacancies that occurs across the barrier layers is such that the vacancies cannot be annihilated, the excess vacancies condense at the periphery of an expanding condensate. This results in separation of the barrier layer from the metal which prevents further penetration of the film above the condensate into the substrate. However, at those regions beyond the condensate, where the barrier layer is still attached to the metal, the film continues to grow into the substrate. Simultaneously, dissolution of the barrier layer at the barrier layer/outer layer interface results in the thinning of the cap over the expanding condensate, with the greatest extent of thinning occurring at the point at which vacancy condensation first occurred because of the longest time since

separation. Thinning of this type at precursor sites to pitting on stainless steels has been observed using microellipsometry[116]. Eventually, the cap over the condensate becomes so thin that it will fracture under the growth stresses that exist in the film, leading to penetration of electrolyte into the cavity (condensate) which marks the initiation of a micropit. The nucleus either promptly repassivates, due to failure to establish a differential aeration cell (DAC), marking a metastable event, or establish a viable DAC resulting in the growth of a macroscopic pit. Establishing differential aeration cell is determined by the ability of the micropit to achieve a critical size (or more correctly, a critical value of i/r, where i is the current density and r is the radius of the semi-spherical nucleus[103-105]). Failure to achieve these conditions, which are critically dependent upon the existence of the cap, at least in the early stages[103, 117], is postulated to result in the passivation of the nucleus.

The survival probability (SP) of a stable pit is defined as:

$$\boldsymbol{SP} = \frac{\mathbf{1}}{(\mathbf{1}+\boldsymbol{N})} \tag{26}$$

where N is the number of metastable events that occur before the formation of a stable pit. The value of SP is typically within the range of 10^{-2} to 10^{-5}, depending upon the material and the environmental conditions[43].

As a result of closer examination of experimental data that were not available when the original PDM was synthesized[96, 113], Macdonald and Yang modified the mechanistic picture stating that vacancy condensation is possible on either the cation sub-lattice of the film or on the metal lattice at the interface, with the two locations being related through the reaction;

$$m + V_M^{\mathrm{X}\prime} \overset{k_1}{\rightarrow} M_M + v_m + \mathrm{X}^{e\prime}$$

where $V_M^{\mathrm{X}\prime}$ is a vacancy on the cation sub-lattice of the barrier layer at the film side of the barrier layer/metal interface and v_m is a vacancy on the metal lattice on the metal side of that same interface. Other processes that generate v_m must also be considered. The process of vacancy annihilation/ condensation at the metal/barrier layer interface has not received in-depth examination. Suffice it to state at this point that annihilation of the vacancy on the metal lattice can occur via a number of processes, including diffusion to a

free interface (or grain boundary) and dislocation climb. In any event, the two-dimensional vacancy condensate continues to grow via vacancy condensation at the periphery. Due to the fact that the film continues to dissolve at the barrier layer/solution interface, the cap over the condensate gradually thins and, at some point, rupture occurs, thereby marking a breakdown event. If the nucleus dies immediately (within milliseconds to seconds), because of prompt repassivation, the event is labelled a "metastable pit". However, as noted above, a small fraction of the breakdown events survive and establish viable micro cells having the appropriate separation between the local anode (in the pit nucleus) and the local cathode (on the external surface), thereby resulting in the growth of stable pits.

Figure 10 illustrates the initiation of pitting due to the accumulation of cation vacancies to form a cation vacancy condensate at the metal/film interface, process leading to the breakdown of passive film according to PDM.

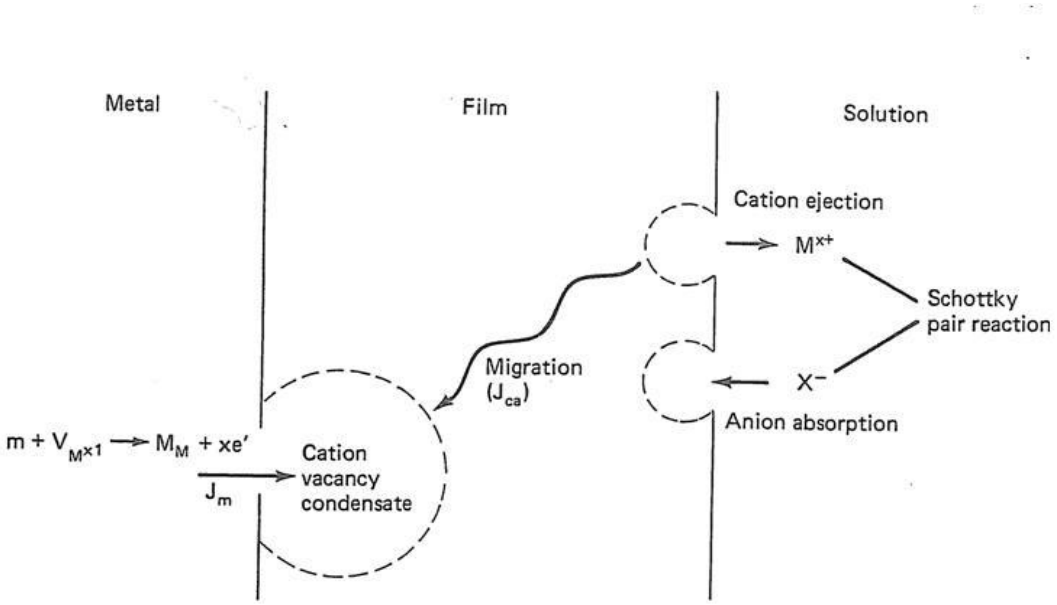

Figure 10: Processes leading to breakdown of passive films according to PDM[99]

Vacancies that are generated on the metal lattice or through other processes, v_m, can also be annihilated by processes such as dislocation climb or diffusion to a free interface (which occurs on the metal side of the metal/barrier layer interface), free surface, void or grain boundary. For metals and alloys that form p-type semiconducting barrier layers, such as nickel[96], in which cation vacancies are the principal point defect;

$m + V_M^{\mathbb{X}'} \overset{k_1}{\rightarrow} M_M + v_m + \mathbb{X}^{e'}$ is postulated to be the primary source of vacancies on the metal lattice at the metal/barrier layer interface.

However, metals and alloys that display n-type electronic character (e.g., Fe, Zn, stainless steel) [96], also suffer passivity breakdown. Hence annihilation of cation vacancies alone via vacancy condensation reaction might not be the sole source of, v_m, in the general case. Generation of cation interstitials can also occur through the following reaction:

$$m \overset{k_2}{\rightarrow} M_i^{\mathbb{X}^+} + v_m + \mathbb{X}^{e^-}.$$

Two fundamental mechanisms have been postulated to be responsible for passivity breakdown, both mechanisms lead to generation of the cation vacancy flux across the barrier layer in response to the absorption of aggressive anions into oxygen vacancies at the barrier layer/outer layer interface. The first mechanism is a Schottky pair reaction while the other is ion desorption/vacancy pair generation. Both Schottky pair generation and ion desorption/vacancy pair generation give rise to the same expressions for the breakdown voltage and induction time. It is also important to note that both mechanisms lead to autocatalytic generation of oxygen vacancies at the barrier layer/outer layer interface above the point of cation vacancy condensation.

The autocatalytic generation of oxygen vacancies at the barrier layer/outer layer interface is an important feature of the PDM because it accounts for the intriguing observation of rings of absorbed chloride at the peripheries of 'blisters' on the surface of aluminium in contact with chloride-containing solutions under spontaneous pitting conditions by Bargeron and Givens. The chloride ring expands with the blister, signalling a continual redistribution of absorbed chloride ion on the surface[118, 119]. This observation is in complete accord with the predictions of the PDM, because of the close spatial relationship between oxygen vacancy generation and cation vacancy condensation. Hence, the oxygen vacancy concentration at the surface, and the concentration of absorbed chloride, is greatest above the location of vacancy condensation, which coincides with the periphery of the blister. The autocatalytic generation of oxygen vacancies, ensures continuous

condensation of cation vacancies at the periphery of the condensate which invariably ensures the continued growth of the blister. Cation vacancy condensation (separation of the barrier layer from the substrate metal) is postulated to occur when the product of the "excess" cation vacancy flux and the time over which condensation occurs exceeds a critical value[113] i.e.

$$(J_{ca} - J_m)(t - \tau) \geq \xi \quad (27)$$

where J_{ca} is the flux of cation vacancies across the barrier layer at the breakdown site, J_m is the annihilation flux, t is the time, τ is the cap dissolution time, and ξ is the critical area concentration of vacancies. From equation 27, it is evident that the critical condition for passivity breakdown at a specific site occurs after an infinite time, (i.e. when t → ∞) or when $J_{ca} = J_m$. This condition results in an expression for the critical breakdown potential for a single site given by Shibata and Takeyama[120], regardless of the fate of the nucleus (i.e., irrespective of whether the breakdown event results in a metastable or stable pit)[96, 113]:

$$V_c = \frac{4.606RT}{\chi\alpha F} log\left[\frac{J_m}{J^o u^{-\chi/2}}\right] - \frac{2.303RT}{\alpha F}\log(a_x) \quad (28)$$

Where R is the universal gas constant, T is the absolute temperature, F is the Faraday constant. J^o in equation 28 is expressed as:

$$J^o = âD \quad (29)$$

where D is the cation vacancy diffusivity, â and u are constants, they depend on the thermodynamic parameters for the absorption of the aggressive ion into an oxygen vacancy at the barrier layer/outer layer interface, a_x is the activity of the aggressive ion at the barrier layer/outer layer interface, and ξ′ is a parameter that depends on the critical area concentration of condensed vacancies, ξ.[113] The expression for critical breakdown voltage explains the ubiquitous observation that V_c varies linearly with $-\log(a_x)$, with a coefficient that exceeds 2.303RT/F (note that a < 1). Substituting the expression for the annihilation flux in equation 27 into equation 28 gives the induction time for passivity breakdown as[113]:

$$t_{ind} = \xi'\left[\exp\left(\frac{\chi\alpha F\Delta V}{2RT}\right) - 1\right]^{-1} + \tau \quad (30)$$

where $\Delta V = V\text{-}V_c > 0$ (i.e. $J_{ca} > J_m$). The expression for the induction time for passivity breakdown explains the form of ($log\ t_{ind}$) vs. ΔV, which is a straight line with a negative slope of $\chi\alpha F\Delta V/2RT$ at small ΔV (but sufficiently large that the exponential >> 1), but in which $t_{ind} = \tau$ is a constant at large ΔV.

Independent of mathematical models and assumptions, over two decades before the postulation of PDM, pitting corrosion had been described as a unique type of anodic autocatalytic process. That is, the corrosion process within a pit produces conditions which are both stimulating and necessary for the continuing activity of the pit. The schematic pit process of a metal, M (e.g. Fe) in aerated sodium chloride solution is illustrated in Figure 11.

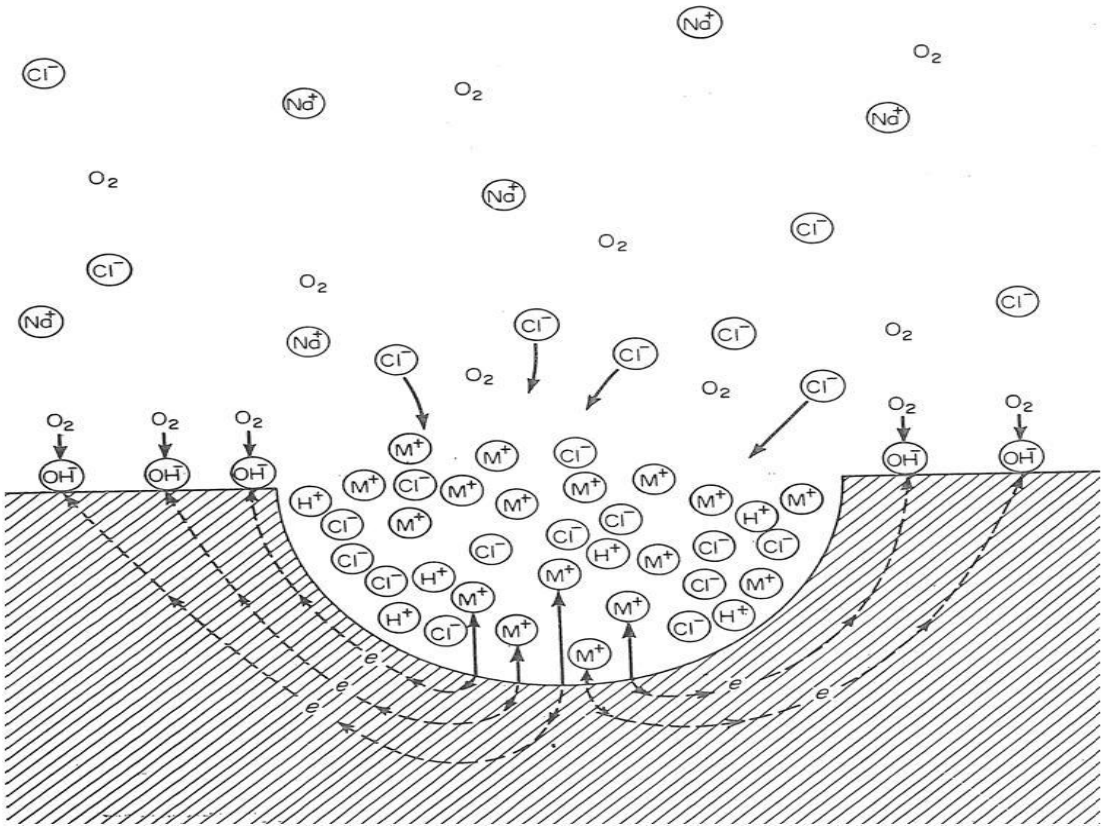

Figure 11: Autocatalytic processes occurring in corrosion pit[99]

Rapid dissolution of the metal occurs within the pit producing excess of positive charges, M^+, (cations) which results in the migration of chloride ions (anions) into the pit to maintain electro-neutrality, while oxygen reduction takes place on adjacent surfaces. It is worth noting that hydroxide ions (OH^-) also migrate from outside of the pit, but they are less mobile than the chloride ions. Hence, in the pit, there is high concentration of MCl. Except for alkali

metals (e.g. sodium and potassium), metal salts including chlorides and sulphates, hydrolyse in water dissociating into an insoluble hydroxide and a free acid as shown below:

$$M^{+}Cl^{-} + H_2O \rightarrow MOH\downarrow + H^{+}Cl^{-}$$

Both hydrogen and chloride ions stimulate the dissolution of most metals and alloys (for reasons yet to be understood) hence the entire process accelerates over time. This process is self stimulating and self propagating leading to pit growth. Since the solubility of oxygen is virtually zero in concentrated solutions, no oxygen reduction occurs within the pit. The cathodic oxygen reduction on the surface adjacent to the pits tends to suppress corrosion due to generation of hydroxyl ions (OH^-) which increases the pH at the cathodic sites. As a result, the pits technically cathodically protect the adjacent surfaces. Before the postulation of the point defect model, in 1951, Evans[121] suggested that the pit initiation process is a result of momentarily high local dissolution induced by a scratch on the surface or other defects or random variation in solution composition leading to migration of the chloride ions to the point on the metal surface where metal dissolution is momentarily high, thereby stimulating metal dissolution which further favours rapid dissolution at that point. It is apparent that during the initiation or early growth stage of the pit, conditions are rather unstable. Evans went further to explain that the pit growth is typically in the direction of gravity because the dense concentrated solution which is necessary for continuous activity of the pit is influenced by gravity. PDM is fully aligned and in agreement with the postulated pit mechanism.

In the original PDM[113], the parameter τ was identified as a 'relaxation time', which described the temporal and spatial response of the vacancy structure to the absorption of an aggressive anion into an oxygen vacancy at the barrier layer/outer layer interface. Upon reinterpreting the data of Cassilas et al[122, 123] for passivity breakdown on titanium by Ellerbrock and Macdonald[114], it became evident that τ is also determined by the time of dissolution of the cap to the point that the cover becomes mechanically unstable. Thus, τ can be defined as;

$$\boldsymbol{\tau} \leq \Delta \boldsymbol{L}/\Omega \mathbf{K_s} \mathbf{C_{H^+}^n} \quad (31)$$

where ΔL is the thickness of the barrier layer over the condensate at the point at which cation vacancy condensation first occurs, and the denominator is the barrier layer dissolution rate; Ω is the mole volume of the barrier layer per gram cation, K_s is the rate constant for the barrier layer dissolution reaction, C_{H^+} is the concentration of hydrogen ion at the barrier layer/solution interface and n is the reaction order.

At sufficiently high overvoltages, ($\Delta V = V - V_c$), where vacancy condensation occurs rapidly, $t_{ind} \sim \tau$ and, unless the rate of dissolution of the cap depends on X^-, τ should be independent of the concentration of the aggressive species in the solution, but should be a function of the pH. With regards to pH, τ should decrease with decreasing pH for pH < pzc, but should decrease with increasing pH for pH > pzc, where pzc is the pH of zero charge[124]. For the case of iron in chloride solutions, τ shows slight dependencies on $[Cl^-]$ and pH[113], but the dependencies are judged to be too small to be of mechanistic significance. Also, assuming that ΔL ~ 2nm, and τ ~ 10s, the maximum dissolution rate of the cap above the cation vacancy condensate is estimated to be ~ 0.2nm/s.

This value corresponds to a minimal corrosion rate (ignoring cation transmission through the film) of ~ 6mm/y, which is too high to be realistic for iron in neutral chloride solution. This probably reflects the fact that only partial dissolution is necessary to cause the residual stresses to induce rupture of the cap. Alternatively, dissolution may be highly non uniform, giving rise to high local penetration rates through the cap. However, once the cap has ruptured, dissolution may occur from both sides to yield patterns that reflect the properties of both the internal and external environments. Indeed, analysis of the 'lace-like' perforations in the caps over pits that forms on stainless steels in chloride-containing solutions by Laycock et al.[117] implied the latter.

However, over the years passivity breakdown is better understood, the induction time for passivity breakdown has been found to comprise of two components. The first component is the time required for the condensation of sufficient vacancies at the metal/barrier layer interface to cause separation of

the barrier layer from the metal, and hence to stop the growth of the barrier layer into the substrate via the following reaction:

$$\boldsymbol{\tau \leq \Omega L_{ss}^{vc} / k_7 \left(C_{H^+} / C_{H^+}^{0} \right)^{n}} \quad (32)$$

Where Ω is the mole volume of the barrier layer per gram cation, L_{ss}^{vc} is the thickness of the barrier layer at the point of initial vacancy condensation, k_7 is the rate constant for the barrier layer dissolution reaction, C_{H^+} is the concentration of hydrogen ion at the barrier layer/solution interface, and $C_{H^+}^{0}$ is a standard state hydrogen ion concentration which was included to ensure that the units of the rate constant, k_7, are independent of the reaction order, n. The second component of induction time is the time for dissolution of the "cap" (remnant of the barrier layer) over the breakdown site to the point that fracture occurs.

The expression for critical breakdown voltage (V_c) and the induction time for passivity breakdown (t_{ind}) have been found to describe passivity breakdown quantitatively in each of the systems that have been analyzed in depth to permit the discrimination between different mechanisms[96]. These systems include (Cu/HCO_3^-, SO_4^{2-})[112], (Fe/Cl^-, Br^-, I^-)[113], (Ni/Cl^-),[125] and with 'quantitative agreement' being taken as the close agreement between the values obtained for the critical breakdown voltage (V_c) and the induction time for passivity breakdown (t_{ind}).

In 1997, Haruna and Macdonald[126] used the potential sweep rate dependence of the critical breakdown voltage to derive the value of ξ (the area concentration of condensed cation vacancies for the separation of the barrier layer from the metal) for Ni in buffered chloride-containing solution. The value obtained was in good agreement with the value obtained from structural considerations. This was a particularly stringent test, because the parameters in the calculation are fairly well defined.

Towards the end of last millennium, Ellerbrock and Macdonald[114] reanalyzed the experimental data of Casillas et al[122, 123] for passivity breakdown on titanium in bromide-containing solutions. They found out that the maximum dissolution rate of the cap, as estimated from the equation derived by Casillas et al for τ, was about 1nm every 1000s, leading to an estimated passive

current density (assuming predominant oxygen vacancy transmission) of ~3.8μA/cm. This value was considered to be reasonable, given the fact that no allowance was made for surface roughness, and noting that Casillas et al did not report passive current densities for their experiments. In retrospect, this value was also considered to be too large. This implies that the inequality in the equation derived by Casillas et al for τ is more appropriate than the equal sign.

The PDM has been criticised as being too 'static', because passivity breakdown is well-known to be a dynamic phenomenon (as shown by the existence of 'metastable' pitting). In Macdonald's opinion, this criticism is as a result lack of understanding of what the PDM attempts to accomplish. The point defect model attempts to describe the initiation event (i.e. the event that leads to rupture of the passive film that subsequently results in the transient in current). The fact that this must involve the physical rupture of the film is self-evident, and the view that initiation is somehow preceded by dissolution of the substrate must be rejected. Just as commonly said, it's like 'putting the cart before the horse'. As demonstrated by Shibata and Takeyama[120] and later by Williams et al.[103, 127], Wu et al[128] and Lunt et al[129], the breakdown parameters are distributed with V_c being near-normally distributed and t_{ind} being described by a left-acute distribution. These workers have chosen to interpret their data in terms of stochastic models, which presuppose that breakdown is a random phenomenon. This is justified on the basis that the breakdown voltage for metastable events is 'normally' distributed, and hence is Poissonian in nature.

The fallacy in this argument is that, while a random breakdown process is expected to yield a normal distribution in V_c, when sampled over many events, the converse is not true; that is, a normally distributed V_c does not necessarily mean that the event is random in nature. Thus, Wu et al[128] and Lunt et al[129] demonstrated that a 'stochastic' process incorporating short-term 'memory' effects does indeed yield the experimentally observed near-normal distributions in V_c and left acute distribution in t_{ind}, even though the process is not strictly 'random'. These workers were apparently unaware that the same distributions was derived deterministically more than a decade earlier[130, 131].

Macdonald concluded that, stochastic models are phenomenological models, and, as such, they cannot provide a satisfactory account of the physico-electrochemistry of the fundamental events involved in passivity breakdown. For example, the nucleation rate, λ, is derived as a model parameter, but nowhere in the stochastic treatment is there a physical model for nucleation rate, nor is there any explanation of the processes that led to the observed rate and its dependencies on various independent variables. According to Macdonald, until this is done, the stochastic models must be regarded as being inadequate and incomplete, and to offer little more than a description of the phenomenon itself. Macdonald went further to state that passivity breakdown is deterministic in nature and actually seem to be self-evident from the data obtained from the stochastic models themselves, which yield model parameters (λ, μ, or τ_c) as functions of potential, inclusion size, flow velocity, temperature, etc. Clearly, there dependencies must reflect underlying mechanisms, which imply a determinism that governs the behaviour of the ensemble of events.

Accepting that the initial event in the nucleation of a micropit is passivity breakdown, and that V_c and t_{ind} describe the breakdown conditions for a given event, then the two most likely parameters in the model that are most appropriate to describe the behaviour of the population of sites on the surface (based on their distribution) are the cation vacancy diffusivity (D) and the thickness of the barrier (L_{ss})[96]. The fact that the thickness of the barrier, Lss varies across a real surface is well-known from microellipsometric studies[116], but distributing this parameter would seem to affect only those instances where the induction time was dominated by the rate of dissolution of the cap (i.e. at high ΔV or for inherently thick films, such as those that form on the valve metals, such as Ti[122, 123]. To describe the more general case, the cation vacancy diffusivity within the population of breakdown sites was assumed to be distributed normally about a mean ($\bar{D}$) with a standard deviation, σ_D. The resulting distributions in V_c and t_{ind} were then derived as[130, 131]:

$$\frac{dN}{dV_c} = -\frac{\gamma' D}{\sqrt{2\pi}.\sigma_D} e^{-(D-\bar{D})^2/2\sigma_D^2} \quad (33)$$

and

$$\frac{dN}{dt_{ind}} = \left[\frac{\xi u^{\chi/2}}{\sqrt{2\pi}.\sigma_D.\hat{a}}\right] e^{-\left(D-\bar{D}\right)^2/2\sigma_D^2} . \frac{e^{-\gamma' v}}{a_x^{\chi/2}(t_{ind}-\tau)^2} \quad (34)$$

where $\gamma' = \chi\alpha F\Delta V/2RT$, and the other parameters are as previously defined. Equations 33 and 34 have been found to account for the distributions in V_c and t_{ind}, as reported by Shibata et al[120] and later by others[127, 128]. These same expressions are applicable[126], whether it is the 'external' distribution (many specimens, as employed by Shibata[120]) or the 'internal' distribution (single specimen as employed by Williams et al[127]) that is sampled.

According to Shibata's calculations for t_{ind}, variation of the standard deviation did not significantly affect the shape of the t_{ind} distribution. Also, the value that was adopted for the distribution in V_c was found to provide an accurate account of the induction time data[130, 131]. Macdonald and co have explored the distributions in V_c and t_{ind} as a function of a_x, applied voltage (N (t_{ind}) only), pH, and obtained the expected dependencies[130, 131]. While changes in $log(a_x)$ induced relatively small changes in the mean critical breakdown potential, they had significant impact on induction time, with t_{ind} greatly decreases as a_x was increased. For this reason, Macdonald termed the passivity breakdown as 'induction time-limited', however since N(V_c) and N(t_{ind}) are not independent, this terminology should be discouraged. It is however important to note that the resulting distributions in V_c and t_{ind} have led to the formulation of a theory for alloying.

According to Macdonald and Urquidi[132], "t*he basis of this theory is the Solute-Vacancy Interaction Model (SVIM), which postulates that alloying elements that are substitutionally present in the cation sub-lattice of the barrier layer in an oxidation state that is higher than that of the host cation (e.g. Mo, where Mo is present as Mo(VI) in the NiO barrier layer) will interact electrostatically with the mobile cation vacancies, with the net result that the mean cation vacancy diffusivity is lowered. This has the result of shifting the breakdown voltage in the positive direction, to produce a more breakdown-resistant barrier layer".* The Solute-Vacancy Interaction Model has been applied to the Type 304 (18Cr:8Ni)/Type 316 (+2.5% Mo) issue. The result of the calculation is graphically represented in Figure 12[101, 132]. The quantity that was plotted on the ordinate is V(X) - V(X = 0), where X is the cation fraction of Mo in the film

(assumed to be the same as that in the metal), eliminates all known parameters in the model except the dielectric constant of the barrier layer. The value of the dielectric constant was taken to be equal to that for the passive film on iron; this can have profound impact on V_c and t_{ind} While the experimental data were highly scattered, the PDM was found to best account for the effect of Mo by assuming that Mo exists in the +6 state, rather than in the +4 state.

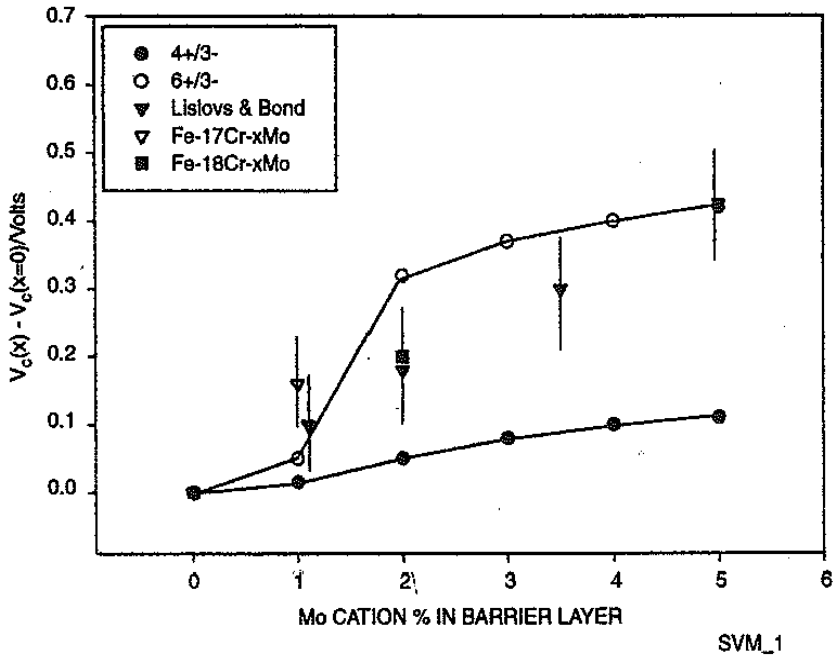

$n_v = 5 \times 10^{20}/cm^3$, $K_1 = 1.13 \times 10^{-16}$ cm^3 (o), $K_1 = 1.13 \times 10^{-16}$ cm^3 (Δ).

▼ Lizlovs & Bond: Fe-18 Cr in 1M NaCl at 25°C.

∇ Shibata: Fe-17 Cr in 3.5% NaCl at 30°C.

∎ Shibata: Fe-18 Cr in 3.5% NaCl at 30°C.

Figure 12: Effect of Molybdenum Concentration on $\overline{V}_c(x)$- $\overline{V}_c(X = 0)$ for 6^+ - 3^-(o) and 4^+-3^-(•) complexes in the passive film on Fe-Cr-Ni-xMo alloys[101]

Another parameter that has a profound effect upon the breakdown parameters is the electric field strength. The electric field strength is buffered by electron/hole generation via band-to-band tunnelling that prevents the field from increasing in an unconstrained manner. However, if an additional e'/h generation process is imposed on the system, such as irradiation with super band gap light, the field will be lowered, with the result that V_c is predicted to shift to more positive values and t_{ind} is predicted to increase to longer times. This is the basis of photo inhibition of passivity breakdown (PIPB), which was

first reported by Lenhart et al.[133] for nickel in 1987 and then subsequently detected by various workers for iron[134, 135], stainless steels[136-138], and copper alloys[139]. In a publication by Shibata et al[140] in 1998, PIPB was confirmed in stainless steel. Using a stochastic model to analyse their data, they found out that the principal effect of super band-gap irradiation was on reducing the pit generation rate, which is precisely the effect predicted by the PDM distribution in t_{ind}. Persistence in photo-inhibition for iron was initially reported by Schmuki and Bohni[134]. This was subsequently confirmed by Heaney and Macdonald[135]. Breslin et al[137, 138] have also demonstrated persistence of PIPB in stainless steels in chloride-containing solutions. In this persistent effect, the resistance to passivity breakdown induced by initial irradiation was found to remain for ≈250h after irradiation had ceased, after which the system then returned to its initial, susceptible state. Schmuki and Bohni[134] explained persistence in terms of the generation of 'surface states' without specifying the nature of those states or how they were formed. On the other hand, persistence was readily accounted for by noting that the photo-quenching of the electric filed modified the vacancy structure, and it was the relaxation of the vacancy structure back to its initial state that determines how long the effect persists [137, 138].

Modification of the vacancy structure in the passive film on stainless steel was detected by Breslin et al. by using Mott-Schottky analysis, the persistence time was found to be in agreement with that estimated from a reasonable value for the vacancy diffusivity[135-138]. Assuming that Schmuki and Bohni's 'surface states' were, oxygen vacancies (which are electronic donors), then the two explanations are equivalent and are within the bounds of the PDM. Based on this finding, it was worth inquiring whether there was any common ground between the stochastic and deterministic views of passivity breakdown. While these two divergent philosophies are not restricted to the present issues, and indeed generally pervade scientific inquiry, there was no question that the evolution of science is towards determinism. Accordingly, 'science' eventually seeks a deterministic explanation of natural phenomena, because it is only through determinism that a deep understanding of mechanisms can be obtained and reliable predictions can be made. The most obvious connection between the stochastic models of Shibata et al[120],

Williams and co-workers[127], and Wu et al[128] is in the pit generation rate. Williams et al.[127] related the rate of generation of stable pits (Λ) to the rate of generation of metastable pits (λ) by;

$$\boldsymbol{\Lambda = \lambda e^{-\mu \tau_c}} \quad (35)$$

where μ is the probability of survival and τ_c is the critical age of the pit nucleus. The metastable pit generation rate, λ is given by the equation for the distribution of t_{ind}, in PDM parlance. Although, a fully deterministic model for describing the transition from metastable pitting to stable pitting is ultimately desired, it is worth stressing that the stochastic approach has considerable merit, because it leads to a natural simulation of the fluctuations in the current[128]. However, for this approach to be truly effective, deterministic models must be developed for estimating μ and τ_c.

Issues associated with commonality in mechanism are of the utmost importance in defining the cause of passivity breakdown. Several mechanisms have been proposed for passivity breakdown in specific systems, ranging from chloride penetration[141], to electrostrictive rupture[115], to inclusion dissolution[142], but in fact all of the systems for which these mechanisms were proposed display common experimental correlations. As an example, they all generally display a linear relationship between the critical breakdown potential (V_c) and the negative logarithm of the activity of the aggressive ion (i.e. $V_c \propto -\log(a_x)$), with the proportional constant being less than 2.303RT/F. Also, $\log(t_{ind})$ varies inversely with $-\Delta V$. It would be a remarkable occurrence if all of these diverse mechanisms gave rise to the same relationships between the dependent (V_c, $t_{in}d$) and independent (a_x, V, pH) variables. Hence it is logical to conclude that a common mechanism for the initial passivity breakdown event exist among all the mechanisms. Macdonald suggested the event is vacancy condensation[96]. It was previously suggested[101] that the intersection between the barrier oxide layer and the sulphide inclusion (in the case of the stainless steels, where the breakdown sites were identified as MnS inclusions), represents a region of great lattice mismatch, and hence a region of high cation vacancy diffusivity. However, according to the PDM, the point of intersection between the barrier layer and the inclusion is the preferred site for cation vacancy condensation that led to

the initial passivity breakdown. It was also concluded that the external surfaces decoration observed[143] was as a result of sulphide dissolution that occurred at a later stage. Breakdown at the point of intersection between the film and the inclusion led to the formation of a crevice, which acidified as spatially separated anodes and cathodes developed at the breakdown site. Acidic conditions in the crevice eventually led to MnS dissolution, HS^- ion produced by this reaction eventually oxidized to thiosulphate ($S_2O_3^{2-}$) and elemental sulphur as it diffuses into the external environment. This postulation provides logical explanation for the dependence of V_c and t_{ind} on a_x observed experimentally, that could not be explained in terms of MnS dissolution alone.

2.5 Repassivation

Apart from understanding the mechanisms for passivity breakdown, the other very important phenomenon in CRA is repassivation. The kinetics of repassivation of localised corrosion events has a profound impact on the accumulation of damage.

Two, fundamentally different passivation mechanisms were readily identified as earlier discussed:

(i) 'Prompt' repassivation which is responsible for the death of the initial event, and gives rise to 'metastable pitting', and

(ii) 'Delayed' passivation which is responsible for the deaths of stable pits at much longer times.

Prompt repassivation has been extensively dealt with by several people including Galvel[144-146], Williams et al.[103], Burstein and co-workers[104, 147], and Frankel et al[105, 148], and it was attributed to the failure of the nucleus to achieve critical conditions. Ezuber and Newman[149] expressed the critical conditions as the product of the pit current density and pit radius or inverse radius exceeding a critical value for an individual pit to transit from metastability to stability. The basic idea is that critical conditions, due to the spatial separation of the partial anode (in the crevice) and the partial cathode (on the external surface) must be achieved for the pit to grow to a self sustaining condition. An important concept in determining the probability of survival of a pit, particularly at an early age, is the continued integrity of the cap. Massive rupture of the cap at a time that is too early in the life of a

nucleus would result in dispersal of the aggressive solution that has accumulated within the crevice; this would lead to repassivation[117]. On the other hand, lack of connectivity between the crevice and the external environment may cause the spatially separated partial anode and partial cathode not to be sustainable, again resulting in death of the embryo. Clearly, the probability that a pit nucleus will survive is a sensitive function of the history of the cap, and any model that is proposed to explain prompt repassivation ultimately will have to address the fate of the post-breakdown barrier layer blister.

Delayed repassivation on the other hand is quite different. The phenomenon was first observed by Macdonald et al[150]. They investigated the nucleation and growth of pits on nickel in buffered chloride solution by observing the surface in situ using optical microscopy. They observed that each pit that nucleated on the surface and grew had associated with it, a 'hemisphere of influence' (HOI), centred on the pit mouth. The HOI, which is produced by a high concentration of hydrolyzed metal ions, is clearly visible under optimal conditions of illumination, increased in radius as the pit aged. They also made two very important observations. The first observation was that no new stable pits nucleated under the HOI of an existing pit. This was attributed to the fact that a pit cathodically protects the external surface under the HOI, due to the preponderance of the cathodic partial current on the surface as later predicted by Liu and Macdonald[151]. The second observation was that the overlap (or more accurately the extent of the impingement) of the HOIs from neighbouring pits inevitably led to the death of one of the pits. This reflects the competition between pits for available resources on the external surface. Hence, if the pits grow independently without any interaction of the two HOIs, sufficient resources were available for each pit to grow and develop independently. However, when the HOIs of neighbouring pits impinged upon each other, the pits compete for the same resources (oxygen reduction) on the external surface. When insufficient resources were available for both pits, then only the fittest pit grows (survival of the fittest). This is in agreement with the competitive adsorption theory which had been previously cited as a mechanism for the inhibition of pitting corrosion by oxyanions[152-156].

2.6 Electrochemical Testing

The potential difference between the anodic and the cathodic reactions is the driving force which permits metal dissolution or corrosion to continue. The total number of electrons generated by oxidation must be equal to the total number of electrons consumed by the reduction processes. Current is a measure of the number of electrons which flow per second. The current provides a measure of the rate at which the reactions are proceeding. Therefore, the measurable values of potential and current are of primary interest in the study of corrosion. When anodic and cathodic reactions occur on the same metal surface, they tend to polarise towards each other to a common potential known as the corrosion potential (E_{cor}). Polarisation is the change in potential of a reaction away from its equilibrium value as a result of passage of current. Electrochemical tests are methods by which either the potential is controlled while the current is measured or the current is controlled while the potential difference and magnitude of polarisation are measured during the corrosion process. The study of potentials as the driving force for electrochemical reactions is founded in thermodynamic principles while the study of current measurements as the measure of rates of electrochemical reactions is founded in kinetics.

Several disciplines play important roles in electrochemical testing. Electrical principles are required to understand current and potential measurements and their relationship. Electronics instruments are used for measurements and control during the test. Knowledge of the chemistry is important because chemical solutions are the corrosive environment in which the tests are conducted while metallurgy is important because alloy composition and thermo mechanical treatments significantly affect the corrosive nature of the metals. Lastly, electrochemistry provides the fundamental principle that governs and defines the corrosion mechanisms and processes that occur during corrosion.

2.6.1 Thermodynamics

The principle of thermodynamics is that materials always seek the lowest energy state. Most metals naturally exist in their stable ore form. However with energy input during the process of refining to the metallic form, they

become thermodynamically unstable and tend to return to their lower energy state. Gibbs free energy (G) is a general term used for energy in a system. For a process such as corrosion to be spontaneous, the change in Gibbs free energy (ΔG) must be negative (i.e. $\Delta G < 0$). The individual oxidation and reduction reactions are referred to as half cell reactions (because together they form a complete electrochemical cell) and can occur locally at adjacent sites on the metal but can also be widely separated as long as electrical connectivity is maintained between the anodic and cathodic sites. The change in Gibbs free energy of each pair of half cell reaction is related to the reversible electromotive force or electrode potential (E) and is given as:

$$\Delta G_{anodic} = nFE_{anodic} \quad (36)$$

$$\Delta G_{cathodic} = -nFE_{cathodic} \quad (37)$$

Where n is the number of electrons associated with the oxidation reaction for anodic and reduction reaction for cathodic and F is the Farady's constant.

The change in Gibbs free energy for a corrosion reaction is the summation of the change in Gibbs free energies for the anodic and the cathodic half cell reactions i.e.

$$\Delta G_{corrosion} = \Delta G_{anodic} + \Delta G_{cathodic} \quad (38)$$

Substituting equations 36 and 37 into equation 38,

$$\Delta G_{corrosion} = nF (E_{anodic} - E_{cathodic}) \quad (39)$$

As earlier stated, for corrosion process to be thermodynamically favoured;

$$\Delta G_{corrosion} =< 0$$

Therefore, from equation 39, for corrosion to proceed, the cathodic potential ($E_{cathodic}$) must be greater than the anodic potential (E_{anodic}).

2.6.2 Kinetics

Kinetics is the study of the rate at which reactions occur. Oxidation and reduction reactions each occur at a potential polarised from its equilibrium value. With the passage of current, the potential of the anode increases to more positive (noble) values while the potential for the cathode decreases to more negative (active) values. Ignoring resistance in the electrochemical cell,

both the anodic and cathodic potentials will approach the corrosion potential. The amount of overpolarisation or overpotential is assigned the symbol eta (η) which is the difference between applied potential and the corrosion potential (E_{cor}) expressed as follows:

$$\eta = \boldsymbol{E} - \boldsymbol{E_{cor}} \tag{40}$$

In an activation controlled polarisation process, the corrosion reaction is limited by the electron transfer reaction to the metal surface. The electron transfer process has associated activation energy and the rate of the process is exponentially related to the free energy change. Since the free energy is directly related to the potential (equations 36 and 37), the relationship between current density and the potential of anodic and cathodic electrode reactions under charge transfer control is given by the Butler-Volmer equation:

$$i = i_{cor}\left(e^{\left(\frac{2.303\eta}{b_a}\right)} + e^{\left(\frac{-2.303\eta}{b_c}\right)}\right) \tag{41}$$

Where i is the measured current density, i_{cor} is the corrosion rate, b_a and b_c are the Tafel constant for the anodic and cathodic reactions respectively. These three parameters can be determined from experimental data. The expressions for Tafel constant for the anodic and cathodic reaction are given in equation 42 and 43 respectively:

$$\boldsymbol{b_a} = \frac{\boldsymbol{-RT}}{\boldsymbol{\alpha nF}} \tag{42}$$

$$\boldsymbol{b_c} = \frac{\boldsymbol{RT}}{\boldsymbol{(1-\alpha)\,nF}} \tag{43}$$

Where R is the universal gas constant, T is the absolute temperature (K), α is the charge transfer coefficient, n is the number of electron charge transferred and F is Faraday constant.

For large anodic overpotentials i.e.$(\eta/b_a \gg 1)$, the Butler-Volmer equation can be simplified to the Tafel equation for the anodic reaction as follows:

$$\eta = \log \boldsymbol{i_{cor}} + \boldsymbol{b_a} \log \boldsymbol{i} \tag{44}$$

Analogously, for large cathodic overpotentials i.e.$(\eta/b_c \ll -1)$, the Butler-Volmer equation can be simplified to the Tafel equation for the cathodic reaction as follows:

$$\eta = \log i_{cor} - b_c \log|i| \quad (45)$$

The Tafel equations (equations 44 and 45) predict a straight line for the variation of the logarithm of current density versus potential, hence currents are usually shown in the semi-logarithmic plots known as the Evans diagram shown in Figure 13.

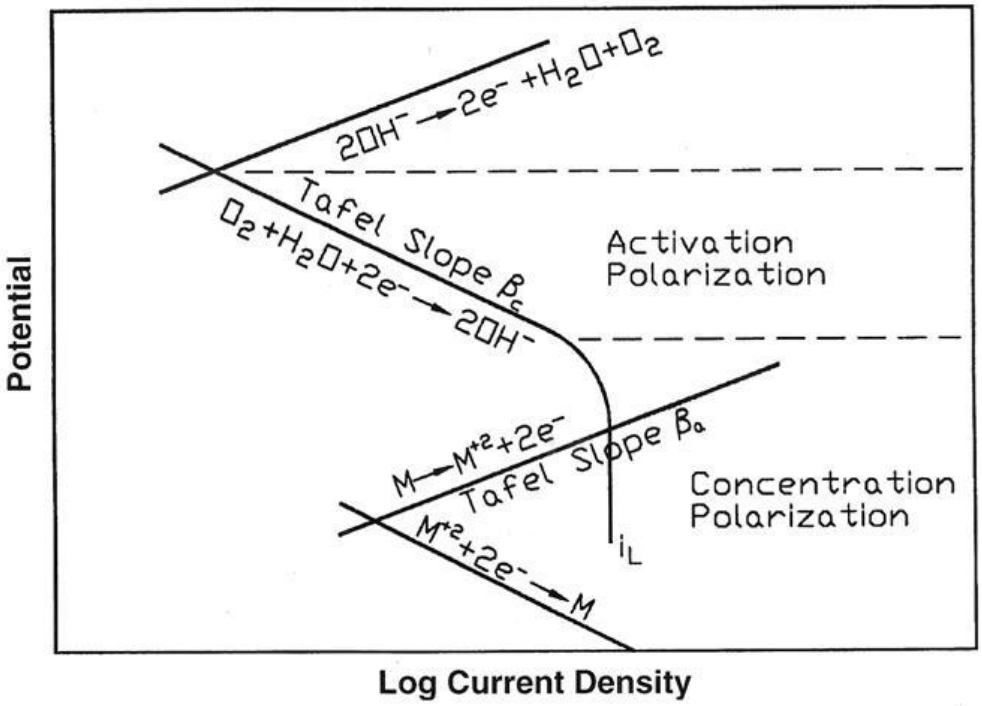

Figure 13: Schematic of Evans diagram for a combined activation/ concentration polarisation[157]

Another type of polarisation commonly observed is the concentration polarisation which is a diffusion controlled process, (typically affects the cathodic reaction). As shown in Figure 13, the corrosion reaction is limited by diffusion of oxygen to the metal surface limits. The rate of the reduction reaction is independent of potential when concentration polarisation occurs.

The slopes of the linear portion of the anodic and cathodic curves are referred to as the Tafel slopes and have units of V per decade (ten-fold change) of current. Generally the anodic and cathodic Tafel slopes are different. An estimate of the Tafel slope corresponds to the slope of the tangent to the polarisation curve in that region. Figure 14a shows schematic diagram of polarisation plots for a system where both the anodic and cathodic reactions

are activation controlled while Figure 14b shows a system where the anodic reaction is activation controlled and the cathodic reaction is diffusion controlled. β_A and β_C are the Tafel slopes for the anodic and the cathodic polarisation curves respectively.

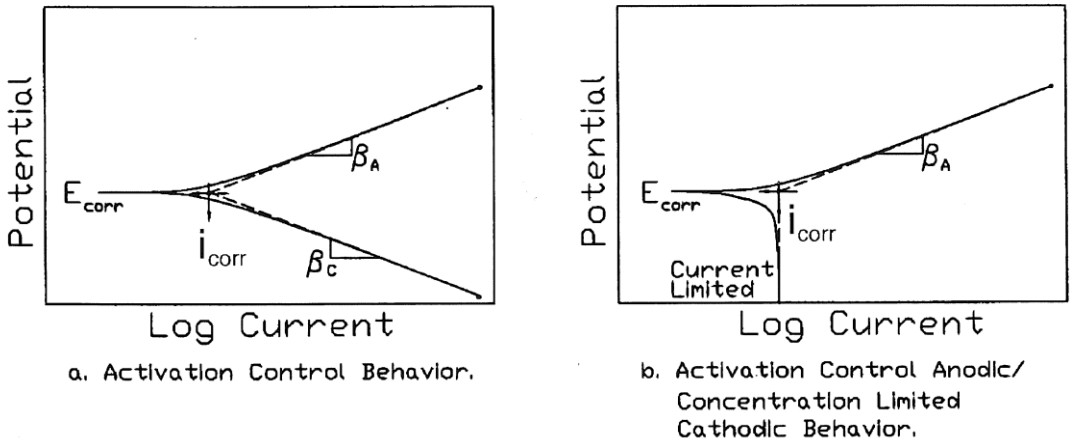

Figure 14: Schematic diagrams of typical polarization plots showing corrosion current extrapolations[157].

Tafel analysis is performed by extrapolating the linear portions of the anodic and cathodic Tafel regions in the log current versus potential plot back to their intersection. The estimated corrosion rate is the value of the current at the point where the two linear segments of the extrapolated anodic and cathodic curves intersect. At the intersection, the rate of the cathodic reaction is equal to the rate of the anodic reaction. Unfortunately, in reality, many corrosion systems do not provide sufficient linear portions of the anodic and cathodic Tafel region to permit accurate extrapolation.

For concentration polarisation the corrosion rate is given as:

$$\boldsymbol{i} = \frac{-\boldsymbol{zFD}(\boldsymbol{C_B} - \boldsymbol{C_S})}{\boldsymbol{\delta}} \quad (46)$$

Where z is the charge on diffusing ion, F is Faraday's constant, D is the coefficient of diffusion, δ is the solution boundary layer thickness, $(C_B - C_S)$ is the concentration gradient, C_B is the bulk concentration and C_S is the concentration at the metal surface. The negative sign is because diffusion is in opposite direction. At the limiting current, Cs $\rightarrow$ 0

$$\therefore \boldsymbol{i_{lim}} = \frac{-\boldsymbol{zFDC_B}}{\boldsymbol{\delta}} \quad (47)$$

Also, the concentration overpotential, η_c, is expressed as:

$$\eta_c = \frac{2.303RT}{zF} Log\left(1 - \frac{i}{i_{lim}}\right) \quad (48)$$

The current at the corrosion potential, I_{cor}, is directly proportional to the corrosion rate. If the surface area over which the current occurs is known, the current can be converted to current density (i) with units in A/cm^2. Using Faraday's Law, the current can be converted to actual corrosion rate (CR);

$$CR = \frac{i M_{wt}}{nFD} \quad (49)$$

where M_{wt} is the atomic weight of the metal in g/mol, n is the number of electrons transferred in g equivalents/mol, D is the density of the metal in g/cm^3 and F is the Faraday's constant. The unit of the corrosion rate is cm/s. However, this is rarely used. Corrosion rate is typically measured in mm/y or mpy. Hence to convert corrosion rate in cm/s to mpy, corrosion rate in cm/s is multiplied by a conversion faction of (1.242 x 10^{10}).

1mpy corrosion rate of iron = 2.17 μA/cm^2 (50)

Linear polarisation resistance (LPR) and polarisation resistance (PR) are analogous terms that refer to a linear approximation of the polarisation behaviour at a potential near the corrosion potential according to the Stern-Geary relationship[158]. Based on stern-Geary approximation, the polarisation current is assumed to change linearly (not logarithmically) with change in potential. In general, this assumption is not valid. It is only a good approximation within 10-20mV from the corrosion potential. Linearity could only be expected for rare case where the anodic Tafel slope β_A is equal to the cathodic Tafel slope β_C[159]. Mansfeld[160] reviewed the issue of linearity of polarization curves in the vicinity of the corrosion potential E_{cor} for commercial corrosion rate meters that employ alternate polarisation with the overpotential within ±10 mV and gave a correction factor that can be used to correct errors arising from the assumption of linearity. It was concluded that the corrosion rate determined is only an estimate[161]. Moreover, the polarization resistance technique is mostly used for corrosion monitoring where it is often not necessary to obtain very accurate values of corrosion rates, it is sufficient to detect large changes in the overall corrosion rates which can give useful information in field applications such as monitoring the effects of corrosion inhibitors, monitoring pH changes during well unloading or monitoring the

effectiveness of a deaeration systems (such as Minox, vacuum deaerator, Seajet, and oxygen scavenger chemical injection), in a waterflood system. From this linear approximation, the corrosion rate can be estimated. The Stern-Geary relationship that describes the change in potential as a function of change in net current, (dE/di) close to the corrosion potential is given as:

$$\boldsymbol{R_p = \frac{dE}{di} = \frac{\beta_A \beta_c}{2.3\,(\beta_A + \beta_c)\, i_{cor}}} \quad (51)$$

Where β_A and β_c are the anodic and cathodic Tafel slopes given as absolute values in volts per decade of current, i_{cor} is the corrosion current density with units of A/m^2, and the polarisation resistance, R_p at the corrosion potential has units of ohm m^2. When the potential near the corrosion potential is plotted on a linear graph against current, the slope of the resulting curve (dE/di) is the polarisation resistance, R_p. This analysis is typically performed within ± 10 to 20mV of the corrosion potential. The preferred method is to calculate R_p as the slope of the tangent of the curve at the corrosion potential where the current is zero as shown in Figure 15a. It is however, not uncommon to approximate this value by taking the average slope as shown in Figure 15b.

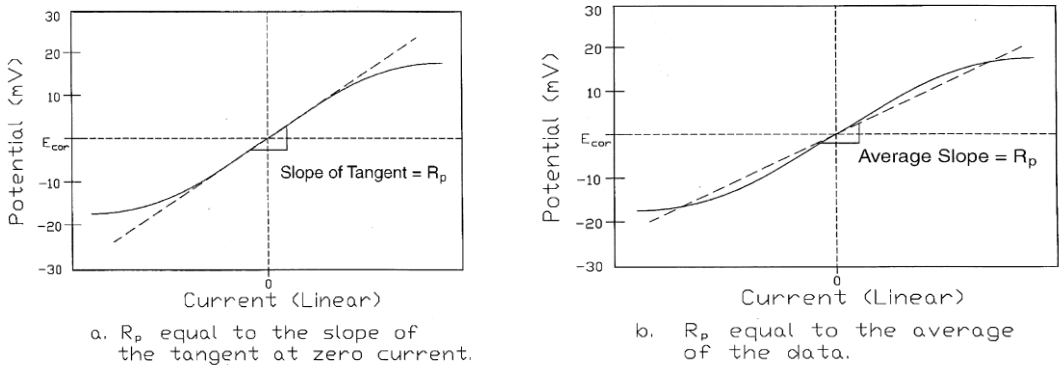

Figure 15: Typical linear polarization resistant curves[157].

With R_p determined, the corrosion current density can be calculated using equation 52:

$$\boldsymbol{i_{cor} = \frac{\beta_A \beta_c}{2.3\,(\beta_A + \beta_c) R_p}} \quad (52)$$

Having calculated i_{cor}, the average penetration rate in mpy or mm/y can be calculated using equation 49. It should be noted that the current measured by this technique or any other electrochemical method is the total oxidation

current. Hence, if a second oxidation reaction is present that is not a corrosion reaction; the calculated corrosion current will be greater than the actual corrosion rate since the corrosion reactions make up only part of the total oxidation current measured. This is a concern when oxidisable species such as sulphide are present in solution or when complex solutions are being examined. The best way to verify if this is a concern is to perform weight loss measurements and compare the results with those obtained from the polarisation resistance measurements.

As mentioned earlier, by plotting the logarithm of the current as a function of the applied potential, the anodic CPP curve of a test material can be obtained. From the CPP curve, the phenomena of active dissolution, passivation, pit initiation, breakdown of the passive film, repassivation and transpassivity can be illustrated. A typical anodic CPP curve of 304 SS in N_2 purged 1N sulphuric acid solution is shown in Figure 16.

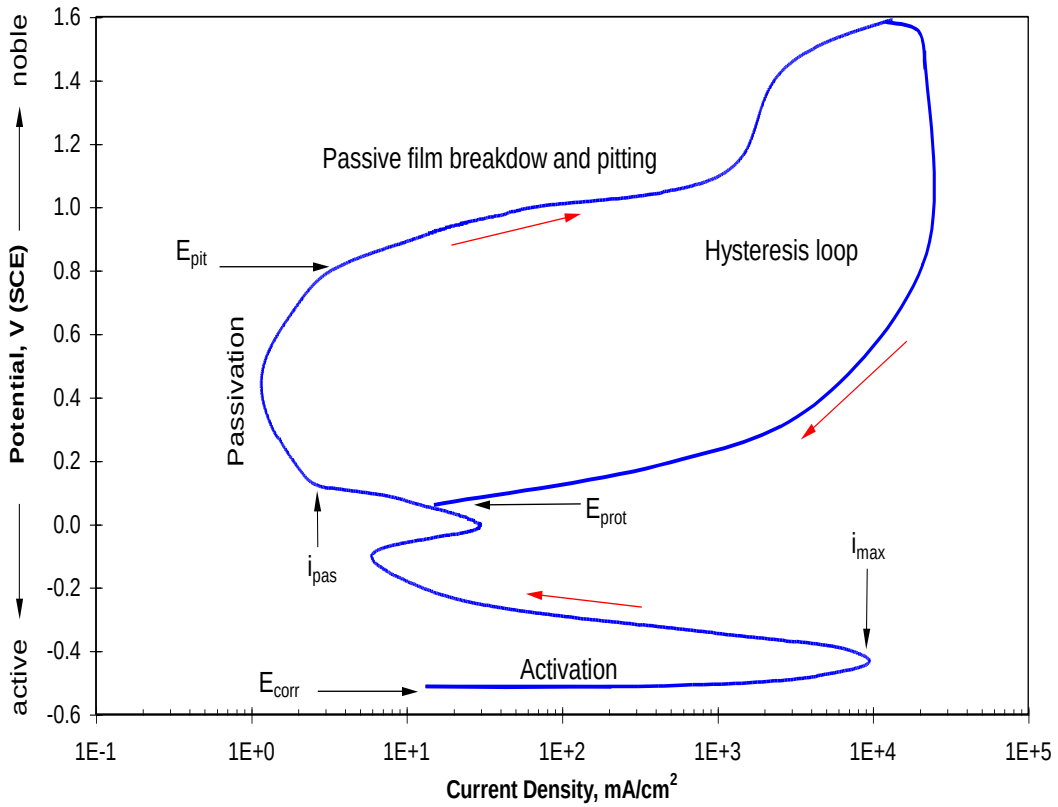

Figure 16: Typical CPP curve of 304 in N_2 purged 1N H_2SO_4 solution[5]

This example has been chosen because it clearly illustrates the various characteristic features of interest to this work. Active corrosion is generally

indicated by a linear anodic curve and coincidence of the forward and reverse scan. The presence of a peak in the anodic portion of the curve, followed by decreasing current generally indicates the onset of passivation. The critical parameters measured for pitting analysis from a CPP curve are the pitting potential (E_{pit}), free corrosion potential (E_{cor}) which is often referred to as the open circuit potential (E_{ocp}) or the rest potential, and protection potential (E_{prot}) which is also sometimes referred to as the repassivation potential, (E_{rp}).

The pitting potential, E_{pit}, also referred to, as the breakdown potential is the potential at which pitting will initiate due to breakdown of passivation. Pitting is characterised by a rapid increase in current with only a small change in potential. The potential at which the current increase was initiated is the pitting potential and the value of E_{pit} is generally taken as the breakdown of passive film in the CPP curve on the forward scan. It should however, be noted that there are other causes for a rapid increase in current such as crevice corrosion and oxidation of water, hence the occurrence of pits on the surface of the working electrode should be verified by visual examination.

The protection potential, (E_{prot}), is the potential at which repassivation occurs (i.e. a stably growing pit or crevice corrosion ceases) during the reverse scan and the current decreases back to (sometimes below) the original passive current density. The value of the protection potential, (E_{prot}), depends on the degree of pitting prior to the reverse scan because the measured repassivation potential decreases with increase in pit depth. Therefore, repassivation potential measured for a very shallow pit might be too high while repassivation potential might be too low for a deep pit[162, 163]. According to Anderko et al[164], “[the reverse dependence of the repassivation potential and the pit depth can be attributed to] ohmic potential drop in the electrolyte in the pit and the current required to maintain an aggressive electrolyte in the pit for sustaining pit growth”. The ohmic potential drop increases with pit depth while the current required to maintain an aggressive electrolyte in the pit decreases.

Anderko et al[164] further stated that the contribution of the ohmic potential drop to the effect of pit depth on the repassivation potential is negligible because the current density at repassivation is low. Also, a significant contribution to the ohmic potential drop occurs within the salt film whose thickness is not

sensitive to pit depth. On the other hand, there is general agreement in literature on the postulation that there is a critical product of current density (i), and pit depth (x) required for sustaining an aggressive pit electrolyte[164]. Therefore, for one dimensional pit, the measured repassivation potential outside the pit, (E_{prot}^{ext}) is given as:

$$\boldsymbol{E_{prot}^{ext} = E_{prot}^{int} + \int i \,.\, \rho dx} \quad (53)$$

Where E_{prot}^{int}, is the potential at the bottom of the pit, and ρ is the resistivity of the electrolyte in the pit. Assuming the dependence of the resistivity of the electrolyte in the pit on pit depth is negligible and considering the product of the current density and pit depth to be a constant (*A*) to sustain a pit, then, the measured repassivation potential outside the pit, (E_{prot}^{ext}) is expressed as:

$$\boldsymbol{E_{prot}^{ext} = E_{prot}^{int} + A\, In(x)} \quad (54)$$

Equation 54 indicates a logarithmic dependence of the repassivation potential and the pit depth. It is however worth noting that although the model predicts a decreased sensitivity for deep pits, it does not predict repassivation potential that is independent of the pit depth for deep pits. The limitation of the model is that it considered ionic transport as the only contributor to potential distribution inside the pit. Several experimental data have confirmed that the repassivation potential becomes insensitive to pit or crevice depth for deep pits[163-168].

In a situation where there had been excessive pitting which could not be repassivated, the protection potential is close to the open circuit potential and sometimes below the open circuit potential. Its value is taken at the point where the reverse scan crosses the passive current measured on the forward scan. Negative hysteresis occurs when the reverse scan current density is less than that for the forward scan while positive hysteresis occurs when the reverse scan current density is greater than that for the forward scan. Positive hysteresis, as depicted in Figure 16, occurs when passive film damage was not repaired and/or pits were initiated. Where the positive hysteresis loop is very large, the protection potential may be close to the corrosion potential, indicating a possibility of pitting corrosion in the test environment.

2.7 Deterministic Modelling of Passivity Breakdown

According to Macdonald[96], *"the deterministic modelling of passivity breakdown as one of the most challenging tasks in corrosion science and electrochemistry because the output of the deterministic theory for passivity breakdown is constrained by relevant natural laws"*. The development of a deterministic theory for passivity breakdown such as the PDM provides an opportunity for predicting localised corrosion damage under conditions that cannot be addressed by empirical methods[101, 151, 169-172]. This goal has been achieved to a significant extent by combining the PDM with a deterministic model for pit growth and assuming a first order kinetic law for delayed repassivation[169].

The damage function provides a convenient definition for the 'failure time' as corresponding to that observation time at which the upper extreme exceeds some critical dimension (e.g. the thickness of a pipe wall). For 'instantaneous' nucleation and growth (i.e. prompt repassivation), the entire population of stable pits nucleate within the first depth increment. The more general case of progressive nucleation and growth (i.e. delayed repassivation) occurs when new (stable) pits nucleate as existing pits grow and die. The ability to separate the damage function into active and inactive components has proven to be of great theoretical importance in developing new strategies to control localised corrosion, because of the emphasis that is placed on the physico-electrochemistry of pit repassivation and survival.

The deterministic prediction of damage is not fully matured; however research work done hitherto demonstrates the practical feasibility of predicting damage in a deterministic manner. This can be further matured into powerful tools for scheduling maintenance, assessing risks, and specifying design parameters in complex industrial systems. Several attempts to elucidate the mechanisms of the formation of passive oxide films have yielded only basic understanding of the chemistry and physics of the growth and breakdown processes.

With the understanding of the common mechanisms for passivity breakdown and the fact that vacancy condensation initiates passivity breakdown, the point defect model provides a robust basis for predicting the occurrence of passivity breakdown in any given system. Realising the importance of the

dissolution of the barrier layer on the model and the ability to differentiate the interfacial reactions on the basis of lattice conservancy, Macdonald combined the point defect model with deterministic models for pit growth and crack growth. By so doing, it became possible to predict the evolution of localised corrosion damage in a wide range of systems.

Until the late nineties, competitive adsorption had been used in conjunction with cation vacancy generation at the metal/film interface to account for the experimental findings. However, based on recent findings, it became necessary to consider the absorption of three absorbed species into surface oxygen vacancies; H_2O resulting in the injection of oxygen ions into the barrier layer, the aggressive anion, X^-, resulting in cation vacancy generation, and the inhibiting species, Y^{z-}, which effectively competes with X^- for the available oxygen vacancies. The equilibria involved for the three absorbed species are written as follows;

$$H_2O + (V_O^{\bullet\bullet})_s \overset{K_o}{\leftrightarrow} (O_o)_s + 2H^+$$

$$X^- \bullet \mathrm{n}H_2O + (V_O^{\bullet\bullet})_s \overset{K_x}{\leftrightarrow} (X_O^{\bullet})_s + \mathrm{n}H_2O$$

$$Y^{z-} \bullet \mathrm{m}H_2O + (V_O^{\bullet\bullet})_s \overset{K_x}{\leftrightarrow} \left(Y_O^{(2-\mathrm{z})\bullet}\right)_s + \mathrm{m}H_2O$$

where $(O_o)_s$, $(X_O^{\bullet})_s$, and $\left(Y_O^{(2-\mathrm{z})\bullet}\right)_s$ are the absorbed species, as expressed in Kroger-Vink notation, and $(V_O^{\bullet\bullet})_s$ represents a surface oxygen vacancy. It should be noted that at least partial dehydration of the anions must occur during the absorption process[96]. Figure 17 shows the reaction scheme for the autocatalytic generation of vacancies at the metal/barrier layer interface, the oxygen vacancies (solid lines) and aggressive anion X^- (broken lines) over the site on the surface where cation vacancy condensation and hence passivity breakdown occurs. Competitive absorption for the surface oxygen vacancies by water, X^-, and the inhibitor, Y^{z-}, is described by the first three reactions at the top of Figure 17. Note that the barrier layer is assumed to comprise of N cation layers with the 0^{th} layer being located at the barrier layer/solution interface and the $-N^{th}$ layer adjacent to the metal/barrier layer interface. Cation vacancy condensation is assumed to occur upon the $-N^{th}$ cation layer. With the cation vacancy annihilation reaction

$$m + V_M^{\mathrm{X}\prime} \overset{k_1}{\rightarrow} M_M + v_m + \mathrm{X}e'$$

where m = metal atom, and v_m = vacancy in the metal phase.

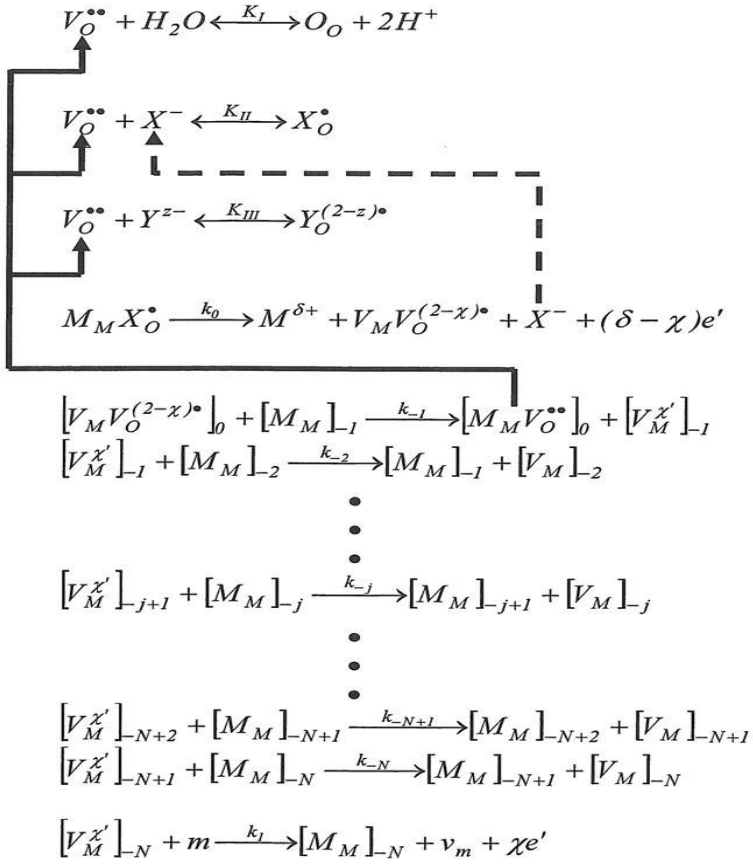

Figure 17: Reaction scheme for the autocatalytic generation of cation vacancies at the metal/barrier layer interface, oxygen vacancies and aggressive anion on the surface where cation vacancy condense[43].

In an effort to study passivity breakdown of 316L SS in the presence of aggressive Cl^- and inhibitive NO_3^-, Macdonald and Yang[43] went further to expand the PDM to include competitive adsorption of aggressive and inhibiting species (such as Cl^- and NO_3^-) into surface oxygen vacancies with the adsorption of X^- culminating in the autocatalytic generation of cation vacancies at the barrier layer/solution interface and subsequent condensation at the metal barrier layer interface[113, 130]. By so doing, they successfully accounted for the critical pitting potential equation that was derived from Nernst equation and expressed as[152]

$$E_{pit} = E_{pit}^{o} - B\log\frac{[Cl^-]}{[A^{z-}]} \tag{55}$$

where E_{pit}^{o} is a constant and is equal to the pitting potential when $\frac{[Cl^-]}{[A^{z-}]} = 1$, B is a constant expressed as $2.303RT/nF$ (in which case R is the universal gas

constant, T is the absolute temperature, F is the Faraday constant) and A^{z-} is the inhibiting oxyanion. The expanded PDM provides clear guidance as to the selection of the most effective inhibitors[96] and can be readily inserted into the pit nucleation function of Damage Function Analysis (DFA)[169], in order to incorporate oxyanion inhibition into the deterministic prediction of localised corrosion damage.

Yang and Macdonald carried out extensive experimental work in the laboratory on the inhibition of chloride ion passivity breakdown on Type 316-SS by nitrate ion in borate buffer solution[74]. CPP tests were performed in deoxygenated NaCl solution containing 0.2M of H_3BO_3 and different concentrations of $NaNO_3$ with the pH adjusted to 8.5. They found out that the critical potential measurements became more reproducible at higher chloride concentration. Their test results indicate that the critical potential rose with increasing H_3BO_3 concentration, with the empirical relationship given as;

$$\boldsymbol{V_c = 0.305 + 0.101 log[H_3BO_3]} \quad (56)$$

Which indicates the buffer itself is an inhibitor of passivity breakdown on Type 316SS in chloride-containing solutions. The expression for critical potential was further expressed as

$$\boldsymbol{V_c = V_o - \frac{\beta}{\alpha} pH - \frac{2.303RT}{\alpha F} log[Cl^-]} \quad (57)$$

where α is the polarisability of the film/solution interface and β is the dependence of the potential drop across the barrier layer/solution interface on pH. By measuring V_c at different pH values and chloride concentrations, α was determined to be 0.338 while β was calculated to be -0.02V. These values are comparable to those previously reported by Lemaitre and Baroux[154] almost 2 decades earlier. Hence, it was confirmed that the critical breakdown potential is a function of $[Cl^-]$ and pH. The excellent agreement of the values for V_0 determined from the two different sources demonstrates the viability of the PDM for describing passivity breakdown on Type 316L SS in chloride-containing solutions. Macdonald and Yang went further to explore the effect of potential scan rate on the critical breakdown potential and found out that the breakdown potential, V_c, increases linearly with $v^{1/2}$, as previously observed by Haruna and Macdonald[126] for nickel, Fonseca et al[173] for

aluminium, Zhang[174] for Type 403 SS, and Zhang and Macdonald[175] also for Type 403 SS, among others[176], and predicted by the Point Defect Model[126]. The theoretical relationship between the critical breakdown potential and potential scan rate can be described by the following equation;

$$\boldsymbol{V_c = 0.198 + 1.71\sqrt{v}} \quad (58)$$

Where v is in units of V/s. For v = 0.5mV/s, the average breakdown potential is 0.236V_{SCE}, which is 0.038V higher than the breakdown potential at zero scan rate; more importantly, is the observation by Haruna and Macdonald[126] and Zhang and Macdonald[175] that the gradient of V_c versus $v^{1/2}$ is essentially independent of the concentration of the aggressive species. Note that the breakdown voltage is a distributed parameter reflecting an underlying distribution in the breakdown sites with regard to the cation vacancy diffusivity[96, 130, 177], it is probably justified to use the measured V_c at a finite voltage sweep rate of, say, 0.5mV/s as a practical way of minimising the number of experiments that must be performed. In any event, the measured breakdown voltage may be corrected to zero scan rate using equation 59. According to the PDM[126], V_c is related to the potential scan rate as:

$$\boldsymbol{V_c\,(V) = \left(\frac{2\xi RT}{J_m \chi F \alpha}\right)^{1/2} v^{1/2} + V_c\,(v = 0)} \quad (59)$$

Using the value of α earlier determined, the value of the critical area (two-dimensional) concentration of condensed vacancies at the metal/barrier layer interface, ξ, can be determined. While J_m is the rate of annihilation of cation vacancies at the metal/barrier layer interface, which should at most be the value of the flux of cation vacancies moving through the passive film from barrier layer/solution interface to metal/barrier layer interface (J_{ca}). However, for a cation vacancy-conducting film (e.g. passive Ni[178]), by measuring the passive current at the point of breakdown (I_{ss}^{bd}), J_{ca} can be calculated using equation 60;

$$\boldsymbol{J_{CA} = \frac{I_{ss}^{bd} N_{AV}}{\chi F}} \quad (60)$$

where N_{AV} is the Avogadro's number and χ = 3, because the passive film is assumed to be defective Cr_2O_3. The value of I_{ss}^{bd} was found to be approximately 2μA/cm^2, J_{ca} was estimated to be 4.1×10^{12} cm^{-2}s^{-1}, and J_m was

at least 4.1×10^{12} $cm^{-2}s^{-1}$. The value of the area (two-dimensional) concentration of condensed cation vacancies, ξ, is therefore at least $2.4\times10^{14}cm^{-2}$. Since the concentrations of cations in the oxide and of metal atoms in the alloy are related to the structures of Cr_2O_3 and the substrate steel, respectively, the values of ξ for vacancy condensation on the cation sub-lattice of the barrier layer on the film side of the interface or on the metal on the substrate side of the boundary lattice were estimated. Considering the fact that the barrier layer on stainless steels comprise of defective chromic oxide, $Cr_{1+x}O_{1-y}$, and recognising that the layer is n-type in electronic character, the principal point defect must be the cation interstitial (x > 0) or oxygen vacancy (y > 0), or both (x, y > 0). They assumed that the metal substrate on the metal side of the interface corresponds to chromium metal. Based on the available structural information, the area atomic density for Cr and Cr_2O_3 were determined to be 1.2×10^{15} cm^{-2} and 4.0×10^{14} cm^{-2}, respectively[174]. These values are in agreement with what was typically observed in other systems[126, 173-175] which further validates the Point Defect Model for describing passivity breakdown.

Based on previous experimental data that the critical breakdown potential, V_c, varies linearly with $log[Cl^-]$, Yang and Macdonald[74] predicted that the critical breakdown potential, V_c, also varies linearly with $log[Cl^-/NO_3^-]$. To confirm their hypothesis, they carried out series of tests on 316L in solutions of NaCl and $NaNO_3$ with borate as the buffering agent and measured critical potential versus $log[Cl^-]$, for solutions with and without nitrate ion.

Figure 18 shows their graph of measured critical potential versus $log[Cl^-]$ for solutions with and without nitrate ion. The linear dependencies are consistent with previous equations for V_c predicted by PDM. The linear proportionality constant between the critical breakdown potential and logarithm of the chloride ion concentration (i.e. slope of the graph of V_c vs. log $[Cl^-]$) was found to be unaffected by nitrate concentration, yielding the same values for the polarisability of the film/solution interface (α), regardless of the nitrate concentration i.e. the fact that the graphs generated for solutions with and without nitrate ion are parallel signifies that the value of α is the same for the two cases.

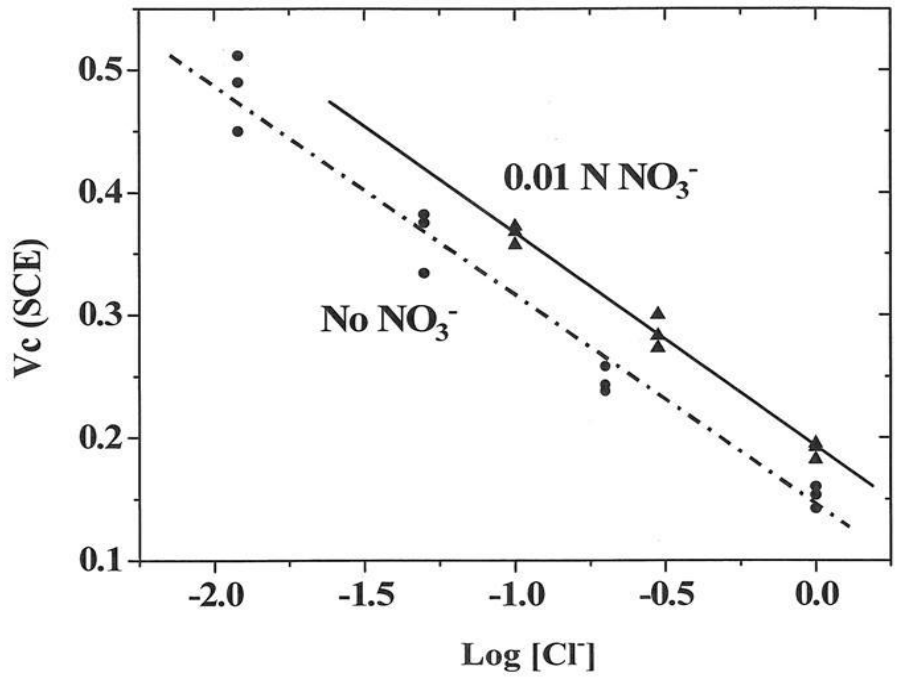

Figure 18: Critical breakdown potential for Type 316 SS in NaCl + borate buffer solution (pH = 8.50 ± 0.05) with and without 0.01N NO_3^-. The voltage scan rate was 0.5mV/s[74]

Similar to the case of V_c versus $log[Cl^-]$, V_c was predicted to decrease linearly with $log[Cl^-/NO_3^-]$ according to the following equation;

$$\boldsymbol{V_c = V_o - \frac{\beta}{\alpha} pH - \frac{2.303RT}{\alpha\alpha_o F} log\left(\frac{[Cl^-]}{[NO_3{}^-]}\right)} \quad (61)$$

where α_o is the transfer coefficient for the cation ejection reaction which was calculated to be 0.994. The value of $\alpha_o \approx 1$ signifies a strong potential dependence. Hence, ejection of the cation from the barrier layer to form $(M_M)_{p-1}\,(V_M V_O)^{(2-\chi)\bullet}$ at the barrier layer/solution interface is a charge transfer process, presumably leading to the formation of Cr (IV) or Cr (VI) in the solution[43]. If the latter is the case, the process might be labelled "chloride catalysed localised transpassive dissolution", in recognition of the fact that transpassive dissolution appears to coincide with the electrochemically mediated ejection of chromate [Cr (VI)] from the surface and concomitant oxidative dissolution of the barrier layer[179]. Substituting calculated values from experimental result into equation 61, the critical breakdown potential was expressed as:

$$\boldsymbol{V_c = 0.543 - 0.176\, log\left(\frac{[Cl^-]}{[NO_3{}^-]}\right)} \quad (62)$$

With the chloride concentration fixed at 0.3M, the critical breakdown potential was measured as a function of the concentration of nitrate, as shown in Figure 19.

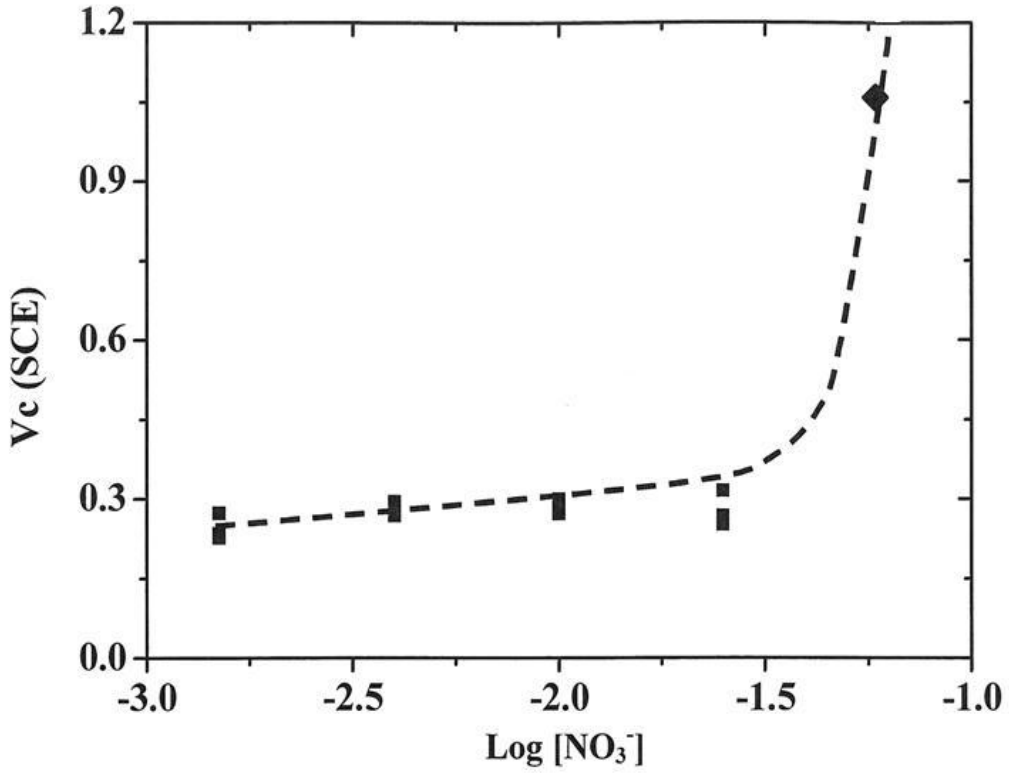

Figure 19: Critical breakdown potential for Type 316 SS as a function of nitrate concentration at ambient temperature (22 ± 2°C) and at pH = 8.50±0.05. The voltage scan rate was 0.5mV/s[74]

At low nitrate concentrations, the critical breakdown potential increased slightly with increasing nitrate concentration but, at a concentration of 0.06M, the critical breakdown potential increased sharply and pitting attack was no longer observed above nitrate concentration of 0.06M. Dahan also reported a similar result for Type 316 SS[180]. This is in agreement with findings from other authors that there is a critical chloride/nitrate concentration required to prevent pitting. Though expected, it is interesting to know that the phenomenon can be directly linked to the breakdown potential of the passive film.

Macdonald and Yang[43] interpreted the sudden increase in V_c as an indication of saturation of the surface oxygen vacancy absorption sites at the barrier layer/solution interface, such that chloride ions were excluded, at least at those sites at which breakdown occurred.

Several studies and experimental evidence indicate that certain oxyanions, such as nitrite (NO_2^-), nitrate (NO_3^-), chromate (CrO_4^{2-}), and sulphate (SO_4^{2-}), inhibit the ability of chloride ion to nucleate pits upon a metal surface (e.g. Fe) by displacing the critical pitting potential in the positive direction and also increasing the induction time at a constant potential[152-156].

The fact that oxyanions have been postulated to absorb into surface oxygen vacancies, hence capable of catalysing cation ejection and generate an enhanced flux of cation vacancies across the barrier oxide layer which, ultimately leads to passivity breakdown has raised the puzzling question as to why the oxyanions themselves do not induce passivity breakdown in a manner that is similar to that for chloride ion. Macdonald and Yang[43] could not provide an adequate answer. However, they postulated that oxyanion absorption is irreversible, and hence cannot aid in cation extraction.

To further verify the viability of the point defect model for accounting for passivity breakdown on Type 316 SS, Macdonald and Yang[43] went further to measure the voltage scan rate dependence of the critical breakdown potential, from which the critical area concentration (two dimensional) of condensed vacancies at the metal/barrier layer interface was derived, and found the experimental value to be in good agreement with those calculated using PDM. Exploring a better answer to the puzzling question is not within the scope of this research work. However, the relationship between the critical breakdown potential and the nitrate concentration would be extended to nitrite concentration to verify the hypothesis that nitrite is an anodic inhibitor and possibly used as a tool to determine the critical nitrite concentration required to inhibit on Type 13Cr-L80 and 25Cr Stainless steel.

Also in the course of this research work, the effect of nitrate/nitrite on the passivity breakdown would be explored further since passivity breakdown is the precursor to the development of all localised corrosion events on metal and alloy surfaces in contact with aggressive aqueous solutions.

Although the processes involved are reasonably well understood[96, 113], the observation that certain species inhibit passivity breakdown has not been fully accounted for theoretically.

2.8 Pitting Resistance

Pitting resistance equivalent number (PRE_N) is a theoretical way of comparing the pitting corrosion resistance of various types of stainless steels, base on their chemical compositions. One of the several ways of expressing the pitting resistance equivalent number of an alloy is given as follows:

$$PRE_N = Cr + 3.3(Mo) + 16(N) \quad (63)$$

Where: Cr is the chromium content, Mo is the molybdenum content and N is the nitrogen content all in weight percent, (%) of elements in solid solution.

Corrosion resistance of alloys in aggressive seawater conditions is of great importance in offshore structures, pipelines, equipment and other subsea hardware. Corrosion resistant alloys (CRAs) exhibit good resistance to CO_2, H_2S and other corrosive species. However, some of them are prone to pitting and crevice corrosion in oxygenated seawater.

Series of tests performed on a wide range of materials showed that only corrosion resistant alloys with high pitting resistant equivalent number, PRE_N are immune to aerated seawater corrosion[5]. These alloys include Hastelloy G-3, Hastelloy C-276 and Inconel 625. Other alloys with low PRE_N like Inconel 825 and duplex stainless steels have limited immunity to pitting and crevice corrosion in aerated seawater. In aerated seawater, $PRE_N \geq 40$ is required to adequately provide pitting resistance. Typical seawater temperature is in the range of 20-30^oC, hence alloys with intermediate PRE_N such as AISI 304, 316L, 718, 825 and 13Cr stainless steel are susceptible to pitting and crevice corrosion in aerated seawater but suitable for use in fully de-aerated seawater[5].

Corrosion Test Data for Critical Pitting Temperature determined using ASTM G150[181] and Critical Crevice Temperature determined using ASTM G48B[182] published by ATI Allegheny Ludlum in their technical data blue sheet for lean duplex Stainless steel ATI 2102^{TM} Alloy[183] are shown in Figure 20 and Figure 21. The figures show the critical pitting temperature (CPT) and the critical crevice temperature (CCP) for AISI 316L, AISI 317L, S32003 and S32205 stainless steel in the form of bar charts.

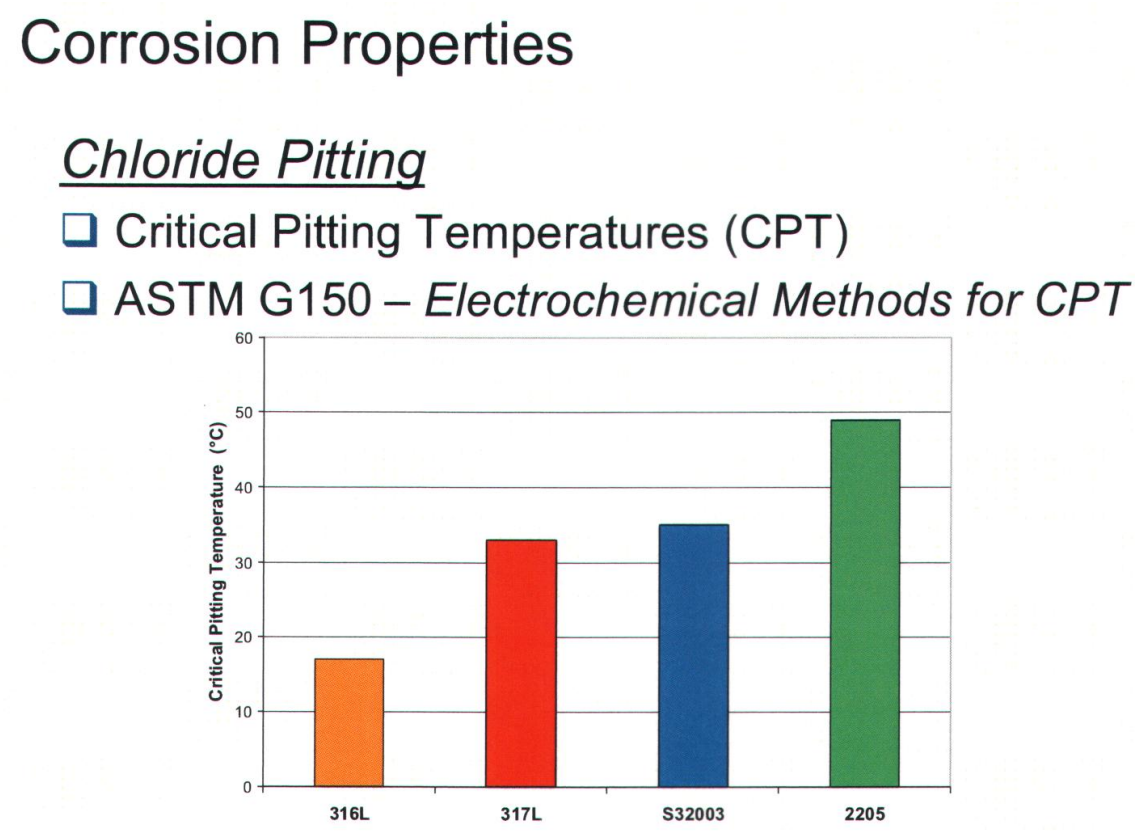

Figure 20: CPT per corrosion data published by ATI Allegheny Ludlum[183]

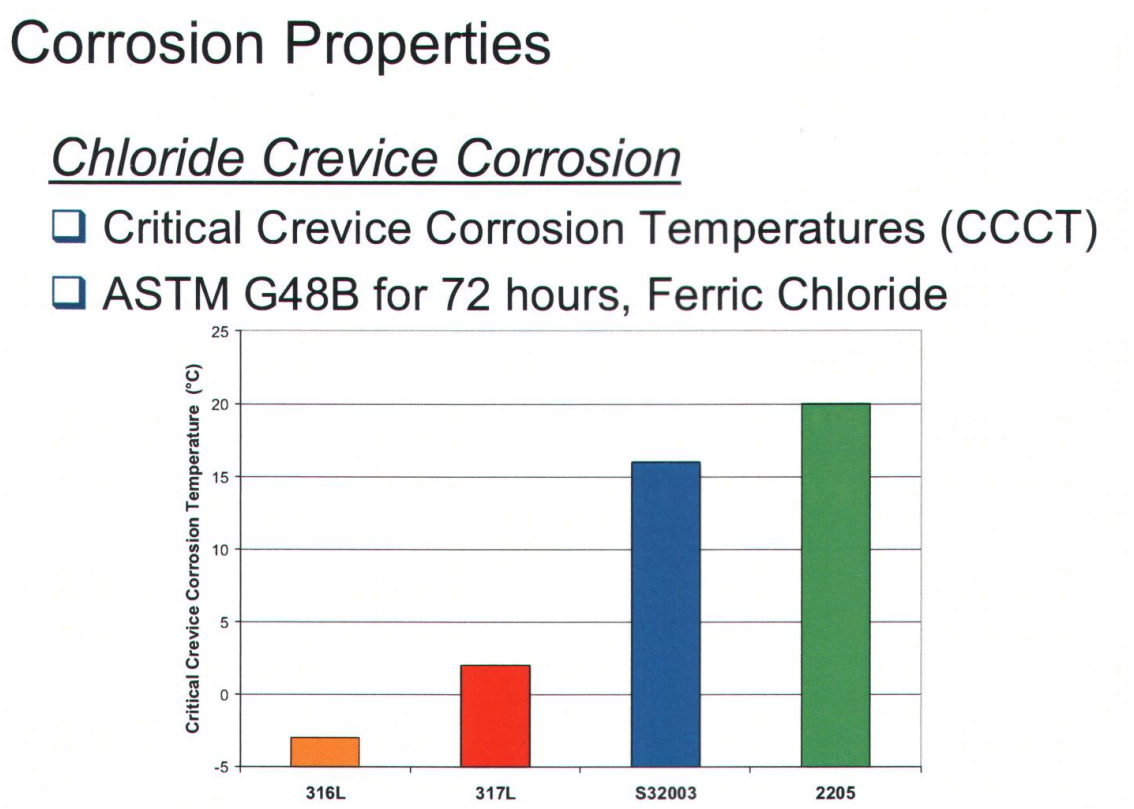

Figure 21: CCCT per corrosion data published by ATI Allegheny Ludlum[183]

2.9 Stress Corrosion Cracking

According to Newman and Procter[184], *"stress corrosion cracking [SCC] is defined as the growth of cracks due to simultaneous action of a stress (nominally static and tensile) and a reactive environment. For metals, the term "reactive" excludes gaseous hydrogen, cathodic polarisation, and liquid metals (liquid metal embrittlement) but includes aqueous and non aqueous electrolytes and reactive atmospheres H_2O, I_2, Cl_2). Static stress includes slow mono-atomic straining or low amplitude cycling known as ripple loading, which accelerates SCC in many metallic systems by promoting oxide film rupture at the crack tip"*.

In practice, stresses arise from either applied loads or residual stress due to welding or non homogeneous plastic deformation. Plasticity plays a key role in SCC of metals unlike the case of inorganic glasses and ceramics that are brittle and crack via reaction of the corrodent with highly stressed bonds at an atomically sharp crack tip[185]. The phenomenon of metal induced fracture, (formerly known as liquid metal embrittlement) is of interest to engineers and scientists however, there is no agreement on its mechanism or relationship with SCC. Magnin and Lepinoux[186] proposed universal models for SCC and fatigue while Lynch[187], and Galvele[188] proposed universal models for environmental assisted fracture in aqueous, gaseous and liquid metal environments. However, according to Newman and Procter[184], these models are not universal since they only apply to particular systems.

Crack initiation and subcritical propagation in structural materials is due to synergistic actions of stress, microstructure of the material and the environment. The mechanisms of crack initiation and propagation have been extensively investigated especially the case of stressed alloys in environments that contain high concentration of anions such as chlorides, phosphates and hydroxides, either in bulk environment (e.g. in the paper, chemical, petrochemical and marine industries) or in localised environments gradients in electrochemical potential, concentration gradient of aggressive species and stress concentration[184]. However, according to Marcus[189], *"it has been recognised that environmentally assisted cracking under static loading (stress corrosion) or cyclic loading (fatigue) can occur in ultra high purity water*

even when the concentration of anions apart from hydroxide is < 10ppb". Although susceptibility to cracking is generally lower in low concentrations than in concentrated environments, it is sufficient to cause concern especially when extended lives or high plant availability is required. There had been several disasters as a result of stress corrosion cracking. It is considered to be a very dangerous form of corrosion because of the marked loss in mechanical strength as a result of very little metal loss; cracks can propagate very fast leading to catastrophic failures. Also, the damages resulting from stress corrosion cracking are typically not obvious during casual inspection.

Fortunately, SCC requires simultaneous occurrence of three conditions: presence of a susceptible material, an environment that causes SCC for that material, and sufficient tensile stress to induce SCC. As shown in Figure 22, elimination of any of the three conditions prevents SCC. Consequently, SCC is relatively rare, but when failure occurs due to SCC, it can be very costly and destructive.

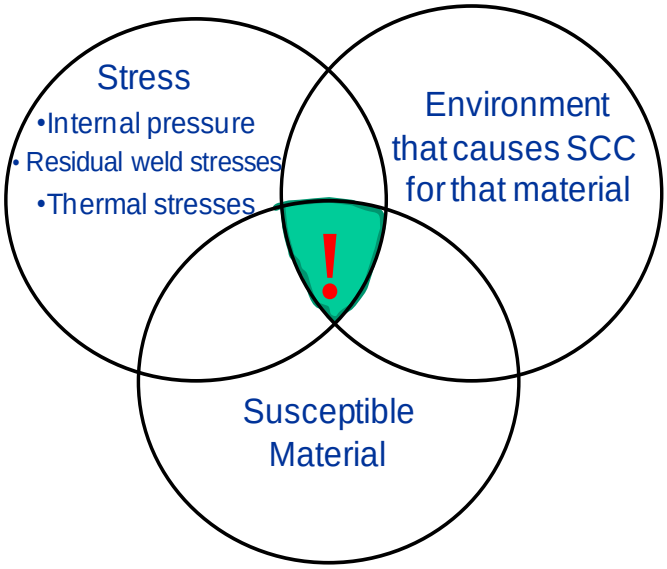

Figure 22: Requirements for occurrence of Stress corrosion cracking

Typically, the first line of defence to stress corrosion cracking is proper materials selection during the design stage. Hence, materials that are susceptible to SCC in the service environments are avoided. Unfortunately, it is not always that simple, some environments are very aggressive (e.g. high temperature water), and most materials are susceptible to SCC. Also some applications require materials with high yield strength which can be very

difficult match with resistance to environmentally assisted cracking such as hydrogen embrittlement.

As shown in Figure 22, elimination of stress (or at least reduction to below the threshold limit for SCC) is another method that can be used to control SCC. Unfortunately this is only feasible in a situation where the stress required for cracking is a residual stress introduced during fabrication process such as welding or forming but, not working stresses that the component is intended to support (e.g. tensile stress in a riser column or umbilical).

For materials with relatively high threshold stress for most environments such as carbon steels, it is relatively easy to reduce the residual stresses to a low enough level with proper fabrication and heat treatment (stress-relief annealing). In contrast, some materials such as austenitic stainless steels have very low threshold stress for chloride SCC which is difficult to achieve with heat treatment. Also, the high annealing temperatures required for stress relief causes other corrosion problems, such as sensitisation and sigma phase embrittlement. Hence, stress relief is not considered a suitable method for controlling SCC for austenitic stainless steels. The logistics and availability of furnaces that are big enough makes full stress-relief annealing difficult and sometimes impossible for large structures hence, partial stress relief around welds and other critical areas are typically carried out using techniques such as induction heating. To avoid creation of new regions of high residual stress, expert advice must be sought to ensure partial stress relief is done in a controlled manner.

Stress relief can also be done mechanically either by hydrostatic testing the material slightly beyond its yield stress, or by shot-peening (or grit-blasting) thereby applying a uniform compressive stress to the entire surface of the material. This tends to ‘even-out’ the stresses and eliminate peak residual stresses if done correctly.

The most direct way of preventing SCC is to control or change the environment that causes the susceptible material to crack but unfortunately, it is rare to have control over the active species that are present in the environment causing the problem.

2.10 Stress Corrosion Cracking Mechanisms

Environmentally assisted cracking like most other localised phenomena has the initiation and propagation periods. To a large extent, the demarcation between these two periods is arbitrary. According to Marcus[189], *"the initiation period is defined as the time at which a crack is detected or when the load has relaxed a specific amount in a strain controlled test*. *[In both cases], the definition of initiation corresponds to a crack depth of significant metallurgical dimension that is greater than or equal to 2mm"*. For modelling purposes, initiation is assumed to be associated with microscopic crack formation at localised corrosion or mechanical defect sites generally associated with pitting, intergranular attack, scratches, weld defects and design notches. It is also generally assumed that there is very high probability that such initiation sites exist (or develop) relatively early in the life of a component. Hence the problem of life prediction requires understanding the growth of small cracks to form a major crack which gets propagated or arrested depending on the specific material, environment and stress conditions.

Figure 23 shows the proposed sequence of crack initiation, coalescence, and growth for steel undergoing subcritical cracking in aqueous environment.

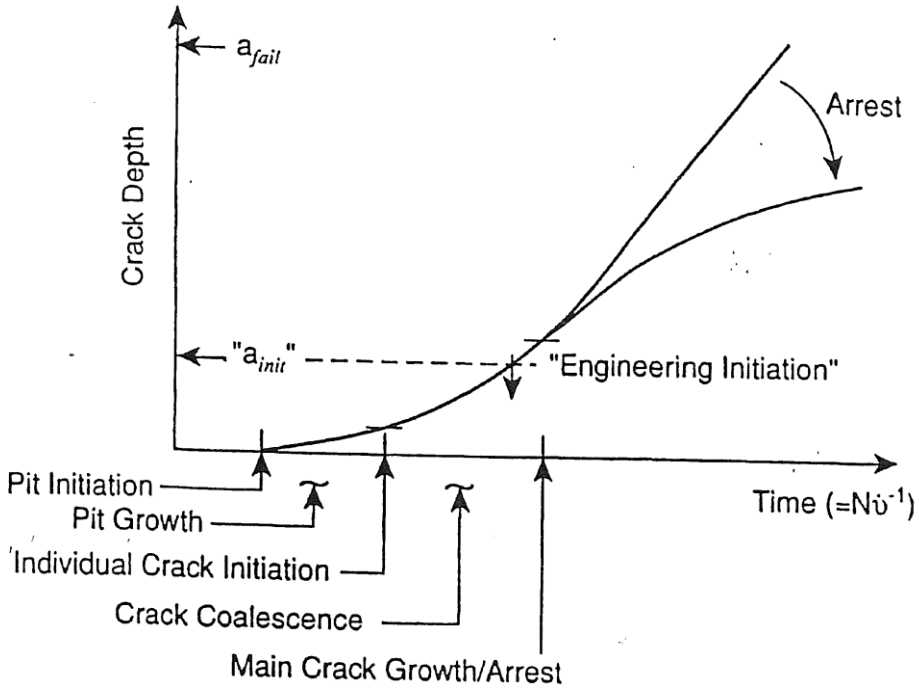

Figure 23: Sequence of crack initiation, coalescence, and growth for steel undergoing subcritical cracking in aqueous environments[189].

An increased resistance against pitting could lead to a delay of crack initiation if cracks are initiated at pits[190]. Fatigue crack can be initiated by a stress corrosion crack[191]. Stress corrosion cracking and corrosion fatigue are strongly linked, both phenomena show similar mechanisms. Various evidence in literature show that corrosion fatigue interferes with SCC especially during crack initiation and propagation[190-195]. Hitherto, there has been very little fundamental work on the growth of microscopically short cracks. Most of the work done had been under fatigue loading with emphasis on the micro-structural interactions required for microscopic crack arrest or propagation, and modifications to linear elastic fracture mechanics analyses to account for the observed behaviour in the range of crack size.

In the area of environmentally assisted cracking, the coalescence of microscopic cracks had been investigated for carbon steel in carbonate-bicarbonate solutions[196, 197], stainless steels and nickel based alloys in high temperature waters[198]. According to Andersen and Vasatis[198], “in all the investigated cases, crack growth rate increased as the cracks coalesced and approached a steady state value when the mean crack depth was about 20-50μm. Thereafter, the crack is termed to be a “deep crack” (~ one grain diameter or more) and its propagation rate could be analysed in terms of linear elastic fracture mechanics”. It should however be recognised that the resultant life prediction could be conservative because the microscopic crack initiation and crack coalescence periods were not taken into account.

According to Ford[199, 200], *"the premise for crack propagation mechanisms for ductile alloys in aqueous solutions is that the crack tip must propagate at a rate faster than the corrosion rate on the unstrained sides in order for the crack not to degrade into a blunt notch*”. The suppression of SCC and fatigue in many systems are attributed to blunting of the cracks during the early stage[189]. A classical illustration is the resistance of mild and low alloy steels to SCC in acidic or concentrated chloride solution except when corrosion blunting is counteracted with chromium or nickel alloying addition[201]. Similarly, at low temperature, carbon steel is not susceptible to SCC in oxygenated high purity water systems because the embryo crack is blunted by pitting. However, at high temperature (above 150^{o}C), cracking is possible due to the

formation of magnetite, Fe_3O_4 which constitute the inner protective film of the duplex surface oxide[202]. As a result, according to Parkins et al[201], *"the material-environment conditions for cracking can be defined based on the thermodynamic criteria for the existence of a protective oxide, salt, or compound film on the crack sides. For example, cracking susceptibility of mild steel in hydroxide, carbonate-bicarbonate, nitrate, phosphate, and molybdate solutions can be predicted in specific potential-pH range where the protective film is thermodynamically stable"*. Similar argument can also be made of the kinetics which requires that the electrochemical reaction rates (e.g. dissolution or oxidation) at the strained crack tip to be significantly higher than those on the crack sides for the crack to propagate[189].

In the late sixties and early seventies, numerous crack propagation mechanisms (such as the pre-existing active path mechanisms, strain assisted active path mechanisms, to hydrogen embrittlement mechanism) were proposed by several authors[203-206]. However with more sensitive experimental and analytical capabilities within the last 2 decades, many of the earlier cracking hypotheses have been shown to be flawed. Only three mechanisms of environmentally assisted crack propagation have been shown to be consistent with experimental data; the slip dissolution, film induced cleavage and hydrogen embrittlement[189]. Other important models involve micro-cleavage[186] or plastic micro-fracture[187] induced by dissolution or adsorption that is more difficult to test experimentally. The surface mobility[188] is another model but there appears to be serious problems with the basic physics of the model[207], although not necessarily with the general concept. Several crack advance theories have been proposed to relate crack propagation to oxidation rates and the stress-strain conditions at the crack tips. Correlation between the average oxidation current density on a strained surface and the crack propagation rate for a number of systems has been used to support these theories[200, 208].

2.10.1 Slip Dissolution mechanism

The slip dissolution model relates the crack propagation to oxidation that occurs when the protective film at the crack tip is ruptured. The model

assumes crack growth occurs by extremely localised anodic dissolution[209-213]; the sides of the crack are protected by a film, (usually an oxide) that is fractured as a result of plastic strain in the metal at the crack tip. Crack growth proceeds by a cyclic process of film rupture, dissolution, and film repassivation.

In most aqueous systems, the protective oxide repassivate at the bared surface and the rate of total oxidation (and crack tip advance) decreases with time. Crack propagation can only be maintained if the protective film ruptures again. Quantitative prediction of the crack propagation rate is based on the relationship between the oxidation charge density on a surface and the amount of metal transformation from the metallic state to the oxidised state. Hence, for a given crack tip environment, corrosion potential and material condition, the crack propagation rate is controlled by the change in oxidation charge density with time and the frequency of film rupture at the strained crack tip. The frequency of film rupture at the strained crack tip is determined by the fracture strain of the film (ϵ_f), and the strain rate at the crack tip, ($\dot{\epsilon}$). According to Faraday's law, the average environmentally controlled crack propagation rate, ($\bar{V}_T$), can be related to the oxidation charge density passed between film rupture events, (Q_f), and the strain rate at the crack tip, ($\dot{\epsilon}$) as:

$$\bar{V}_T = \frac{M}{n\rho F} \cdot \frac{Q_f}{\epsilon_f} \dot{\epsilon} \quad (64)$$

Where M and ρ are the atomic weight and density of the crack tip metal respectively, F is the Faraday's constant and n is the number of electrons involved in the overall oxidation of an atom of the metal.

The oxidation charge density on a bare metal surface varies with time at a rate that depends on the material and the composition of the environment that controls the passivation rate of the crack tip; hence equation 64 can be expressed in terms of power law relationship as:

$$\bar{V}_T = A(\dot{\epsilon})^z \quad (65)$$

Where *A* and *z* are constants that depends on the material and environment compositions at the crack tip. They are related to the oxidation reaction rates or current densities in the specific crack tip material-environment system[214].

Once the passive film is ruptured, the initial dissolution current density i_o at the bare surface is high for a short time t_o, thereafter, oxide formation or precipitation leads to decay in the oxidation current density. The current density i_t at time, (t), can be expressed as follows using a general power law relationship:

$$\boldsymbol{i_t = i_o \left(\frac{t}{t_o}\right)^{-z}} \quad (66)$$

This equation provides the quantitative basis for the empirical observation relating oxidation current density on a straining surface and the crack propagation rate.

For alloys in concentrated solutions under dynamic straining conditions, if a bare surface condition is maintained at the crack tip (i.e $\epsilon_f/\dot{\epsilon} < t_o$), then integrating equation 66, the maximum predicted crack propagation is given as:

$$\boldsymbol{\overline{V}_{max} = \frac{M}{n\rho F}\, i_o} \quad (67)$$

In relatively dilute solution, the passivation rate will be high, hence, z will be high, while t_o will be short. Under constant load or displacement conditions, the periodicity of oxide rupture, $(\epsilon_f/\dot{\epsilon}) >> t_o$. In this situation, a bare surface will not be maintained at the crack tip, and the crack propagation rate is given as:

$$\boldsymbol{\overline{V}_T = \frac{M}{n\rho F} \cdot \frac{i_o t_o^z}{(1-z)\epsilon_f^z}\, \dot{\epsilon}^z} \quad (68)$$

Equation 68 is an expanded version of equation 65 and relates the parameters *A* and z to the specific oxidation rates and the fracture strain of the oxide at the crack tip.

Under constant load or displacement conditions, the crack tip strain rate can be related to the creep processes at a moving crack tip[214] while under monotonically or cyclically changing bulk strain conditions, $\dot{\epsilon}$ can be related to an applied strain rate $\dot{\epsilon}_{app}$. Hence, the slip dissolution mechanism can be applied not only to stress corrosion but also to strain induced cracking[215] and corrosion fatigue. However, under cyclic loading conditions, the crack is also moving forward due to irreversible cyclic plastic deformation such as fatigue striation formation. According to Marcus[189], the mechanical crack propagation

is independent of the crack propagating by oxidation processes [hence], the crack propagation and oxidation crack propagation mechanisms are considered additive. According to Sieradzki and Newman[216], "the faradaic equivalent of the oxidation change density at the strained crack tip is not sufficient to account for the observed crack propagation in some incidences of transgranular cracking". Also, the cleavage-like crystallographic features observed on fractured surfaces were difficult to convincingly rationalise in terms of dissolution oxidation model hence, several authors[216-220] have proposed that transgranular environmentally controlled crack propagation may occur by a combination of oxidation and brittle fracture mechanism. Slip dissolution was initially favoured for both intergranular and transgranular SCC in a wide variety of systems[208]. Lately, it is mainly applied to intergranular cracking of ferrite steels in passivating environments like carbonate-bicarbonate solution[199, 213] and sensitised stainless steel[220].

2.10.2 Film Induced Cleavage Mechanism

The suggestion by Edeleanu and Forty[220] that superficial dezincfication of α-brass in ammonia solution could trigger a brittle fracture through several micrometers of the un-attacked substrate was the origin of the film induced cleavage model. The authors believed the material through which the crack propagated between slip bands was embrittled by short range ordering. Using optical microscopy, they postulated the crack jumping phenomenon which was later confirmed by Beavers and Pugh[217], and others[221-224], using scanning electron microscope (SEM).

According to Sieradzki and Newman[216], "*in the modern theory of film induced cleavage, there is no special property of the face centred cubic (fcc) substrate through which the crack jumps; the special properties actually lie in the thin film itself and must be able to trigger a crack with a velocity of hundreds of meters per second within less than 100nm"*.

According to Newman and Satio[212], "nano-porous metallic layers produced by de-alloying have been effective because they can be brittle and epitaxial, or at least strongly bonded to the substrate". Tests of the film induced cleavage model have relied on producing single shot brittle events through thin alloy

foils which have shown that intergranular fracture can also be triggered by de-alloyed layers in gold alloys[212, 225-231]. The general consensus is that the reality of the phenomenon is well established however, film induced fracture might actually involve slower and more plastic process than originally envisaged by Sieradzki and Newman[216].

In the film induced cleavage mechanism, the crack front is envisioned to move forward by an oxidation process controlled by the same rate determining steps as those in the slip dissolution model. However, when the film ruptures, the crack in the film may rapidly penetrate a small amount, a*, into the underlying ductile metal matrix as shown in Figure 24 which shows the schematic illustration of the elements of the film induced cleavage mechanism of crack propagation. The figure also shows the similarity of the film induced cleavage mechanism and the slip dissolution mechanism during the initial stages of the crack propagation cycle. For the film induced cleavage mechanism, the average environmentally controlled crack propagation rate, ($\bar{V}_T$), is obtained by modify equation 64 used for the slip dissolution model:

$$\bar{V}_T = \left(\frac{M}{n\rho F} Q_f + a^*\right).\frac{\dot{\epsilon}}{\epsilon_f} \quad (69)$$

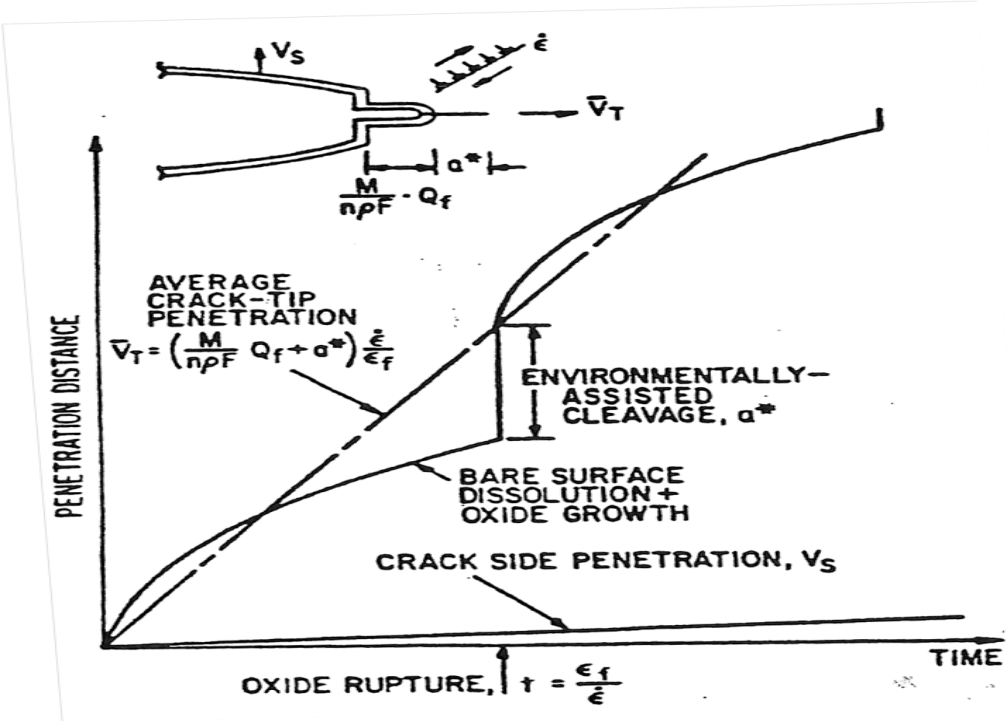

Figure 24: Illustration of the elements of the film induced cleavage mechanism of crack propagation[189]

According to Sieradzki and Newman[216], "*the extent of the additional film induced cleavage component of the crack propagation, a*, is governed by the state of coherence between the surface film and matrix, the fracture toughness of the substrate, the film thickness, and the initial velocity of the cleavage crack emerging from the surface film*".

Traditionally, the surface film has been considered to be an oxide. However, recent investigation by Newman[219], Thompson and Bernstein[232] have shown that de-alloyed films (e.g. copper rich films in CU-Zn or nickel rich film in Fe-Cr-Ni alloys) can exhibit passive behavior and be very brittle. According to Marcus[189], "the extent of cleavage propagation into the matrix has been estimated to be in the order of 1μm depending on the plasticity and micro-structural factors".

2.10.3 Hydrogen Embrittlement Mechanism

Several different theories have been proposed to explain the detailed mechanisms of hydrogen embrittlement. However, the distinction between SCC and hydrogen embrittlement is rather arbitrary because the mechanisms of SCC are often not certain, and many failures that are actually due to the effects of hydrogen have conventionally been ascribed to SCC. When cracking is clearly a result of hydrogen absorption, it is termed hydrogen embrittlement. Application of cathodic protection to metallic components can lead to generation of hydrogen at the metal surface. The amount of hydrogen generated and rate of hydrogen ingress into the metal component is a function of the environment (in particular pH and oxygen content), the type of metal, applied current density and over-potential generated. Dissolved hydrogen concentrate in regions of high stress concentration (such as notches or crack-tips) lead to reduced strength and toughness of the metal at these locations. However, when the crack propagation is too fast, the crack could actually leave the region of high hydrogen concentration. On the other hand, due to hydrogen charging and diffusion, hydrogen concentration can keep pace with slower growing cracks such that, the region around the crack tip is always embitter[233]. As stated by Chuang et al[234, 235] and Tsay et al[236], "resistance of steel to hydrogen embrittlement is largely affected by hydrogen concentration in trapping sites contained by their microstructure". Trapped

hydrogen interactions with micro-structural heterogeneities (which are potential trapping sites for the diffusing hydrogen) initiate a series of actions that eventually lead to failure. The interaction of hydrogen with these sites affects the hydrogen embrittlement resistance of steels.

According to Serna et al[237], "the build-up of molecular hydrogen at these sites promotes micro void initiation by fracturing particles or weakening of the particle-matrix interfaces. In contrast, metals containing strong traps that are more diffusedly distributed, even when they are occupied with hydrogen, generally exhibit little susceptibility to embrittlement".

According to Kerns et al[238], "hydrogen absorption is clearly responsible for SCC of high strength steel in aqueous environment, notably in the presence of H_2S where almost all the discharged hydrogen is absorbed by the metal due to poisoning of the recombination reaction ($H_{ad} + H_{ad} = H_2$) by sulphur adsorption[239]. Once hydrogen is absorbed into the metal, it can promote cleavage, intergranular separation or a high localised plastic fracture". However, transgranular SCC of stable austenitic stainless steel at high temperatures such as 300^oC does not have any correlation with its susceptibility to hydrogen embrittlement[189].

According to Ford[240], "the subcritical crack propagation rate due to hydrogen embrittlement in aqueous environments depends on sequence of events [as illustrated in Figure 25]; diffusion of a reducible hydrogen containing specie such as H_3O^+ to the crack tip region, reduction of the hydrogen containing ions to give adsorbed hydrogen atoms, absorption of the hydrogen atom (H_{ad}) followed by interstitial diffusion of these hydrogen atoms to a "process" zone at a distance (X) in front of the crack tip, localised crack initiation within the "process" zone once the hydrogen concentration in the "process" zone has reached the critical level (C_{crit}) over a critical volume, (d_{crit}), and rapid crack propagation back to the main crack tip[241]".

The hydrogen embrittlement models predict discontinuous crack propagation at an average rate, ($\bar{V}_T$) given as:

$$\bar{V}_T = \frac{X}{t_c} \tag{70}$$

Where X is the distance from the main crack tip to the "process" zone and t_c is the time for the concentration of the absorbed hydrogen, C_H, to reach a critical value, C_{crit}, over the volume d_{crit}.

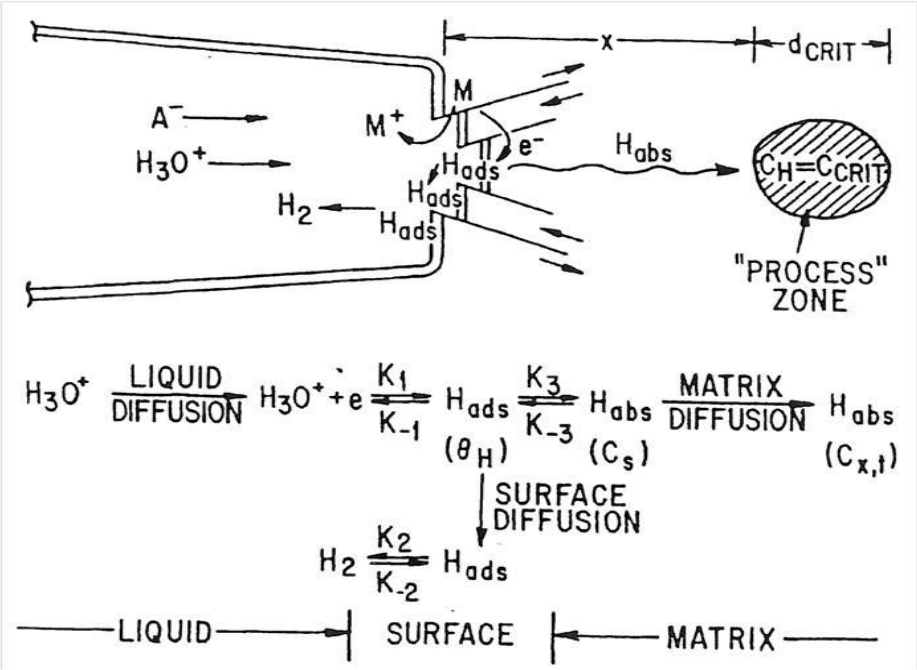

Figure 25: Schematics of various reactions at the crack tip associated with hydrogen embrittlement mechanisms in aqueous environments[214].

Similarly, other specific stress corrosion cracking processes have acquired their own names e.g. 'season cracking' for the cracking of brass in environments containing ammonia, 'caustic cracking' for the cracking of steel in strong alkalis etc.

Another mechanism for SCC is active path dissolution. This process involves accelerated corrosion along a preferred path of higher than normal corrosion susceptibility, with the bulk of the material typically being passive. The most common active path is the grain boundary, where segregation of impurity elements can make it marginally more difficult for passivation to occur. For example, when an austenitic stainless steel has been sensitised by precipitation of chromium carbide along the grain boundary, the local chromium concentration at the grain boundary is reduced, and this region will slightly be more difficult to passivate. Consequently, the grain boundary preferentially corrodes, with the specimen surface and the crack walls remaining passive. This process can occur in the absence of stress, giving

rise to intergranular corrosion that is uniformly distributed over the specimen. The effect of the applied stress is mainly to open up the cracks, thereby allowing easier diffusion of corrosion products away from the crack tip hence, allowing the crack tip to corrode faster. According to Cottis[242], "*active path corrosion processes are inherently limited by the rate of corrosion of the metal at the crack tip, which limits the maximum crack growth rate to around 10^{-2} mm/s, and crack growth rates are often much lower, down to around 10^{-8} mm/s (about 0.3mm/y) or less"*.

Bursle and Pugh[243] reviewed several different stress corrosion cracking (SCC) models and concluded that the film rupture model[208, 244] involving anodic dissolution at the crack tip explains most examples of intergranular SCC. The principal feature of rupture model is that the protective surface film in the vicinity of the crack tip is ruptured by localised plastic deformation but the protective film away from the crack tip remains intact. Consequently, an electrolytic cell is created with the bare metal at the crack tip acting as the anode and the unbroken passive film adjacent to it acting as the cathode, which is sacrificially protected by the exposed bare metal at the crack tip. As a result, the exposed bare metal suffers rapid anodic dissolution which allows the crack to grow. According to Macdonald and Yang[43], "the rate of anodic dissolution and associated crack extension depends partly on the repassivation rate. SCC process is known to be maximised at intermediate passive rates. When the rate of repassivation is low, the crack tip becomes blunt because of excessive dissolution on the crack sides. On the other hand, when the repassivation rate is high, the amount of crack tip penetration per film rupture event is minimised". Hitherto, SCC observed due to the presence of nitrate is intergranular in nature.

2.11 Effect of Stress Intensity Factor on the rate of SCC

Various analytical methods have been used to evaluate the critical value of plane-strain stress intensity factor (K_I). Gdoutos[245] plotted the stress-strain curve and determined the yielding load using the load-displacement data from the notched slow strain rate test. He took the yielding load as the point of crack initiation. The diameter of the fractured specimens was measured from the SEM micrographs of the final surface. The portion of the stress-strain

curve between the yielding load and the final load (plastic component) was used to generate a second-order polynomial fit which was later used to generate the corresponding polynomial equation. The J-Integral area or the fracture energy area was determined by integrating the resultant equation given as follows:

$$\boldsymbol{J = \int \sigma d\varepsilon = \oint_C \frac{F}{A} \frac{du}{dl_o}} \quad (71)$$

Where σ is the stress function (psi), dƐ is the strain limits, F is the force applied at the crack tip (lb), A is the area of the crack tip (sq inch) while $\frac{du}{dl_o}$ is the change in energy per unit length.

Gdoutos calculated the mode I stress intensity factor from the J-integral using the following equation:

$$\boldsymbol{K_I = \sqrt{\frac{J\,E}{1-\nu^2}}} \quad (72)$$

Where E is the modulus of elasticity and ν is the Poisson's ratio. Yang and Kuang[246], and Couroneau and Royer[247] utilised similar analytical method used by Gdoutos[245] except that they incorporated dimensionless stress-intensity factor (SIF) into their computation to account for the geometry effects of the test specimens. They used values of the final load and diameters to compute the fracture stress (σ_{net}) which was used to derive the mode I stress intensity-factor expressed as follows:

$$\boldsymbol{K_I = \sigma_{net}\sqrt{\pi\, D\, K_I^*}} \quad (73)$$

Where D is the nominal diameter (inch), K_I^* is the dimensionless stress intensity factor which was based on ratios of (a/R) and (a/b) from Yang and Kuang[246] for pure tension. Where a is the notch depth (inch), b is the minor axis of crack depth (inch), R is the radius of the test specimen (inch) and (a/R) is the relative crack depth.

Also, the finite-element analysis (FEA) was used to determine the stress intensity factor. In the purely elastic case, the mode I stress intensity factor (K_I) is given as:

$$\boldsymbol{K_I = \sigma Y\sqrt{\pi a}} \quad (74)$$

Where σ is the nominal stress, *a* is the notch depth, and Y is the geometrical correction factor which is »1. For the elastic finite-element analysis case, Y was inferred to be 1.18

For the elastic – plastic case, the overall J-Integral area or the fracture energy area is the summation of the J-Integral area for elastic ($J_{Elastic}$) and the J-Integral area for plastic ($J_{Plastic}$) i.e.:

$$\boldsymbol{J = J_{Elastic} + J_{Plastic}} \tag{75}$$

$J_{Elastic}$ is given as:

$$\boldsymbol{J_{Elastic} = \frac{K_I^2(1-\nu^2)}{E}} \tag{76}$$

and $J_{Plastic}$ is given as:

$$\boldsymbol{J_{Plastic} = \frac{Y\,A}{\pi\, r_n^2}} \tag{77}$$

Where Y is the geometrical correction factor inferred to be 0.08 from finite-element analysis for plastic case, A is the plastic area under the load-displacement curve, r_n is net section radius at the notch, E is the modulus of elasticity and ν is the Poisson's ratio. The mode I stress intensity factor (K_I) was obtained using Gdoutos expression as given in equation 72.

Venkatesh and Kane[248] evaluated the stress-intensity values of steel in ethanol determined using different analytical methods and found out that the K_I value varied from 38 to 81MPa $m^{½}$ depending on the composition of ethanol used for the test. Also air fracture toughness values were predominantly in the range of 101-113MPa $m^{½}$ as expected for this grade of steel tested. They found out that the variation in the results obtained by finite element analysis was mainly due to the different geometric factors (Y) used for the elastic-plastic analysis which was derived from the results of the software computation.

According to Marcus[189], *"SCC phenomena such as cracking of brass in aqueous ammonia are classical because they occur at low stresses and at high rates (10^{-9} to 10^{-6} m/s) while the crack velocity varies with the mode I stress intensity factor (K_I)"*.

As shown in Figure 26, Dickson et al[249] plotted the crack velocity against the stress intensity to illustrate the effects of alloy composition and cold work on SCC of austenitic stainless steels in a hot chloride solution. They identified the threshold stress intensity (K_{ISCC}), and the region II crack velocity, v_{II} as two significant parameters. The threshold stress intensity, (K_{ISCC}), gives the threshold stress intensity factor for stress corrosion crack growth in mode I plane strain loading. Below the threshold stress intensity (K_{ISCC}), stress corrosion cracks will not propagate. However, once the threshold stress intensity was exceeded, the crack growth rate increased rapidly until a limiting rate, known as the plateau crack growth rate or velocity was reached. Dickson et al[249] postulated that having the plateau at intermediate values of K_I indicates that the crack rate is controlled by chemical phenomenon (such as dissolution, diffusion or adsorption) not mechanical control. As the stress intensity factor is increased further, the crack growth rate eventually starts to increase slightly and the stress intensity factor approaches the critical stress intensity factor for fast fracture, (K_{IC}). In this regime part of the crack growth occurs by purely mechanical processes, with the environment serving only to propagate the crack through the toughest regions of the microstructure.

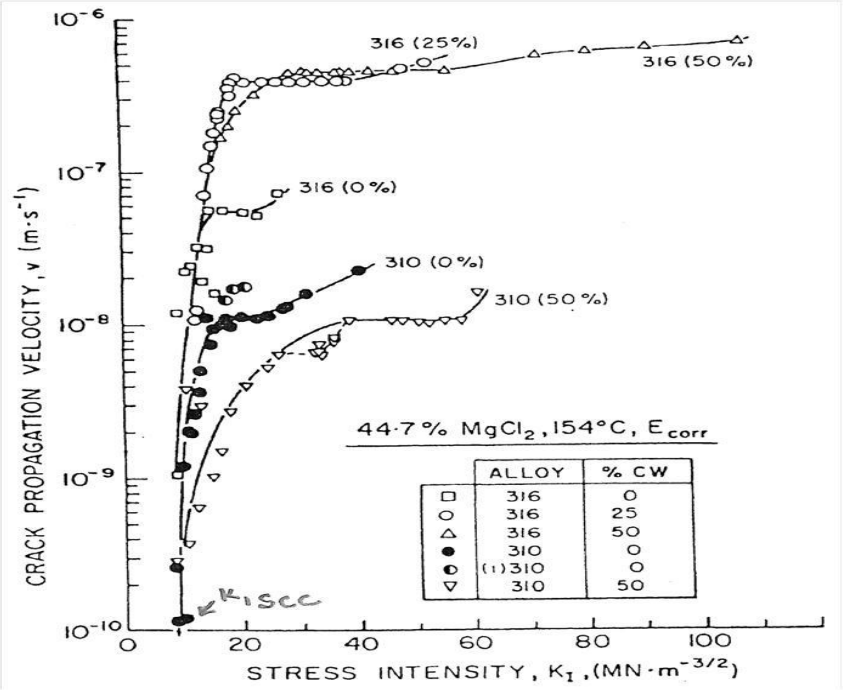

Figure 26: Crack velocity – stress intensity curves for annealed and cold worked 310 and 316 austenitic stainless steels in boiling (154°C) aqueous $MgCl_2$ Solution[249].

Failure of high strength material due to fast fracture is usually catastrophic while ductile alloys fail by leakage. Classical SCC systems have low K_{ISCC} values, e.g. austenitic stainless steel in hot chloride have values are as low as 1MPa $m^{½}$. However, values as high as 12MPa $m^{½}$ have been reported in literature[189]. Marcus[189] further stated that superior performance of duplex stainless steel in hot chloride is associated with higher K_{ISCC} values (3-10 times). Hence duplex must be highly stress or defective in order to fail by SCC in hot chloride solution. It is however worth noting that even the K_{ISCC} value of 1MPa $m^{½}$ is high enough to cause yielding at the crack tip.

According to Cottis[242], "In principle K_{ISCC} provides a good basis for managing stress corrosion cracking. Crack growth, and invariably stress corrosion failure can be avoided by ensuring that the combination of stress and maximum defect size give a stress intensity factor that is below K_{ISCC}. However, it should be appreciated that K_{ISCC} is not an invariant material property, all material and environmental factors that influence other aspects of SCC will also affect K_{ISCC}. Consequently it is important to be sure that an appropriate value of K_{ISCC} is used". Also, the effects of alloying additions are not consistent from one environment to another. For example, higher molybdenum content improves the resistance of low alloy steel to carbonate-bicarbonate cracking, but makes it more susceptible to caustic cracking[189].

As mentioned earlier, the probability of crack propagation (in the absence of SCC effects) is a function of the applied stress intensity factor being greater than a critical value, known as the fracture toughness, K_{IC}. Similarly, the general observation is that SCC will only occur if K is greater than K_{ISCC}. This provides a method of determining the likelihood of SCC failure for a given component. It also indicates the requirements for crack detection during inspection. If the stress (σ) that the component is subjected to is known, then the critical crack length (a_{crit}) required for crack propagation at a known stress intensity factor, K_{ISCC} is given by:

$$\boldsymbol{a_{crit} = \frac{1}{\pi}\left[\frac{K_{ISCC}}{\sigma Y}\right]^2} \quad (78)$$

Provided the crack detection limit of the system used is greater than or equal to the critical crack length, technically there is high confidence that SCC

failure is unlikely. In situations where critical crack length (a_{crit}) cannot be reliably detected, it must be assumed that such cracks exist, and the inspection frequency should be based on the time required for the largest crack that could not be detected to grow to the size required to achieve K_{IC}. If the plateau crack growth rate is reasonably low, this may give an acceptable time between inspections, but for many systems the crack growth rate is too rapid and failure will occur in an unacceptably short time[242].

Pits are generally believed to be common sites for the initiation of cracks. Hence as a conservative approach, a pit can be treated as a crack with the same cross-section. A fracture mechanics approach is then used to determine the size of pit necessary to exceed K_{ISCC} and invariably cause cracking. Fracture mechanics is concerned with the mechanical conditions at the tip of a crack, and the properties of the material that determine whether or not that crack will propagate. Hence, techniques of fracture mechanics are very valuable in determining both the probability of failure and the consequence of failure by cracking processes.

2.12 Managing Stress corrosion cracking

Typically operating in conditions where the material is susceptible to SSC is avoided during the design, execute and operating phase. However, due to unanticipated system changes, it might be required to operate in conditions where the system is susceptible to SCC. In such conditions active surveillance is required. The risk-based inspection, (RBI) is typically adopted to monitor for cracks and other defects and also ensure proactive measures are taken before failure occurs. This technique is a valuable tool for scheduling and managing inspection frequency. Susceptibility to failure is determined by comparing measured degradation rate with design degradation rate for the components. Each component is categorised in terms of probability of failure and consequence of failure. Typically, three consequence categories are considered for each failure mode, i.e. economic, health/safety and environment while four probability classes for each mode, i.e. High (H), Medium (M), Low (L) and Negligible (N). In addition the RBI matrix defines five consequence classes, i.e. Extreme (E), High (H), Medium (M), Low (L) and Negligible (N) as shown in Table 1.

Table 1: RBI Critical Matrix

		Susceptibility to Failure	RBI Criticality Class				
Probability class	H	Very susceptible to degradation	L	H	E	X	X
	M	Susceptible to degradation under normal conditions	L	M	H	E	X
	L	Susceptible to degradation under upset conditions	N	L	M	H	E
	N	Not susceptible under any foreseen conditions	N	N	L	M	H
Consequence Category	Economics (USD)		Slight Damage <10k	Minor Damage 10-100k	Local Damage 0.1 – 1M	Major Damage 1 – 10M	Extensive Damage >10M
	Health and Safety		Slight Injury	Minor Injury	Major Injury	Single Fatality	Multiple Fatalities
	Environment		Slight Effect	Minor Effect	Localized Effect	Major Effect	Massive Effect
Consequence class			N	L	M	H	E

Equipments with Extreme (X) criticality class are unacceptable; a management of change (MOC) must be implemented immediately to reduce the criticality class. Management of change typically require upgrading the susceptible material and/or the operating environment/parameters. On the other hand, equipments with negligible (N) criticality class do not require any inspection. Only equipments with High (H), Medium (M) and Low (L) criticality class are inspected. The system is inspected in order of decreasing estimated risk over the life of the equipment just as the technique is named “risk based inspection”. The technique provides a good guidance for setting the priorities for inspection. Components with High (H) criticality class are given first priority. In practice, use of components in this category is generally discouraged. The inspection priorities then move down through the grid with second priority given to components with Medium (M) criticality class and third priority given to components with Low (L) criticality class. In practice, components with Low (L) criticality class are typically not inspected, but simply replaced when they fail. While the basic principle of risk-based inspection is very simple, it has proved to be a powerful tool. For example, it has been claimed that 90% reduction in failures and 50% reduction in inspection costs has been achieved by using RBI[242].

In the course of this work, electrochemical techniques (mainly CPP and potentiostatic tests), C-ring exposure tests and SSR test have been conducted as the test methods to investigate the susceptibility of CRA materials to localised corrosion and stress corrosion cracking in the presence of nitrite. The SSR test was proposed as a test method to test the susceptibility of 13Cr-L80 and 25Cr-F225 to SCC in the presence of nitrite because it ensures that the passive protective barrier is breached and the bare metal is exposed to the test environment.

Based on literature search, work done to date was better understood and gaps to be filled by the research work identified. Work to date had focused on carbon steel with different school of thought on the susceptibility of carbon steel to pitting corrosion and SCC in the presence of nitrite. The consistent postulation is that below the critical nitrite concentration, carbon steel is susceptible to both pitting and SCC.

3 EXPERIMENTAL PROCEDURE

3.1 EL400 Working Electrodes for Electrochemical Tests

The EL400 working electrodes used for the tests were fabricated from 91.4cm × 61cm × 2.54cm (3'×2'×1") plates of the 13Cr, 22Cr and 25Cr that were carefully machined into cylinders. The flat ends of the cylinder were tapped and threaded. The total surface area of the carefully machined surface finished of the EL400 working electrodes exposed were calculated and recorded. A schematic drawing of the EL400 electrodes that were used for electrochemical tests in this work is shown in Figure 27.

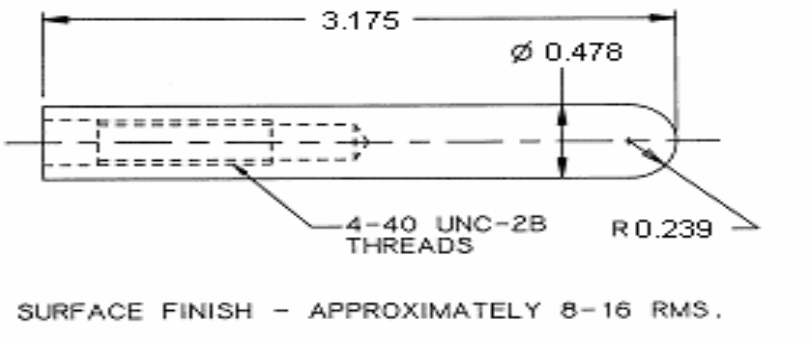

Figure 27: Engineering drawing of the EL400 working electrodes used for electrochemical tests (units in cm)

The chemical composition of the 13Cr, 22Cr and 25Cr EL400 working electrodes as given in the material test result (MTR) are shown in Figure 28, Figure 29 and Figure 30 respectively.

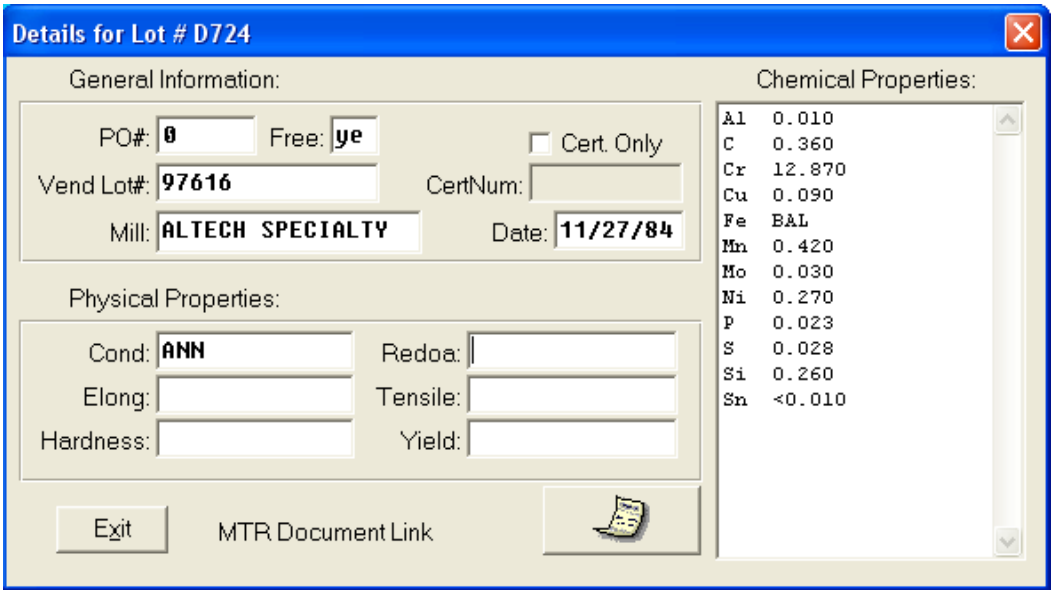

Figure 28: MTR for 13Cr EL400 Probes

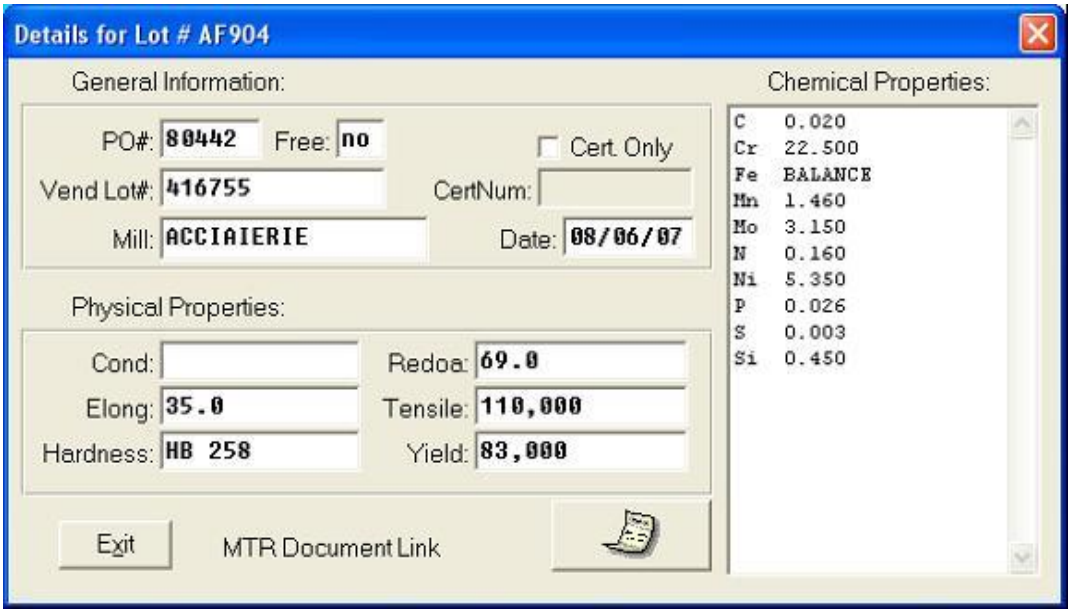

Figure 29: MTR for 2205 – UNS # S32205 EL400 Probes

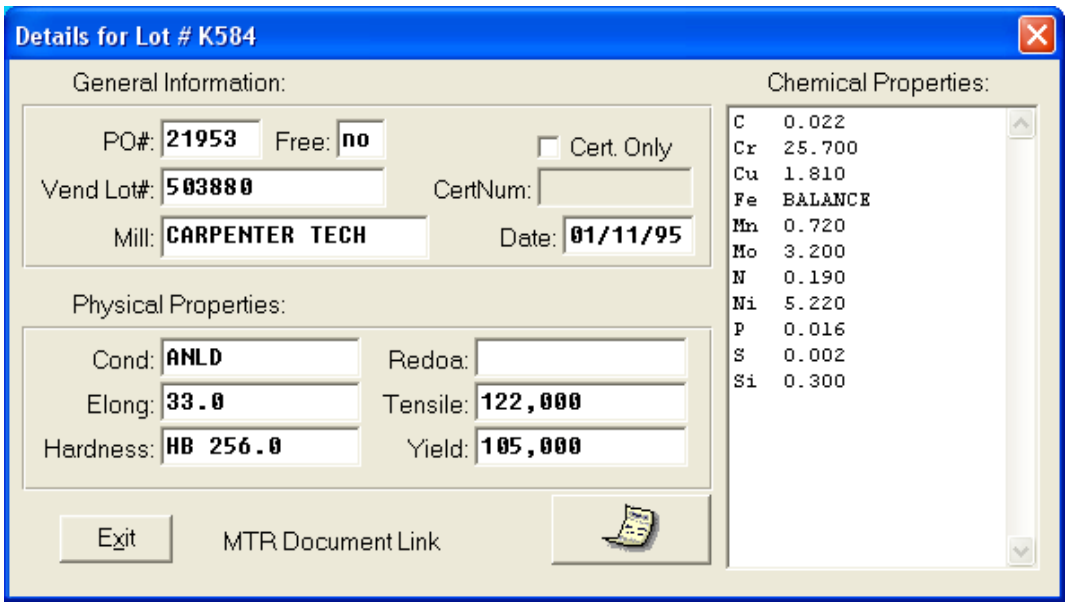

Figure 30: MTR for F255 - UNS # S32550 EL400 Probes

3.2 Preparation of Test Solution

As substitute for seawater, synthetic seawater was prepared using ready mixed synthetic seawater salt prepared in accordance with ASTM D1141[7]. The chemical composition of synthetic seawater is shown in Table 2.

To prepare 10L of synthetic seawater, 419.53g of synthetic seawater salt was dissolved in 8 to 9L of deionised water in a 10 litre conical flask. The solution was vigorously stirred until all the salt was completely dissolved and further

diluted with deionised water to 10L. Prior to use, depending on the current pH measurement of the freshly prepared synthetic seawater solution dilute solution of either sodium hydroxide or hydrochloric acid was used to adjust the pH to 8.2

Table 2: Chemical composition of synthetic seawater

Compound	Concentration (g/L)
NaCl	24.530
$MgCl_2$	5.200
Na_2SO_4	4.090
$CaCl_2$	1.160
KCl	0.695
$NaHCO_3$	0.201
KBr	0.101
H_3BO_3	0.027
$SrCl_2$	0.025
NaF	0.003

3.3 Electrochemical Cell Setup

To ensure consistent results were obtained, the same 1 litre, round bottom flask glassware with 5 necks was used for all the electrochemical tests. The working electrode, counter electrode, reference electrode, gas inlet and outlet tubes, and the thermocouple were inserted into the solution chamber through the necks.

The Luggin probe-salt bridge separated the bulk solution from the saturated calomel reference electrode. The probe tip of the Luggin probe was adjusted to bring it in close proximity with the working electrode. Figure 31 shows the close up picture of the glass cell.

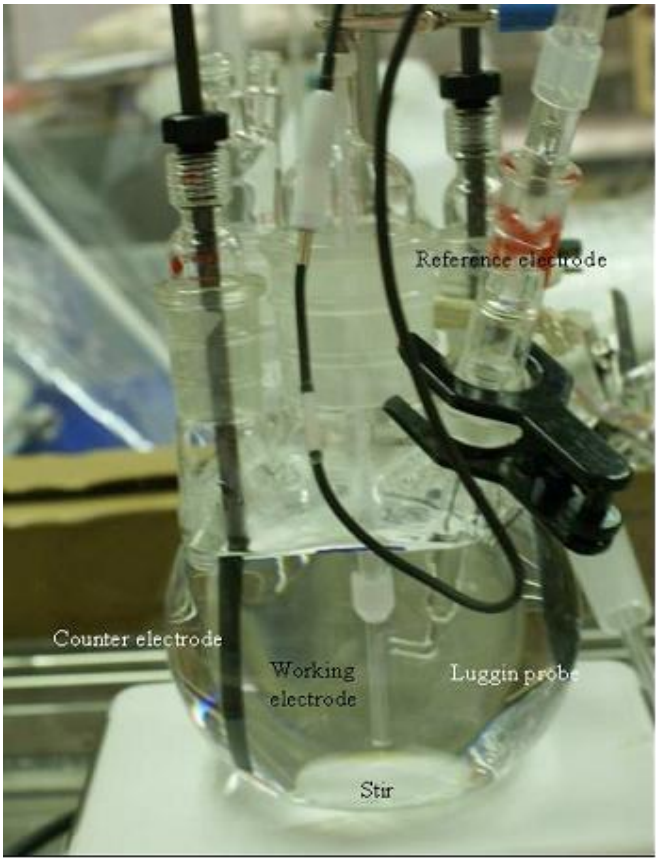

Figure 31: Figure showing Close up of the glass cell

At the beginning of each electrochemical test, the glass cell was placed on a magnetic stirrer plate and filled with 800ml of the synthetic seawater with the pH of the test solution already adjusted to 8.2. Sodium nitrate/nitrite was injected into the test solution to achieve the desired nitrate/nitrite concentration. A stirring bar was used to agitate the test solution for the duration of the test. The rotating speed of the magnetic stirring bar was set at about 700 rpm for consistency for all the tests carried out. For tests performed at elevated temperature, the solution was heated with a heat tape wrapped and taped around the glassware. The temperature of the solution was maintained by a temperature control system. The electrodes were installed in their appropriate glass necks. Saturated calomel electrode, SCE was used as the reference electrode and graphite as counter electrode. Other parts such as the gas dispenser (both inlet and outlet) and thermocouple were installed in the glass cell; the test solution was purged with nitrogen gas (0.0125% O_2 and N_2 balance) for an hour per ASTM G61[250] to obtain anaerobic conditions. The gas flow rate used for purging was controlled using a regulator. While

purging the test solution, the tapped and threaded ends of the EL400 working electrode was rinsed with acetone and de-ionised water, then attached to the electrode holder threaded bar and hand tightened until the TFE-fluorocarbon gasket was sufficiently compressed to avoid leakage in the gasket in order to avoid crevices. The entire surface area of the EL400 working electrode was rinsed with acetone and de-ionised water, dried and stored in a safe place.

After purging the test solution for an hour, the dissolved oxygen concentration in the test solution was measured using CheMets Kit K-7540 self-filling ampoules for colorimetric analysis (0-40ppb range). The dissolved oxygen concentration measured ranged from 17 - 26ppb at 25^{o}C to 5ppb at 80^{o}C. The working electrode was then immersed in the test solution for an hour before polarisation per ASTM G61[250]. The Luggin probe for the reference electrode was adjusted to ensure its tip was located approximately 1mm from the working electrode. The working, counter and reference electrodes were then connected to the multifunction Gamry 6500 series potentiostat. After the working electrode had been immersed in the test solution for an hour, the polarisation scan was initiated. Nitrogen purging was maintained throughout the duration of the test providing nitrogen blanket. The outlet gas was bubbled into a water column to ensure there was no oxygen ingress. Figure 32 shows the photograph of the experimental setup.

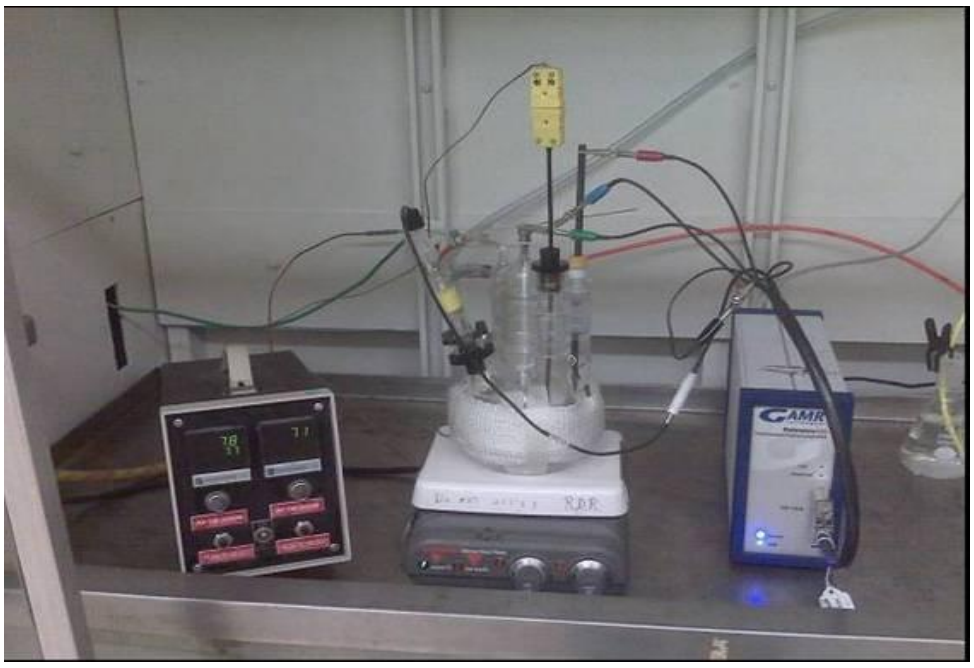

Figure 32: Figure showing the experimental setup of the glass cell

3.4 Electrochemical Test Methods

3.4.1 Open Circuit Potential

For the open circuit potential tests, the setup for electrochemical cell as described in 3.3 was followed. However, the desired sample period and the duration of the test were set in the potentiostat before potential measurement was initiated.

3.4.2 Cyclic Potentiodynamic Polarisation (CPP) Test

After setting up the electrochemical cell as described in 3.3, the CPP test was performed per ASTM G61.

3.4.2.1 Anodic Polarisation

For anodic polarisation curves, the initial potential was set at approximately 50mV more negative than the corrosion potential. The forward sweep rate was set at 0.2mV/s. Hence, the initial current measured was cathodic but the current switched to anodic once a potential more positive than the corrosion potential was reached. This permitted a quick check to confirm that the current went through zero (i.e. extremely low current) at the corrosion potential. In situations where the current did not go through zero at the corrosion potential, the circuit was checked for AC noise and other problems such ground loop currents. Any detected issue was rectified immediately before proceeding with the test.

To reduce the scatter in the protection potential determined from the series of tests, the amount of pitting allowed prior to repassivation was controlled by the potential sweep rate and the maximum current attained during the forward scan before reversing the potential.

The setting was such that either a maximum potential of 1V with reference to E_{cor} or current density of 1mA/cm^2 (which ever was attained first) activated the reverse sweep at the same sweep rate of 0.2mV/s until the hysteresis loop closed or until a corrosion potential 50mV more negative than the corrosion potential (E_{cor}) was reached before terminating the test.

The initial setting for the Gamry potentiostat for anodic CPP test is as shown in Table 3.

Table 3: Initial settings for the Gamry potentiostat for anodic CPP test

Initial potential, E_i	-50mV vs. E_{cor}
Forward scan	0.2mV/s
Apex potential, E_{max}	1.0V vs. E_{cor}
Reverse scan	0.2mV/s
Final potential, E_f	-50mV vs. E_{cor}
Apex current, I_{max}	1mA/cm^2
Sample period	10s
Sample area	4.75cm^2
Density	7.87gm/cm^3
Equivalent weight	27.92

3.4.2.2 Cathodic Polarisation

For cathodic polarisation curves, due to the limitations of the Garmy 6500 potentiostat, cathodic polarisation curves were started at the open circuit potential with the apex potential set at 50mV more positive than the corrosion potential to initiate reverse scan. Hence, the initial currents measured were anodic and the current switched to cathodic once a potential more negative than the corrosion potential was reached. The cathodic polarisation curve was terminated at a final potential of 500mV more negative than the corrosion potential. Table 4 shows the initial setting for the Gamry potentiostat for cathodic CPP test.

Table 4: Initial settings for the Gamry potentiostat for cathodic CPP test

Initial potential, E_i	E_{cor}
Forward scan	0.2mV/s
Apex potential, E_{max}	50mV vs. E_{cor}
Reverse scan	0.2mV/s
Final potential, E_f	-500mV vs. E_{cor}
Apex current, I_{max}	1mA/cm^2
Sample period	10s
Sample area	4.75cm^2
Density	7.87gm/cm^3
Equivalent weight	27.92

3.5 Potentiostatic Polarisation Test

The potentiostatic polarisation test was used to investigate long-term pitting corrosion behaviour of the test materials and also to determine the critical concentration of nitrite as an anodic inhibitor. The CPP results served as a guide to determine the polarisation level for the potentiostatic polarisation test. When the pitting potential from CPP testing was much more-noble than the corrosion potential and protection margin of 200 mV was achieved, it was not necessary to perform potentiostatic polarisation test. Otherwise, the material was tested at a selected potential between free corrosion potential (E_{cor}) and pitting potential (E_{pit}). The corrosion current was recorded every 10s for the duration of the potentiostatic polarisation test and plotted as a function of time. At certain polarisation level, increase in current with time indicates the initiation of pitting or damage of the passive film, while a decrease in current indicates passivation or recovery of a damaged passive film.

3.5.1 Determination of Critical Nitrite Concentration

To determine the critical concentration of nitrite as an anodic inhibitor, the potentiostatic polarisation test was conducted at a given potential taken from the CPP result typically close to the pitting potential (E_{pit}) and the nitrite concentration increased at intervals. The corrosion current was recorded during the potentiostatic polarisation test and plotted as a function of time. The critical nitrite concentration is indicated by a drastic decrease in current, which was maintained for a considerable amount of time.

3.6 C-ring Test

C-ring exposure test was predetermined as the primary technique for determining the susceptibility of the CRA materials to stress corrosion cracking (SCC) in nitrite environment with the fallback option of utilising slow strain rate test. Two different grades of CRA; 13Cr-L80 and 25Cr, were tested at two different temperatures and two different nitrite concentrations. Table 5 shows the test matrix that was used for the each of the C-ring test material. Each exposure test was carried out in duplicate for proper validation hence a total of 16 C-rings were tested. 8 C-rings for each material. Each exposure test was performed such that the two different C-rings of each test material

was exposed to the same environment in one glass autoclave but properly partitioned to prevent interference. Hence total of 4 C-rings were in each glass autoclave with total of 4 autoclave tests conducted.

Table 5: C-Ring Test Matrix

Test ID Number	Environment for each test material	Test Temperature (°C)
Test 1.	Blank deoxygenated seawater	25
Test 2.	Blank deoxygenated seawater	80
Test 3.	Deoxygenated seawater with1000ppm Nitrite Solution	25
Test 4.	Deoxygenated seawater with1000ppm Nitrite Solution	80

Figure 33 shows the decision tree for the C-ring test protocol.

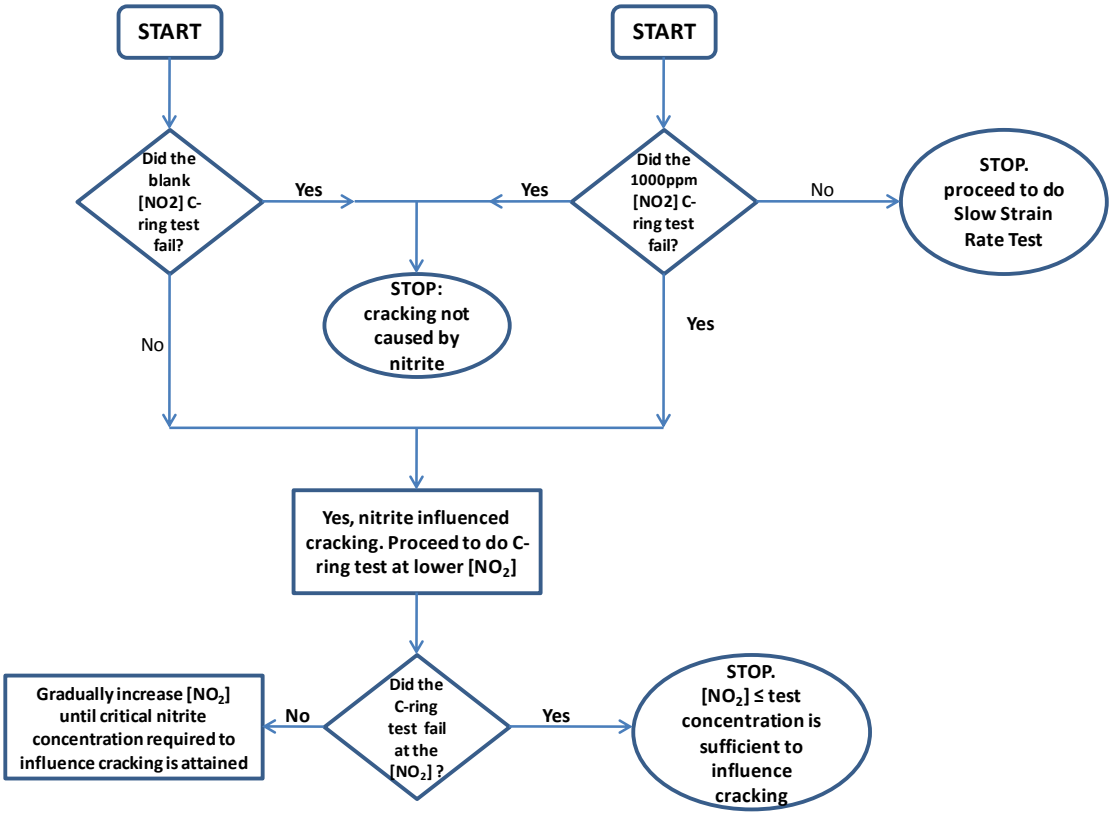

Figure 33: Decision Tree for C-ring Test Protocol

The strategy was to do the blank and 1000ppm nitrite concentration being the critical test/worst case scenario likely to be susceptible to stress corrosion cracking and localised corrosion but if required proceed straight to the fallback option of using slow strain rate test. However, if the tests at 1000ppm nitrite

concentration cracked, then test at lower nitrite concentration would be carried out to determine the critical nitrite concentration necessary to influence cracking.

The test vessels used for C-ring tests must be constructed from materials that are inert to the test environment. In the past, some plastic test vessels gave satisfactory service, while others caused varying test results from the time they were new until after they had been in continuous use while glass test vessels have not exhibited this tendency. The only limitation for glass autoclave is the low pressure restriction however, since the tests required for this research work are to be carried out at relatively low pressures, glassware vessels were used.

All C-ring samples were prepared from pipes in accordance with the NACE standard TM0177-2005[251]. The C-ring specimens were machined from a section of pipe with all the mill scale on the as-received pipe already removed and the C-ring specimen surface polished to give a shiny surface finish. The schematic of a C-ring specimen is shown in Figure 34.

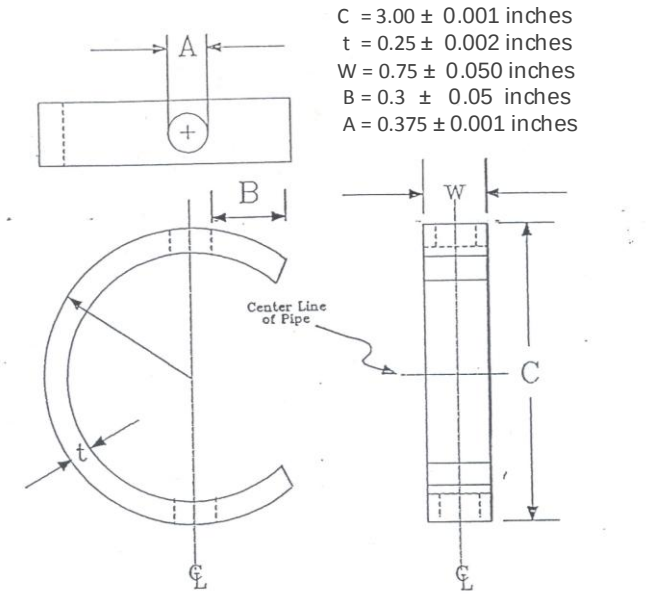

Figure 34: Schematics of the 13Cr-L80 C-ring Specimen

The diameter (C) and wall thickness (t) of the C-ring varied based on the diameter and the wall thickness of the as-received pipe. It was ensured that the wall thickness of the C-rings was within the preferred range of 0.25 inches (6.35mm) and 0.30 inches (7.62mm) to avoid the difficulty associated with

deflecting pipe with wall thickness greater than 0.32 inches (8.13mm). The diameter of the bolt hole (A) and the width of the C-ring specimen (W) were measured. The dimensions of the ring can affect the stress state. The stress of principal interest in the C-ring specimen is the circumferential stress. It should be recognized that this stress is not uniform[252].

First, there is a gradient through the thickness, varying from a maximum tension on one surface to a maximum compression on the opposite surface. Secondly, the stress varies around the circumference of the C-ring from zero at each bolt hole to a maximum at the middle of the arc opposite the stressing bolt; the nominal stress is present only along a line across the ring at the middle of the arc. Thus, when the specimen is stressed by measuring the strain on the tension surface of the C-ring, the strain gage should be positioned at the middle of the arc in order to indicate the maximum strain. Thirdly, the circumferential stress may vary across the width of the ring, the extent of the variation depending on the width-thickness and diameter-thickness ratios of the C-ring. Hence, it was ensured that the C/t ratio and the w/t ratio were within the recommended range of 10-100 and 2-10 respectively because of increased difficulties in machining and decreased precision in stressing.

After all the necessary verifications were done on the as received C-rings from the machine shop, the C-rings were thoroughly cleaned with acetone to remove grease from machining work. Each C-ring was stamped at one edge of the finished (near the end) for identification as shown in Figure 35A, then flipped to the other side, where a Tic-mark was punched on each edge at the centre of each bolt hole using a pointed centre punch as shown in Figure 35B. Using a digital calliper, the following C-ring dimensions were measured and recorded:

- Outside diameter, (C).
- Wall thickness, t, measured at the apex of the C-ring.
- Tic-mark to Tic-mark length, L, measured by placing the pointed end of the calliper in one Tic-mark and sliding the measuring blade such that the other pointed end of the calliper is placed in the other Tic-mark.

A: Stamped

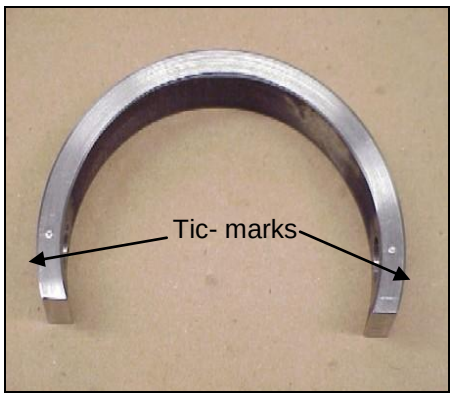

B: Tic Mark

Figure 35: Stamped and Tic marked C-rings from 3.0" (7.62cm) OD 13Cr

The deflection of each C-ring was calculated using the following equation:

$$\delta = \frac{\pi r[r - 0.5t]}{t}\varepsilon \tag{79}$$

The yield stress at 0.2% strain was used as the desired applied Stress for the C-ring deflection calculation.

where:

δ = Deflection of C-ring across the two Tic-marks (inches);
r = Outer radius of C-ring (inches);
t = Wall thickness of C-ring (inches);
ε = Outer fibre strain at C-ring apex, calculated using the following equation:

$$\varepsilon = \frac{\sigma_{ys}}{E} + 0.002 \tag{80}$$

where σ_{ys} is the yield stress (psi) and E is the Modulus of elasticity (psi). Substituting equation 80 into equation 79 gives the desired deflection of each C-ring as:

$$\delta = \frac{\pi r[r - 0.5t]}{t}\left(\frac{\sigma_{ys}}{E} + 0.002\right) \quad (81)$$

After calculating the deflection for each of the C-rings, they were deflected and held in place by means of bolts and nuts. All bolts and nuts were made from noble material, Hastelloy C-276.

Galvanic effects between dissimilar metals can either accelerate or suppress cracking susceptibility. For example, reduced cracking has been observed in some duplex stainless steels when these materials were coupled to electrochemically less noble materials such as carbon and low-alloy steels[251] hence to prevent galvanic corrosion, all fixtures were properly wrapped with Teflon tape to electrically isolate them from the C-ring specimens.

Figure 36 shows picture of the C-rings and Teflon wrapped couplings before deflection.

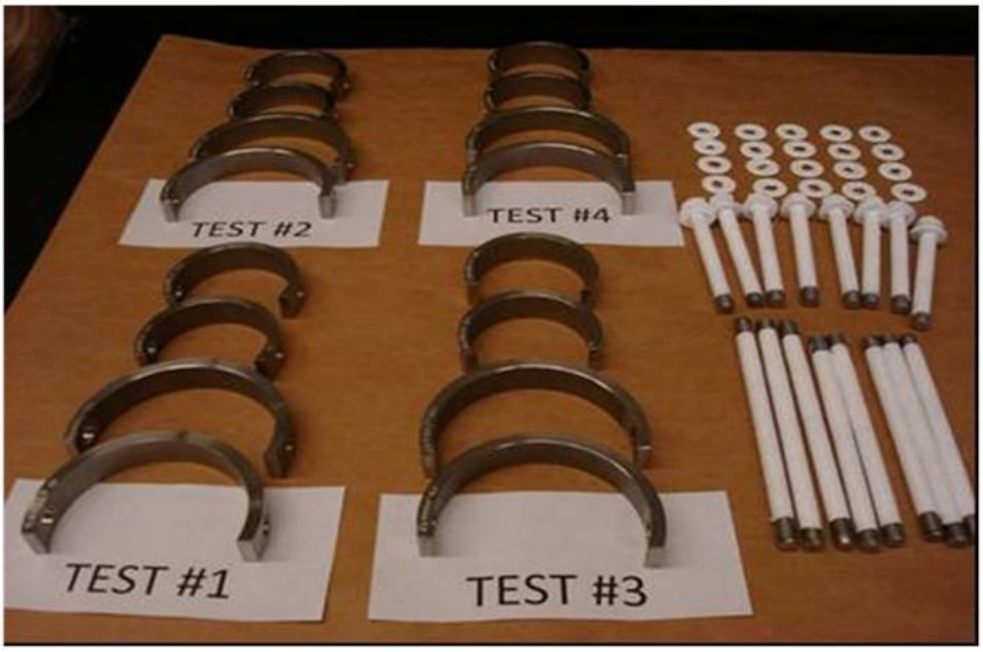

Figure 36: Picture of the C-rings and Teflon wrapped couplings before deflection

Deflection of the C-rings was achieved by inserting the teflon wrapped bolt affix with washers and nuts through the C-ring holes and one end of the bolt was clamped to a vice as shown in Figure 37, then the nut on the other end was gradually tighten measuring the distance between the two Tic-marks with callipers until the desired strain of the C-ring, (L – δ), was achieved.

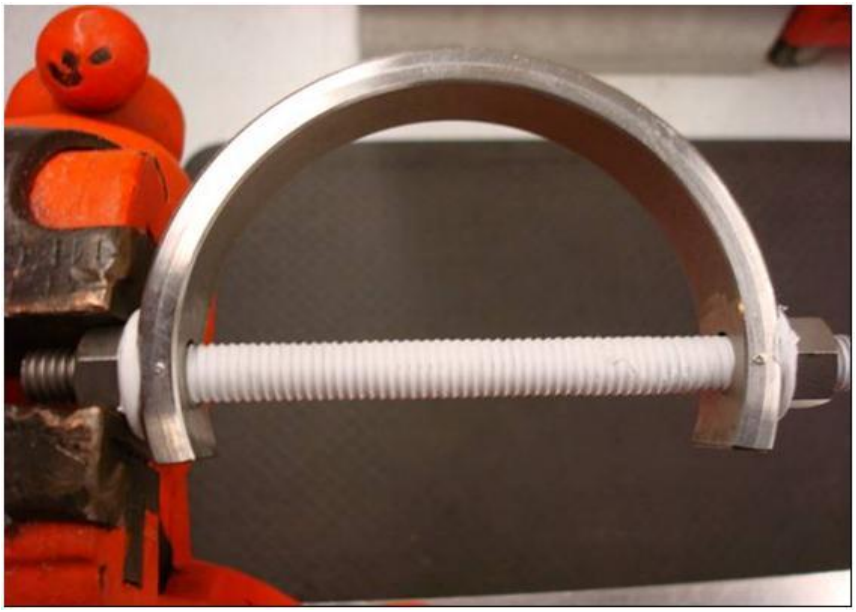

Figure 37: C-ring clamped to the vice for deflection

Deflecting the C-ring was carefully performed because deflecting beyond the required value meant higher stress was applied and the C-ring can no longer be used for the test. The nut, washers, and C-ring were then cleaned with acetone and de-ionized water and dried by blowing nitrogen gas. The deflected C-rings were kept in a safe place pending the time they would be loaded in the autoclave. Figure 38 show pictures of the C-rings and Teflon wrapped coupling after deflection of the C-rings.

Figure 38: Picture of the C-rings after deflection

The glass autoclave was cleaned with acetone, and the four already deflected C-rings were carefully placed in the autoclave such that C-rings with dissimilar metal were properly separated with a dielectric material to avoid galvanic coupling which might interfere with the test. The thermocouple, dip tube and autoclave seal ring were also wrapped with Teflon tape. Hastelloy C-276 needle valves in closed position were attached to the dip tube and the vent port on the autoclave cover. Pressure gauge was also installed. The thermocouple was inserted into the thermowell of the autoclave ensuring the thermocouple leads were properly plugged into the temperature controller. The threads on the autoclave bolts were lubricated, the seal rings were inserted and the autoclave sealed using 100 ft/lbs of torque. A vacuum was pulled on the autoclave (via vent valve) and held for approximately 10 minutes. The autoclave was then backfilled with nitrogen to approximately 500 psig and held for about 30 minutes to check for leaks.

Test solution prepared per 3.2 was added into another glass autoclave with sodium nitrite solution added to achieve the required concentration. The autoclave was then sealed using the same procedure described above. The gas inlet dip tube was connected to the nitrogen gas system while the vent line was connected to the scrubber. The needle valves for the inlet tube and vent were opened. Using the regulator on the nitrogen test gas (0.0127% Oxygen bal. N_2) system, vigorous purging of the test solution was commenced. The test solution was purged for 3 hours to de-aerate the solution, after which the gas flow was stopped and the inlet and vent valves closed.

After purging, the inlet line of the autoclave containing the de-aerated solution was disconnected from the nitrogen system and connected to the inlet dip of the autoclave loaded with the C-rings. Also the vent line of the autoclave containing the de-aerated solution was disconnected from the scrubber and connected to the nitrogen system while the vent line of the autoclave containing the C-rings was rigged up to the scrubber. The needle valves on the inlet tubes and vent lines of both autoclaves were opened. Using the nitrogen pressure, the de-aerated solution was transferred into the autoclave containing the C-rings until the desired level was attained. The inlet tube of

the autoclave containing the C-ring was then closed, disconnected from the other autoclave and connected to the nitrogen system to maintain a nitrogen blanket for the duration of the exposure test. Figure 39 shows the setup of the two autoclaves for the test solution transfer.

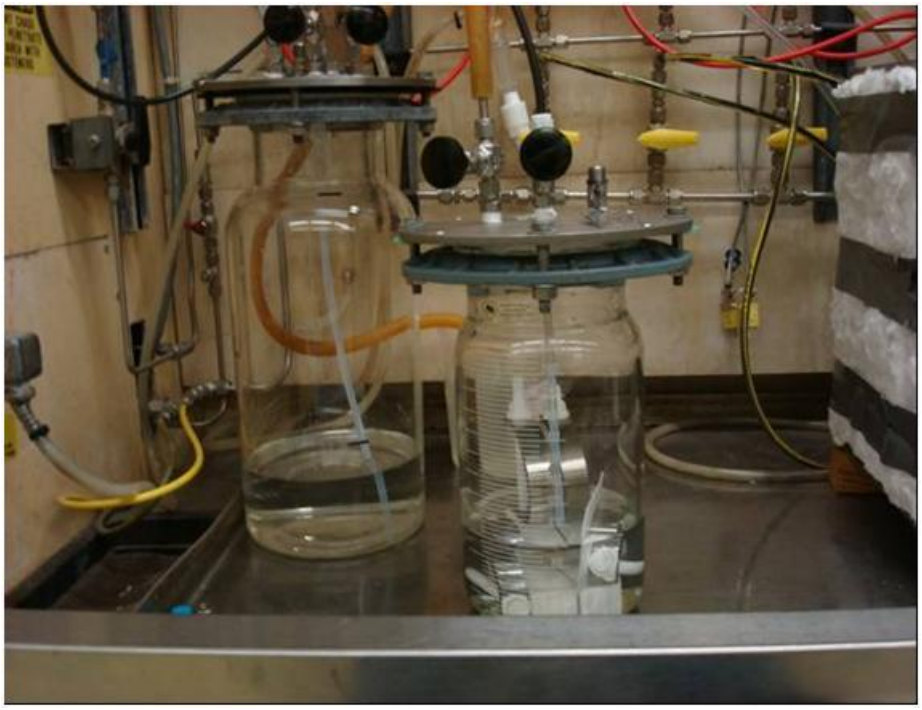

Figure 39: Picture showing setup for test solution transfer

For the test conducted at elevated temperatures, the autoclave containing the C-rings was then carefully loaded into already prepared oil bath. The oil level was such that the entire liquid in the glass autoclave was submerged in the oil bath to ensure heat transfer was proportional with no localised hot spots.

The heater and the thermocouple for the oil bath were connected to a temperature controller (to maintain the set temperature) and turned on. Insulating plastic balls were used to cover the entire surface of the oil bath to prevent heat loss. The temperature of the oil bath, nitrogen flow and pressure were monitored throughout the 30 day exposure test, recording any visible change observed.

Figure 40 and Figure 41 show pictures of the C-ring test setup and a close up picture showing four C-rings in a glass autoclave respectively.

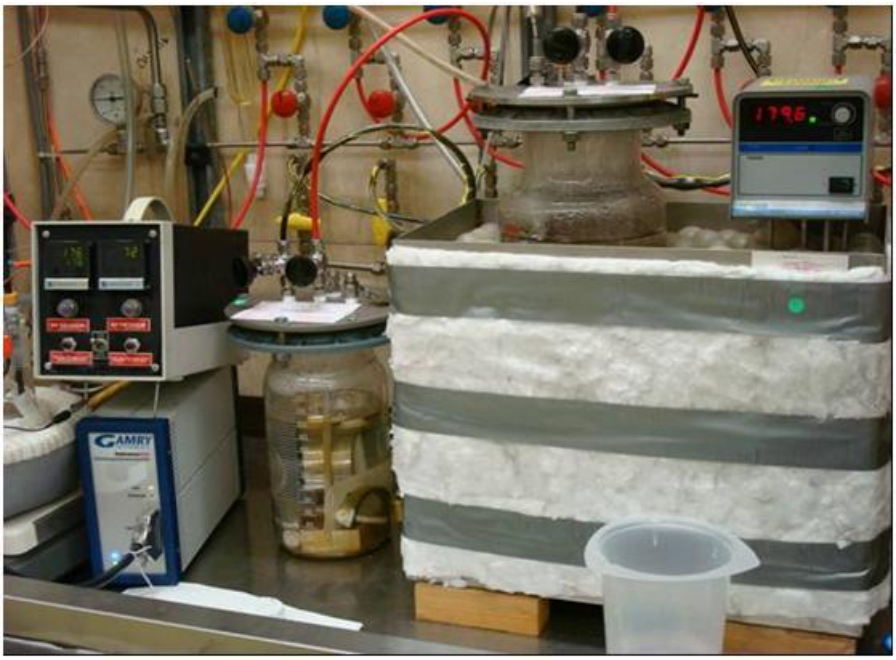

Figure 40: Picture of the C-ring setup for both 25^{o}C and 80^{o}C in a bath

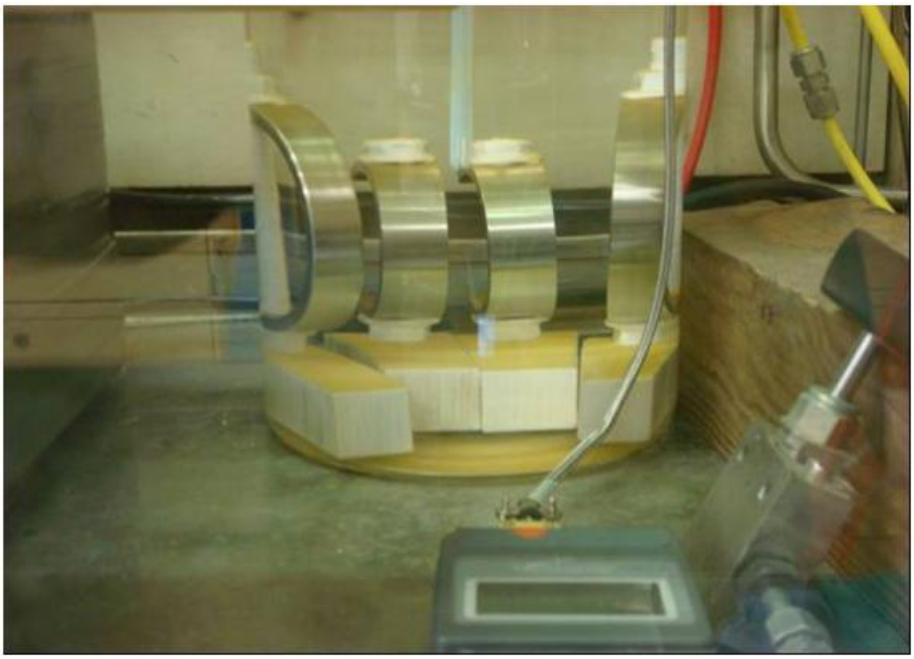

Figure 41: Picture showing close up of the 4 C-rings in a glass autoclave

After the 30 days exposure test, the autoclave was opened and the C-rings were removed from the autoclave. All the C-rings were rinsed with deionised water, then all the fixtures on the C-rings were removed.

The C-rings were stored in an oxygen free dry box prior to examination. A stereo-microscope at magnifications up to 10X was used to examine the C-rings for cracking and pitting. In cases where metallographic examination was

required for more precise examinations, a 2-inch (5.08cm) section of the C-ring was cut from the apex and mounted. The mounted specimens were wet ground with silicon carbide abrasive paper to reveal the surface of the metal. They were then ground in succession with finer and finer abrasive media and polished with soft cloth until a scratch-free mirror finish was obtained. The specimens were examined with an optical microscope at magnifications up to 400X for cracks and pitting both in the etched and un-etched conditions.

3.7 Slow Strain Rate Test

Slow strain rate test was used as an alternative technique for determining the susceptibility of the CRA materials to stress corrosion cracking (SCC) in nitrite environment. Apart from the fact that the tests were fast, the technique ensures the passive layer is destroyed and the bare metal is exposed to the environment.

Slow strain rate (SSR) tests were conducted, per NACE TM0198-2004[253] and ASTM G129[254] to determine the cracking susceptibility of 13Cr-L80 and 25Cr-F255 materials to stress corrosion cracking in seawater at various sodium nitrite concentrations at 80°C. During the fabrication process of the SSR test samples, materials close to welds were avoided to ensure consistent microstructures. Specimens were machined from longitudinal axis orientation of thick walled piping with at least 0.25mm removed by cylindrical wet grinding to produce a surface finish of 0.25µm. This was followed by longitudinal polish, finishing at 1200 grit to remove all circumferential marks from the gauge length and then wet ground threads on each end. All the SSR tests were carried out using the specimen dimension shown in Figure 42.

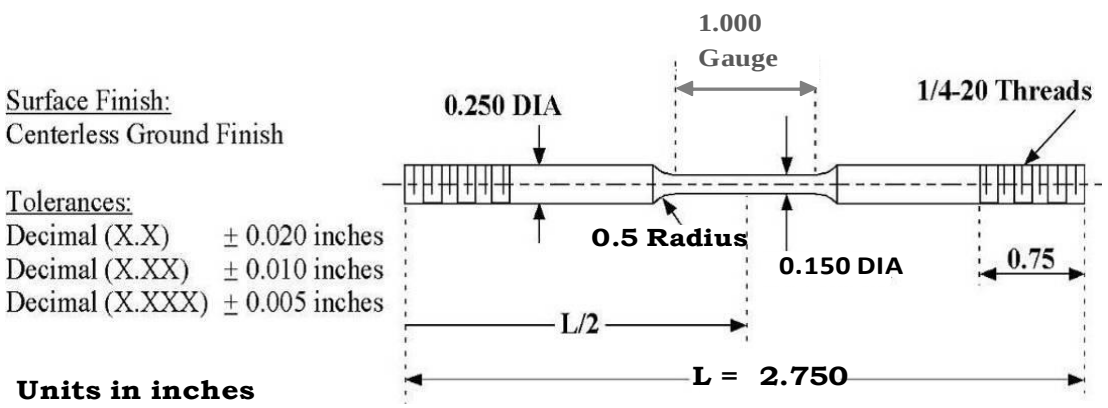

Figure 42: Engineering drawing of the SSR rate test specimen

The gauge section has diameter of 0.15 ±0.002 inch, gauge length of 1.000 inch, radius of curvature of the shoulder section at the ends of the gauge section was 0.5 inch to minimise stress concentrations and fillet failures. The as-received specimens were rinsed with acetone and deionised water to remove grease from machining work, then air dried and kept in a safe place.

Two different grades of CRA, 13Cr-L80 and 25Cr (F255), were tested all at the same strain rate of $4x10^{-6}$ /s. Most of the tests were carried out at the open circuit potential but some of the tests were carried out with an applied potential close to the pitting potentials of the test material (per CPP test results) for the duration of the SSR test. Table 6 and Table 7 show the test matrix that was used for the slow strain rate tests for 13Cr-L80 and 25Cr-F255 respectively. Each test was carried out in duplicate for proper validation hence a total of 40 SSR tests were carried out, 20 specimens for each material. The SSR tests were conducted in a 0.5L Hastelloy C-276 autoclave ensuring the solution volume-to-exposed specimen surface area was more than 30 ml/cm^2. The autoclave used for the SSR tests had suitable ports to facilitate gas inlet and vent line, inlet line to fill the solution into the autoclave, slots for the thermocouple, counter electrode and reference electrode.

Table 6: Slow Strain Rate Test Matrix for 13Cr-L80

	Test Solution	Applied Potential (mV vs. SCE)	Test ID
Air	Open air	OCP	91413-344
Env. 1	Blank deoxygenated seawater (i.e. 0ppm Nitrite)	OCP	91413-341
Env. 2	Deoxygenated Seawater with 100ppm Sodium Nitrite.	OCP	91413-343
Env. 3	Deoxygenated Seawater with 1000ppm Sodium Nitrite.	OCP	91413-345
Env. 4	Deoxygenated Seawater with 6000ppm Sodium Nitrite.	OCP	91413-347
Env. 5	Blank deoxygenated seawater (i.e. 0ppm Nitrite)	-250	91413-348
Env. 6	Deoxygenated seawater with 1000ppm Nitrite	-250	91413-349
Env. 7	Deoxygenated seawater with 4000ppm Nitrite	-250	91413-342
Env. 8	Blank deoxygenated seawater (i.e. 0ppm Nitrite)	-150	91413-346
Env. 9	Deoxygenated seawater with 1000ppm Nitrite	-150	91413-365

Table 7: Slow Strain Rate Test Matrix for 25Cr-F255

	Test Solution	Applied Potential (mV vs. SCE)	Test ID
Air	Open air	OCP	91414-358
Env. 1	Blank deoxygenated seawater (i.e. 0ppm Nitrite)	OCP	91414-352
Env. 2	Deoxygenated Seawater with 100ppm Sodium Nitrite.	OCP	91414-353
Env. 3	Deoxygenated Seawater with 1000ppm Sodium Nitrite	OCP	91414-354
Env. 4	Deoxygenated Seawater with 6000ppm Sodium Nitrite	OCP	91414-355
Env. 5	Blank deoxygenated seawater (i.e. 0ppm Nitrite)	250	91414-356
Env. 6	Deoxygenated seawater with 1000ppm Nitrite	250	91414-359
Env. 7	Deoxygenated seawater with 4000ppm Nitrite	250	91414-360
Env. 8	Blank deoxygenated seawater (i.e. 0ppm Nitrite)	500	91414-362
Env. 9	Deoxygenated seawater with 1000ppm Nitrite	500	91414-357

At the beginning of each SSR test, the gauge section diameter of the test specimen was measured to the nearest 0.001inch (25.4µm) and recorded. The test specimen, pull rods, and the internal surface of the autoclave were thoroughly cleaned, degreased and dried prior to use. The thread portion of the specimen was taped with Teflon and carefully screwed into the pull rods. The pull rods were installed through the autoclave and held in place with sliding ceramic seals ensuring the gauge section and the autoclave were not contaminated during installation. Teflon tape and ceramic seal were used to electrically isolate the test specimen from the various metallic components of the gripping fixtures and autoclave.

The autoclave with the coupled specimen was then installed into the load frame. About 500ml of the test solution already prepared per section 3.2 was poured into a sealed glass purging vessel and deaerated by purging with nitrogen for an hour. While purging the test solution, the autoclave was sealed and pressurised with inert gas to approximately 500psig (3.45MPa) and held for about 30 minutes to check for leaks. The autoclave was cycled from vacuum to pressurisation with nitrogen for 3 cycles to deaerate the autoclave. The purged test solution was drawn into the autoclave via the transfer line under a vacuum. Approximately 380ml of the deaerated test solution was

transferred into the autoclave to completely immerse the gauge length of the specimen. Bubbling of nitrogen test gas (0.0127% Oxygen bal. N_2) into the test solution was commenced and the test solution heated to 80°C using heat pads strapped to the autoclave.

Figure 43 shows the setup of the autoclave with the gauge length completely immersed in the test solution. During heating, all necessary checks were carried out to ensure the test had initiated successfully. The SSR test specimen was preloaded to 200lb, and the slow strain rate test commenced at a strain rate of $4x10^{-6}$ /s.

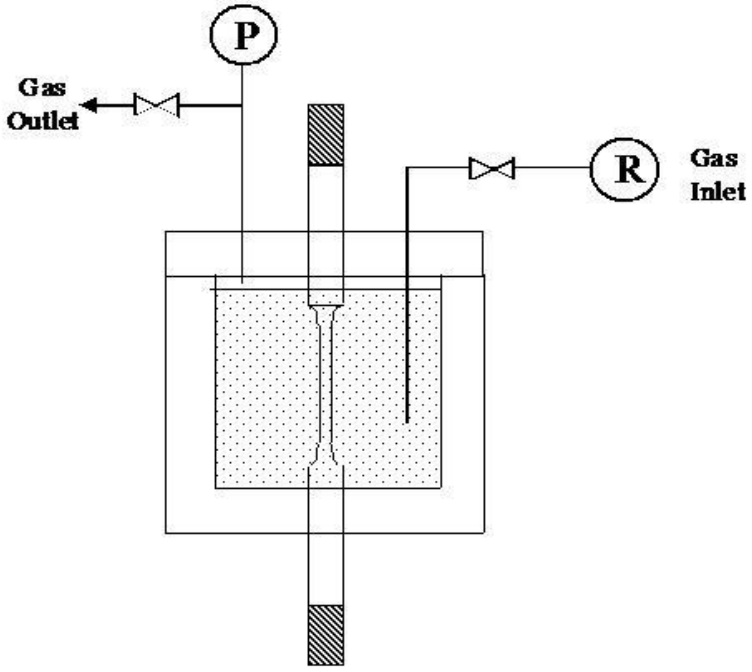

Figure 43: Setup of autoclave showing gauge length completely immersed in the test solution

For SSR tests conducted with an applied potential, a saturated calomel electrode (SCE) reference electrode was maintained at room temperature using a Luggin probe/salt bridge filled with test solution, platinum was used as the counter electrode and the test specimen as working electrode. All connected to the potentiostat and desired potential applied before commencing the slow strain.

The test specimens were pulled to failure. Figure 44 shows the setup of the SSR test.

Figure 44: Picture of the SSR test setup

At the end of each slow strain test, the pH of the test solution was measured; the failed specimens were removed from the autoclave and cleaned in acetone. Visual examination was performed for evidence of cracking under low power optical microscope at a magnification of at least 20X. The nature of the primary fracture was evaluated whether it was a brittle or ductile fracture. Any secondary crack away from the primary fracture was noted. When necessary, metallographic sectioning of the test specimen gauge section was performed and sections observed at a magnification of 100X or under the Scanning Electron Microscope (SEM) to fully characterise the failed test specimens with respect to stress corrosion cracking behaviour.

4 RESULTS AND DISCUSSION

4.1 Open Circuit Potential Measurements

The potentials of corroding metals are influenced by the oxidising/reducing power of the environment however; the potential is typically controlled by the corrosion reactions of the metal. Hence if a true measurement of the oxidising power of a solution is desired, an inert metal such as platinum must be used to measure the potential, in which case the measured potential is referred to as the redox potential of the solution. The corrosion potential on the other hand provides the basis for evaluating the corrosion conditions of a given metal with respect to the oxidising power of a given solution. Knowledge of the oxidising power of a given solution is very essential in the materials selection process. The open circuit potential of 13Cr was measured as the nitrite concentration was increased over time at 80^{o}C with the objective of investigating the effect of increased nitrite concentration, [NO_2^-], on the open circuit potential for 13Cr. Figure 45 shows the graph of corrosion potential over time as the nitrite concentration was gradually increased. The test was carried out for 1 week allowing sufficient time for the corrosion potential to stabilise in between the dosing of sodium nitrite solution.

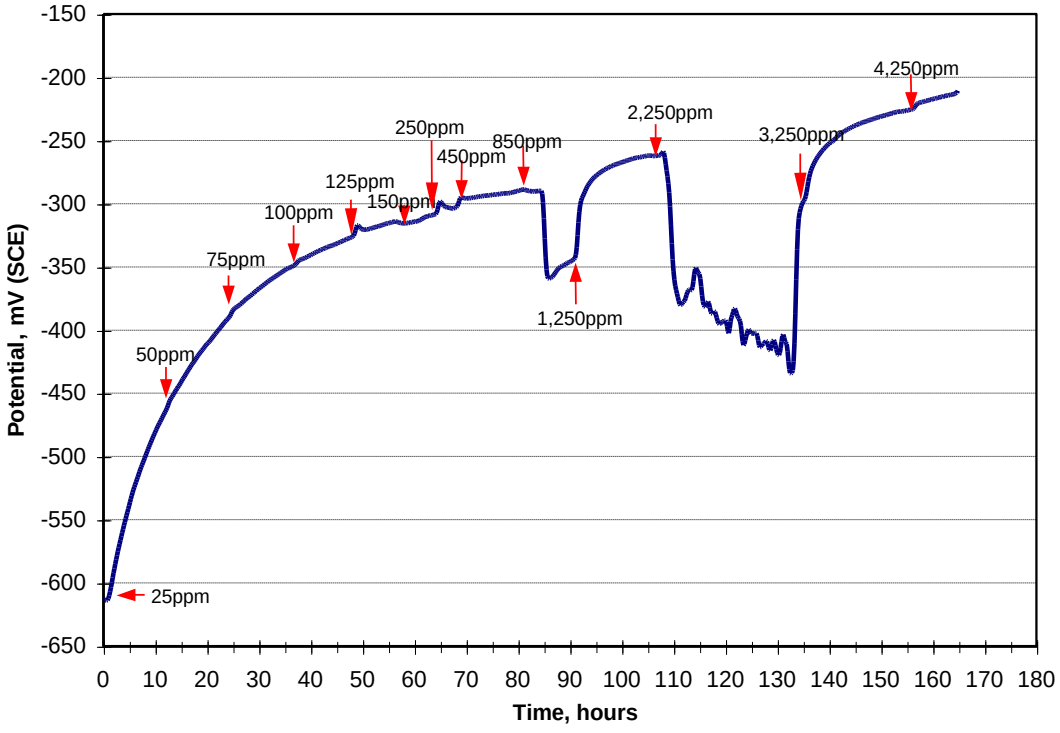

Figure 45: Corrosion potential of 13Cr with increasing [NO_2^-] at 80^{O}C

As shown in Figure 45, the open circuit potential of 13Cr increased in the anodic direction as the nitrite concentration increased making the 13Cr, working electrode more passive (i.e. exhibiting more noble properties). Up till about 100ppm nitrite concentration, a slight increase in nitrite concentration led to a significant increase in corrosion potential. An increase in corrosion potential to more positive values is one of the characteristics of an anodic inhibitor. Anodic inhibitors shift the anodic polarisation curve to lower currents and leave the cathodic curve with a net reduction in the corrosion rate. CPP tests were later used to confirm the other two attributes of nitrite as an anodic inhibitor.

The shift in potential to more noble potentials could be as a result of any or combination of the following factors;

1. Nitrite passivation potential; nitrites although sometimes regarded as reducing agents especially at low concentration, possess oxidizing properties and tend to render iron passive thereby stopping corrosion in weakly alkaline solution. Hence at low concentration up to 850ppm, 13Cr was passivated by nitrite. The passive film was more stable thereby shifting to more passive corrosion potential indicated by the anodic polarisation.
2. Also nitrite is considered to act like chromates, converting any ferrous salts formed at susceptible points to ferric hydroxide so that the attack is stifled. In such conditions, nitrite leads to anodic polarisation, which facilitates the formation of protective films and causes the metal to assume a passive state. With the onset of the passive state, the passive film formed retards further oxidation of the metal into the ionic state; hence the anode potential becomes more positive. This phenomenon may shift the potential of iron electrode to exceed 1V[86].

As the sodium nitrite concentration increased, the open circuit potential of the specimen was steadily increased in the anodic direction reaching a plateau at a nitrite concentration of 850ppm and a corresponding potential of about –290mV. Shortly after, there was a drop in potential, shifting towards more active corrosion. Same behaviour was observed just after increasing the concentration from 1250ppm to 2,250ppm.

The drop in potential to more active corrosion potential shortly after the nitrite concentration was increased to 850ppm could be attributed to breakdown of the passive film and pit initiation. Pitting causes decrease in pH which, further distorts the passive film and eventually switches the anodic reaction from oxidation of chromium to oxidation of iron.

Another school of thought is the introduction of oxygen into the deoxygenated solution since the sodium nitrite injected was not deoxygenated. Increasing the sodium nitrite concentration from 450ppm to 850ppm was achieved by injecting 4ml of 80,000ppm sodium nitrite solution to 800ml deoxygenated test solution giving a dilution ratio of 40ppb dissolved oxygen (assuming 8,000ppb in fully oxygenated solution). Introduction of 40ppb, dissolved oxygen into the solution could shift the dominating cathodic reaction in the presence of oxygen to oxygen reduction.

$$O_2 + 2H_2O + 4e^- \leftrightharpoons 4OH^-$$

Shift towards active corrosion is similar to what is expected with oxygen reduction. The second shift to active corrosion was observed after increasing the nitrite concentration from 1250ppm to 2250ppm by injecting 10ml of 80,000ppm sodium nitrite solution to the deoxygenated test solution. Also assuming 8,000ppb in fully oxygenated solution, gives a dilution ratio of 100ppb, dissolved oxygen introduced into the system. It is remarkable to state that the magnitude of the shift towards active corrosion in both instances were proportional to the amount of oxygen introduced in both cases. So also was the duration before returning to steady potential.

The shift to more active corrosion and reverting to initial potential before introduction of dissolved oxygen exhibits a depletion pattern. Hence it was possible that the potential dropped when fresh oxygen was introduced and the potential reverted back to its initial state when the oxygen was depleted via oxygen reduction reaction given above. To confirm this hypothesis, the test was repeated using higher concentration of sodium nitrite solution to reduce the amount of sodium nitrite injected each time to increase the nitrite concentration and invariably reduce the amount of oxygen introduced. The drop in potential was also observed in the repeated test. However, to

completely rule out oxygen reduction, it must be ensured that dissolved oxygen in the injected sodium nitrite solution was the only source of introducing oxygen into the system and not via oxygen ingress during injection and switching of the injection syringe. Bigger injection syringe containing sufficient sodium nitrite solution was used during the repeated test and the syringe was never removed. Also there was continuous purging with nitrogen for the duration of the test, but this does not completely eliminate oxygen ingress into the system.

Another school of thought for the shift to more active corrosion is the possibility of switching from one redox reaction to another, particularly switch in the predominant cathodic reaction. In a deoxygenated sodium nitrite solution, the possible nitrite cathodic reduction reactions together with their standard reduction potential are listed below[255]:

(i) $NO_2^- + H_2O + e^- \leftrightharpoons NO + 2OH^-$ -460mV

(ii) $2NO_2^- + 2H_2O + 4e^- \leftrightharpoons N_2O_2^{2-} + 4OH^-$ -180mV

(iii) $2NO_2^- + 3H_2O + 4e^- \leftrightharpoons N_2O + 6OH^-$ +150mV

Also there is the possibility of intermediate reaction when nitrite was spent. Hence the reaction products from equations (i) and (iii) serves as the reactant. The possible intermediate reactions, together with their standard reduction potential are listed below:

(iv) $2NO + 2e^- \leftrightharpoons N_2O_2^{2-}$ +0.10v

(v) $2NO + H2O + 2e- \leftrightharpoons N_2O + 2OH-$ +0.76v

(vi) $2NO + 2H^+ + 2e^- \leftrightharpoons N_2O + H_2O$ +1.59v

(vii) $N_2O + 2H^+ + 2e^- \leftrightharpoons N_2 + H_2O$ +1.77v

A possible explanation for the shift in potential to a more active potential and later reverting to its initial potential is that the nitrite got spent due to nitrite reduction and a switch to one of the intermediate reactions led to the drop in potential to a more active corrosion potential but when nitrite was replenished (injected), the cathodic reaction switched back to nitrite reduction. Alternatively, it could be that the nitrite anodically protected 13Cr but nitrite got spent (due to nitrite reduction), which led to the drop in potential to a more active corrosion potential however when nitrite was replenished, anodic inhibition was re-established hence, the potential switched back to a more

noble potential. The benefit of nitrite as an oxidising inhibitor is that it does not require oxygen to form a passive film on iron. This benefit makes nitrite a useful inhibitor in a deoxygenated system.

The disadvantage however is that the nitrite can be reduced and depleted hence loosing the passivation ability i.e. shift in potential to more active corrosion. The nitrite concentration, [NO_2^-], required for inhibition in diluted seawater is in the order of 10^{-3}M. However the critical concentration required for inhibition increases with the presence of aggressive ions (such as Cl^-, SO_4^{2-} and NO_3^-). Determination of the critical nitrite concentration (4.3.1) is part of the scope of this research.

The last possible explanation for the shift in potential to more active potential could also be attributed to switch in the predominate cathodic reaction but this time rather than having the switch as a result of nitrite depletion, the switch could be thermodynamically influenced in a situation where the nitrite concentration reached a critical concentration and the concentration gradient favoured a less favourable thermodynamic reduction of nitrite.

As shown above, the most favourable thermodynamic reduction of nitrite is the reduction to nitric oxide (nitrogen monoxide, NO), equation (i), but nitrite concentration gradient could make reduction of nitrite to nitrous oxide (N_2O), equation (iii), thermodynamically possible. When part of the nitrite was spent and the concentration was not sufficient to thermodynamically favour reduction of nitrite to nitrous oxide, it switched back to reduction of nitrite to nitric oxide hence returns to the initial potential.

It should however be noted that by comparing the open circuit potentials of 13Cr working electrode (that was immersed in solution for almost 160 hours) at different nitrite concentrations in Figure 45 with the corresponding open circuit potentials of 13Cr work electrodes that were immersed in solution for 1 hour per ASTM G61[250] before the cyclic potentiodynamic polarisation tests were initiated as shown in Figure 53, there are discrepancies in the data which indicates that the 13Cr working electrode used for the open circuit measurement was probably contaminated due to long exposure. The error margin reduced significantly at nitrite concentrations of 1000ppm and above.

4.2 Cyclic Potentiodynamic Polarisation (CPP) Test

The relative corrosion resistance of CRA cannot be differentiated or screened in a relative short period of time by a simple immersion test in seawater solution because of their very low corrosion rate in seawater solution. In order to evaluate CRA materials, their corrosion process must be accelerated. The cyclic potentiodynamic polarisation (CPP) method is one of the electrochemical techniques used to accelerate the corrosion process in order to evaluate test samples in a test solution in a reasonable time period. Plotting the logarithm of the current as a function of the applied potential, the anodic CPP curve of the test material can be obtained. From the CPP results, the information about the potential corrosion types (uniform corrosion or pitting susceptibility) and the extension of activation and passivity for the alloy/environment combination can be obtained. This can be used to rank the pitting resistance of the test materials in a specified environment.

Pitting and repassivation potentials are usually determined by either cyclic potentiodynamic polarisation (CPP) tests or potentiostatic tests. However for the purpose of this work, CPP test was performed first and the pitting potentials obtained directly from the CPP curve at the potential where current increased dramatically. In situations where the CPP curve had two slope changes on the forward scan in the transpassive region, the potential where the second slope change occurred was selected as the pitting potential to be conservative. Similarly, the repassivation potentials were obtained directly from the CPP curve at the zero current potential on the reversal scan.

For curves where the protective margin was less than 200mV, potentiostatic tests were performed at potentials range slightly higher than the open circuit potential but slightly lower than the pitting potential. The potentiostatic test was started at the potential of interest and change in current as a function of time was monitored for a period of 24 hours usually or longer. Other testing conditions remained the same as what was used in the CPP tests.

If the current increased with time, it indicates the applied potential was more noble than repassivation potential however, if the current decreased with time or remained small, it’s an indication that the applied potential was below the repassivation potential.

For cyclic potentiodynamic polarisation tests, selection of appropriate sweep rate for metal/environment combination is very important, especially if near steady state condition is desired because the selected sweep rate can affect the polarisation behaviour. The magnitude of the current measured at each potential is a function of the sweep rate. Generally, faster sweep rates give higher current at any given potential than lower sweep rates. At the start of each potential step increase, there is a spike in the polarising current, which gradually decays until the next potential step increase. Therefore if the sweep rate is too fast and does not allow enough time for the spike to decay, high currents would be measured. The passive current density, for instance can vary by almost two orders of magnitude depending on the sweep rate.

The best practice is to run the polarisation test at near steady state condition. Hence the sweep rate was selected such that it was as fast as possible to minimise the test duration but slow enough to ensure that further decrease in sweep rate does not significantly change the measured current. ASTM G5 standard specifies a sweep rate of 10mV/min (0.167mV/s) for 430-stainless steel in 1N H_2SO_4 combination which is a good average value that can be used for many metal/environment conditions[256]. It is also very important to use a consistent sweep rate for similar test conditions for proper bench marking. For this research work, a sweep rate of 0.2mV/s was used throughout.

Typically, anodic polarisation curves are scanned to positive potential until anodic current significantly increases due to pitting, active corrosion or water breakdown due to oxidation of water. Once such potential and corresponding increase in current is reached, the sweep direction is reversed. For the purpose of this research work, maximum potential of 1V or current density of 1mA/cm^2 (whichever comes first) was set to activate the reverse sweep. The sweep rate of the reverse sweep was kept the same as that of the forward sweep. The final potential on the reverse sweep was set at 50mV below E_{cor} to ensure the repassivation behaviour after passivation breakdown was observed. However, the reverse-scan was terminated when the reversed curve crossed that of the forward sweep or when the current becomes cathodic and continues to increase cathodically. For this research work, CPP tests were used to determine susceptibility of 13Cr, 22Cr and 25Cr to

localised corrosion, investigate their active/passive behaviour and relative pitting resistance in seawater solution with different concentrations of nitrate/nitrite at 25°C and 80°C. The CPP result provided information about the potential corrosion types in nitrate/nitrite environment; whether the test material exhibits a uniform corrosion or was susceptible to localised corrosion. The CPP results also provided information on the extension of passivity for the test material in nitrate/nitrite environment.

Based on the CPP results, the susceptibility of 13Cr, 22Cr and 25Cr to localised corrosion in the test solutions was determined using the protection margin, (E_{rp} - E_{corr}) as the criterion. A minimum protection margin of 200 mV is often used as a pass/fail criterion. It is very important to use consistent test procedure within the given set of experiments in order to draw valid conclusions from the test data.

Figure 46 shows CPP curves of 13Cr, 22Cr and 25Cr polarised in fully oxygenated blank seawater at 25°C (room temperature).

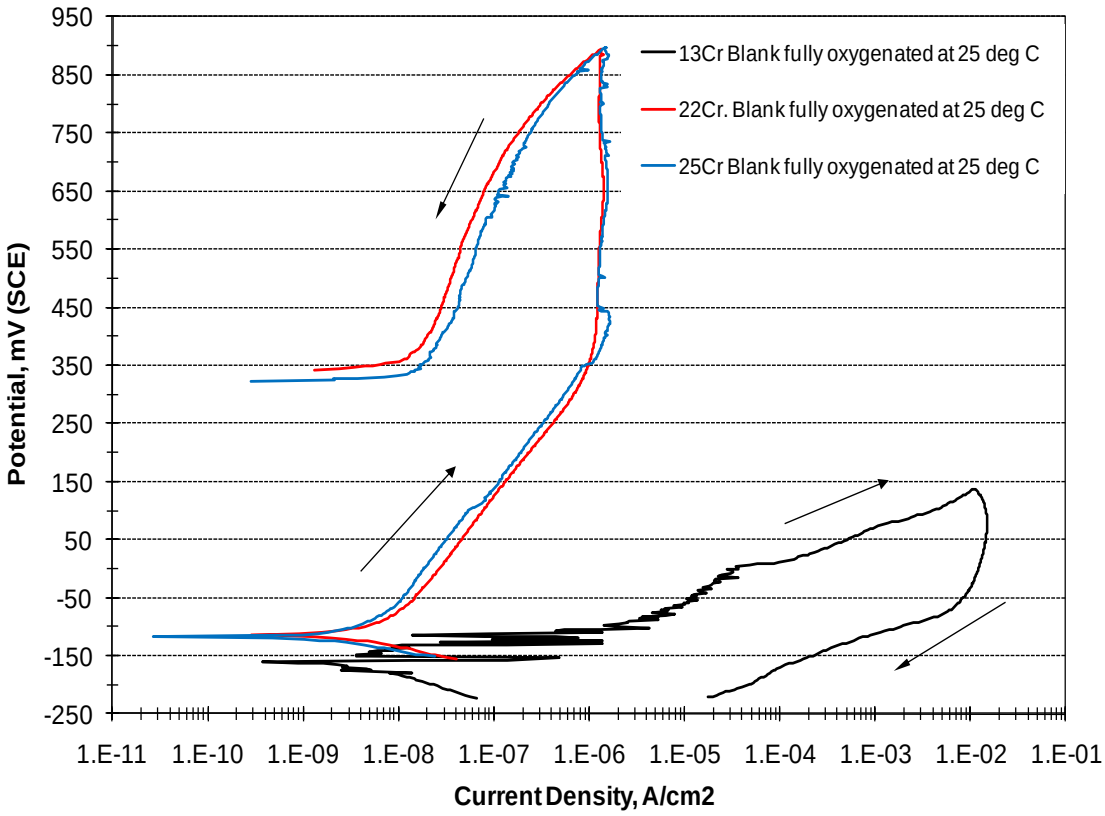

Figure 46: CPP for 13Cr, 22Cr and 25Cr in fully oxygenated blank seawater at 25°C

There are several publications on the Fe-Cr alloys in sodium chloride solution confirming chromium oxidation is preferred during the first steps of the film growth. Hence the protective barrier is a very thin film mainly composed of chromium oxide Cr_2O_3. Several literatures also emphasise the fact that chromium content greater than 15% is required for complete Cr_2O_3 passive layers on the metal surface[257-262].

Figure 46 shows the difference in corrosion characteristics expected for different materials exposed to the same environment. As stated in the material test results shown in Figure 28, Figure 29, and Figure 30 the chromium content for 13Cr, 22Cr and 25Cr used for this test were 12.87%, 22.50% and 25.70% respectively. Hence it is not surprising that 13Cr is more active compared to 22Cr and 25Cr. Also because the chromium content in 13Cr was not sufficient to completely protect the metal, there was early passive film breakdown followed by pitting initiation as indicated by the noisy region shown in the anodic curve for 13Cr.

Pitting corrosion was active until the maximum polarisation current density was reached and the reverse polarisation initiated. The reverse scan produced positive hysteresis without closure indicating the repassivation potential is below the corrosion potential. Hence, 13Cr is susceptible in these test conditions. However, the anodic curves for 22Cr and 25Cr exhibit typical active-passive behaviour with no passive film breakdown or pitting initiation until maximum forward potential of 1V with respect to the corrosion potentials were reached, at which point the reverse sweeps were initiated. The current densities of the reverse scans were less than those of the forward scan hence given negative hysteresis loops which indicates 22Cr and 25Cr are not susceptible in the test conditions. The open circuit potential and the active passive behaviour of 22Cr and 25Cr were very similar both in the forward and reversed scan since they both had chromium oxide Cr_2O_3 passive and the environment was not aggressive enough to cause a breakdown of the passive film.

The appearance of post-test specimens for 13Cr, 22Cr and 25Cr polarised in blank fully oxygenated seawater at 25^{o}C (room temperature) are shown in Figure 47A/B/C respectively.

A: 13Cr fully oxygenated, 7600ppb blank at 25^{o}C

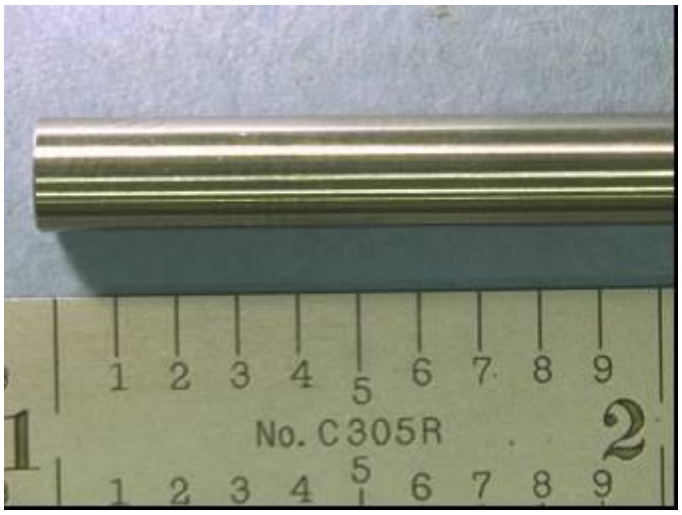

B: 22Cr fully oxygenated, 7600ppb blank at 25^{o}C

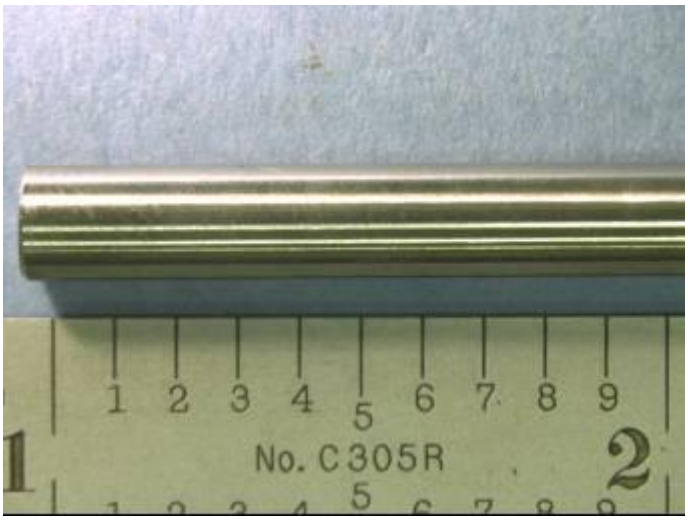

C: 25Cr fully oxygenated, 7600ppb blank at 25^{o}C

Figure 47: Photographs of post-test specimens of 13Cr, 22Cr and 25Cr polarised in fully oxygenated seawater at 25^{o}C

Figure 48 shows CPP curves of 13Cr with fully oxygenated blank solution, deoxygenated blank solution, 100ppm sodium nitrate solution and 100ppm sodium nitrite solution at 25^{o}C (room temperature).

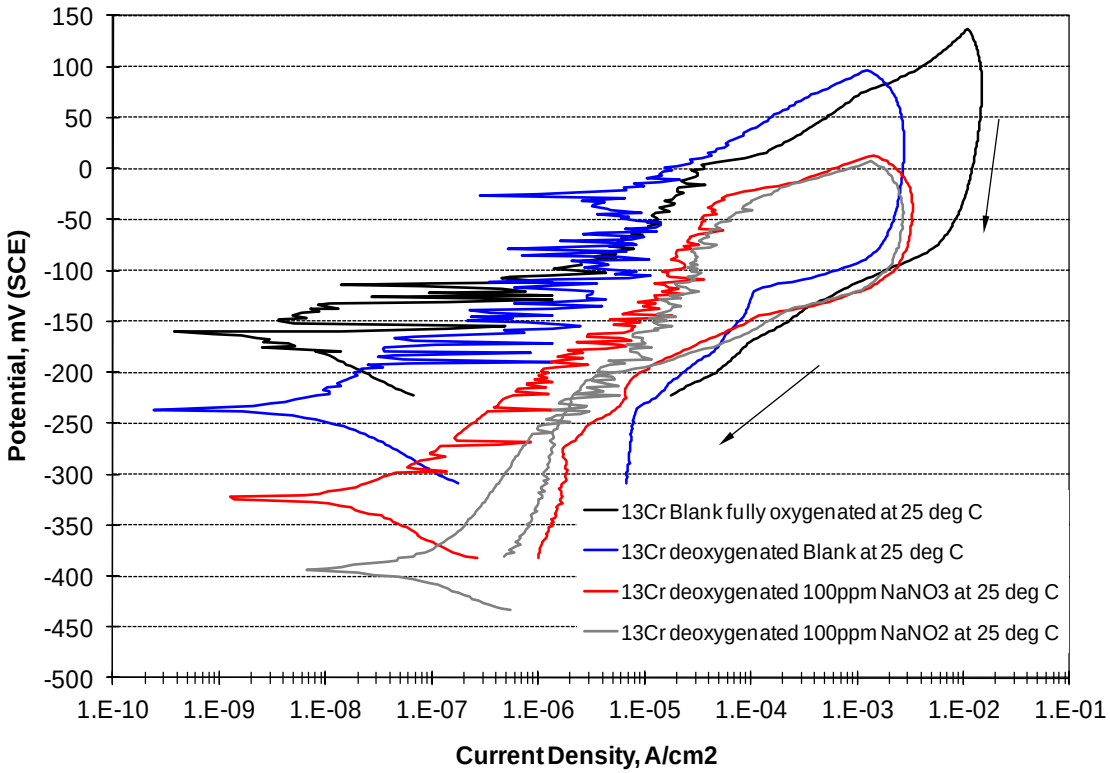

Figure 48: CPP curves for 13Cr at 25^{o}C

Even at low anodic polarisation levels, all the curves at room temperature (Figure 48) exhibit some fluctuations (a very noisy region) on the forward scan. The fluctuations were probably due to breakdown of passive film and/or occurrence of unstable pits in the mesoscopic stage of pit initiation, which then repassivated. The curves show early passive film breakdown followed by pitting initiation and propagation except in the case of blank deoxygenated where there was no oxygen to promote pit propagation. Pitting corrosion was active for some time even after reversing the scan direction thereby resulting in higher current at potentials where passive behaviour was observed during the forward sweep hence producing positive hysteresis in the reverse scan. The positive hysteresis loops were without closure except for the 100ppm sodium nitrite solution, which had a closure about 198mV away from the corrosion potential. Production of positive hysteresis when the sweep scan was reversed after a significant increase in current is another indication that

pitting corrosion had occurred. However the passivation current density was in the order of 1μA/cm^2. A minimum protection margin (difference between the repassivation potential, $E_{rp,}$ and the corrosion potential) of 200mV is considered protective. The early noisy region suggests that the initial passive oxide film immediately broke down and/or 13Cr could not form a stable passive film in all the seawater solutions tested. This indicates that 13Cr is susceptible to pitting corrosion at room temperature in all the tested cases.

13Cr in fully oxygenated seawater had the highest corrosion potential, followed by that deoxygenated blank solution, 100ppm sodium nitrate and lastly 100ppm sodium nitrite. High corrosion potential observed for 13Cr in fully oxygenated was probably due to the fact that both the thermodynamics and the kinetics of chromium oxidation to chromium oxide was improved since there was sufficient oxygen in the solution to form chromium oxide protective film on the sample thereby making it to be more noble. The passive film however broke down almost immediately as indicated by the early noise.

Injection of 100ppm sodium nitrate and 100ppm sodium nitrite shifted the corrosion potential in the direction of active corrosion by 87mV and 157mV respectively when compared to the CPP curve for 13Cr with the blank deoxygenated solution. Also the corrosion rates increased from 2.43E-10 A/cm^2 for blank solution to 1.28E-9 A/cm^2 for 100ppm sodium nitrate solution and 6.69E-9 A/cm^2 for 100ppm sodium nitrite solution. This implies that injection of 100ppm sodium nitrate and 100ppm sodium nitrite to seawater actually significantly increased the corrosion rate of 13Cr.

Similarly, field data from Shell Bonga and Ursa Princess Platforms, where actual corrosion rates were measured on carbon steel to check the effect of injection of 100ppm sodium nitrate into deoxygenated water injection system as a means for controlling reservoir souring indicates that the corrosion rates were higher than the expected rates for oxygen corrosion[5].

The appearance of post-test specimens for 13Cr in fully oxygenated seawater, blank deoxygenated seawater, deoxygenated seawater with 100ppm sodium nitrate and deoxygenated seawater with 100ppm sodium nitrite at 25^{o}C are as shown in Figure 49A/B/C/D respectively.

A: 13Cr fully oxygenated blank solution, 7600ppb [O] at 25^{o}C

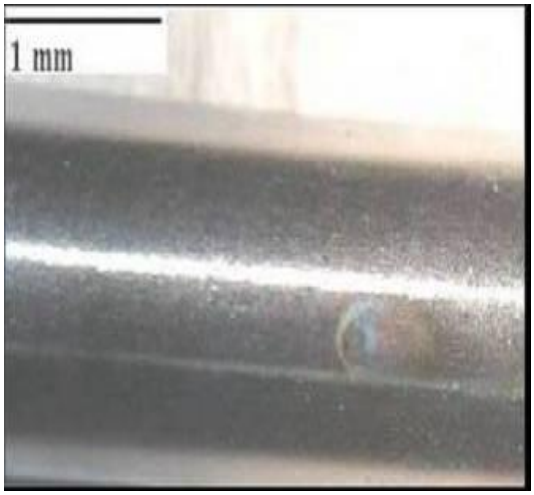

B: 13Cr deoxygenated blank solution, 17ppb [O] at 25^{o}C

C: 13Cr deoxygenated solution 17ppb [O], with 100ppm $NaNO_3$ at 25^{o}C

D: 13Cr deoxygenated solution 17ppb [O], with 100ppm $NaNO_2$

Figure 49: Photographs of post-test specimens of 13Cr polarised in 17ppb [O] seawater at 25^{o}C

Pits/localised active areas and/or discoloration/etched patches were found on most of the 13Cr specimens in various test conditions. 13Cr in fully oxygenated seawater had the highest pit density while 13Cr specimen in deoxygenated blank seawater solution had the least pit density possibly because the presence of oxygen though improved the passivation of 13Cr but also helped to speed up the pitting kinetics in the fully oxygenated seawater solution more than the influence of 100ppm nitrate/nitrite as an oxidising agent. However, in the case of Figure 49B, the oxygen concentration was not high enough to promote pit propagation, hence repassivation occurred and no

pit was observed on the sample but etched patches. Also the pit density observed in Figure 49C and Figure 49D were not as much compared to Figure 49A where the pits where all over the entire surface of the specimen.

Figure 50 shows CPP curves of 13Cr with fully oxygenated blank solution, deoxygenated blank solution, 100ppm sodium nitrate solution, 100ppm sodium nitrite solution and 400ppm sodium nitrite solution all at 80^{o}C.

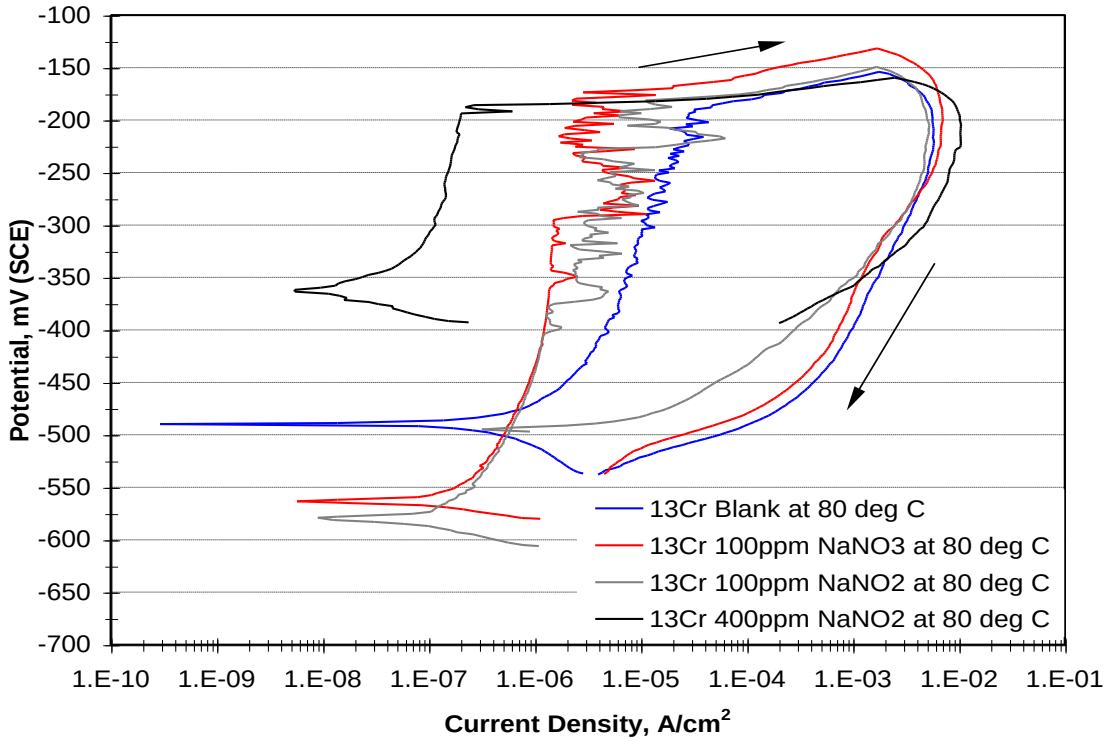

Figure 50: CPP curves for 13Cr at 80^{o}C

Figure 50 indicates that 13Cr is more susceptible to pitting corrosion in all the tested conditions at higher temperatures when compared with the curves in Figure 48 at 25^{o}C. All the curves at 80^{o}C shown in Figure 50 have lower corrosion potentials (i.e. more active corrosion) and higher corrosion rate compared with their corresponding curves at 25^{o}C even though the dissolved oxygen concentration dropped from 17ppb at 25^{o}C to 5ppb at 80^{o}C. This is not surprising, although increase in temperature reduces the amount of dissolved oxygen in solution but increases the rate of almost all chemical reactions. Generally for strong oxidisers, increase in temperature greatly increases the oxidising power. The effect of temperature on corrosion rate is well known to be rapid or exponential increase as the temperature increases. Also for stainless

steel in the passive state, close to the transpassive region, there could be a negligible increase in corrosion rate as temperature increases until a critical temperature that influences the switch from passive to transpassive state is attained, at which stage very rapid increase in corrosion rate is observed. Even at low anodic polarisation levels, all the curves in Figure 50 exhibit some fluctuations (a very noisy region) during the forward scan similar to those curves at room temperature. However, the fluctuations were not immediate. The curves show typical activation-passivation behaviour followed by pitting initiation and positive hysteresis. The extent of the passive region were more pronounced in the 13Cr specimens in deoxygenated seawater with 100ppm sodium nitrate, 100ppm and 400ppm sodium nitrite which implies that increase in temperature improved the ability for sodium nitrate and sodium nitrite to facilitate a protective film on 13Cr. This however cannot be over emphasised because the blank solution also exhibited similar behaviour, it was just not as pronounced. It is more logical to conclude that the passivation was attributed to increase in temperature. It is also worth noting that positive hysteresis loop for 13Cr in deoxygenated seawater with 100ppm sodium nitrite at 80^{o}C also had a closed loop as experienced at 25^{o}C however, the protection margin dropped from 198mV at 25^{o}C to 86mV at 80^{o}C. This implies that increasing the temperature dropped the protection margin by over 100mV rendering 13Cr more susceptible to pitting at 80^{o}C than 25^{o}C. It is possible that at a critical temperature, 13Cr could switch from the passive state to the transpassive region. This was however not explored further because it is outside the scope of this research work.

Contrary to what was observed for 13Cr in 100ppm sodium nitrite solution at 25^{o}C, at 80^{o}C 100ppm of sodium nitrite did not increase the corrosion rate compared to the blank solution. It actually dropped the corrosion rate slightly. This gives an indication of the temperature dependence on the effect of low concentration of nitrite (below critical concentration) on 13Cr. This is a very important point to note because the increase in corrosion rate due to injection of 100ppm sodium nitrate in field applications (which was reduced to nitrite by the nitrate reducing bacteria, NRB) as observed on topside piping, subsea flow lines and risers on both Shell Bonga and Usra Princess platforms is not necessarily what should be expected in the sub-surface components

(especially water Injector wells downhole components) because the temperature are higher. As shown in Figure 2, 13Cr is extensively used as construction material for downhole components such as parkers, sleeves and tail pipe assembly and the base pipe for the screens in a typical water injection well that would be exposed to nitrate/nitrite used as anti souring control agent. Due to high pressure and high flow velocities, heat is generated due to friction; the temperature of injected seawater downstream of the choke is around 80^{o}C. Hence the presence of low concentration of nitrite in the seawaters could actually lower the corrosion rate. Hence, 13Cr is a suitable material for downhole components provided it is not polarised beyond the passivation potential.

In a publication made by Shell Global Solution in 2008 on the selection of Sand Screen Materials for Seawater Injection Wells, it was concluded that 13Cr is susceptible to pitting corrosion at dissolved oxygen concentrations (DOC) ranging from 17ppb to 7.8ppm. When 316L and 825 stainless materials were used for the bottom-hole sand-screen assembly and coupled to casing made of low alloy or carbon steel similar to P110 Cr-Mo, (but not 13Cr-80), it provides acceptable lifecycle performance in seawater injection service, exposed to intermittently oxygen control excursions due to the low oxygen exposure or being galvanically protected in this service[5].

It is worth noting that an additional CPP curve for 13Cr specimen immersed in deoxygenated seawater with 400ppm sodium nitrite solution overnight for over 12hours before polarisation was initiated.

Figure 51 shows the open corrosion potential measured overnight before initiating polarisation, the graph shows rapid decline in the corrosion potential in the direction of active corrosion in the first hour indicating active corrosion before either the inhibiting effect of nitrite or repassivation of 13Cr began. The open circuit potential after the first hour was –533.9mV, after which the open circuit potential started to fluctuate such that for every drop in potential, there was a corresponding increase in potential indicating pitting and repassivation. The fluctuation is understandable considering the fact that the chromium content in 13Cr-L80 is slightly less than the critical concentration of 15% required for self healing process of chromium (III) oxide passive film[257].

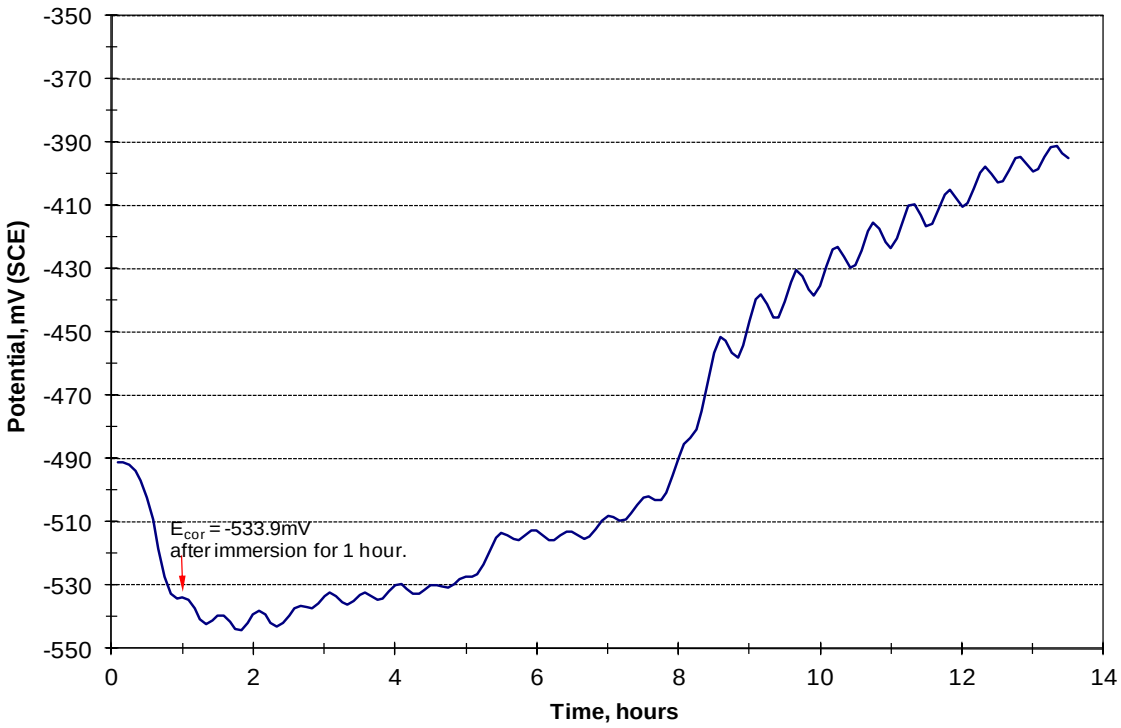

Figure 51: Graph showing open circuit potential for 13Cr in deoxygenated seawater with 400ppm $NaNO_2$ at 80^oC

By the 5th hour, the potential slightly increased. By the 8th hour, there was a more significant increase in the potential after which every slight decrease in potential due to active corrosion was repassivated with a gradual increase in potential in the more noble direction until the test was stopped. The value of the open circuit potential at the beginning of the test before the drop in potential started was not attained until after 8 hours.

The graph validates the methodology as prescribed by ASTM G61[250] indicating that soaking the specimen for an hour gives a conservative corrosion potential. It also indicates the need to use similar soaking period for all the tests for consistency.

As shown in Figure 50, the CPP curve for 13Cr in deoxygenated seawater with 400ppm sodium nitrite at 80^oC indicates more pronounced anodic polarisation compared to the other curves. When compared to that of 100ppm sodium nitrite solution, it was anodically polarised by over 215mV which indicates it was more passive. Also the corrosion rate dropped substantially. The forward scan showed full passivation with no fluctuation (i.e. no pit). The passive film was actually preserved until it transitioned from passive region to

transpassive region where the passive film broke down and there was significant corrosion.

At transpassivity, the oxidation state of chromium changed from Cr^{3+} (Cr_2O_3) to Cr^{6+} (CrO_4^{2-}) as illustrated in the following reaction;

$$5H_2O + Cr_2O_3 \rightarrow 2CrO_4^{2-} + 10H^+ + 6e^-$$

However, there was water zone stability and Cr^{6+} is unstable because its potential is higher than that of oxygen evolution (i.e. $E_{anode} > E_{cathode}$) hence solution oxidation occurred resulting in further polarisation.

The specimen was over-polarised to the maximum polarisation current density of 1mA/cm^2 before the reverse polarisation was initiated. This indicates that 400ppm of sodium nitrite was able to protect 13Cr from active dissolution in seawater however, if for any reason, 13Cr is polarised 200mV above the corrosion potential, it transitions from passivation to transpassivation and a corresponding corrosion rate in the order of 1mA/cm^2 is expected. The pH of the solution dropped from 8.2 before polarisation to 7.08 after polarisation. This is understandable as the oxidation of chromium from oxidation state of III to VI and/or oxygen evolution reaction generate hydrogen protons (H^+). The clear solution at the beginning of the test changed to dirty brown solution probably as a result of high oxidation state salts of ferric.

Lastly, the pitting potentials of 13Cr in the various test solutions were almost the same except for the solution with 100ppm sodium nitrate which was slightly higher. However, the corresponding corrosion rates at the pitting potentials were different. The range of nitrate/nitrite concentration was however very low, (below the critical nitrate/nitrite concentration for inhibition), this possibly explains why their pitting potentials were close. This was further explored when higher sodium nitrite concentrations were used. It was found that with sodium nitrite concentration above 400ppm, the pitting potential substantially increased.

The appearance of post-test specimens for 13Cr in blank deoxygenated seawater, deoxygenated seawater with 100ppm sodium nitrate, deoxygenated seawater with 100ppm and 400ppm sodium Nitrite at 80^{o}C are as shown in Figure 52A/B/C/D respectively.

A: 13Cr blank solution at 80°C, 5ppb [O]

B: 13Cr 100ppm $NaNO_3$ at 80°C, 5ppb [O]

C: 13Cr 100ppm $NaNO_2$ at 80°C, 5ppb [O]

D: 13Cr 400ppm $NaNO_2$ at 80°C, 5ppb [O]

Figure 52: Photographs of post-test specimens of 13Cr polarised in 5ppb [O] seawater at 80°C

Pits and etched patches were found on most of the 13Cr specimens in various test conditions. The intensity of the pits increased with the increase in sodium nitrite concentration. This is consistent with the CPP curves. Although the open circuit potential increased anodically with the sodium nitrite concentration making the thermodynamics of the corrosion less favourable with increased nitrite concentration due to the passive film formation. However, as the samples were polarised, the kinetics of the reaction at the pitting potential increased. It was highest at 400ppm Sodium nitrite. Also pitting corrosion was active for some time after reversing the scan direction. Figure 53 shows the CPP curves of 13Cr in deoxygenated seawater solution with different sodium nitrite concentrations: 0ppm 100ppm, 400ppm, 1000ppm, 5000ppm, 8,250ppm and 12,500ppm.

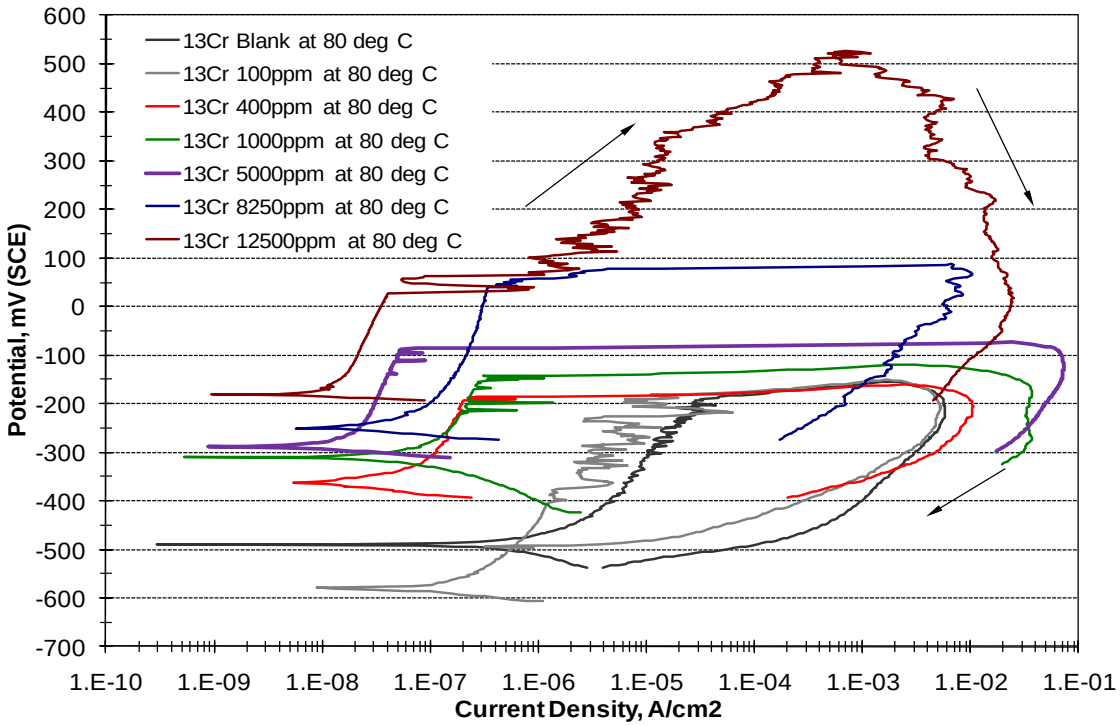

Figure 53: CPP curves for 13Cr with different sodium nitrite concentrations at 80^{o}C

The curves show a regular trend; as the sodium nitrite concentration increased the corrosion potential became more-noble and the anodic polarisation curves shifted to lower currents given a net reduction in corrosion rate due to passivation. As described in section 2.6.2 and illustrated in Figure 14, the corrosion rates for each of the CPP curves generated at various sodium nitrate concentrations tested were estimated by extrapolating the linear portions of the anodic and cathodic Tafel regions in the log current versus potential plot back to their intersection. The estimated corrosion rate is the value of the current at the point where the two linear segments of the extrapolated anodic and cathodic curves intersect. At the point of intersection, the rate of the cathodic reaction and the rate of the anodic reaction are equal. Comparing CPP curves in Figure 53 with those in Figure 48, the CPP curves at 80^{o}C temperatures have more drastic transition from active corrosion to passivity and the linear region of the curves were very close to E_{cor} but at 25^{o}C, the transition from active corrosion to passivity were not as drastic and linear region of the curves were further away from E_{cor}. Since the CPP curves were polarised by close to 500mV away from $E_{cor,}$ in order to properly identify the linear portions of the anodic and cathodic of Tafel regions in the log

current versus potential plot, the scale of the x and y axes were changed to show the cathodic curves and only the active corrosion transitioning into the passive region of the anodic curve, ensuring linear region with at least one decade of current density. For anodic curves where the linear region was not sufficiently long enough, best fit straight lines were draw through the linear section ensuring the line was tangential to the curve at the section where it transitioned from active corrosion to passive corrosion i.e. where the increase in current density stops and increase in potential starts. Based on the extrapolated data, graphs of the open circuit potential and the corresponding current density were plotted as a function of the sodium nitrite concentration in deoxygenated seawater solution as shown in Figure 54.

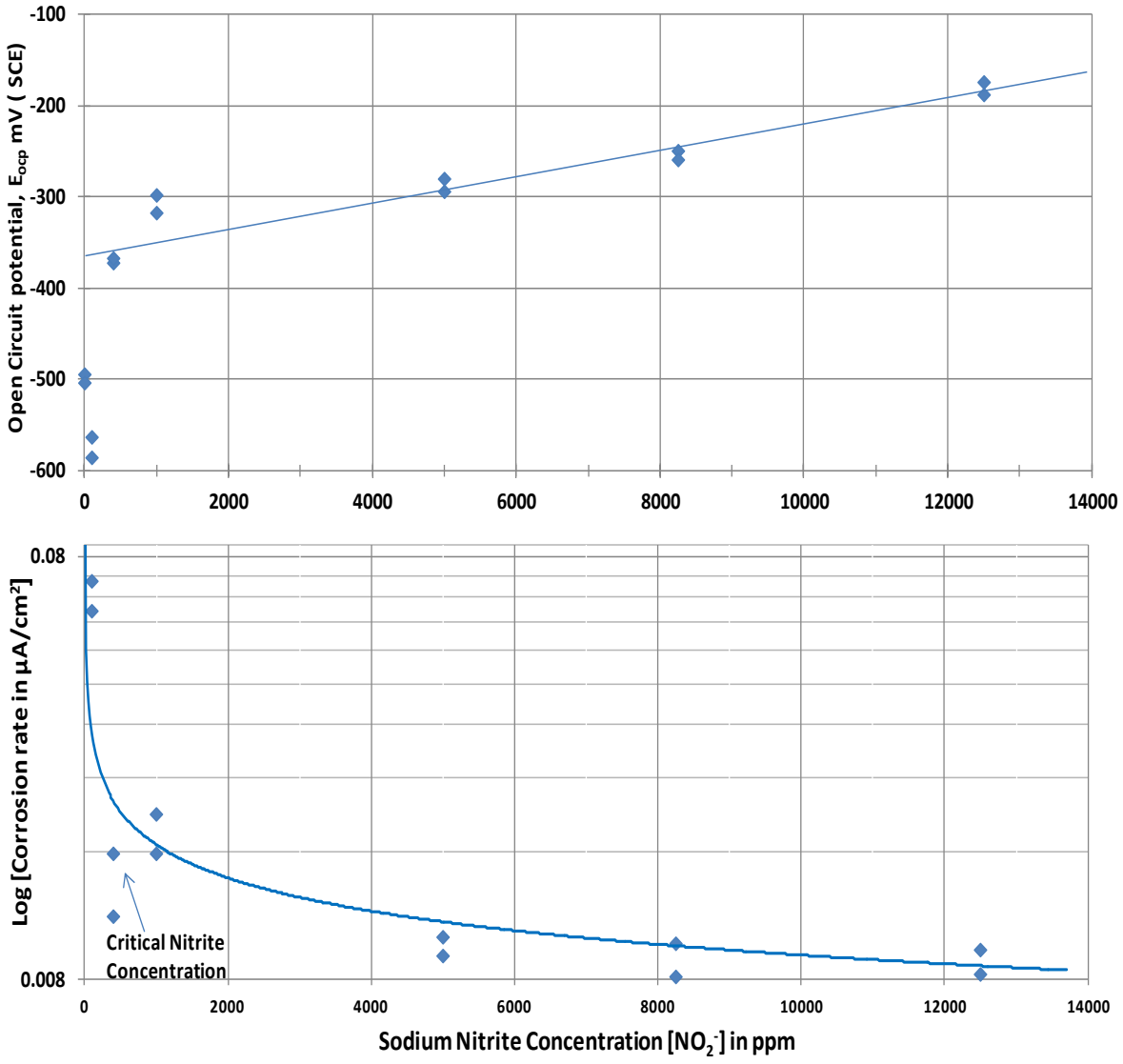

Figure 54: Open circuit potential and current density as a function of nitrite concentration in deoxygenated seawater in type 13Cr-L80

There were two regions on the potential versus nitrite concentration graph. The first region was from 0ppm to the critical nitrite concentration of 400ppm which shows unstable potential probably due to pitting and repassivation of the pits happening simultaneously. Above the critical nitrite concentration of 400ppm, the potential was pretty stable and shows a linear increase in potential as the nitrite concentration increased. Formation of chromium oxide (Cr_2O_3) passive film on stainless steel could be spontaneous, at a point in the passive state, the film growth results in increased potential. Hence it is logical to infer that increase in nitrite concentration influenced the chromium oxide (Cr_2O_3) passive film growth. The chromium oxide passive film is electrically semi-conductive.

It is well known that anodic passive current density is attributed to the semi-conductivity of passive film; however, how the semi-conductive passive film influences the kinetics of cathodic reactions is not well known. Increased passivity led to a corresponding decrease in corrosion rate, as shown in the CPP curves in Figure 53 and the graph of current density as a function of nitrite concentration in Figure 54. As the nitrite concentration increased, the corrosion rate decreased. The decrease in corrosion rate is more pronounced after the critical nitrite concentration.

As shown in Figure 54, the graph for $Log(i_{cor})$ against sodium nitrite concentration shows an asymptotic curve. Once the critical sodium nitrite concentration of 400ppm was attained, further increase in sodium nitrite concentration did not significantly change the corrosion rate. This phenomenon is illustrated in Figure 55 which shows the typical effect of anodic inhibitors, with the corrosion potential increased in the anodic direction (more-noble) and a corresponding shift in the anodic polarisation curve to lower currents and a net reduction in the corrosion rate. Anodic inhibitors do not have any significant effect on the cathodic curve. The effect of increased sodium nitrite concentration on the cathodic CPP curves was covered in 4.2.1.

According to Figure 53, all the CPP curves show typical activation-passivation behaviour followed by pitting initiation and positive hysteresis loops. The passivation transition was more pronounced in the 13Cr specimens at nitrite

concentration of 400ppm and above. For the blank and 100ppm, the forward scan showed early fluctuation implying pitting at about -550mV while for the other CPP curves, the passive film was preserved until very close to the pitting potential when it transitioned from passive region to transpassive region where the passive film broke down and there was significant corrosion reaching a corrosion rate of the order of 1mA/cm^2 before the reverse scan.

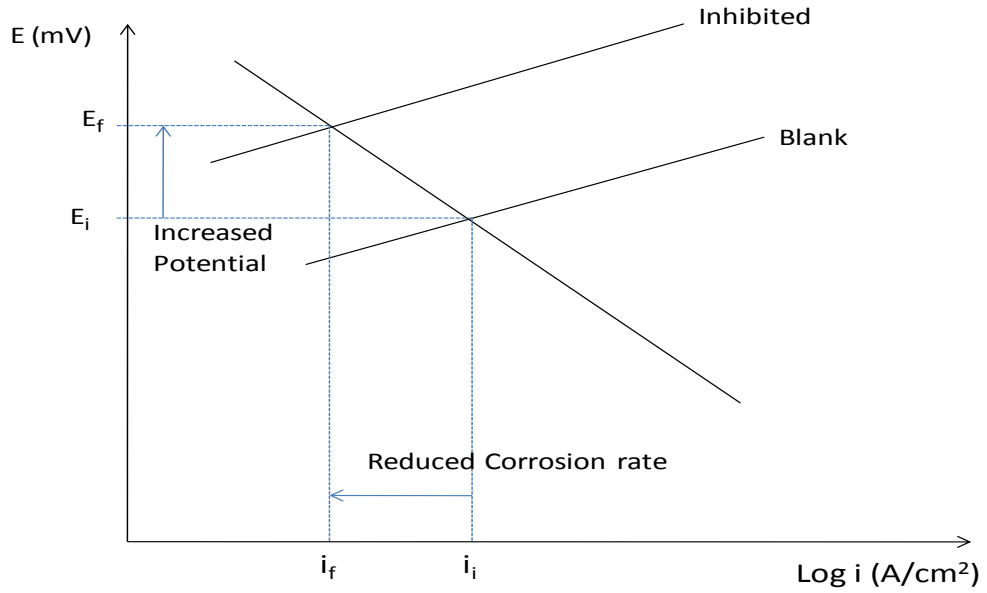

Figure 55: Typical effect of anodic inhibitors

Unlike the other curves with instantaneous increase in the current density, at nitrite concentration of 12,500ppm the forward scan showed full passivation with no fluctuation (i.e. no pit). The passive film was preserved until it transitioned from passive region to transpassive region however, the destroyed passive film tried to repair and repassivate but was not able to completely repassivate. This is evident by the fluctuation observed after breakdown of the passive film. The resistance developed due to attempt of the passive film trying to repassivate and/or excessive solid reddish brown rust deposit suspected to be iron (III) oxide, Fe_2O_3 probably led to significant increase in the potential reaching almost 550mV before attaining the maximum current density of 1mA/cm^2 that activated the reverse sweep.

Except for the curve at 100ppm, none of the other curves had a closed hysteresis. Even the curve at 100ppm sodium nitrite that had a closed hysteresis only has a protection margin of 86mV. This indicates that at 80^{o}C,

13Cr is susceptible to pitting in deoxygenated seawater (5ppb) at all sodium nitrite concentration up to 12,500ppm, even though nitrite polarised 13Cr to more noble potential and significantly reduced the corrosion rate. It is worth noting that the pitting potential for 13Cr was almost the same up to sodium nitrite concentration of 400ppm after which it increased significantly with increase in sodium nitrite concentration. This indicates that between 400ppm and 1000ppm sodium nitrite concentration, there was a change in the passivation which was capable of shifting the pitting potential by over 50mV in the anodic direction. Hence it was inferred that a minimum of 400ppm sodium nitrite and a critical concentration between 400ppm and 1000ppm is required to form a complete passive film. Beyond 1000ppm, the passive film grows and increases the pitting potential. Figure 56 shows the critical breakdown potential for Type 13Cr-L80 as a function of nitrite concentration at 80^{o}C, pH 8.2 with a voltage scan rate of 0.2mV/s.

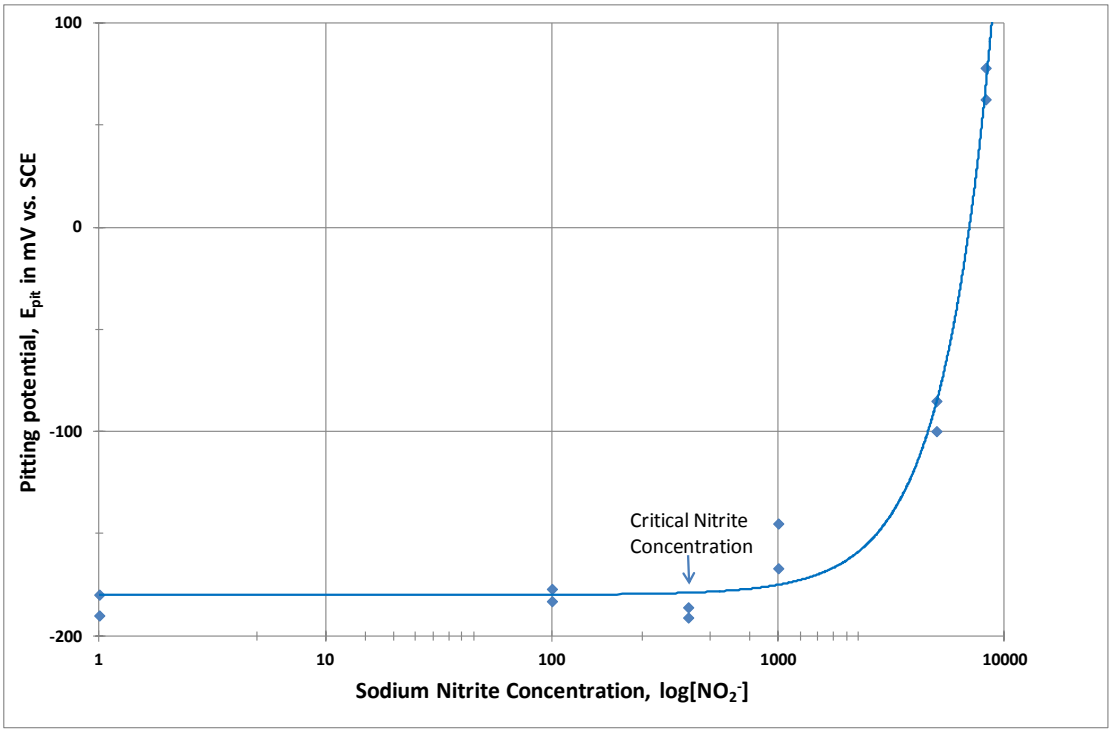

Figure 56: Critical breakdown potential for Type 13Cr-L80 as a function of nitrite concentration at 80^{o}C, pH 8.2 with a voltage scan rate of 0.2mV/s

As shown, at low nitrite concentration, the critical breakdown potential increased slightly with increasing nitrite concentration until the critical nitrite concentration of 400ppm was reached.

At higher concentrations, the pitting potential increased very quickly and as shown in Figure 57, the pitting density observed was greatly reduced. This result is similar to the test results previously reported by Macdonald[43] and Dahan[180] for nitrate on Type 316 stainless steel. The test result further validates the point defect model[43] and the sudden increase in pitting potential indicates saturation of the surface oxygen vacancy absorption sites at the barrier layer/solution interface, such that chloride ions are excluded, at least at those sites at which breakdown occurred.

This test result also validates the inhibiting ability of oxyanion (nitrite in this case). Inhibition is attributed to competitive adsorption of the oxyanions into surface oxygen vacancies in a manner that does not result in cation vacancy generation, thereby depriving chloride ion from absorption sites at the barrier layer/solution interface. It is also a confirmation of Macdonald and Yang's postulation[43] that oxyanion absorption is irreversible hence cannot aid in cation extraction. It is however worth noting that pitting was observed at the tip of the working electrode and under solid deposits above 1000ppm, this was probably due to the fact that the electrodes were polarised to the transpassivity region as shown in Figure 53 hence it is inferred that the pitting observed occurred during transpassivity. The test results confirm the postulation that the critical nitrite concentration for 13Cr-L80 determined in 4.3.1 is actually the critical concentration required to repassivate 13Cr-L80 after pitting. As shown in Figure 54 and Figure 56, the actual critical nitrite concentration required to inhibit pitting is about 400ppm however the test method used in section 4.3.1 was not fast enough to demonstrate pitting inhibition before pitting occurred. Also the corrosion rate measured after inhibition in section 4.3.1 corresponds to repassivation current density for 13Cr-L80 at potential of -250mV (SCE) on the CPP curve for 400ppm sodium nitrite solution shown on Figure 50.

Lastly, as observed from the curves in Figure 48, injection of nitrate/nitrite led to increase in the current density (rather than decrease in current density) at low concentrations but at high concentration, nitrite injection actually led to decrease in current density. Figure 53, Figure 54 and Figure 56 show that the decrease in current density was more pronounced once the nitrite concentration was above the critical concentration indicating that increase in

current density observed at low nitrite concentration was probably due to the fact that nitrite present was not sufficient to protect the entire metal surface hence causing a partial protection and the unprotected surface experienced increased localised corrosion due to smaller anode surface area. However at higher temperature (80^{o}C), increased current density was not observed in Figure 50 and Figure 53 with the same low concentrations of nitrate/nitrite, contrary to what was observed at room temperature. This is consistent with the results of the classic corrosion program conducted at the National Physical Laboratory, United Kingdom in the 1960's[44-50], and also preliminary assessment of effect of nitrate treatment conducted by Shell Global Solution in United State[6], which states that at low concentrations; nitrate is classified as non-oxidising, however test results showed some evidence of nitrate electro-reduction only in high concentrated solutions which may be more prominent at higher temperatures[44]. It is however worth stating that the classic corrosion program conducted at the National Physical Laboratory in UK were performed using mild steel while the preliminary assessment done in the USA used carbon steel and 13Cr.

Figure 57A/B/C/D/E/F and Figure 58 show the photographs of the post-test specimens of 13Cr polarised in 5ppb [O] seawater with 0ppm, 100ppm, 400ppm, 1000ppm, 5000ppm, 8250ppm and 12500ppm sodium nitrite concentrations respectively at 80^{o}C.

Figure 57A/B/C show progression of small pits all over the specimen as the nitrite concentration increases up to 400ppm. At nitrite concentration of 1000ppm few pits were observed but more of general corrosion with slight brownish deposit on the specimen as shown in Figure 57D. This is consistent with the observation on the CPP curves and further supports the inference that at 1000ppm, the sodium nitrite concentration was sufficient to form a complete passive film on the metal surface. As the sodium nitrite concentration was increased to 5000ppm, as shown in Figure 57E brown solid deposits concentrated at the tip of the specimen and massive metal loss probably resulted from propagation of several pits observed underneath the solid deposit. The specimen was fabricated from plates and carefully machined into cylindrical form.

A: 13Cr blank solution

B: 13Cr 100ppm $NaNO_2$

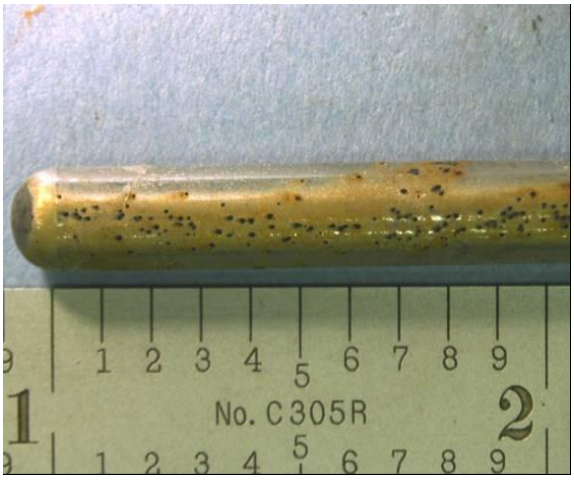

C: 13Cr 400ppm $NaNO_2$

D: 13Cr 1000ppm $NaNO_2$

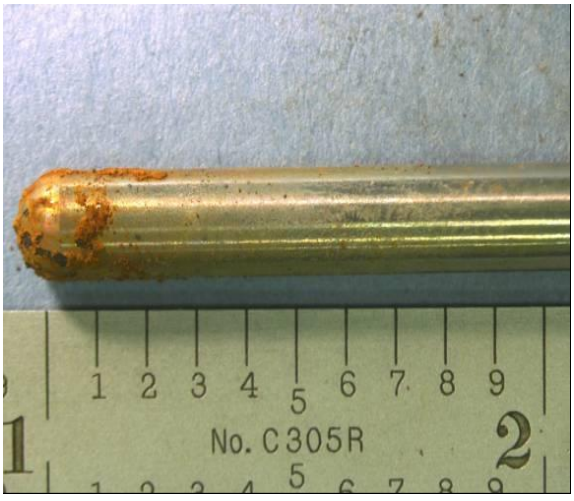

E: 13Cr 5000ppm $NaNO_2$

F: 13Cr with 8,250ppm $NaNO_2$

Figure 57: Photographs of post-test specimens of 13Cr polarised in 5ppb [O] seawater with different Sodium nitrite concentrations at 80°C

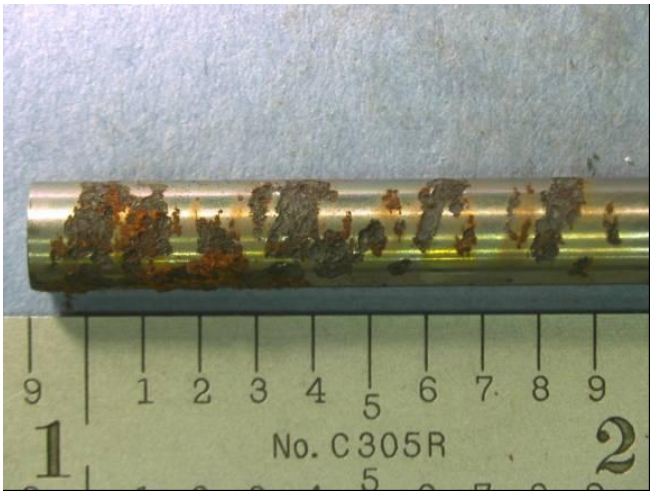

13Cr with 12,500ppm $NaNO_2$ at 80^oC

Figure 58: Photograph of post-test specimens of 13Cr polarised in 5ppb [O] seawater with Sodium nitrite concentration of 12,500ppm at 80^oC

Although the edges were rounded, the tip of the specimen is probably an area of high stress concentration hence has high tendency for pit initiation and propagation. Also the tip of the specimen is typically difficult to be completely covered by a thin protective film layer because of its shape. No pit was observed along the specimen but tiny solid deposits. Hence it was inferred that the actual passive film breakdown was at the tip of the specimen and the increased current density measured was as a result of corrosion at the tip of the specimen. This is an important point to be noted in the design of a system to be protected by inhibition.

Stress concentration areas must be avoided; all angles, tips and corners must be properly rounded. Unfortunately such areas of high stress concentration and potential spots for pitting initiation are also areas that are difficult to protect by the thin film of the anodic inhibitor. As the sodium nitrite concentration increased from 5,000ppm to 8,250ppm and 12,500ppm, there was excessive reddish brown solid deposit almost covering the entire specimen.

Figure 57F shows the specimen in 8,250ppm sodium nitrite solution with substantial amount of solid brown deposit on the entire specimen. Unlike Figure 57F where the solid brown deposit was preserved, Figure 58 shows the specimen in 12,500ppm sodium nitrite solution after the brown deposit on

the specimen had been washed in deionised water and dried using nitrogen to reveal the under deposit corrosion.

The photograph reveals severe localised corrosion attack under the solid deposit. This is not surprising as the CPP curve for 13Cr at sodium nitrite concentration of 12,500ppm shown in Figure 53 shows fluctuations (a very noisy region) on both the forward and reverse scans after breakdown of passivity, with the current density attaining over 20mA/cm^2. The severe localised corrosion is probably as a result of several pit initiation, and pit propagation with small pits merging with adjacent pits to form a bigger pit.

Figure 59 shows the CPP curves of 22Cr in fully oxygenated blank solution, deoxygenated blank solution, 100ppm sodium nitrate solution and 100ppm sodium nitrite solution all at 25^{o}C (room temperature).

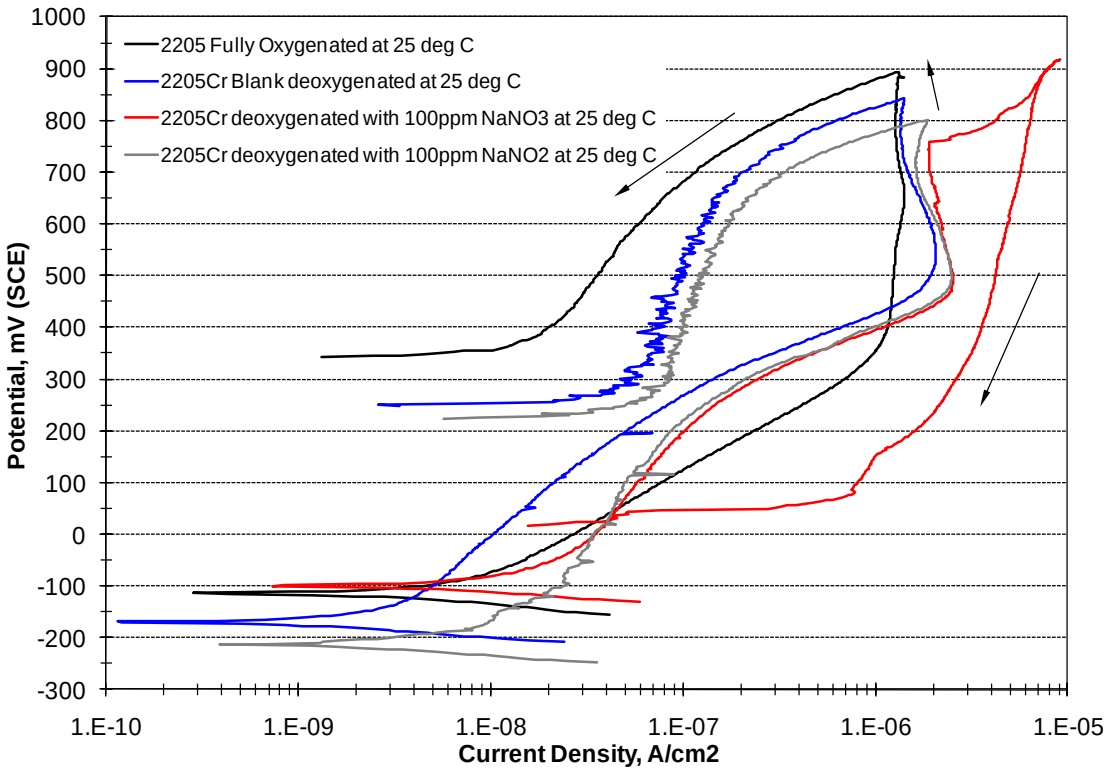

Figure 59: CPP curves for 22Cr at 25^{o}C

As shown in Figure 59**,** at room temperature, 22Cr in fully oxygenated seawater solution exhibits typical activation-passivation behaviour with no passive film breakdown or pitting initiation. The passive film continued to grow as the potential increased until a peak forward potential of 1V versus E_{cor} was reached, at which stage the reverse sweep was initiated. Since the passive

film was not destroyed, it is not surprising that the current density of the reverse scan was less than that of the forward scan hence given negative hysteresis loop. The curves for 22Cr in blank deoxygenated seawater and deoxygenated seawater with 100ppm sodium nitrite also exhibit typical activation-passivation behaviour with current fluctuation in the active stage and later transitioned into the passive zone until the peak forward potential of 1V versus E_{cor} was reached, at which point the reverse sweep was initiated. The current densities of the reverse scan of both curves were less than those of the forward scans hence given negative hysteresis loops. The slight fluctuations experienced during the forward and reverse sweep is probably due to partial breakdown of the passive film, which was quickly repaired (i.e. prompt repassivation) but not pitted. As shown in Figure 29, Alloy S32205 has 22.5% chromium, which is more than the 15% critical concentration[257] required for self healing process of the Chromium (III) oxide (Cr_2O_3) passive film. Chromium is known to have a strong tendency to form oxy-hydroxide compounds and the presence of chromium in the passive film on Fe-Cr alloys is believed to ensure a somewhat hydrated structure for the oxide[263]. In fact, it has been suggested that bound water is present in the film which helps to facilitate film repair after film breakdown[264].

Alloy S32205 also contains Nickel, Manganese and Nitrogen, the three most common elements used to stabilise austenite. It also contains Molybdenum which improves the stability of the passive film especially in the presence of chloride ions. The passive film formed on austenitic stainless steel is often reported to be duplex consisting of an inner barrier oxide film and an outer deposit hydroxide or salt film. Passivation is generally believed to take place by the rapid formation of surface-adsorbed hydrated complexes of metals that are sufficiently stable on the alloy surface. The hydrated complexes further react with water to form hydroxide which, rapidly losses their proton (deprotonate) to form an insoluble surface oxide film that has corrosion rate that is too low (range of 0.05$\mu A/cm^2$) to sustain pit propagation

The curve for 22Cr in deoxygenated seawater with 100ppm sodium nitrate solution also exhibits typical activation-passivation behaviour but with passive film breakdown or pitting shortly after passivation was initiated leading to

increased current at about 750mV. The current density of the reverse scan was more than that of the forward scan hence giving a positive hysteresis loop. The reverse sweep crossed the forward sweep in the active dissolution region and had a protection margin of only 127mV. Hence 22Cr is susceptible to pitting at room temperature in 100ppm solution of $NaNO_3$ but not susceptible in all the other test conditions at room temperature (negative hysteresis). This inferred that injection of sodium nitrate into seawater solution has a significant effect on the use of 22Cr. It initially passivates the surface of 22Cr thereby making it to have a more positive potential (i.e. more-noble) than even the fully oxygenated seawater solution but the passive film could not be sustained hence 22Cr eventually became susceptible to pitting corrosion with nitrate injection as low as 100ppm. Studying the effect of higher concentration of sodium nitrate was not included in the scope of the work because typical nitrate treatment is 100ppm of sodium nitrate. However the study of increased concentration of sodium nitrite was in the scope since the philosophy of nitrate injection as a means of preventing reservoir souring advocates the reduction of nitrate to nitrites, nitrous oxide or even nitrogen by nitrate reducing bacteria (NRB) and also nitrate reducing Sulphide Oxidizing Bacteria (NRSOB) hence the chances of nitrate accumulation is very slim. Addition of 100ppm $NaNO_2$ on the other hand shifted the initial potential to more active corrosion potential and slightly increased the corrosion rate. This is similar to what was observed in the case of 13Cr at room temperature and low concentrations of nitrite but the increase in corrosion rate was not as pronounced as that of 13Cr. This further supports the inference that the increase current density observed was as a result of localised action of the unprotected surface. However, the effect of the localised action was not as bad because 22Cr has better passive protection. It is worth noting that the corrosion rate in all the test conditions were in the same range with the curves reaching their maximum corrosion rate at a potential of about 500mV except in the case of fully oxygenated seawater solution. In which case, the maximum corrosion rate was attained around 400mV. Given a 100mV shift compared to others. This is probably due to the fact that the fully oxygenated solution had more oxygen available to drive the corrosion process more than others. The Tafel slope during active corrosion which is an activation controlled process for 22Cr in fully

oxygenated seawater solution was slightly lower than those of the deoxygenated blank seawater solution, 100ppm sodium nitrate and 100ppm sodium nitrite solution. Hence slight increase in potential results in higher corrosion rates compared to the other curves.

Figure 60A/B/C/D show the photographs of the post test specimens for 22Cr in seawater solution with fully oxygenated blank, deoxygenated blank, 100ppm sodium nitrate and 100ppm sodium nitrite respectively.

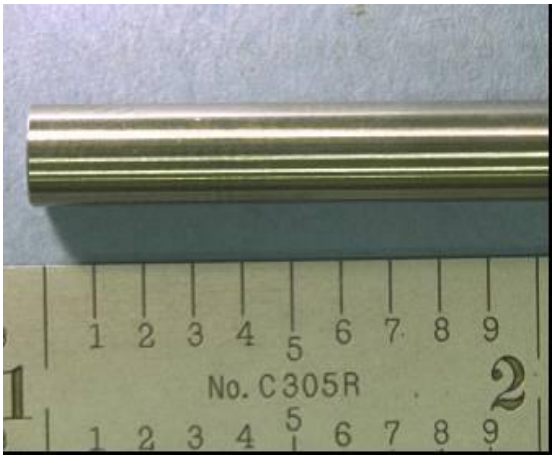

A: Blank fully oxygenated, 7600ppb [O]

B: Blank deoxygenated, 17ppb [O]

C: 100ppm $NaNO_3$, 17ppb [O]

D: 100ppm $NaNO_2$, 17ppb [O]

Figure 60: Photographs of post-test specimens of 22Cr in seawater at 25^{o}C

Figure 60A shows the post specimen photograph for 22Cr in fully oxygenated seawater at room temperature with no pit observed. Inputting the chemical composition data from the materials test report for S2205 provided in Figure 29 into the pitting resistance equivalent number equation 63, the PRE_N for S32205 is 35.46. From corrosion test data published by ATI Allegheny Ludlum in their technical data blue sheet for lean duplex Stainless steel ATI 2102^{TM}

Alloy[183] shown in Figure 20 and Figure 21, the critical pitting temperature (CPT) for S32205 is 48^{o}C while the critical crevice temperature (CCP) is 20^{o}C.

Pitting resistance equivalent numbers (PRE_N) is a theoretical way of comparing the pitting corrosion resistance of various types of stainless steels, based on their chemical compositions. Typically, $PRE_N \geq 40$ is required to adequately provide pitting resistance. However, the PRE_N for S32205 is close enough to 40 and the test temperature is lower than the critical pitting temperature. Hence it is not surprising that no pit was observed in the test sample at room temperature. Also since the test specimen was properly mounted on the electrode holder ensuring no crevice between the test specimen and the TFE-Fluorocarbon compression gasket, no localised corrosion was anticipated for 22Cr in deoxygenated seawater at 25^{o}C. Had this not been the case, crevice corrosion could easily have occupied between the test specimen and the TFE-Fluorocarbon compression gasket since the critical crevice temperature was lower than the test temperature. The solution at the end of the test was clear and the pH only dropped from 8.2 at the beginning of the test to 8.18 at the end of the test. This is consistent with the fact that the CPP curve gave a negative hysteresis loop and the reverse sweep of the sample kicked off shortly after the transition from active dissolution to passive region and the current density was only 1.43μA/cm^2.

Figure 60B shows the post specimen photograph for 22Cr in deoxygenated blank seawater at room temperature. There was no visible pit; the solution at the end of the test was clear and the pH did not change substantially. This is consistent with the fact that the CPP curve gave a negative hysteresis loop and the reverse sweep of the sample was initiated shortly after the transition from active dissolution to passive region just like the fully oxygenated solution. Also the passivation current density was only 1.38μA/cm^2.

Figure 60C shows the post specimen photograph for 22Cr in deoxygenated seawater with 100ppm sodium nitrate at room temperature. There was no visible pit; the solution at the end of the test was clear and there was no substantial change in pH. The reverse sweep was initiated shortly after the transition from active dissolution to passive region just like the fully oxygenated solution however, the CPP curve gave a closed positive

hysteresis with a protection margin of 127mv. Although the rule of thumb is to have a protection margin > 200mV to adequately protect, however because the sample was not polarised beyond the passivation zone and the maximum current density was only 8.76μA/cm^2 hence, the test sample did not suffer any localised attack. Nevertheless, 22Cr is susceptible to localised attack in this test condition. Had the sample been polarised above 1000mV, there might have been localised attack. Figure 60D shows the post specimen photograph for 22Cr in deoxygenated seawater with 100ppm sodium nitrite at room temperature. There was no visible pit; the solution at the end of the test was clear and the pH did not substantially change. This is consistent with the fact that the CPP curve gave a negative hysteresis and the reverse sweep of the sample kicked off shortly after the transition from active dissolution to passive region just like the fully oxygenated solution. Also the passivation current density was only 1.79μA/cm^2.

Figure 61 shows CPP curves of 22Cr with deoxygenated blank solution, 100ppm sodium nitrate solution and 100ppm sodium nitrite solution at 80^{o}C.

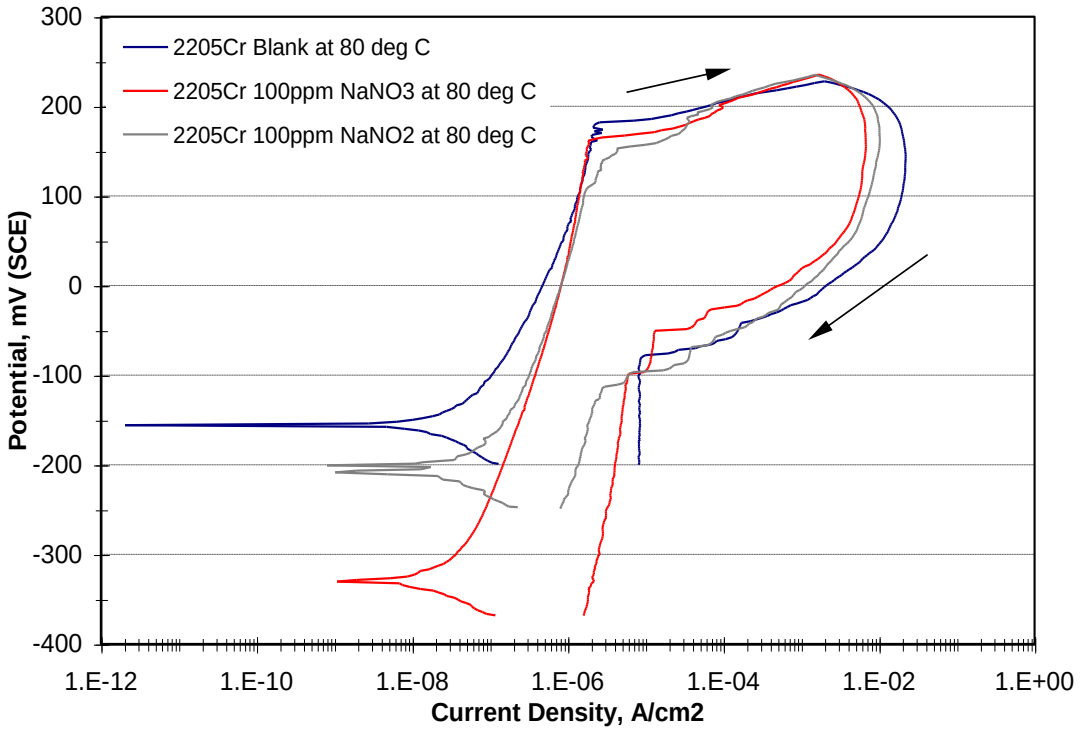

Figure 61: CPP curves for 22Cr in deoxygenated seawater at 80^{o}C

The curves illustrate the fact that increase in temperature increases susceptibility to corrosion. All the CPP curves exhibited active passive

behaviour however the transition from active to passive stage was almost instantaneous and passive region was more pronounced. Similar to the curves at 25^{o}C, the passivation current for all the curves were almost the same. All the curves showed passive film breakdown at a potential around 160mV (i.e. pitting potential) with increased corrosion rate up to 1mA/cm^{2} which initiated the reverse sweep. The corrosion rate in the reversed sweep were higher than those measured at the same potential in the forward sweep hence all the 3 curves had positive hysteresis contrary to what was observed at room temperature where only the solution with 100ppm sodium nitrate had positive hysteresis. The repassivation potentials for all the curves were below the corrosion potential hence they all had open loops with none of the reverse sweep crossing the forward sweep. The curve with 100ppm sodium nitrate was actually polarised to a more active corrosion potential indicating that nitrate probably inhibited the formation of passive film at 80^{o}C.The open circuit potential for 22Cr at both temperatures (i.e. 25^{o}C and 80^{o}C) were very similar for all the curves with the exception of deoxygenated seawater with 100ppm sodium nitrate where the open circuit potential shifted by over 200mV from -100mV at 25^{o}C to -330mV at 80^{o}C hence moving to more active corrosion potential with increased temperature whereas it had the most positive potential compared to the other curves at 25^{o}C. The magnitude of the increase in corrosion rate was in the order of 10 in all the test cases at 80^{o}C compared to their rates at 25^{o}C. Also the maximum current density for all the 3 curves were achieved at lower potential of about 140mV at 80^{o}C compared to 500mV at 25^{o}C giving a potential shift of over 300mV compared to the curves at room temperature. The three curves had similar characteristics, similar corrosion rates but different corrosion potential inferring that the addition of 100ppm sodium nitrate or sodium nitrite mainly affected the thermodynamics not the kinetics at 80^{o}C. The temperature increase mainly aided the passive film formation but as observed, once the passive film broke down, the corrosion rate was very high. The fact that all the curves have open positive hysteresis indicate that 22Cr is susceptible to pitting and localised corrosion in deoxygenated blank seawater solution, 100ppm sodium nitrate and 100ppm sodium nitrite seawater solution at 80^{o}C. The test temperature was higher than the critical pitting temperature of the test material hence it is

not surprising that the test material is susceptible to pitting and localised corrosion.

Figure 62A/B/C show the post specimen photographs for 22Cr in deoxygenated blank seawater solution, deoxygenated seawater solution with 100ppm sodium nitrate and 100ppm sodium nitrite at 80^{o}C respectively.

A: 22Cr blank solution at 80^{o}C, 5ppb [O]

B: 22Cr 100ppm $NaNO_3$ at 80^{o}C, 5ppb [O]

C: 22Cr 100ppm $NaNO_2$ at 80^{o}C, 5ppb [O]

Figure 62: Photographs of post-test specimens of 22Cr polarised in 5ppb [O] seawater at 80^{o}C

All the photographs exhibit similar characteristics with several minor pits and etched patches. This is not surprising as the experiment was conducted above the critical pitting temperature for S32205. Also the PRE_N is less than 40 hence susceptible to pitting. At the end of each test, the test solutions had slightly dirty rusty colour and some dirty brown solid deposits observed at the bottom of the glassware. The pH drop from 8.2 at the beginning of the test to about 7.83 at the end, this is probably as a result of the polarisation to 1mA/cm^2 (transpassivity) observed in all the CPP curves prior to the reverse sweep.

Figure 63 shows the CPP curves of 25Cr with fully oxygenated blank solution, deoxygenated blank solution, 100ppm sodium nitrate solution and 100ppm sodium nitrite solution at 25^{o}C (room temperature).

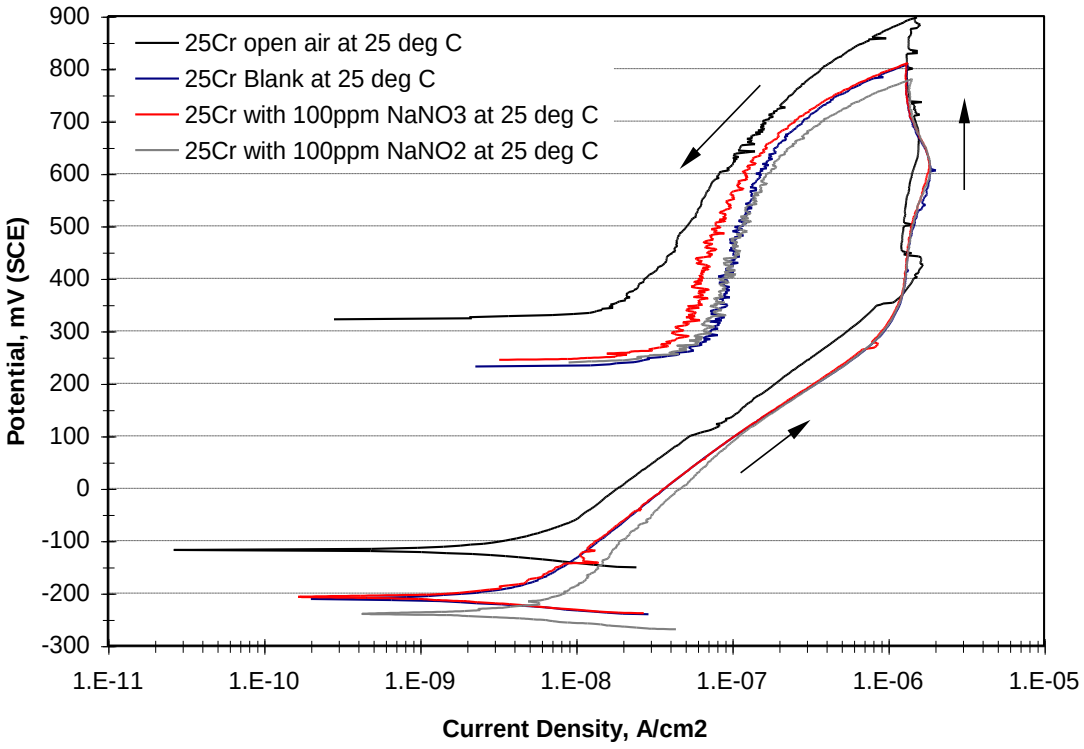

Figure 63: CPP curves for 25Cr at 25^{o}C

All the curves show typical activation-passivation behaviour with no passive film breakdown or pitting initiation up till maximum forward potential of 1V vs. E_{cor} was reached, at which point the reverse sweep was initiated. The current densities of the reverse scans were less than those of the forward scan hence giving negative hysteresis loops. 25Cr with fully oxygenated seawater solution

exhibits a more noble potential with a potential shift of about 85mV compared to 25Cr in deoxygenated blank solution. This is probably because of the presence of dissolved oxygen in the solution, which helped in the formation of the protective film, making it more passive compared to others. For 25Cr in fully oxygenated seawater, the maximum current density was attained around 400mV while it was around 600mV for others. This further shows the effect of oxygen on both the anodic and cathodic reactions making the corrosion to proceed at lower potential. Also the corrosion rate was slightly lower compared to other. Some fluctuations were observed in the passive region, indicating breakdown in passivation, which quickly healed and repassivated before pit formation and growth could occur.

Addition of 100ppm sodium nitrate to deoxygenated seawater had no effect on 25Cr. The curves with blank deoxygenated seawater and deoxygenated seawater with 100ppm sodium nitrate were very identical, following the same path in the forward sweep but slightly different path in the reverse sweep. Interestingly, the reverse sweep for 25Cr in 100ppm sodium nitrate and 100ppm sodium nitrite followed the same path. Hence having identical corrosion potential and corrosion rates, it is worth noting that 25Cr in blank deoxygenated seawater also had some fluctuations in the passive region during forward sweep similar to those observed in the fully oxygenated seawater solution which also indicates breakdown in passivation, but quickly healed and repassivated before pit formation and growth could occur.

Addition of 100ppm sodium nitrite to deoxygenated seawater had a slight effect on 25Cr, the corrosion potential dropped by about 40mV toward active corrosion compared to blank deoxygenated solution and that with 100ppm sodium nitrate. This indicates that 100ppm nitrite lowered the passivation potential of 25Cr and also slightly increased the corrosion rate. This is probably due to the partial protection of part of the specimen by nitrite leading to increased corrosion of the unprotected sections as earlier discussed in the case of 13Cr and 22Cr. No fluctuation was observed in the passive region during the forward sweep of 25Cr in both the 100ppm sodium nitrate and 100ppm sodium nitrite solutions, this indicates that these two solutions either assisted in passivation or prevented breakdown of the passive film. All the

curves however showed fluctuation in the reverse sweep but less pronounced in 25Cr in fully oxygenated seawater which was probably due to the presence of complete passive film of chromium (III) oxide (Cr_2O_3) which was aided by the presence of oxygen.

Figure 64A/B/C/D show photographs of the post test specimen for 25Cr in fully oxygenated seawater, deoxygenated blank seawater, deoxygenated seawater with 100ppm sodium nitrate and deoxygenated seawater with 100ppm sodium nitrite respectively. None of the photographs show any pit neither was there any discoloration.

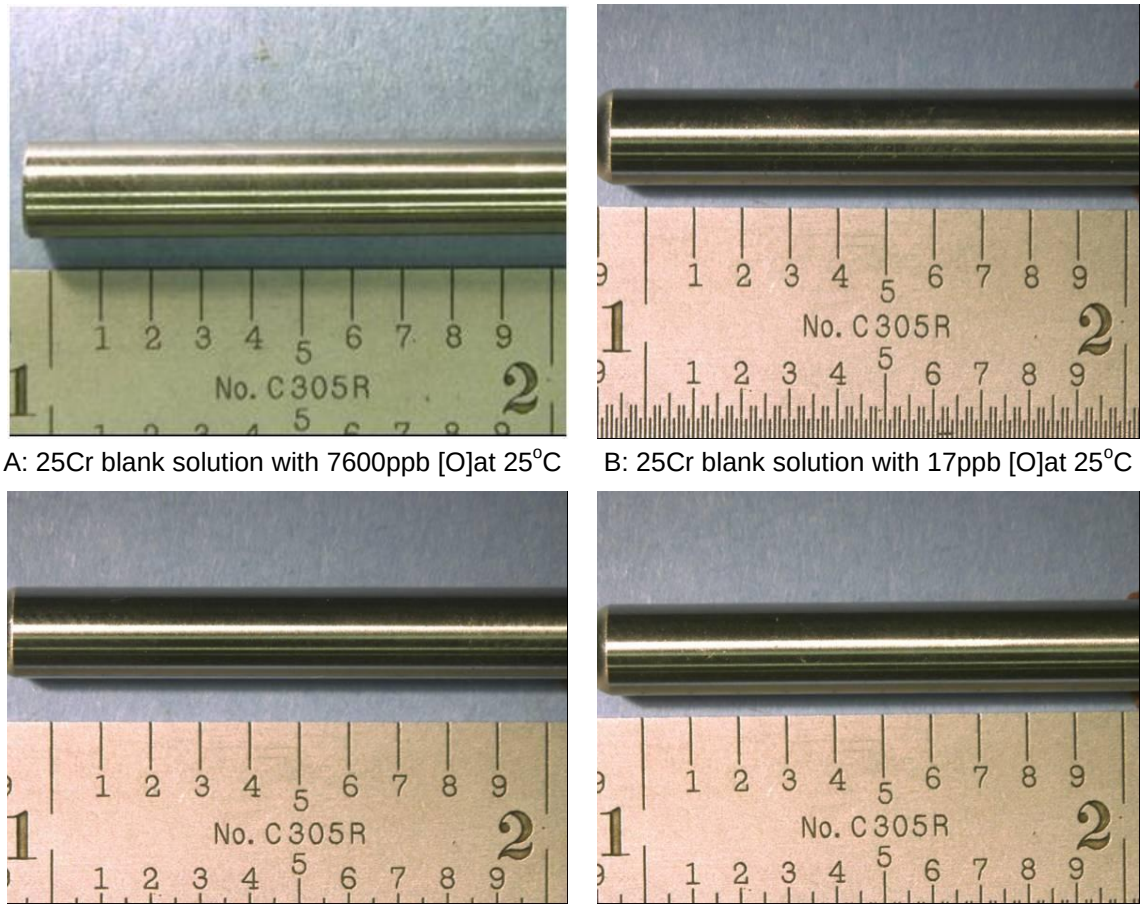

A: 25Cr blank solution with 7600ppb [O]at 25°C

B: 25Cr blank solution with 17ppb [O]at 25°C

C: 25Cr 100ppm $NaNO_3$ at 25°C, 17ppb [O]

D: 25Cr 100ppm $NaNO_2$ at 25°C, 17ppb [O]

Figure 64: Photographs of post-test specimens of 25Cr polarised in seawater at different oxygen concentration at 25°C

The material test result for the 25Cr as shown in Figure 30 indicates chromium content of 25.7%, Molybdenum content of 3.2% and Nitrogen content of 0.19% hence a PRE_N of 39.3 The critical pitting temperature for S32550 (Ferralium 255) is 50°C[265]. Hence it is not surprising that there was no

pit since the test was performed well below the critical pitting temperature and the PRE_N is almost 40. At the end of each of the tests, the test solution was clear and there was no substantial change in pH. This is consistent with the fact that the CPP curves gave negative hysteresis loops and the reverse sweep of the tests initiated shortly after the transition from active dissolution to passive region.

Figure 65 shows CPP curves of 25Cr with deoxygenated blank solution, deoxygenated solution with 100ppm sodium nitrate solution, 100ppm and 400ppm sodium nitrite solution at 80^{o}C respectively.

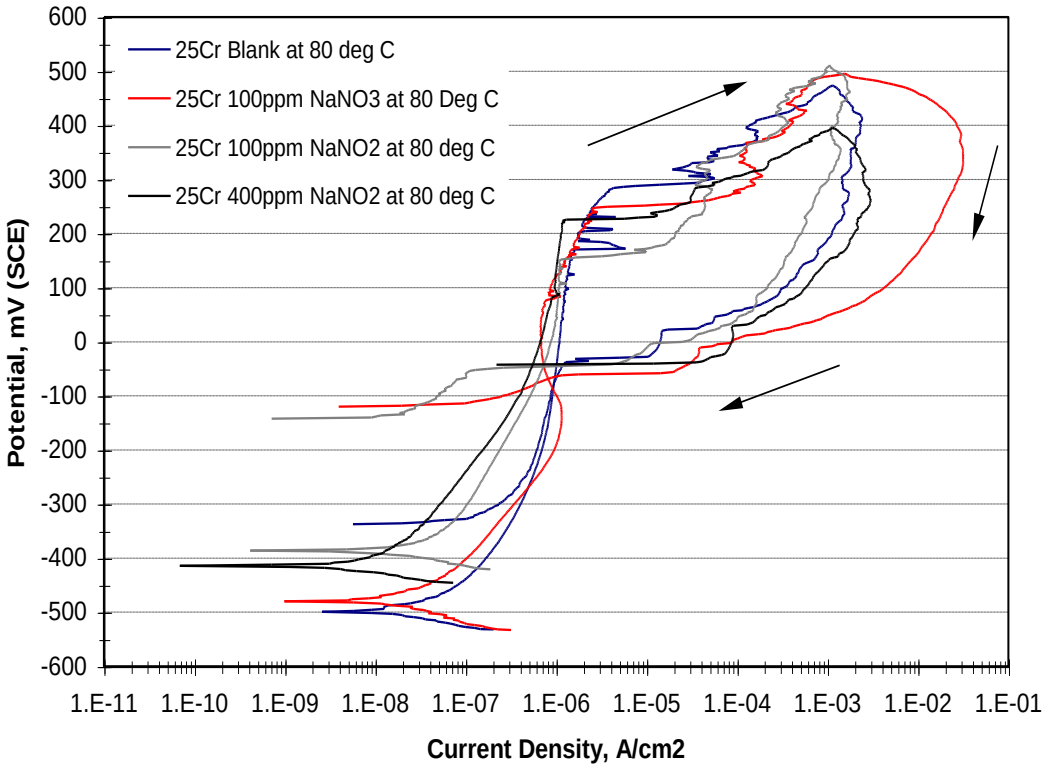

Figure 65: CPP curves for 25Cr at 80^{o}C

Just as was observed in the case of 22Cr, these CPP curves also show the tremendous effect of temperature in increasing the susceptibility of the test material to corrosion. All the curves had positive hysteresis loops contrary to what was observed at room temperature where they all had negative hysteresis loops. All the curves show typical activation-passivation behaviour with pronounced passivation. This is expected of 25Cr in neutral and slightly alkaline solution because of the high chromium content. Also the presence of Nickel, Manganese and Nitrogen which are the three most common elements

used to stabilise austenite, all contribute to passivity while Molybdenum improves the stability of the passive film especially in the presence of chloride ions, coupled with the high temperature and presence of oxidisers which promote passivation. All the curves show minor fluctuation in the forward sweep, indicating breakdown in passivation, which quickly healed and repassivated before pit formation and growth could occur. The fluctuation was however more pronounced in the blank solution. This is consistent with what was observed at room temperature where nitrate and nitrite assisted in passivation and preventing breakdown. Within the potential range of 150-300mV all the passive films broke down causing a huge current surge up to 1mA/cm^2 which initiated the reversed sweep due to high current contrary to what was observed at room temperature where the reversed sweep was initiated by high potential. Apart from 25Cr in the deoxygenated seawater solution with 400ppm that completely broke down after the pitting potential, all the others exhibit a couple of sequence of passive film breakdown and self-healing (repassivation) and further breakdown, showing a region of instability between 1μA/cm^2 and 2mA/cm^2.

All the curves gave a closed hysteresis loop with a protection margin way above the 200mV indicating that 25Cr is not susceptible to pitting/localised corrosion in all the test conditions. Unlike what was observed at room temperature where 100ppm sodium nitrate had no effect on the anodic curve, at 80^{o}C the anodic curve for 100ppm sodium nitrate shifted slightly into more active corrosion compared to blank solution. At 80^{o}C both 100ppm sodium nitrate and 100ppm sodium nitrite polarised 25Cr in the anodic direction making it more passive. The degree of polarisation was however different. 100ppm sodium nitrate only polarised 25Cr by about 20mV compared to the blank solution while 100ppm and 400ppm polarised 25Cr by 115mV and 85mV respectively. All the CPP tests were conducted following the procedure as stated in ASTM G 61[250], which requires the specimen to be immersed in the test solution for minimum of 1 hour before initiating polarisation. However, in an attempt to study the effect of soaking for longer duration, the specimen for 400ppm sodium nitrite was actually immersed in the deoxygenated solution overnight for about 14 hours before initiating polarisation.

Figure 66 shows the open corrosion potential for 25Cr immersed in deoxygenated seawater solution with 400ppm sodium nitrite overnight before initiating polarisation.

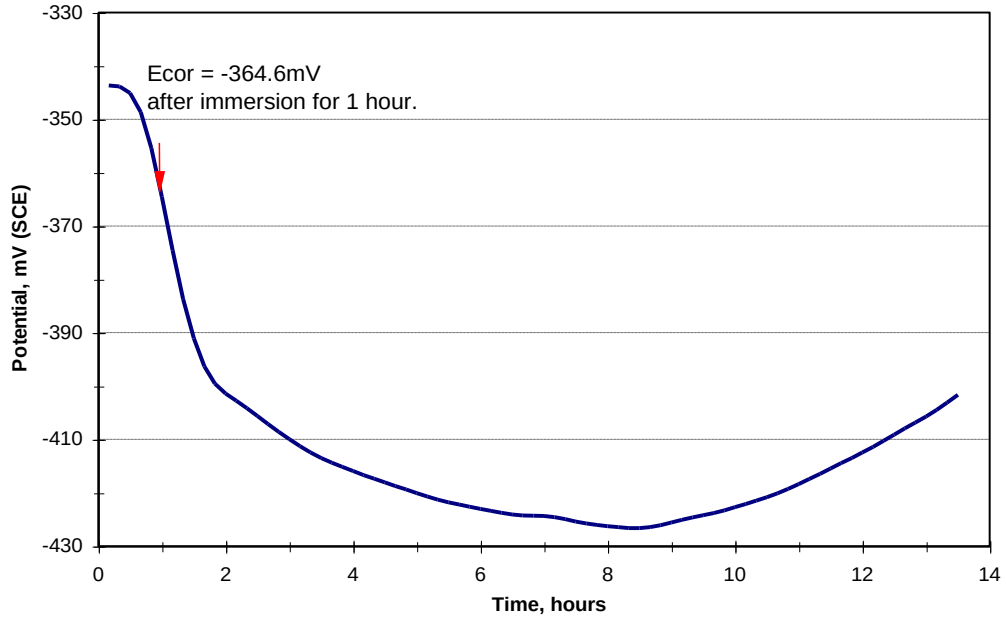

Figure 66: Graph showing open circuit potential, for 25Cr in deoxygenated seawater with 400ppm $NaNO_2$ at 80°C

The graph shows rapid decline in the corrosion potential in the direction of active corrosion for the first two hours after which there was steady decline for another 6 hours before the potential started to increase towards the noble direction. The rapid decrease in corrosion potential indicates free corrosion which probably slowed down as a result of partial passivation while the gradual increase in potential is an indication of complete passivation and growth of the passive film. After the first hour the potential was –364.6mV, which implies that if the polarisation had been initiated after an hour, like the rest of the tests in Figure 65, the potential for 25Cr with 400ppm sodium nitrite would have been more anodic than that of 100ppm sodium nitrite, which logically was the expectation. The graph in Figure 66 further validates the methodology as prescribed by ASTM G61[250] indicating that soaking the specimen for an hour gives a conservative corrosion potential similar to what is expected after an extended immersion. It also indicates the need to use similar soaking period for all the tests for consistency. 25Cr immersed in 100ppm $NaNO_3$ deoxygenated seawater solution had the highest corrosion rate compared to others while that of 100ppm $NaNO_2$ had the lowest. This

indicates that necessary precautions must be taken in the selection of 25Cr for downhole components for water injectors (Figure 2 show that 25Cr is typically used as components in the subsurface critical safety shutdown valve (SCSSV), production parker and blank pipe for the sand screen) where nitrate injection is utilised to control reservoir souring. It is essential to check for galvanic couplings and/or mixed potentials to ensure there was nothing that could anodically polarise 25Cr beyond its pitting potential because the corrosion rate is quite high beyond the pitting potential. The good news however, is that all literature search hitherto, suggest that nitrate would have been reduced by the nitrate reducing bacteria, NRB, to nitrite or even nitrogen by the time it gets downhole.

Figure 67A/B/C/D show the photographs of the post test specimens for 25Cr at 80^{o}C in blank deoxygenated seawater, deoxygenated seawater with 100ppm sodium nitrate, 100ppm and 400ppm sodium nitrite respectively.

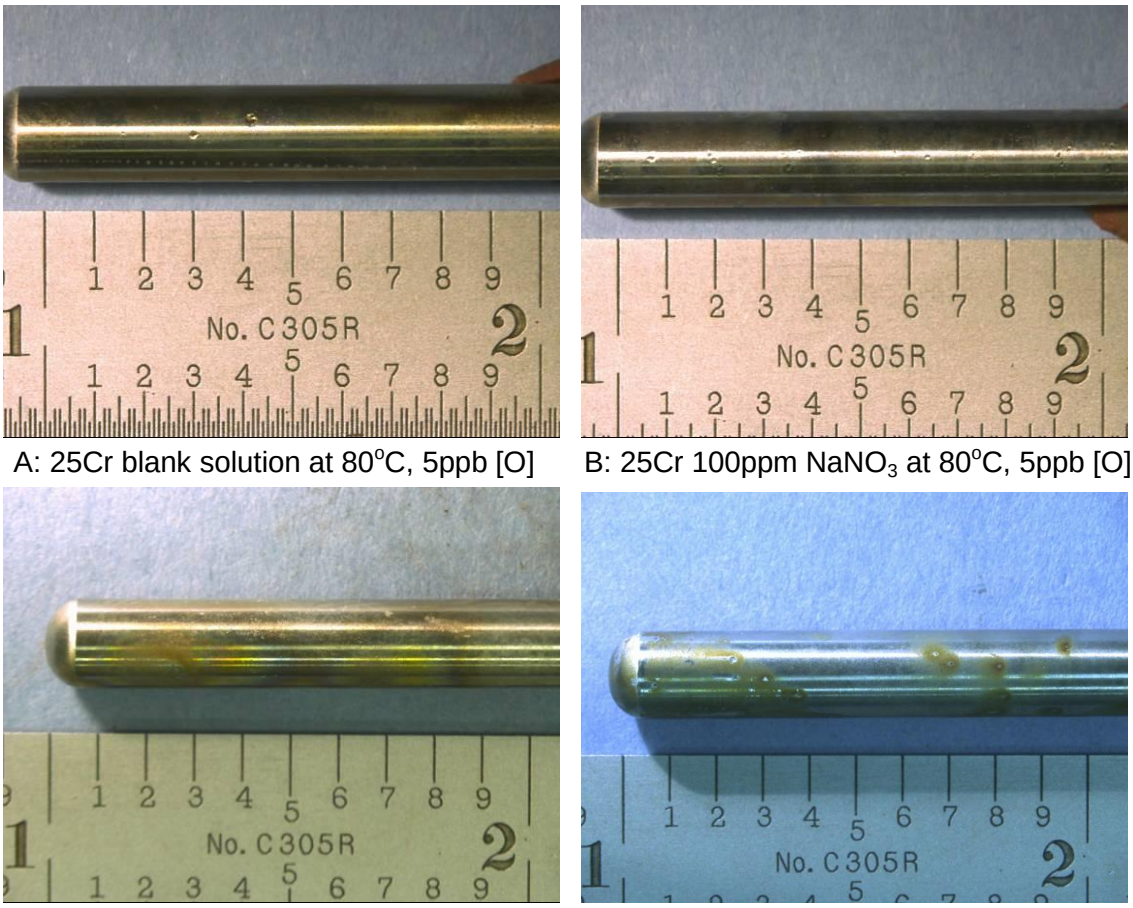

A: 25Cr blank solution at 80^{o}C, 5ppb [O]

B: 25Cr 100ppm $NaNO_3$ at 80^{o}C, 5ppb [O]

C: 25Cr 100ppm $NaNO_2$ at 80^{o}C, 5ppb [O]

D: 25Cr 400ppm $NaNO_2$ at 80^{o}C, 5ppb [O]

Figure 67: Photographs of post-test specimens of 25Cr polarised in deoxygenated seawater at 80^{o}C

All the photographs show etched patches and pitting however the 25Cr in deoxygenated seawater with 100ppm sodium nitrite shows the least amount of pits. This is consistent with the CPP curve which indicates that 25Cr in deoxygenated seawater with 100ppm sodium nitrite, showed the least corrosion rate. Although all the curves showed closed hysteresis loops with more than 200mV protection margin, which suggests they are not susceptible to pitting/localised corrosion. However, during the CPP testing, the test specimens were over-polarised beyond the passive region to the transpassive region with corresponding current densities reaching the maximum value of 1mA/cm^2 before the reserves sweep was initiated. Most likely, pitting occurred while the specimens were polarised to the transpassivity region.To fully understand the effect of nitrite on 25Cr at 80^{o}C, CPP tests were performed at various sodium nitrite concentrations ranging from 0ppm to 8000ppm similar to what was done for 13Cr.

Figure 68 shows the CPP curves of 25Cr in deoxygenated seawater solution with different sodium nitrite concentrations: 0ppm, 100ppm, 400ppm, 1000ppm, 2500ppm, 4000ppm, 6000ppm and 8000ppm.

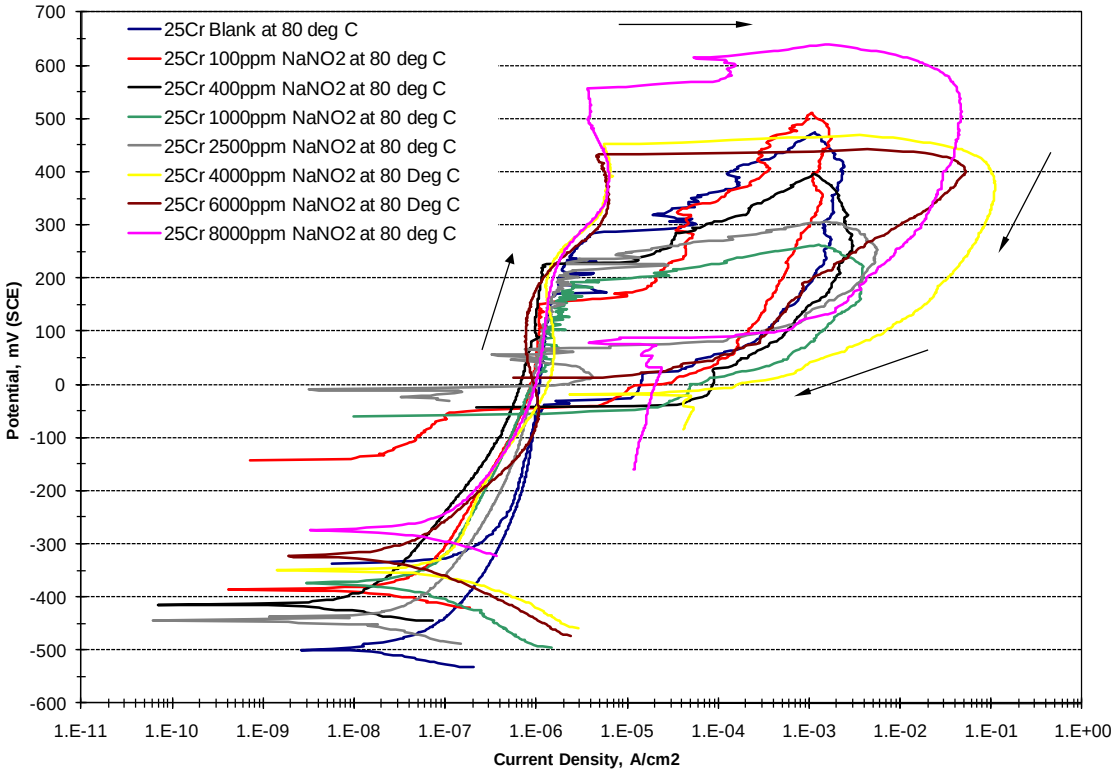

Figure 68: CPP curves for 25Cr at deoxygenated seawater at different sodium nitrite concentrations at 80^{o}C

The CPP curves for 25Cr in Figure 68 show a similar trend with those obtained in the case of 13Cr; as the sodium nitrite concentration increased the corrosion potential shift to more-noble values with corresponding shift in the anodic polarisation curve to lower currents and a net reduction in the corrosion rate. However, the CPP curve at sodium nitrite concentration of 2500ppm did not follow the same trend as others; its corrosion potential was lower than those obtained at sodium nitrate concentrations of 100ppm and 400ppm however, its corrosion rate was lower than those at 100ppm and 400ppm. The shift to more active corrosion at nitrite concentration of 2500ppm could not be adequately explained. It is however obvious that above sodium nitrite concentration of 400ppm there was a switch from partial passivation to complete passivation. From the CPP curves obtained between sodium nitrite concentration of 0ppm and 400ppm, the forward scan showed early fluctuations implying pitting and repassivation. The passive film eventually broke down but it tried to repassivate. The passive film was unable to completely repassivate before it broke down again. Repassivation and resistance to pitting further increased the potentials until maximum potential of 1V with respect to the corrosion potentials were attained and the reverse sweeps were initiated. However, above sodium nitrite concentration of 400ppm, the passive film was preserved until the pitting potentials were attained at which stage the damaged passive film led to very high corrosion rates and the reversed sweeps were initiated when the maximum corrosion rate of 1mA/cm^2 was attained.

Using the same methodology that was used in the case of 13Cr, the corrosion rates for each of the CPP curves at various sodium nitrate concentrations were estimated by extrapolating the linear portions of the anodic and cathodic Tafel regions in the log current versus potential plot back to their intersection. The estimated corrosion rate is the value of the current at the point where the two linear segments of the extrapolated anodic and cathodic curves intersect. In order to properly identify the linear portions of the anodic and cathodic of Tafel regions in the log current versus potential plot, the scale of the x and y axes were changed to show the cathodic curves and only the active corrosion transitioning into the passive region of the anodic curve, ensuring linear region

with at least one decade of current density. For anodic curves where the linear region was not sufficiently long enough, best fit straight lines were draw through the linear section ensuring the line was tangential to the curve at the section where it transitioned from active corrosion to passive corrosion i.e. where the increase in current density stops and increase in potential starts.

Figure 69 shows the graphs of the open circuit potential and the corresponding current density as a function of the nitrite concentration in deoxygenated seawater solution. Similar to what was observed in the case of 13Cr, there was unstable region between sodium nitrite concentration of 0ppm and the critical nitrite concentration of about 400ppm. Above the critical nitrite concentration, the potentials were pretty stable and show a linear increase in potential as the nitrite concentration increased.

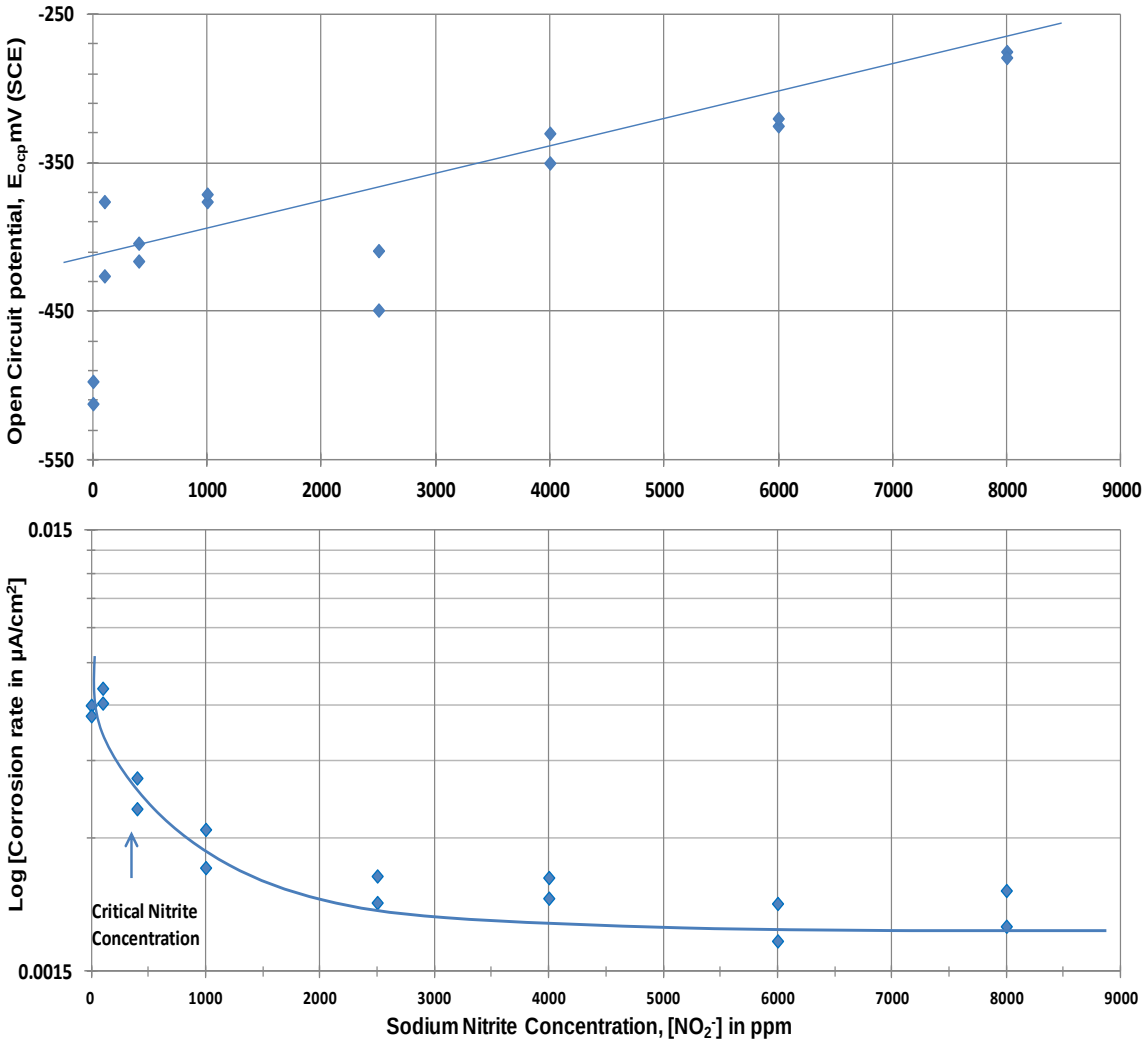

Figure 69: Open circuit potential and current density as a function of sodium nitrite concentration on type 25Cr-F255

Also, the graph for $Log(i_{cor})$ against sodium nitrite concentration shows an asymptotic curve. The corrosion rate continued to reduce with increase in sodium nitrite concentration while the potential increased to more noble potential however once the critical sodium nitrite concentration of about 400ppm was attained, further increase in sodium nitrite concentration did not significantly affect the corrosion rate even the potential increased. The observed response of 13Cr and 25Cr to increase in sodium nitrite concentration confirms that nitrite is indeed an anodic inhibitor; with increase in nitrite concentration, the corrosion potential increased in the anodic direction (more-noble) and a the anodic polarisation curves shifted to lower currents giving a net reduction in the corrosion rate.

Figure 70 shows the critical breakdown potential for Type 25Cr-F255 as a function of nitrite concentration at 80^{o}C, pH 8.2 with a voltage scan rate of 0.2mV/s.

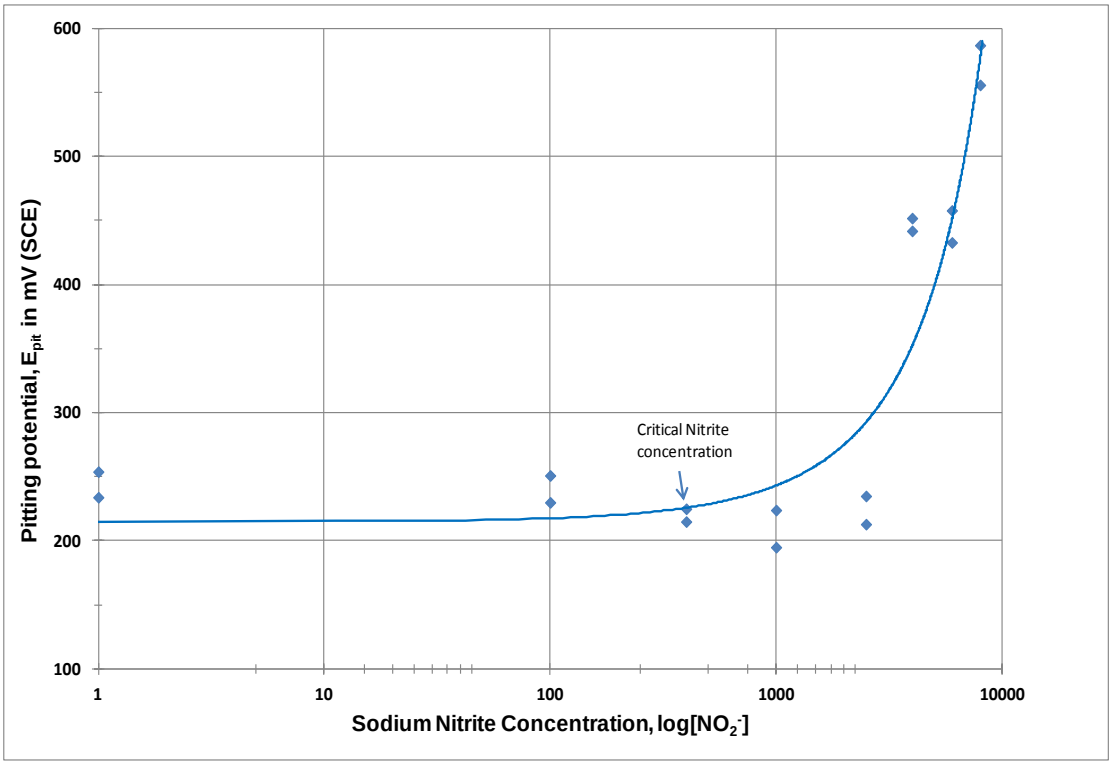

Figure 70: Critical breakdown potential for Type 25Cr-F255 as a function of nitrite concentration at 80^{o}C, pH 8.2 with a voltage scan rate of 0.2mV/s

Similar to what was observed in the case of 13Cr-L80, initially, at low nitrite concentrations, the critical breakdown potential did not significantly change with increasing nitrite concentration until the critical nitrite concentration of

400ppm was reached. At higher concentrations, the pitting potential increased very quickly as shown in Figure 70. This indicates that above the critical nitrite concentration, pitting is unlikely to occur. This result is similar to the test results previously reported by Macdonald[43] and Dahan[180] for nitrate on Type 316 stainless steel.

Figure 71 shows photographs of the post test specimens of 25Cr at various sodium nitrite concentrations. Contrary to Macdonald and Dahan's observation that pitting stopped after the critical nitrite concentration was attained, in Figure 71 pitting was observed on the working electrode and under solid deposits above the critical nitrite concentration particularly in post test samples with high sodium nitrite concentration of 2500ppm and above.This was probably due to the fact that the electrodes were polarised to the transpassivity region as shown in Figure 68 hence it is inferred that the pitting observed occurred during transpassivity. Also increase in pitting potential means that from thermodynamic point of view the anodic reaction is unlikely to occur. However, increase in nitrite concentration is capable of influencing both the thermodynamics and the kinetics of the cathodic reaction. Once $E_{cathode} > E_{anode}$ corrosion will proceed. As shown in Figure 71, all the photographs show etched patches and pitting. The density of pits observed on the specimen and the pit depth increased with the sodium nitrite concentration. At low nitrite concentrations, very few pits were observed on the surface of the specimen however, beyond sodium nitrite concentration of 2500ppm there was excessive pit propagation with some of the pit grown to merge with other pits thereby forming a bigger pit with extensive metal loss. Also above 2500ppm, there was progressive increase in the general corrosion and the amount of rust deposit on the specimen. The observed trend of corrosion on the specimens is consistent with the result of the CPP curves in Figure 68. The test result validates the point defect model[43]. Just as was inferred for 13Cr, the sudden increase in pitting potential observed in Figure 70 indicates saturation of the surface oxygen vacancy absorption sites at the barrier layer/solution interface, such that chloride ion are excluded, at least at those sites at which breakdown occurred. This test result further validates the inhibiting ability of oxyanion (nitrite in this case).

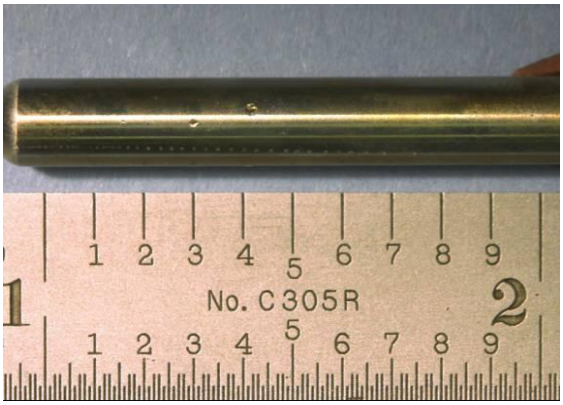

A: 25Cr blank solution at 80°C, 5ppb [O]

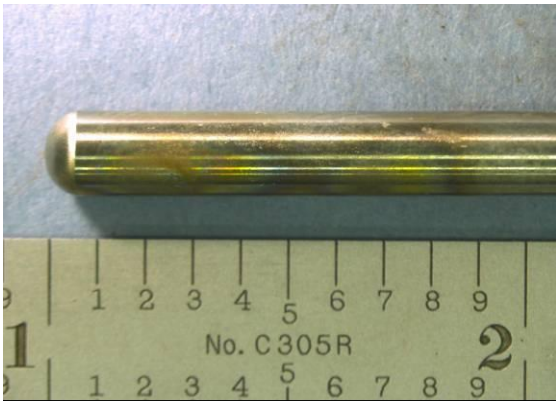

B: 25Cr 100ppm $NaNO_2$ at 80°C, 5ppb [O]

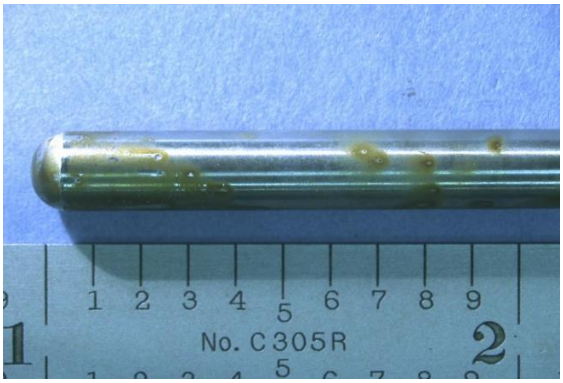

C: 25Cr 400ppm $NaNO_2$ at 80°C, 5ppb [O]

D: 25Cr 1000ppm $NaNO_2$ at 80°C, 5ppb [O]

E: 25Cr 2500ppm $NaNO_2$ at 80°C, 5ppb [O]

F: 25Cr 4000ppm $NaNO_2$ at 80°C, 5ppb [O]

G: 25Cr 6000ppm $NaNO_2$ at 80°C, 5ppb [O]

H: 25Cr 8000ppm $NaNO_2$ at 80°C, 5ppb [O]

Figure 71: Post-test specimens of 25Cr with different $NaNO_2$ concentrations at 80°C

Lastly, the test result confirms 400ppm as the critical nitrite concentration for 25Cr-F255. It should however be noted that the critical concentration determined is what is required to inhibit prior to pitting. As shown in section 4.3.1, the critical nitrite concentration required for repassivation of 25Cr-F255 after pitting had occurred is actually higher. Also the critical nitrite concentration required to inhibit 25Cr-F255 prior to pitting initiation could actually be as low as 200ppm since the decrease in current density actually started just after 150ppm but there was a lot of passivity breakdown and prompt repassivation activities on the metal surface, just as seen in Figure 70, the data points were less scattered at lower nitrite concentration compared to the case of 13Cr-L80. This is not surprising because the chromium content in 25Cr-F255 is more than the 15% critical concentration[257] required for self healing process of the chromium (III) oxide (Cr_2O_3) passive film.

Table 8 gives the summary of all the CPP results and the key corrosion parameters.

Table 8: Summary of CPP Testing Results

Test Materials	Solution	Temp (^oC)	E_{corr} (mV) wrt SCE	I_{corr} A/cm^2	E_{pit} (mV) wrt SCE	E_{rp} (mV) wrt SCE	Protection margin* (mV)	Post-coupon appearance	Comments
13Cr	Blank fully oxygenated (open air)	25	-160	1.64E-9	6	< E_{corr}	0	Pitted	Susceptible
22Cr			-118	1.21E-9	>850	Negative Hysteresis	Negative Hysteresis	Not pitted	Not susceptible
25Cr			-118	9.62E-10	>850	Negative Hysteresis	Negative Hysteresis	Not pitted	Not susceptible
13Cr	Blank	25	-237	2.10E-9	-9	< E_{corr}	0	Pitted	Susceptible
	100ppm $NaNO_3$		-323	1.28E-9	-29	< E_{corr}	0	Pitted	Susceptible
	100ppm $NaNO_2$		-391	1.38E-8	-35	-223	168	Pitted	Susceptible
13Cr	Blank	80	-494	1.72E-7	-190	< E_{corr}	0	Pitted	Susceptible
	100ppm $NaNO_3$		-565	1.92E-8	-174	< E_{corr}	0	Pitted	Susceptible
	100ppm $NaNO_2$		-584	5.95E-8	-183	-493	88	Pitted	Susceptible
	400ppm $NaNO_2$		-372	1.59E-8	-186	< E_{corr}	0	Pitted	Susceptible

Test Materials	Solution	Temp (^oC)	E_{corr} (mV) wrt SCE	I_{corr} A/cm^2	E_{pit} (mV) wrt SCE	E_{rp} (mV) wrt SCE	Protection margin* (mV)	Post-coupon appearance	Comments
13Cr	1000ppm $NaNO_2$	80	-297	1.97E-8	-145	< E_{corr}	0	Pitted	Susceptible
	5000ppm $NaNO_2$		-293	1.01E-8	-85	< E_{corr}	0	Pitted	Susceptible
	8500ppm $NaNO_2$		-249	1.43E-8	78	< E_{corr}	0	Pitted	Susceptible
	12500ppm $NaNO_2$		-174	9.42E-9	71	< E_{corr}	0	Pitted	Susceptible
22Cr	Blank	25	-173	5.08E-10	>850	Negative Hysteresis	Negative Hysteresis	Not pitted	Not susceptible
	100ppm $NaNO_3$		-95	3.40E-9	751	31	126	Not pitted	Susceptible
	100ppm $NaNO_2$		-208	1.34E-9	>850	Negative Hysteresis	Negative Hysteresis	Not pitted	Not susceptible
22Cr	Blank	80	-154	2.76E-9	182	< E_{corr}	0	Pitted	Susceptible
	100ppm $NaNO_3$		-327	1.94E-9	163	< E_{corr}	0	Pitted	Susceptible
	100ppm $NaNO_2$		-207	1.95E-9	153	< E_{corr}	0	Pitted	Susceptible

Test Materials	Solution	Temp (^oC)	E_{corr} (mV) wrt SCE	I_{corr} A/cm^2	E_{pit} (mV) wrt SCE	E_{rp} (mV) wrt SCE	Protection margin* (mV)	Post-coupon appearance	Comments
25Cr	Blank	25	-207	8.25E-10	>850	Negative Hysteresis	Negative Hysteresis	Not pitted	Not susceptible
	100ppm $NaNO_3$		-211	9.86E-10	>850	Negative Hysteresis	Negative Hysteresis	Not pitted	Not susceptible
	100ppm $NaNO_2$		-234	1.94E-9	>850	Negative Hysteresis	Negative Hysteresis	Not pitted	Not susceptible
25Cr	Blank	80	-503	9.14E-9	284	-74	422	Pitted	*Not susceptible
	100ppm $NaNO_3$		-474	8.49E-9	248	-70	404	Pitted	*Not susceptible
	100ppm $NaNO_2$		-373	6.11E-9	152	-30	360	Pitted	*Not susceptible
	400ppm $NaNO_2$		-404	2.76E-9	225	-31	387	Pitted	*Not susceptible
	1000ppm $NaNO_2$		-376	6.09E-9	195	-52	322	Pitted	*Not susceptible
	2500ppm $NaNO_2$		-449	1.88E-9	235	3	450	Pitted	*Not susceptible
	4000ppm $NaNO_2$		-350	1.38E-8	452	< E_{corr}	0	Pitted	Susceptible
	6000ppm $NaNO_2$		-325	4.76E-9	433	23	344	Pitted	*Not susceptible

Test Materials	Solution	Temp (^oC)	E_{corr} (mV) wrt SCE	I_{corr} A/cm^2	E_{pit} (mV) wrt SCE	E_{rp} (mV) wrt SCE	Protection margin* (mV)	Post-coupon appearance	Comments
25Cr	8000ppm $NaNO_2$		-275	8.90E-9	556	< E_{corr}	0	Pitted	Susceptible

- A minimum of 200 mV is considered protective.

* Although the protection margin was >200 mV however, pits were observed in the post-test specimen. This is deceptive, because these pits actually resulted from the fact that the specimen was over-polarised during the CPP testing and the maximum polarization current was up to 1mA/cm^2

4.2.1 Effect of nitrite on the cathodic curve

Anodic inhibitors typically increase the corrosion potential in the anodic direction (more-noble) with a corresponding shift in the anodic polarisation curve to lower currents and a net reduction in the corrosion rate. However, anodic inhibitors do not have significant effect on the cathodic curve.

In section 4.2, the effect of nitrite as an anodic inhibitor, increasing the corrosion potential in a more noble direction and decreasing the corrosion rate within a concentration range was demonstrated. In this section, the last attribute of nitrite as an anodic inhibitor with no significant effect on the cathodic curve was explored.

Figure 72, Figure 73 and Figure 74 show the cathodic curves for three different alloys, ½Cr-L80, 13Cr-L80 and 25Cr-F255 respectively at three different sodium nitrite concentrations (0ppm, 1000ppm and 6000ppm).

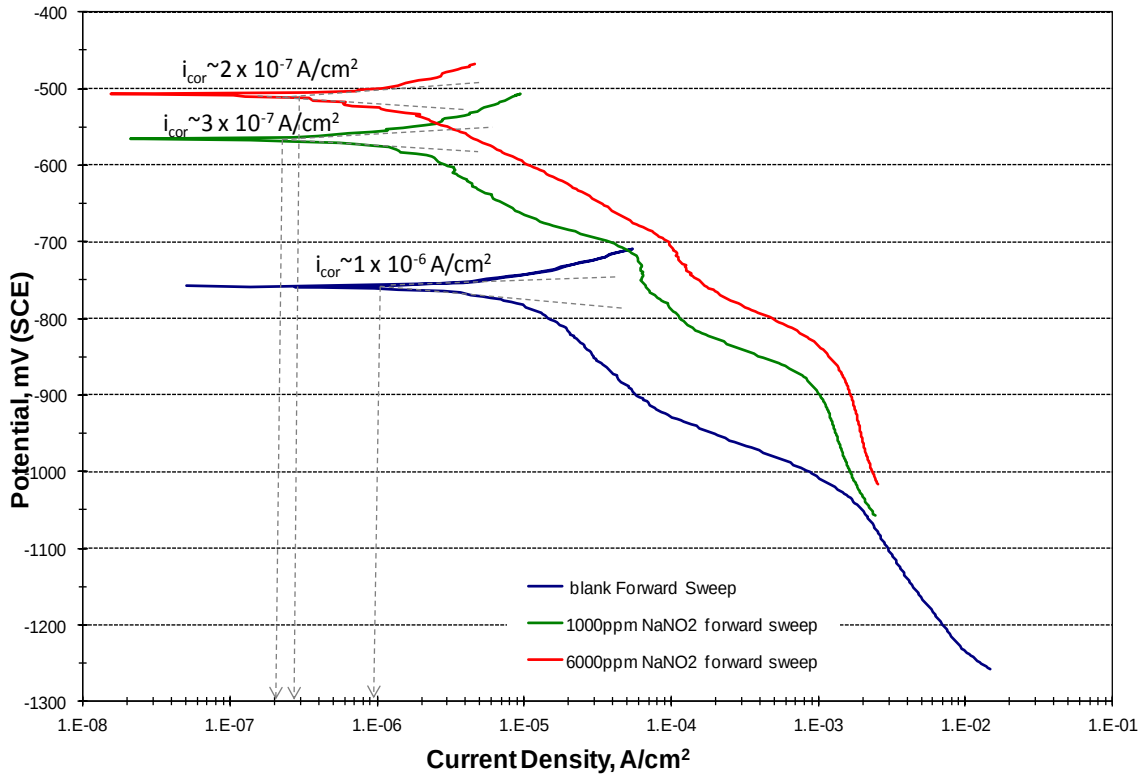

Figure 72: Cathodic curves of ½Cr low alloy steel with different sodium nitrite concentration at 80°C

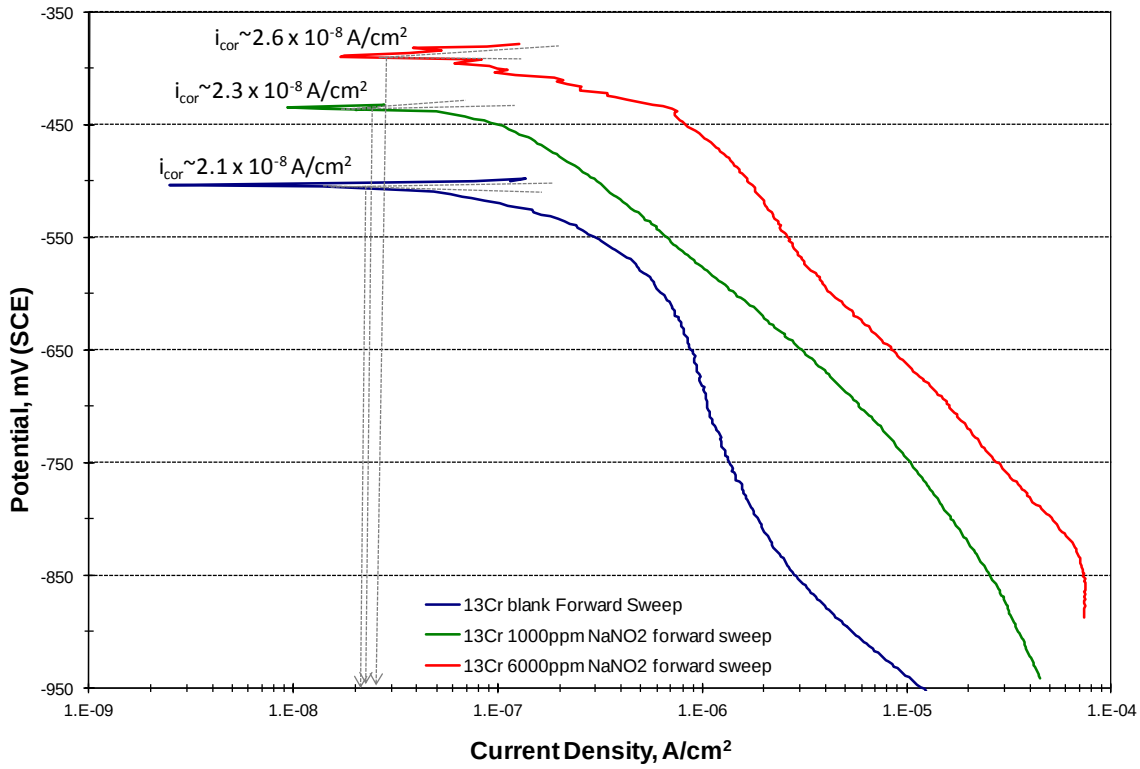

Figure 73: Cathodic curves of 13Cr with different sodium nitrite concentration at 80°C

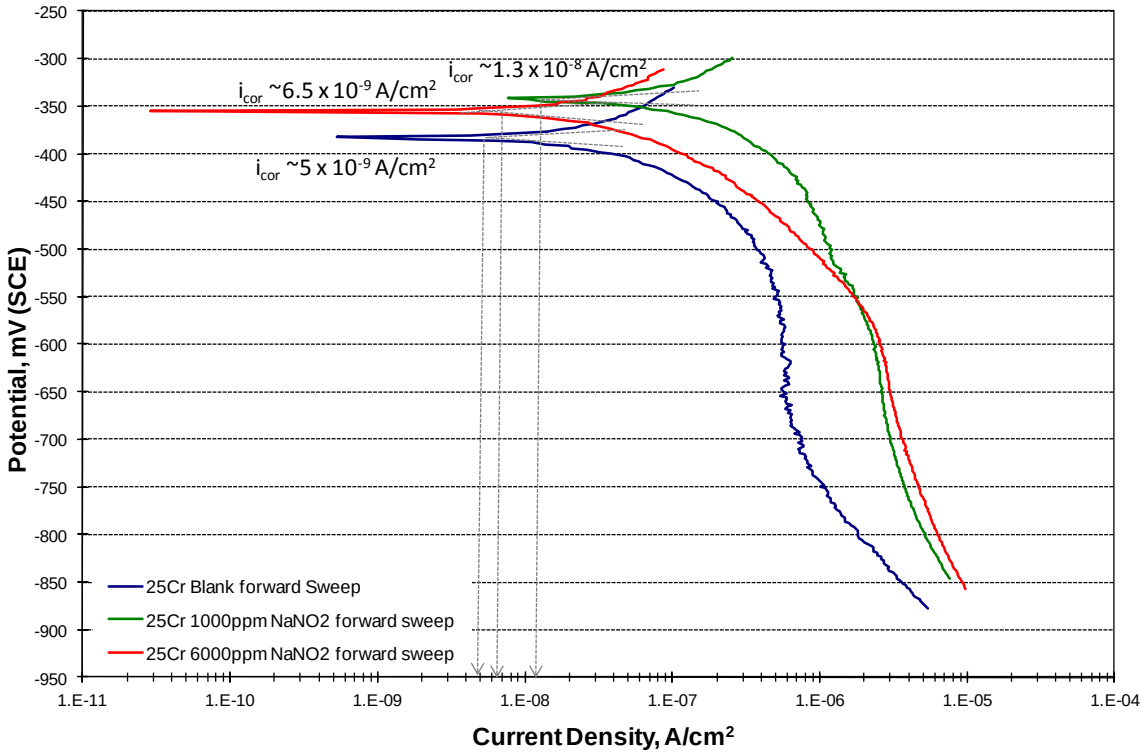

Figure 74: Cathodic curves of 25Cr with different sodium nitrite concentration at 80°C

As shown in Figure 72, Figure 73 and Figure 74, the corrosion rates for each of the CPP curves at various sodium nitrate concentrations were estimated by extrapolating the linear portions of the anodic and cathodic Tafel regions in the log current versus potential plot back to their intersection. The estimated corrosion rate is the value of the current at the point where the two linear segments of the extrapolated anodic and cathodic curves intersect. In order to properly identify the linear portions of the anodic and cathodic of Tafel regions in the log current versus potential plot, the scale of the x and y axes were changed to show the cathodic curves and only the active corrosion transitioning into the passive region of the anodic curve, ensuring linear region with at least one decade of current density.

The three figures show that change in sodium nitrite concentration from 0ppm to 6000ppm significantly changed the corrosion rates for ½Cr-L80, and 25Cr-F255 but the corrosion rate for 13Cr-L80 did not significantly change. Also addition of sodium nitrite increased the corrosion potential to more noble potentials for all the materials tested.

As shown in Figure 72, the estimated corrosion rates for ½Cr-L80 at 0ppm, 1000ppm and 6000ppm sodium nitrite concentrations are 1μA/cm^2, 0.3μA/cm^2, and 0.2μA/cm^2 respectively while their corresponding corrosion potentials were -758mV, -565 mV and -507mV respectively. Indicating that increase in the sodium nitrite concentration led to increase in the corrosion potential (to more noble potential) and corresponding decrease in the corrosion rate. This behaviour is consistent with the effect of anodic inhibitors in carbon steel and low alloy steel. Change in sodium nitrite concentration from 1000ppm to 6000ppm did not significantly change the corrosion rates of ½Cr-L80. However, when the sodium nitrite concentration was increased from 0ppm to 1000ppm, the corrosion rate increased with a magnitude of 3.The three curves have very similar shapes. The cathodic curves show the initial cathodic reaction reaching its limiting current density around 0.1mA/cm^2 and the second cathodic reaction reaching its limiting current density around 1.0mA/cm^2.

Figure 73 shows the estimated corrosion rates for 13Cr-L80 at 0ppm, 1000ppm and 6000ppm sodium nitrite concentrations are 21ηA/cm^2,

2.3ηA/cm^2, and 2.6ηA/cm^2 respectively with corresponding corrosion potentials of -503mV, -434mV and -388mV respectively. This indicates that increase in the sodium nitrite concentration from 0ppm to 6000ppm did not significantly change the corrosion rates of 13Cr-L80. However, the corrosion potential increased to more noble potentials.

Figure 74 shows that the corrosion rate for 25Cr at 0ppm, 1000ppm and 6000ppm sodium nitrite concentrations are 5ηA/cm^2, 13ηA/cm^2, and 6.5ηA/cm^2 respectively with corresponding corrosion potentials of -382mV, -341mV and -355mV respectively. This indicates that increase in nitrite concentration increased both the corrosion rates and the corrosion potential. Increasing the sodium nitrite concentration from 0ppm to 1000ppm increased the corrosion rate by a magnitude of almost 3 however when sodium nitrite concentration was increased to 6000ppm (which is above the critical sodium nitrite concentration as earlier mentioned), the corrosion rate dropped by 50% when compared with the result at 1000ppm. Similar behaviour was observed in the anodic CPP curves for at room temperature and low sodium nitrite concentrations as shown in Figure 48, Figure 59, and Figure 63 for 13Cr, 22Cr and 25Cr respectively. As suggested earlier, the increase in corrosion rate at low nitrite concentration is probably due to the fact that the amount of nitrite present was not sufficient to protect the entire metal surface. This led to partial protection and increased localised corrosion of the unprotected surfaces due to small anode big cathode phenomenon.

As shown in Figure 73, the cathodic curves for 13Cr-L80 reached their initial limiting current density around 1μA/cm^2 in blank seawater solution and 75μA/cm^2 in sodium nitrite solution while Figure 74 shows the cathodic curves for 25Cr reached their initial limiting current density around 0.6μA/cm^2 in blank seawater solution and 3μA/cm^2 in sodium nitrite solution. Typical corrosion rate of stainless steels in seawater is about 1μA/cm^2 (~0.5mpy) hence it was inferred that the limiting current densities measured in blank seawater solution was due to oxygen reduction while the limiting current measured in seawater containing sodium nitrate shows the effect of nitrite and is probably due to nitrite reduction. The test demonstrates that effect of increased sodium nitrite concentration from 0-6000ppm in seawater solution varies from metal to

metal. In some cases it was not significant while in others it was significant. This indicates the surface activity of the metal has some effect on the cathodic curves. Although, Vera, Shirah, and Song[266] had reported similar cathodic reaction kinetics on both X65 carbon steel and Alloy 625 surface in CO_2-saturated brine at 66°C.

To accurately determine the effect of nitrite as an anodic inhibitor on the cathodic curve, an inert metal such as platinum or gold electrode should be used for the test.

4.3 Potentiostatic Polarisation Test

Potentiostatic Polarisation test is typically used to investigate the relationship between the long-term pitting behaviour and various electrochemical parameters in situations where the protection margin (E_{rp}-E_{corr}) from the CPP testing was less than 200mV. It is not necessary to perform additional potentiostatic polarisation test in situations where the protection margin was more than 200mV.

The protection margin obtained from CPP result in Table 8 indicates the protection margin for 13Cr was less than 200mV while that for 25Cr was more than 200mV. Hence potentiostatic test was carried out only for 13Cr. Figure 75 shows the step change in potential and the corresponding current density plotted over time during the potentiostatic test for 13Cr in 1000ppm nitrite at 80^oC.

13Cr test specimen was polarised over a range of potential between the corrosion potential (E_{cor}), and pitting potential, (E_{pit}) for a relatively longer time than what was achieved from the CPP sweep. The selection of polarisation range was based on the results from CPP test result in Table 8. The potentiostatic polarisation test was commenced at -400mV wrt SCE with 25mV step change every 15 minutes.

Corrosion rates and potentials were recorded every 10s for the duration of the test. As shown in Figure 75, at -400mV, the current fluctuated indicating breakdown of passivation followed by repassivation but overall, the corrosion rate gradually increased from 9.2ηA/cm^2 to 0.1μA/cm^2 indicating that the

applied potential was more-noble than repassivation potential. After 15 minutes the potential was increased to -375mV. As expected in any potential sweep change, there was a corresponding instantaneous increase in corrosion rate from 0.1µA/cm^2 to 0.5µA/cm^2. Six minutes after the potential sweep, there was a significant instantaneous jump in the corrosion rate from 0.17µA/cm^2 to 3.39mA/cm^2.

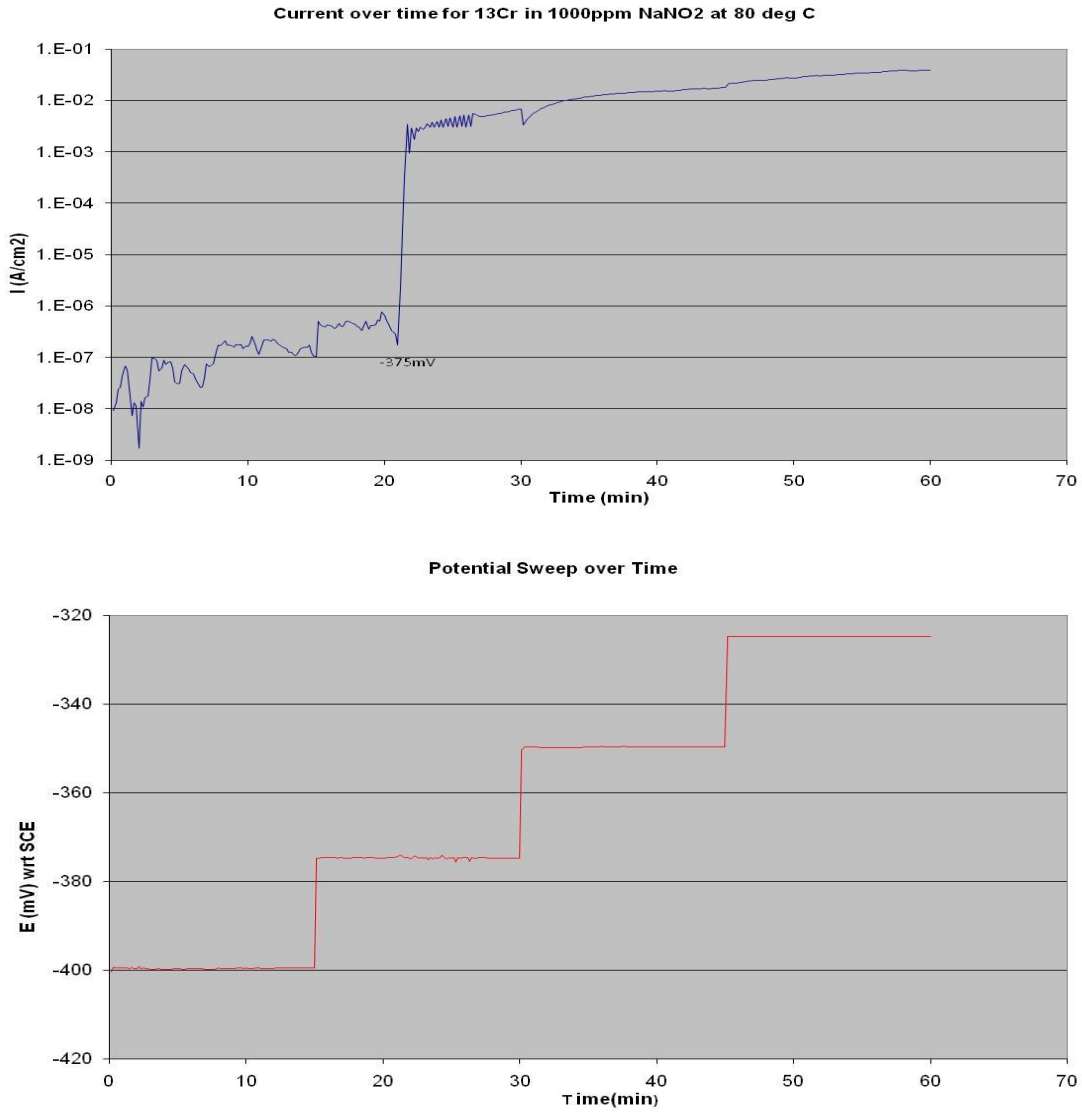

Figure 75: Potentiostatic sweep of 13Cr in 1000ppm nitrite solution at 80^{o}C

This was followed by a noisy region on the curve indicating active/passive behaviour initially. This was followed by gradual increase in corrosion rate which indicates active corrosion. Further sweep to higher potentials did not

significantly increase the corrosion rate. The potential at which the instantaneous significant increase in corrosion rate occurs indicates the pitting potential and marks the transition from passive region to transpassive region hence further increase in potential can only increase the corrosion rate. The test result indicates that -375mV wrt SCE is the pitting potential for 13Cr in 1000ppm nitrite solution at 80^{o}C.

4.3.1 Determination of Critical Nitrite Concentration

Nitrite as an anodic inhibitor, possess the following characteristics just like most anodic inhibitors:

1. Metal specific
2. Sensitive to Aggressive species e.g. Cl^-, NO_3^-, SO_4^{2-}
3. There is a critical concentration required for effective performance
4. There is a critical pH required for effective performance
5. Corrosion rate is greatly reduced to almost zero when effective.

In the course of this research, three different corrosion resistant alloys, 13Cr, 22Cr and 25Cr were used as test metals. Several cyclic potentiodynamic polarisation tests were carried out using the 3 test materials at two different temperatures (25^{o}C and 80^{o}C) and different sodium nitrate and sodium nitrite concentrations.

All inhibitors are required to be present at a certain critical concentration[267] in the aqueous environment, and the critical concentration depends on the composition and nature of the inhibitor. The objective of this section was to determine the critical nitrite concentration required for inhibition of 13Cr-L80 and 25Cr-F255 and to confirm that the corrosion rate was greatly reduced to almost zero as stipulated for anodic inhibitor. This was achieved by running potentiostatic polarisation tests with an applied potential close to the pitting potential (determined from the CPP tests in 4.2) and measuring the corrosion rate over time as the nitrite concentration was increased. The test for 13Cr-L80 was carried out for a duration of almost 18 hours with an applied voltage of -250mv (SCE), slightly below the pitting potential of 13Cr in blank seawater solution (lowest pitting potential) as shown in Figure 50. Nitrite concentration was gradually increased and the corrosion rate monitored.

Figure 76 shows the graph of corrosion rate measured over time as the nitrite concentration was increased in potentiostatic polarisation test of 13Cr-L80 at an applied potential of -250mV with respect to the SCE.

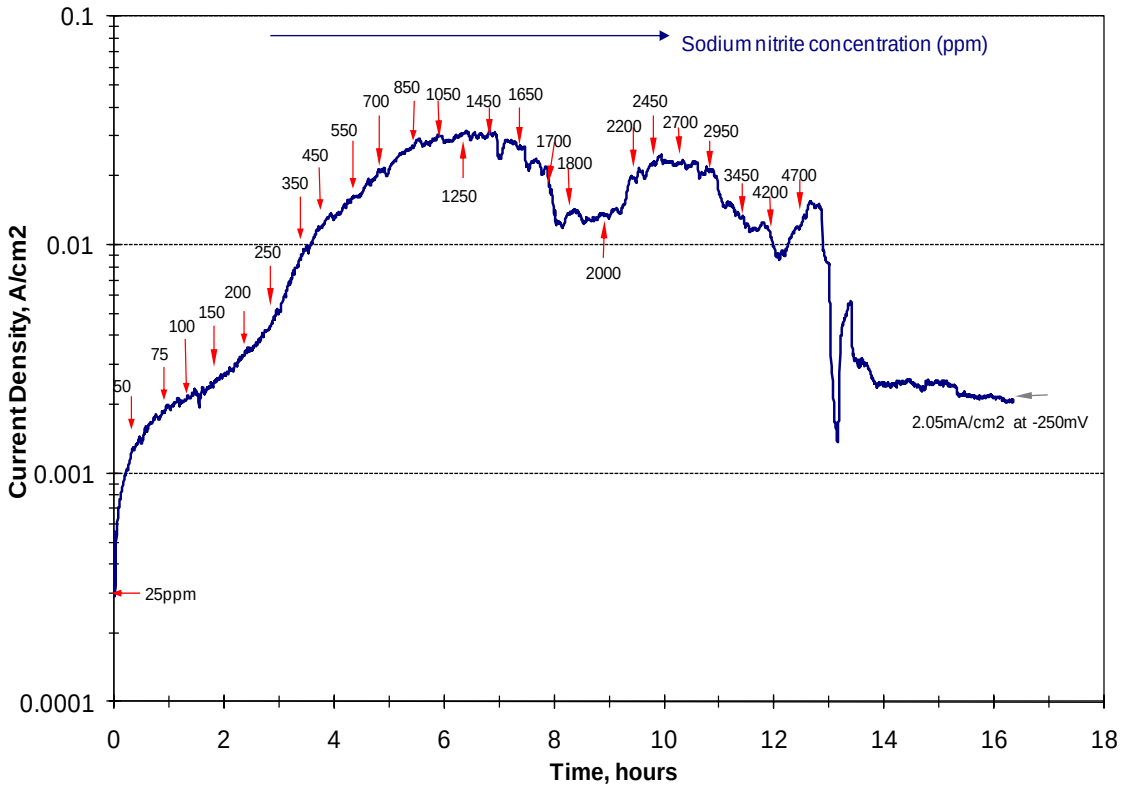

Figure 76: Determination of Critical nitrite concentration for 13Cr-L80 at 80^{o}C and applied potential of -250mV with respect to SCE

The figure shows a gradual increase in the corrosion rate over time, reaching a peak of approximately 30mA/cm^2 at a nitrite concentration of about 1450ppm. Then the corrosion rate gradually decreased indicating initiation of passivation. The fluctuations observed on the curve indicates breakdown in passivation and repassivation. At nitrite concentration of 1700ppm, the corrosion rate drastically dropped from about 22mA/cm^2 to 13mA/cm^2 indicating partial passivation. However after about 90 minutes, the corrosion rate gradually increased back to its initial peak of 22mA/cm^2 indicating a breakdown in the passive film that was formed. A similar drop in corrosion rate from 20mA/cm^2 to 8.93mA/cm^2 was observed at nitrite concentration within the range of 3000ppm and 4200ppm. The corrosion rate gradually rose back to about 14mA/cm^2. The fact that the current did not rise back to its initial

peak of 22mA/cm^2 indicates a passivation did not completely breakdown. At nitrite concentration of 4700ppm, there was a drastic drop in corrosion rate from 14mA/cm^2 to 1.38mA/cm^2 followed by a sharp raise to 5.2mA/cm^2 and another sharp fall which eventually remained constant at 2.05mA/cm^2 for almost 3 hours before the test was stopped. A drastic drop in corrosion rate which remaining constant for a reasonable amount of time indicate a complete passivation was achieved at that nitrite concentration. Hence 4700ppm is inferred to be the critical nitrite concentration for 13Cr-L80. The corrosion rate though greatly reduced, did not drop to almost zero as stipulated when anodic inhibitor is effective on a carbon steel, because the sample had been polarised, pitted and re-passivated hence the corrosion rate measured was actually the repassivation current hence it is not surprising that measured current is higher that the corrosion rate at the beginning of the test prior to pitting. The measured current indeed corresponds with the repassivation current of 13Cr-L80 at -250mV wrt SCE on the CPP curve for 4000ppm sodium nitrite solution as shown in Figure 50.

It is also worth stating that the critical nitrite concentration could actually be lower in a situation where passivation was achieved before pitting occurred. The test was actually repeated for a shorter duration and faster nitrite concentration increment to see if the critical nitrite concentration and corresponding passivation could be achieved before pitting occurred however this was unsuccessful.

The test for 25Cr-F255 was carried out with an applied voltage of 250mv wrt SCE, slightly below the pitting potential of 25Cr-F255 in blank seawater solution as shown Figure 65 for duration of almost 7 hours compared to the 18 hours for 13Cr-L80. This is expected as 25Cr has more Cr, Ni, and Mo to promote passive film formation. This also further stresses the fact that anodic inhibitor is metal specific. Similar to what was done for 13Cr-L80, nitrite concentration was gradually increased and the corrosion rate monitored.

Figure 77 shows the graph of corrosion rate measured over time as the nitrite concentration was increased in potentiostatic polarisation test of 25Cr-F255 at an applied potential of 250mV with respect to the SCE.

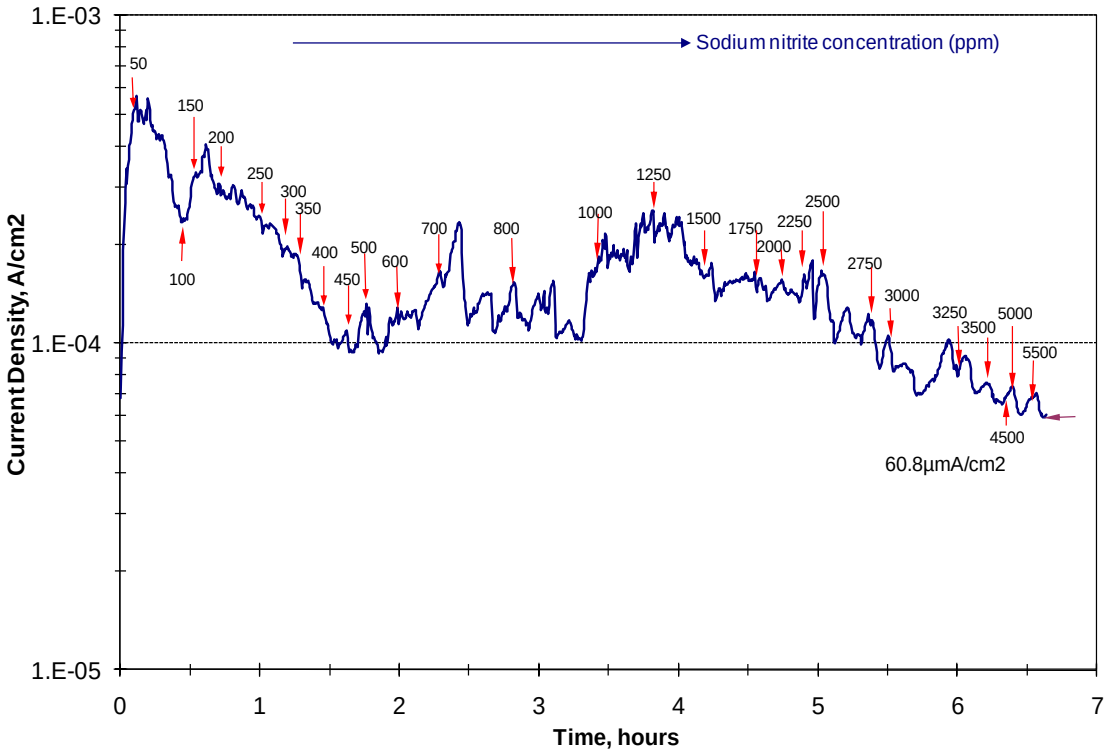

Figure 77: Determination of Critical nitrite concentration for 25Cr-F255 at 80^{o}C and applied potential of 250mV wrt SCE

Similar to what was observed in the case of 13Cr-L80, the corrosion rate gradually increased reaching its peak of 0.5mA/cm^2 within 15 minutes at nitrite concentration of 50ppm. After reaching its peak, there was a drastic drop to 0.25mA/cm^2 indicating initiation of passive film and instantaneous increase to 0.32mA/cm^2 and 0.39mA/cm^2 when the nitrite concentration was increased to 100ppm and 150ppm respectively.

At nitrite concentration of 200ppm the corrosion rate started to drop gradually with increase in nitrite concentration up till 400ppm dropping the corrosion rate to as low as 99µA/cm^2. But the low corrosion rate could not be sustained, it gradually increased after few minutes and there were several spikes followed by drop of the corrosion rate as the concentration of nitrite was gradually increased up till 5500ppm before it stayed constant at 60.8µA/cm^2 and the test was stopped. The fluctuations in current density indicates breakdown in passivation and repassivation. From the test, two critical nitrite concentrations could be drawn; the first being at 400ppm which is inferred to be the critical nitrite concentration for passivating 25Cr-F255 in sodium nitrite

solution. While the second critical concentration is 5500ppm which is the concentration required for repassivation after breakdown in passivation and pitting. It is worth noting that the corrosion rate of 99μA/cm2 corresponds to the passivation current observed from the CPP curve of 25Cr-F255 at 80^{o}C shown in Figure 65.

Lastly, unlike what was observed in the case of 13Cr-L80, the corrosion rate of 60.8μA/cm^{2} measured at the critical nitrite concentration after repassivation is lower than the corrosion rate of blank solution at the beginning of the test. This demonstrates the ability of 25Cr to completely repassivate since it has more chromium than the critical concentration required for self healing process of the passive film[257].

4.4 C-ring test for Stress Corrosion Cracking

At the end of the 30 days test, a stereo-microscope, at magnifications up to 10X, was used to examine the C-rings for cracking and pitting. Neither the 13Cr C-rings nor the 25Cr C-rings showed any form of primary or secondary cracks. Figure 78 shows digital pictures of the C-rings for 13Cr after the 30 days for Test 1(blank seawater at 25^{o}C), Test 2 (blank seawater at 80^{o}C), Test 3 (seawater with 1000ppm sodium nitrite at 25^{o}C) and Test 4 (seawater with 1000ppm sodium nitrite at 80^{o}C).

As shown in Figure 78, the 13Cr C-rings tested in blank seawater exhibited pitting corrosion but no cracks when visually examined. Comparing the photographs, the pit density observed on the 13Cr C-rings tested in blank seawater at 80^{o}C was higher than for those tested at 25^{o}C in blank seawater. This is expected and consistent with what was observed in the CPP tests for 13Cr at 25^{o}C (Figure 48) and 13Cr at 80^{o}C (Figure 50), that the pitting corrosion rate increases with temperature.

However the 13Cr C-rings tested in seawater with 1000ppm sodium nitrite at 25^{o}C and 80^{o}C did not show any sign of pitting nor cracking. Their solutions did not show slight brown coloration and solid deposits that was observed in the blank solution. This further validates the inhibiting potential of nitrite especially when the concentration was above the critical concentration of 400ppm as previously mentioned.

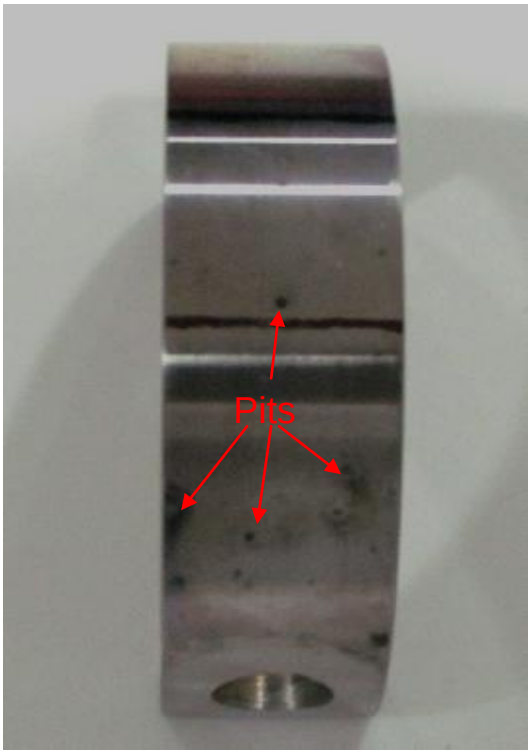

Test 1: 13Cr blank seawater at 25°C

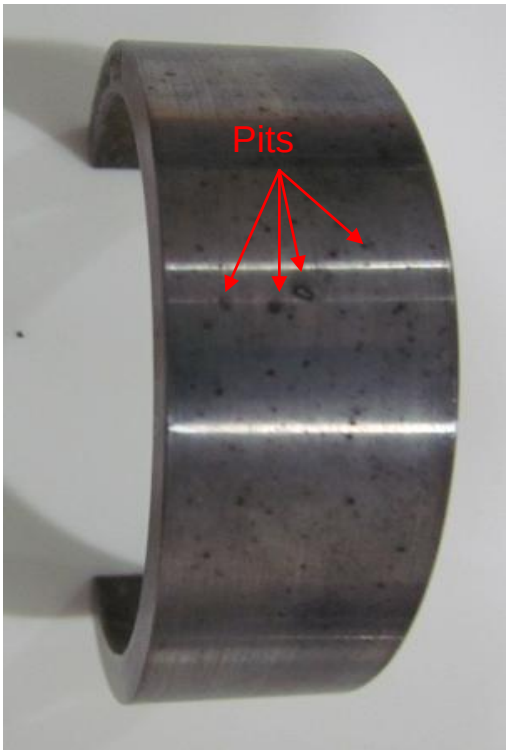

Test 2: 13Cr blank seawater at 80°C

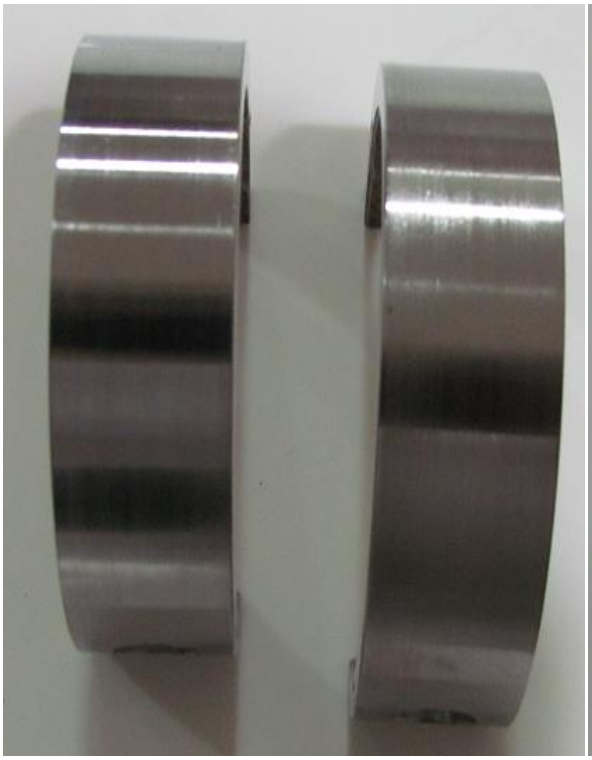

Test 3: 13Cr seawater 1000ppm $NaNO_2$ at 25°C

Test 4: 13Cr seawater 1000ppm $NaNO_2$ at 80°C

Figure 78: Photographs of 13Cr-L80 C-rings after 30 days exposure test

The 13Cr C-rings tested in seawater with 1000ppm sodium nitrite at 25^{o}C maintained shining surface whereas those exposed to 80^{o}C had some etched patches but no pits.

Just in case there were micro cracks that could not be observed under low magnification, metallographic examination was performed on the C-ring that had the highest amount of pitting corrosion, in this case 13Cr C-rings tested in blank seawater at 80^{o}C (Test 2) were selected. To verify the effect of nitrite, the C-rings tested in seawater with 1000ppm sodium nitrite at 80^{o}C (Test 4) were also selected.

For more precise examinations, 2-inch section of the C-rings of 13Cr-L80 used for Test 2 and Test 4 were cut from the apex and mounted to examine the cross section of the C-rings. The mounted specimens were wet ground with silicon carbide abrasive paper to reveal the surface of the metal. They were then ground in succession with finer and finer abrasive media and then polished with soft clothe until a scratch-free mirror finish was obtained. The specimens were examined for cracks and pit with an optical microscope at magnifications up to 200X.

Figure 79 shows Micrograph image of a cross section of C-ring apex of 13 Cr-L80 tested in blank seawater at 80^{o}C after 30 days exposure test at a magnification of 200X (not etched) while Figure 80 shows Micrograph image of a cross section of C-ring apex of 13 Cr-L80 tested in seawater with 1000ppm sodium nitrite at 80^{o}C after 30 days exposure test also at a magnification of 200X (not etched).

As shown in Figure 79 and Figure 80, neither cracks nor pits were identified on either of the apex of C-ring apex tested in blank seawater solution or seawater with 1000ppm sodium nitrite solution. The fact that pits were not observed on both samples indicates that the several pits observed on the sample tested in blank seawater at 80^{o}C at low magnification prior to metallographic operations as shown in Figure 78 were not deep and were removed during grinding and polishing of the specimen.

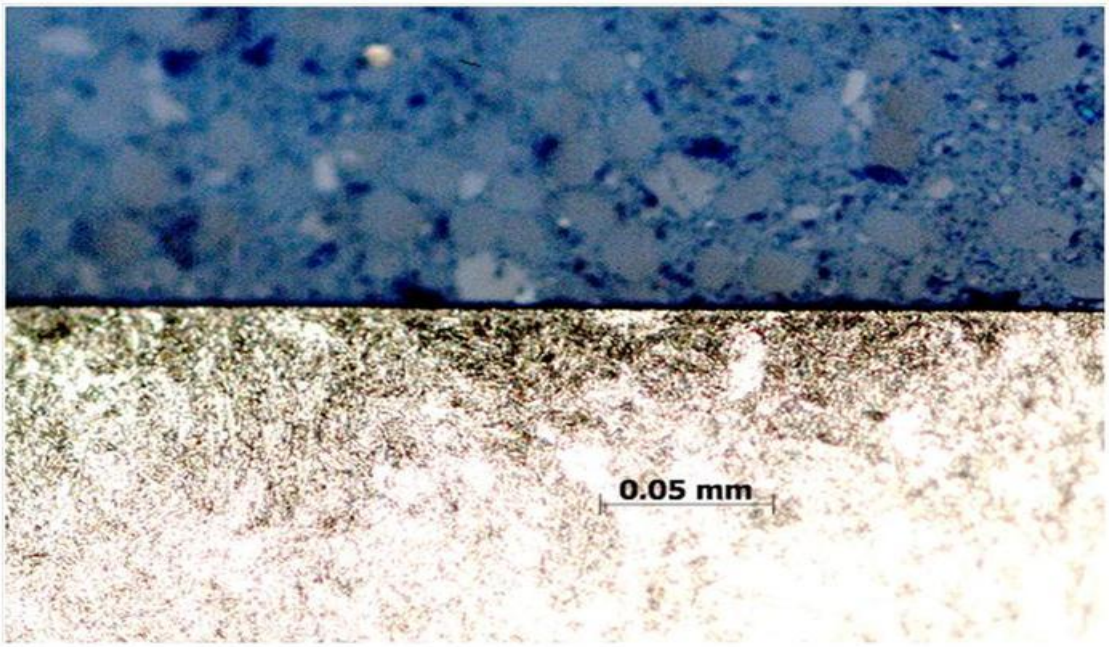

Figure 79: Micrograph image of a cross section of C-ring apex of 13 Cr-L80 in blank seawater at 80^{o}C after 30 days exposure test at a magnification of 200X (un-etched)

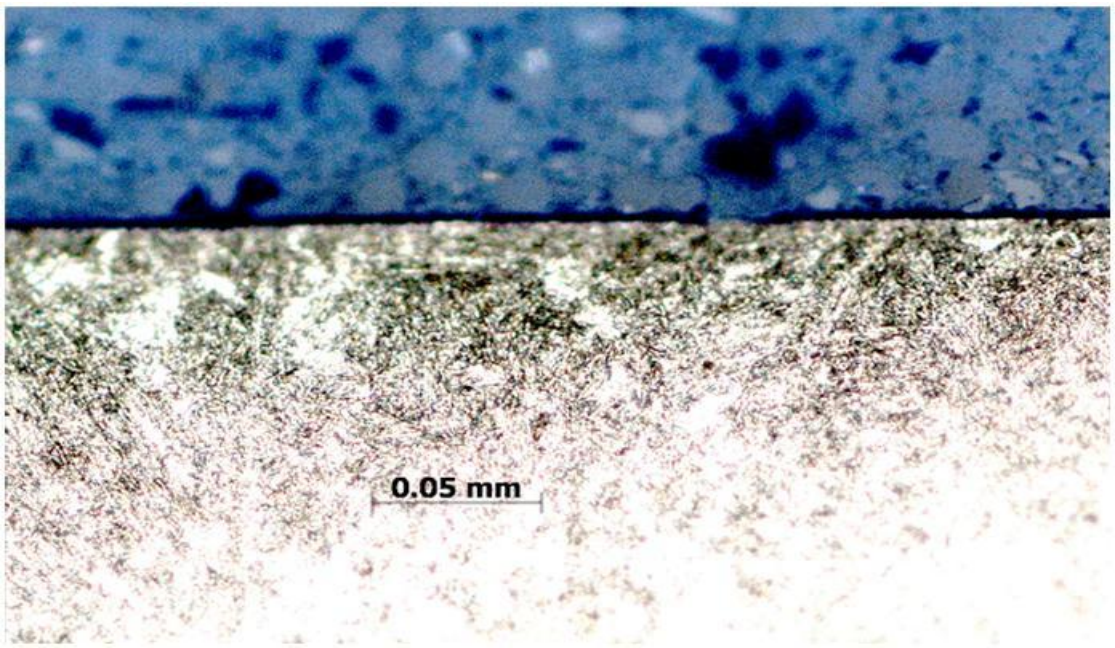

Figure 80: Micrograph image of a cross section of C-ring apex of 13 Cr-L80 in seawater with 1000ppm Sodium nitrite at 80^{o}C after 30 days exposure test at a magnification of 200X (un-etched)

Figure 81 shows digital photograph of the C-rings of 25Cr after the 30 days for Test 1 (blank seawater at 25^{o}C), Test 2 (blank seawater at 80^{o}C), Test 3 (seawater with 1000ppm sodium nitrite at 25^{o}C) and Test 4 (seawater with 1000ppm sodium nitrite at 80^{o}C).

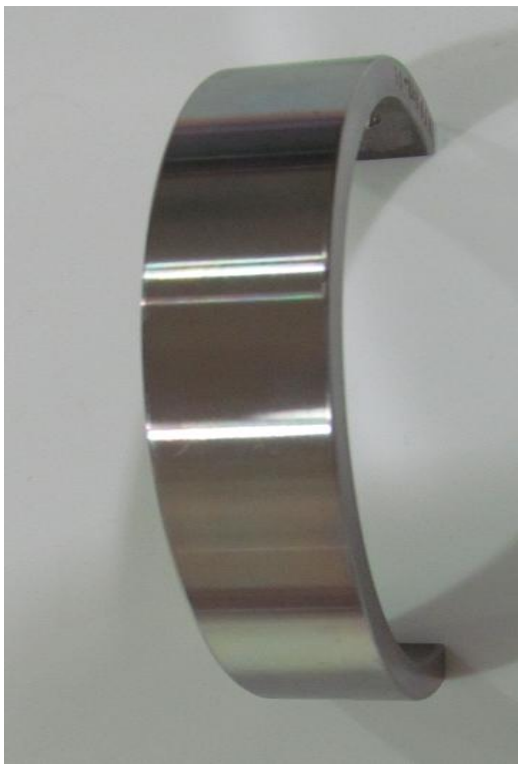

Test 1: 25Cr blank seawater at 25°C

Test 2: 25Cr blank seawater at 80°C

Test 3: 25Cr seawater 1000ppm $NaNO_2$ at 25°C

Test 4: 25Cr seawater 1000ppm $NaNO_2$ at 80°C

Figure 81: Photographs of 25Cr-F255 C-Rings after 30 days exposure test

As shown in Figure 81, none of the 25Cr C-rings tested exhibited pitting corrosion or cracking when visually inspected. The C-rings tested in blank

seawater at 25^{o}C and those tested in seawater with 1000ppm sodium nitrite at 25^{o}C and 80^{o}C all remained in their shining mirror like conditions however the C-rings tested in blank seawater at 80^{o}C had some etched patches but no pit. The fact that C-rings tested in blank seawater at 80^{o}C had some etched patches while those tested in seawater with 1000ppm sodium nitrite at the same temperature did not have etched patches also demonstrates the inhibiting potential of nitrite.

Although examination at low magnification did not reveal cracks, metallographic examination were performed on the C-rings tested in blank seawater at 80^{o}C and C-rings tested in seawater with 1000ppm sodium nitrite at 80^{o}C. 2-inch sections of the C-rings were cut from the apex and mounted to examine the cross section of the C-rings. The mounted specimens were wet ground with silicon carbide abrasive paper to reveal the surface of the metal. They were then ground in succession with finer and finer abrasive media and then polished with soft cloth until a scratch-free mirror finish was obtained. In order to reveal grain structure of duplex stainless steel, the specimens were etched using Kalling's No. 2 (5g of $CuCl_2$, 100ml of Hydrochloric acid and 100ml of Ethanol). The specimens were then examined with an optical microscope at magnifications up to 100X for cracks and pit.

Figure 82 shows a micrograph image of a cross section of C-ring apex of 25Cr-F255 tested in blank seawater at 80^{o}C after 30 days exposure test at a magnification of 100X (etched). The figure revealed several pits that were not observed at low magnifications. The figure also shows preferential or intergranular corrosion along the grain boundaries. This is not surprising because grain boundaries are typically nucleation sites for localised corrosion. The PDM postulates that passivity breakdown occurs as a result of cation vacancy condensation at the metal/barrier layer interface at sites in the passive film that are characterised by high cation vacancy fluxes, due to the aggressive anion induced, autocatalytic generation of cation vacancies at the barrier layer/solution interface. As a result, the excess vacancies condense to form a two -dimensional vacancy condensate beneath the “weak points” in the barrier layer that are characterised by high cation vacancy diffusivity. Vacancy condensation effectively causes local separation between the barrier layer

and the metal. These sites correspond to regions of structural discontinuity, such as (but not limited to) grain boundaries, emergent dislocations, and the points of intersection between the barrier layer and precipitates, inclusions (e.g. MnS in stainless steels), and other second phase particles[96].

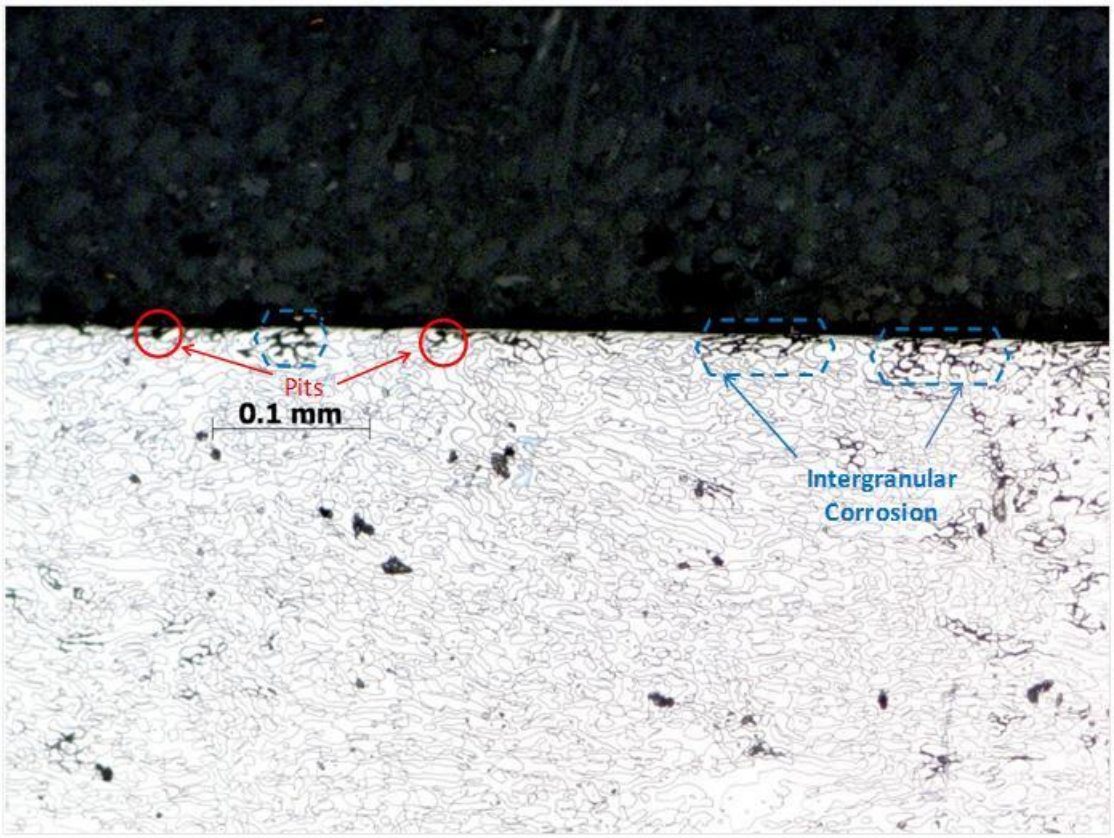

Figure 82: Micrograph image of a cross section of C-ring apex for 25 Cr-F255 in blank seawater at 80°C after 30 days exposure test at a magnification of 100X (etched)

Preferential corrosion along the grain boundaries are typical sites for crack initiation however, no crack was observed in this case. Some of the pits that initiated along the metal surface had propagated through the grain boundaries and could have possibly developed into a crack if there was sufficient tensile stress and the corrosion process was accelerated or performed over a longer period.

Figure 83 and Figure 84 show Micrograph images of cross sections of two different apex sections of C-rings from 25Cr-F255 tested in seawater with 1000ppm sodium nitrite at 80°C after 30 days exposure test at magnification of 100X (etched).

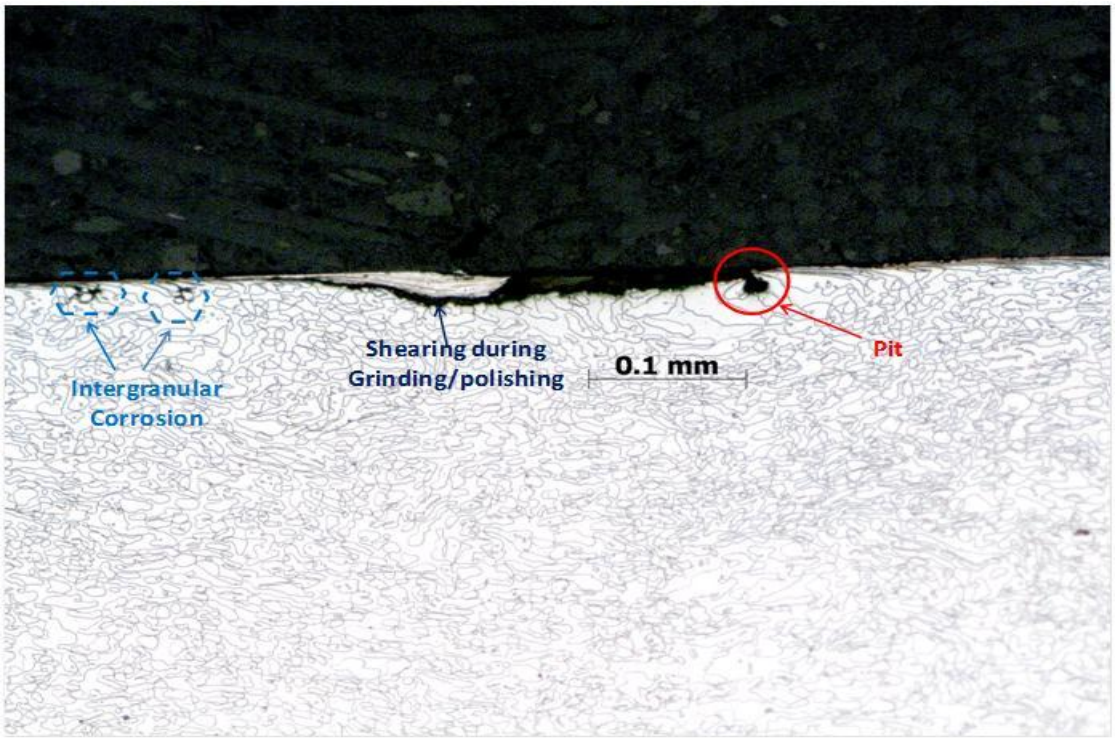

Figure 83: Micrograph image of a cross section of C-ring apex for 25 Cr-F255 in seawater with 1000ppm sodium nitrite at 80°C after 30 days exposure test at a magnification of 100X (etched)

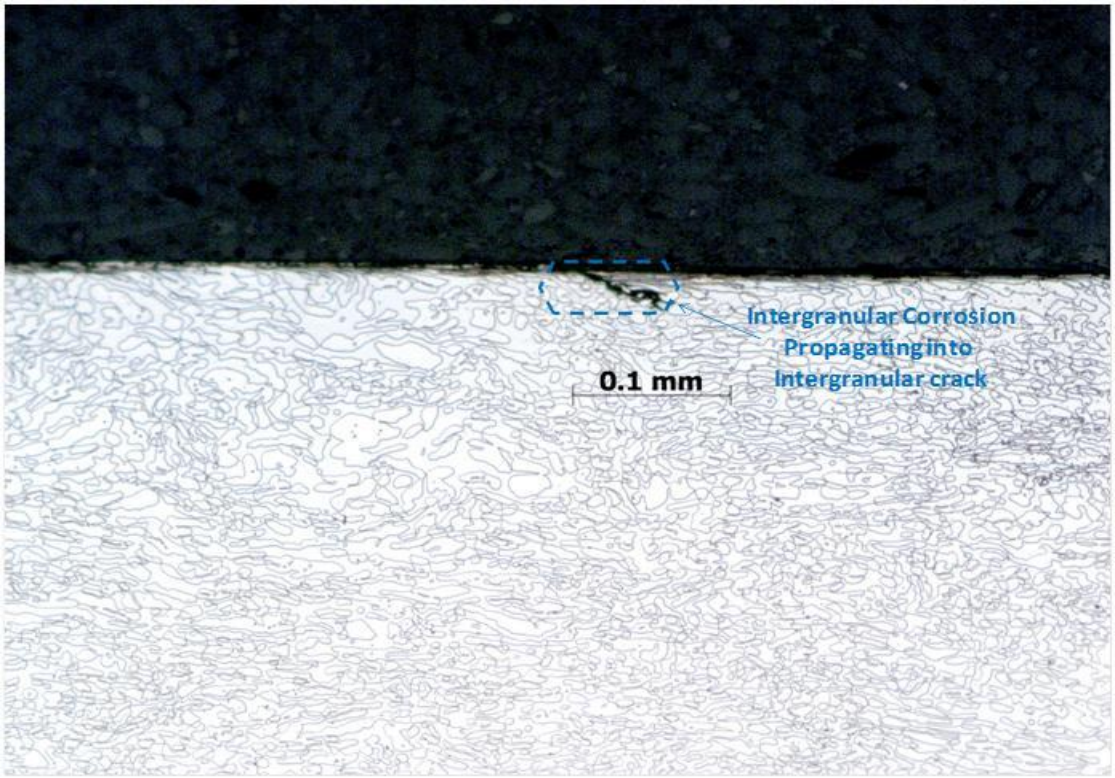

Figure 84: Micrograph image of another cross section of C-ring apex for 25 Cr-F255 in seawater with 1000ppm sodium nitrite at 80°C after 30 days exposure test at a magnification of 100X (etched)

Intergranular corrosion observed in Figure 83 (specimen exposed to seawater with 1000ppm sodium nitrite concentration) was not as severe as those observed in Figure 82 (specimen exposed to blank seawater). Also, the number of pits was reduced, only one pit was observed in Figure 83 however the pit was bigger than the pits observed in Figure 82 indicating that sodium nitrite probably reduced pitting and intergranular corrosion but enhanced the kinetics of pit propagation.

Figure 83 shows a degradation that has typical pit morphology and a crack which probably initiated at the tip of the pit and propagated circumferentially along the outer surface of the apex where the highest level of stress is expected. The crack was however very super facial and did not propagate through the wall thickness. The image also shows that some part of the specimen has either corroded away or chipped off. The latter is believed to be the reason for the loss of part of the specimen since the duration of the test was short and 25Cr is not expected to have such a high corrosion rate in the test solution. Circumferential cracks are not unusual since the principal stress in the C-ring specimen is mainly circumferential however; the crack is not believed to be as a result of stress corrosion cracking. It was probably caused by shearing during grinding/polishing operation. To the left of the crack are secondary cracks or intergranular attack.

Figure 84 shows the image of the duplicate C-ring, which also indicates a crack that initiated at the outer circumference of the apex and had propagated with a crack length of about 0.05mm preferentially orientated along the grain boundaries. This crack was probably initiated by the intergranular attack which progressed into an intergranular stress corrosion crack. For the deflection calculations of the C-rings, the yield stress of the test material was used as the applied stress on the C-rings during the 30 days exposure tests. Per the materials test results for 25Cr-F255 shown in Figure 30, its yield stress is 105kpsi (724MPa).

Using the equation for stress intensity factor (K_I) as stated in equation 71, measured crack length, a, of 0.05mm from Figure 84, and geometrical correction factor (Y) of 1, gives a stress intensity factor of 9.45MPa $m^{½}$. This

value is definitely high enough to cause failure of super duplex stainless steel. Literature has reported values as high as 12MPa $m^{½}$ for austenitic stainless steel in hot chloride solution[189]. The crack growth rate is 2 x 10^{-8} mm/s (~0.6mm/y) which is also consistent with literature for SCC caused by active path dissolution mechanism where accelerated corrosion along a preferred path of higher than normal corrosion susceptibility, with the bulk of the material typically being passive. The most common active path is the grain boundary, where segregation of impurity elements can make it marginally more difficult for passivation to occur hence, the grain boundary preferentially corrodes, with the specimen surface and the crack walls remaining passive. This process does not require substantial amount of stress to proceed, the applied stress is mainly to open up the cracks and allow easier diffusion of corrosion products away from the crack tip hence, allowing the crack tip to corrode faster. Active path corrosion processes are inherently limited by the rate of corrosion of the metal at the crack tip, which limits the maximum crack growth rate to around 10^{-2}mm/s, and crack growth rates are often much lower, around 10^{-8} mm/s (about 0.3mm/y) or less[242].

Considering the fact that sample in Figure 82 with no nitrite did not crack, while sample in Figure 84 that cracked was exposed to the same test conditions except for the presence of 1000ppm concentration of sodium nitrite in the test solution of the C-ring that cracked, it was inferred that the presence of nitrite caused 25Cr to be susceptible to stress corrosion cracking.

It is very surprising that cracks were detected in 25Cr duplex stainless steel but not in 13Cr-L80 which is martensitic possibly because the passive layer was not completely destroyed and the bare metal exposed to the environment. Even then, one would expect that the passive film on 25Cr would heal faster than that of the 13Cr considering the chromium content. Another school of thought that possibly provides a more logical explanation is the fact that 13Cr martensitic only has a single phase while the duplex as a dual phase (ferritic and austenitic phase) hence it is possible that the interface between the two phases served as the weak points on the barrier layer where the excess vacancies condense to form a two -dimensional vacancy condensate which are possible sites for pit nucleation due to presence of

aggressive anion (nitrite ion in this case) which lead to induced autocatalytic generation of cation vacancies at the barrier layer/solution interface. On the contrary however, martensitic materials have higher hardness and are more brittle hence have higher tendency to crack. This can however not be over emphasised because dilution of the passive film into the metal causes a localised hardness at the passive film/metal interface which could easily influence cracking phenomenon.

Lastly, according to the film rupture model, most intergranular SCC involves anodic dissolution at the crack tip[208, 244]. The principal feature of rupture model is that the protective surface film in the vicinity of the crack tip is ruptured by localised plastic deformation but the protective film away from the crack tip remains intact. Hence, an electrolytic cell is created with the bare metal at the crack tip acting as the anode and the unbroken passive film adjacent to it (cathode) sacrificially protected by the exposed bare metal at the crack tip. As a result, the exposed bare metal suffers rapid anodic dissolution which allows the crack to grow. The rate of anodic dissolution and associated crack extension depends partly on the repassivation rate. In the case of 13Cr where the chromium content is below the 15% critical concentration required for self healing process[257], the rate of repassivation is low. Hence, the crack tip becomes blunt because of excessive dissolution on the crack sides thereby stopping the crack propagation. However, in the case of 25Cr, the rate of repassivation is sufficient to support crack propagation.

The result of the C-ring test was not conclusive hence the decision was taken to go ahead with the slow strain rate test which was already a fall back option.

Table 9 gives a summary of the C-ring tests performed.

Table 9: Summary of C-Ring Tests

Test ID Number	Stamp Number	Test Material	Temp (°C)	Test Solution	Visual Observation		Metallographic Observation	
					Post-coupon appearance	Cracks	Post-coupon appearance	Cracks
Test 1	ST0064-15	13Cr	25	Blank deoxygenated seawater	Pitted	No	Pitted	No
	ST0064-16				Pitted	No	Pitted	No
Test 2	ST0064-17		80		Pitted	No	Pitted	No
	ST0064-18				Pitted	No	Pitted	No
Test 3	ST0064-19		25	Deoxygenated seawater with1000ppm Sodium Nitrite Solution	Not pitted	No	N/A	N/A
	ST0064-20				Not pitted	No	N/A	N/A
Test 4	ST0064-21		80		Not pitted	No	Pitted	No
	ST0064-22				Not pitted	No	Not pitted	No
Test 1	X10063-13	25Cr	25	Blank deoxygenated seawater	Not pitted	No	N/A	N/A
	X10063-14				Not pitted	No	N/A	N/A
Test 2	X10063-15		80		Not pitted	No	Pitted	No
	X10063-16				Not pitted	No	Pitted	No
Test 3	X10063-17		25	Deoxygenated seawater with1000ppm Sodium Nitrite Solution	Not pitted	No	N/A	N/A
	X10063-18				Not pitted	No	N/A	N/A
Test 4	X10063-19		80		Not pitted	No	Pitted	Yes
	X10063-20				Not pitted	No	Pitted	Yes

4.5 Slow Strain Rate Test

The slow strain rate test has emerged as a relatively quick and simple method for evaluating metals and alloys for resistance to a variety of environmental cracking phenomena, including stress corrosion cracking, hydrogen embrittlement, and liquid metal cracking. SSR test is particularly used as a screening test for CRA evaluation for downhole applications.

For the purpose of this research work, slow strain rate (SSR) tests were conducted, per NACE TM0198-2004[253] and ASTM G129[254] to determine the cracking susceptibility of 13Cr-L80 and 25Cr-F255 materials to environmental assisted cracking in sea water with nitrite at 80^{o}C. SSR tests were performed at constant tensile strain rate of 4 x 10^{-6} /s to ensure repeatability. All tests were performed in duplicates. The baseline SSR tests were performed in air while the other tests were performed in deoxygenated seawater with different sodium nitrite concentrations. Some of the tests were performed at open circuit potential of the test specimen, while others were performed with an applied constant potential with respect to the saturated calomel reference electrode (SCE) to polarise the test specimen in the pitting susceptibility region. Table 6 and Table 7 show the test conditions for 13Cr and 25Cr respectively. Test results were compared with the baseline test conducted at the same strain rate and temperature in air.

Basically two types of results were obtained from the SSR test; the first being the visual of the test specimen gauge section for evidence of cracking, while the other was the measurement of the ductility parameters of the test specimen and the comparison with the baseline material properties determined in air.

For the visual examination, both halves of the failed gauge section of the test specimen for each SSR test were visually examined under low power optical microscope at a magnification of at least 20X to check for the nature of the primary fracture; whether it was a brittle or ductile fracture. Also, secondary cracks away from the primary fracture were noted. Based on the visual examination, the test samples were classified per NACE TM0198[253].

When necessary, metallographic sectioning of the test specimen gauge was performed and sections observed at a magnification of 100X or under the Scanning Electron Microscope (SEM) to fully characterize the failed test specimens with respect to stress corrosion cracking behaviour.

The key parameters used to evaluate the test specimen for ductility are Percentage Elongation (%EI), and Percentage Reduction of Area (%RA). These key parameters were determined for each test specimen. Also the ductility ratios were calculated for each test by dividing the parameters measured in each test environment by the same parameter measured when the test was conducted in air. The ratios of Time to Failure (TTF), Percentage Elongation (%EI), Percentage Reduction of Area (%RA), in test environment to air provide information on stress corrosion cracking (SCC) susceptibility in the test environment. In accordance with NACE TM0198, ductility ratios of reduction in area in the test medium to the reduction in area in air (RA/RA_{air}) around 1 generally indicate high resistance to environmental cracking in that test medium, whereas low values generally indicate low resistance to environmental cracking in that test medium. For the purpose of this research work, the susceptibility limit as been defined as 0.85. Hence, materials with ductility ratio < 0.85 were inferred to be susceptible to environmental cracking in the test environment. Samples of such failed specimens were further examined under the Scanning Electron Microscope (SEM) to analyse the type of facture and also to check for primary and/or secondary cracks. Ratio of Time to Failure (TTF_{ratio}), is the ratio of time to failure (TTF) in test environment to time to failure in air, expressed as follows:

$$\boldsymbol{TTF_{ratio}} = \frac{\boldsymbol{TTF_{Environment}}}{\boldsymbol{TTF_{air}}} \tag{82}$$

The percentage Elongation (%EI) is expressed as:

$$(\%\boldsymbol{EI}) = \frac{(\boldsymbol{l_f - l_o})}{\boldsymbol{l_o}} \times \mathbf{100} \tag{83}$$

where l_f is the final gauge length and l_o is the initial gauge length.

The ratio of percentage elongation, $(\%EI)_{ratio}$, is the ratio of the percentage elongation in the test environment to the percentage elongation in air, which is expressed as:

$$(\%\boldsymbol{EI})_{\boldsymbol{ratio}} = \frac{(\%\boldsymbol{EI})_{\boldsymbol{Environment}}}{(\%\boldsymbol{EI})_{\boldsymbol{air}}} \quad (84)$$

For circular fracture surfaces, the percentage reduction in cross-sectional area (%RA) of the test specimens was calculated using the following equation:

$$(\%\boldsymbol{RA}) = \frac{\boldsymbol{D_i^2 - D_f^2}}{\boldsymbol{D_i^2}}\ \boldsymbol{x\ 100} \quad (85)$$

Where D_i is the initial gauge section diameter (in.) and D_f is the final gauge section diameter at fracture location (in.)

For noncircular fracture surfaces, the percentage reduction in cross-sectional area (%RA) of the test specimens was calculated using the following equation:

$$(\%\boldsymbol{RA}) = \frac{[\boldsymbol{D_i^2 - (C_{fa} \times C_{fb})}]}{\boldsymbol{D_i^2}}\ \boldsymbol{x\ 100} \quad (86)$$

where C_{fa} is the major axis of fracture surface (in) and C_{fb} is the minor axis of fracture surface (in).

The ratio of reduction in cross sectional area of the sample in the test medium to the reduction in cross sectional area in air $(\%RA)_{ratio}$ is expressed as follows:

$$(\%\boldsymbol{RA})_{\boldsymbol{ratio}} = \frac{(\%\boldsymbol{RA})_{\boldsymbol{Environment}}}{(\%\boldsymbol{RA})_{\boldsymbol{air}}} \quad (87)$$

Table 10 and Table 11 give the result of the SSR test parameters for 13Cr-L80 and 25Cr-F255 respectively.

Table 10: Slow Strain Rate Test Results for 13Cr-L80 Material.

Test Identification number	91413-344	91413-341	91413-343	91413-345	91413-347	91413-348	91413-349	91413-342	91413-346	91413-365
Environment	Air	Env. 1	Env. 2	Env. 3	Env. 4	Env. 5	Env. 6	Env. 7	Env. 8	Env.9
Initial pH	N/A	8.2	8.2	8.2	8.2	8.2	8.2	8.2	8.2	8.2
Final pH	N/A	7.7	7.7	7.6	7.7	8.0	6.3	7.5	8.0	6.9
Initial Diameter (in)	0.152	0.152	0.152	0.153	0.153	0.153	0.153	0.155	0.153	0.151
Initial Gage Area (in^2)	0.018	0.018	0.018	0.018	0.018	0.018	0.018	0.019	0.018	0.018
Maximum Load (Ibs)	1902	1845	1907	1888	1869	1898	1888	1951	1857	1875
UTS (ksi)	104.8	101.7	105.1	102.7	101.7	103.2	102.7	102.6	101.1	104.7
Fracture Load (Ibs)	1206	1143	968	1188	1152	1153	1138	1155	1137	1002
Was Cracking Observed?	No	No	No	No	No	No	No	No	No	Yes
Time to Failure, TTF (hrs)	12.5	12.6	24.1	13.1	12.6	13.0	12.9	12.5	12.8	10.7
TTF/TTF in air	1.00	1.01	1.94	1.05	1.01	1.04	1.04	1.00	1.03	0.86
Elongation (%)	15.7	16.0	32.9	16.6	16.2	16.7	16.6	15.7	16.5	13.8
Elongation/Elongation in air	1.00	1.02	2.09	1.06	1.03	1.06	1.06	1.00	1.05	0.88
Reduction of Area, RA (%)	68.6	64.1	76.6	62.4	66.2	65.7	64.8	73.1	73.0	57.5
RA/RA in air	1.00	0.93	1.12	0.91	0.97	0.96	0.95	1.07	1.06	0.84

Table 11: Slow Strain Rate Test Results for 25Cr-F255 Material.

Test Identification number	91414-358	91414-352	91414-353	91414-354	91414-355	91414-356	91414-359	91414-360	91414-362	91414-357
Environment	Air	Env. 1	Env. 2	Env. 3	Env. 4	Env. 5	Env. 6	Env. 7	Env. 8	Env.9
Initial pH	N/A	8.2	8.2	8.2	8.2	8.2	8.2	8.2	8.2	8.2
Final pH	N/A	7.6	7.8	7.6	7.7	7.6	7.7	7.6	8.0	5.1
Initial Diameter (in)	0.153	0.153	0.152	0.153	0.153	0.153	0.153	0.152	0.151	0.153
Initial Gage Area (in^2)	0.018	0.018	0.018	0.018	0.018	0.018	0.018	0.018	0.018	0.018
Maximum Load (Ibs)	1832	1901	1883	1898	1904	1935	1934	1956	1931	1730
UTS (ksi)	99.6	103.4	103.8	103.2	103.5	105.3	105.2	107.8	107.8	94.1
Fracture Load (Ibs)	887	972	981	908	920	998	1011	1070	1001	1219
Was Cracking Observed?	No	No	No	No	No	No	No	No	No	Yes
Time to Failure, TTF (hrs)	28.3	27.1	26.2	28.8	29.3	26.6	29.9	30.4	28.3	14.7
TTF/TTF in air	1.00	0.96	0.92	1.02	1.03	0.94	1.05	1.07	1.00	0.52
Elongation (%)	39.0	37.2	36.0	39.8	40.5	36.4	40.9	41.5	38.7	18.7
Elongation/Elongation in air	1.00	0.95	0.92	1.02	1.04	0.93	1.05	1.06	0.99	0.48
Reduction of Area, RA (%)	81.6	79.8	80.9	74.3	83.4	79.5	79.0	78.5	80.3	40.9
RA/RA in air	1.00	0.98	0.99	0.91	1.02	0.97	0.97	0.96	0.98	0.50

Susceptibility to environmental assisted cracking was observed only on the 13Cr-L80 specimen exposed to Environment 9 (deoxygenated seawater with 1000ppm sodium nitrite with an applied potential of -150mV wrt SCE which was selected based on the CPP curves for 13Cr-L80 (Figure 73) to ensure material susceptibility was in the pitting region during the test). The ductility ratios were 0.86 for time to failure, 0.88 for elongation and 0.84 for reduction of area. Severe pitting and cracking were observed on the gauge section as shown in several SEM sample images in Figure 85 to Figure 90.

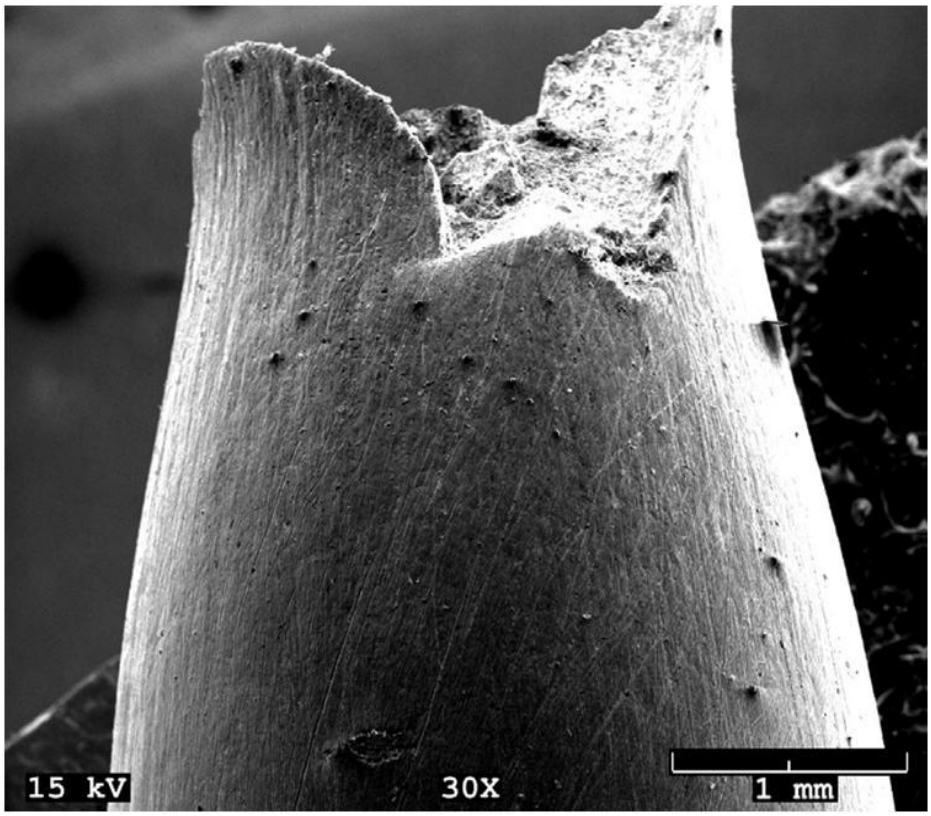

Figure 85: Fracture front of 13Cr-L80 in deoxygenated seawater with 1000ppm sodium nitrite with an applied potential of -150mV (SCE) at magnification of 30X

Figure 85 and Figure 86 show different fracture fronts of 13Cr-L80 after SSR test to failure. The pictures show necking as illustrated by the reduction in gauge diameter. The fracture surface indicates that necking was followed by a brittle fracture. The dull fractured surface is an indication of strain hardening just before the brittle fracture. The stress vs strain curve for the sample shown in Figure 96 confirms the strain hardening.

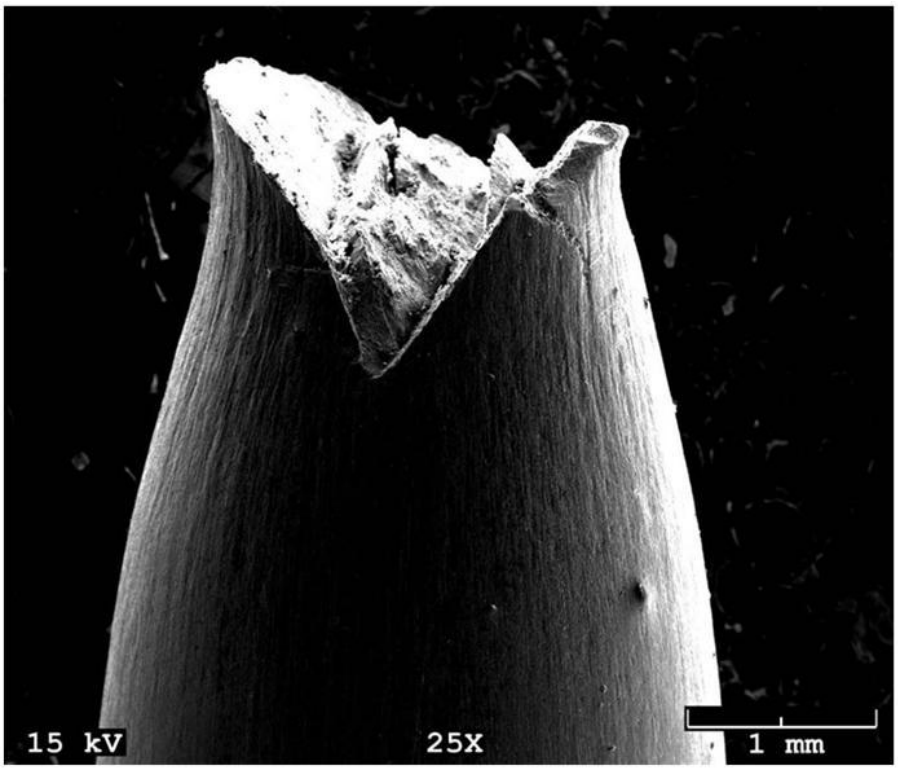

Figure 86: Another Fracture front of 13Cr-L80 in deoxygenated seawater with 1000ppm sodium nitrite with an applied potential of -150mV (SCE) at magnification of 25X

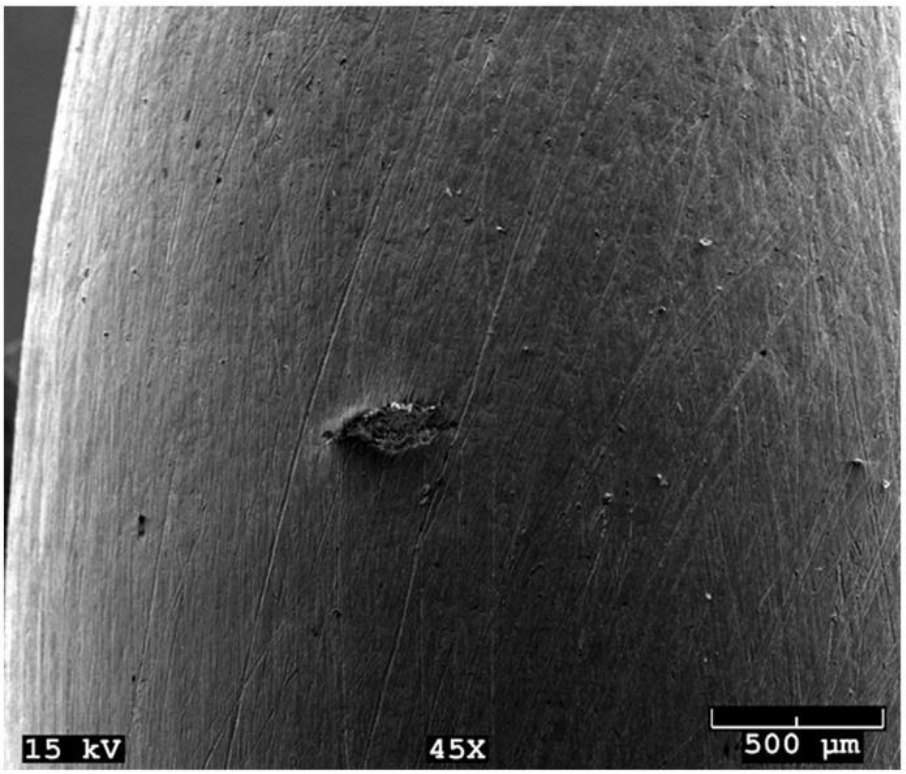

Figure 87: Secondary crack initiation from a pit on 13Cr-L80 in deoxygenated seawater with 1000ppm sodium nitrite with an applied potential of -150mV (SCE) at magnification of 45X

Figure 87 shows initiation of secondary crack from a pit on the gauge of 13Cr-L80. The figure also shows a couple of micro pits along the gauge length.

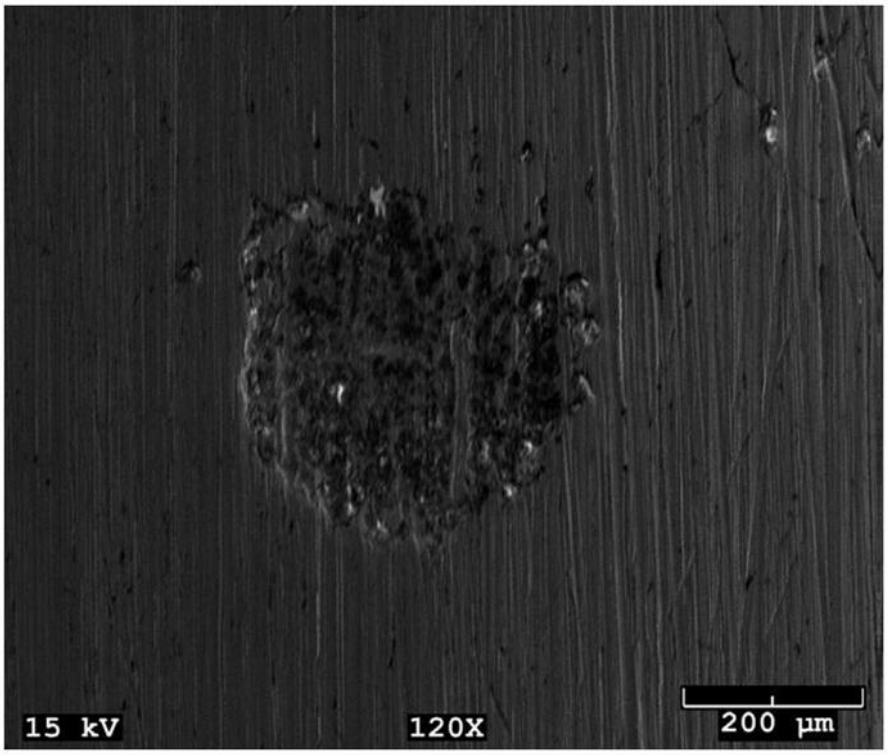

Figure 88: Pitting attack with secondary cracks on 13Cr-L80 in deoxygenated seawater with 1000ppm sodium nitrite with an applied potential of -150mV (SCE) at magnification of 120X

Figure 88 and Figure 89 show several pits and secondary crack initiation. Figure 88 shows a very big pit probably as a result of propagation of small pits that all merged to form a big pit.

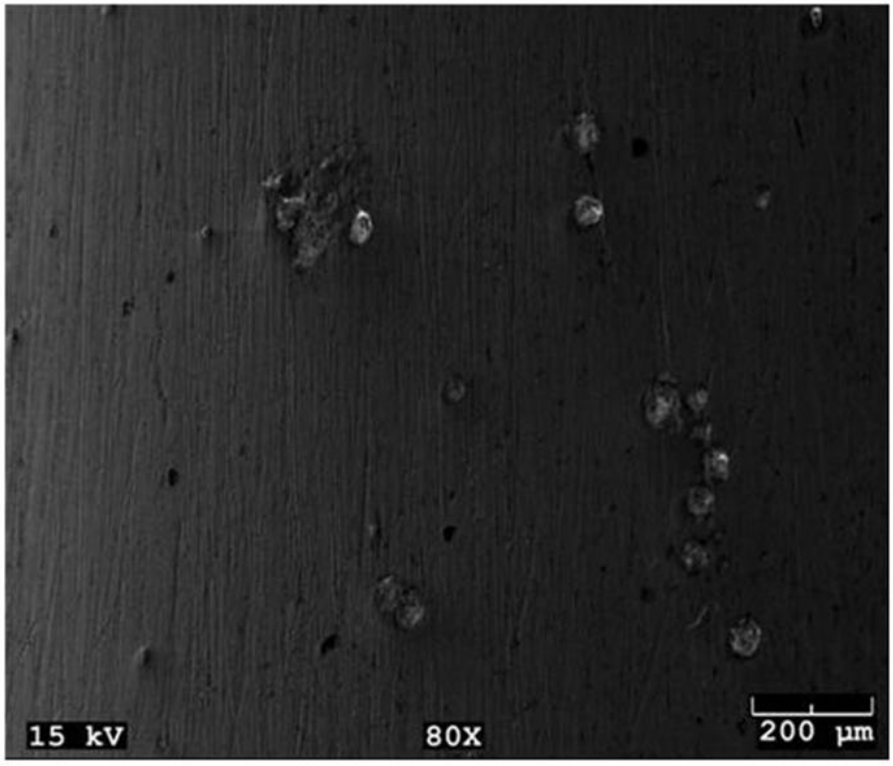

Figure 89: Several small pitting attacks on 13Cr-L80 in deoxygenated seawater with 1000ppm sodium nitrite with an applied potential of -150mV wrt SCE at magnification of 80X.

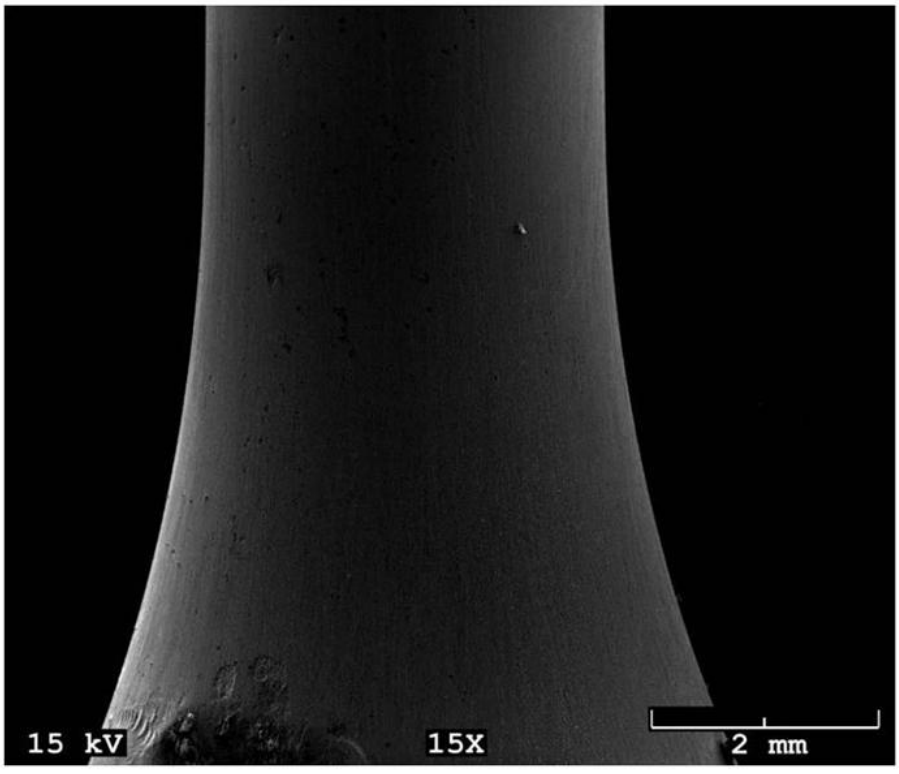

Figure 90: Gauge section with small pits - 13Cr-L80 in deoxygenated seawater with 1000ppm sodium nitrite with an applied potential of -150mV (SCE) at magnification of 15X

Figure 90 shows the plastic deformation of 13Cr before fracture as illustrated by the significant reduction in the diameter of the gauge length. Environmentally assisted cracking of 13Cr-L80 specimen exposed to deoxygenated seawater with 1000ppm sodium nitrite under potentiostatic charge of -150mV wrt SCE was reproduced with the same test conditions confirming susceptibility of 13Cr-L80 to the test medium.

The fact that pitting and cracking was not observed in the test sample exposed to blank deoxygenated seawater that was also under potentiostatic charge of -150mV wrt SCE infers the susceptibility of 13Cr-L80 in the test condition in Environment 9 was as a result of the presence of 1000ppm of sodium nitrite in the test solution.

Injection of up to 6000ppm of sodium nitrite to deoxygenated seawater did not make 13Cr-L80 susceptible when the SSR tests were carried out at open circuit potential. CPP test results from 4.2 actually indicate that above the critical nitrite concentration, nitrite actually inhibits corrosion by shifting the open circuit potential to a more positive level with a corresponding shift in the anodic polarisation curve to lower currents thereby reducing the net corrosion rate. However by applying potential to polarise the test sample close to its pitting potential, increased the oxidising power of nitrite leading to nitrite reduction and corresponding oxidation of iron thereby inducing localised pitting.

A material is termed not to be susceptible to environmentally assisted cracking if the passive film can be preserved (i.e. no breakdown of passive, pit stabilisation and pit growth). Cracks are postulated to initiate from pits and other defect, hence when there is no pit and/or defect, it is a generally assumed that cracks cannot initiate. Environmental assisted cracking was also observed on the 25Cr-F255 but only on specimen exposed to Environment 9 (deoxygenated seawater with 1000ppm of sodium nitrite under potentiostatic charge of 500mV wrt SCE).

The ductility ratios were 0.52 for time to failure, 0.48 for elongation and 0.50 for reduction of area. Severe pitting attacks were observed on the gauge section and at the fractured surface as shown in Figure 91 to Figure 95.

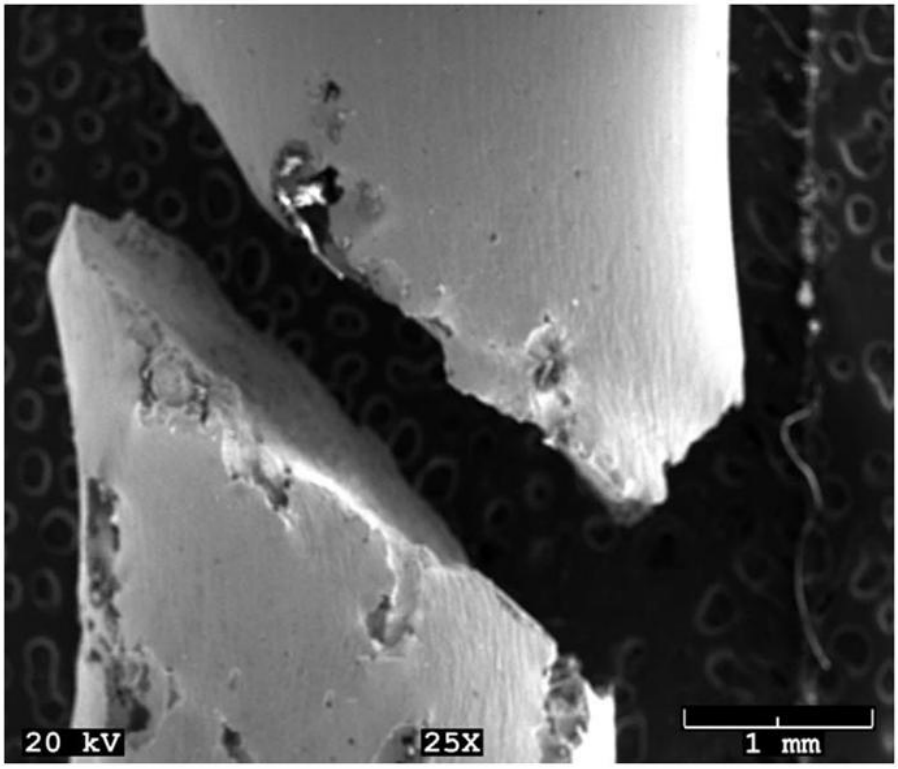

Figure 91: Brittle fracture and pitting of 25Cr-F255 in deoxygenated seawater with 1000ppm sodium nitrite with an applied potential of 500mV (SCE) at magnification of 25X

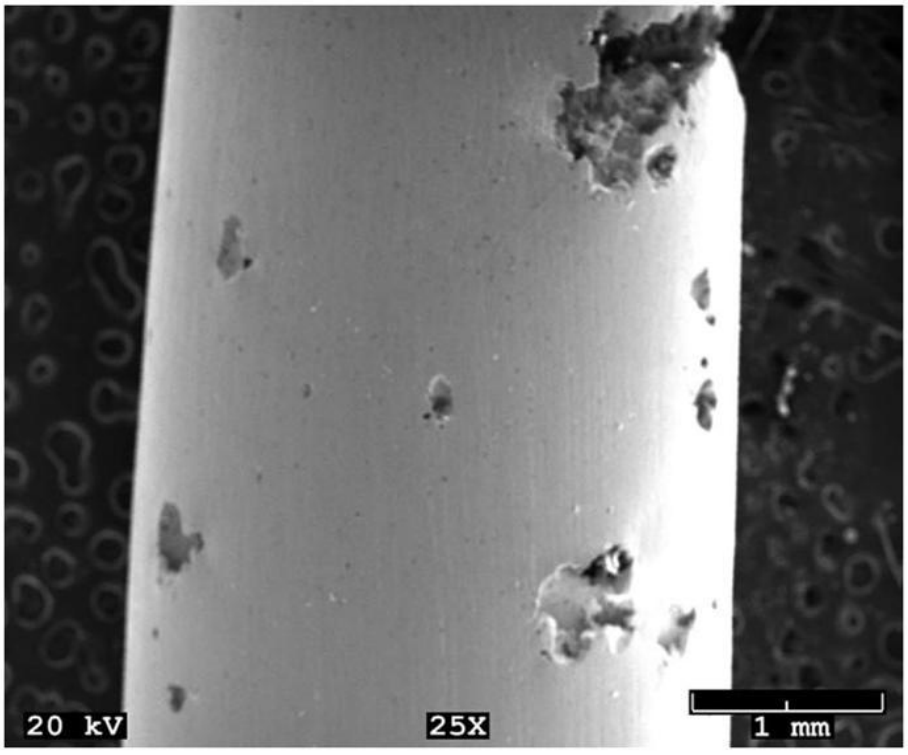

Figure 92: Severe pitting on gauge section of 25Cr-F255 in deoxygenated seawater with 1000ppm sodium nitrite with an applied potential of 500mV (SCE) at magnification of 25X

Excessive corrosion shown in Figure 91 and Figure 92 coupled with the premature fracture observed could not be reproduced in the duplicate test under the same test conditions. It is suspected that there might have been a loss in the potentiostatic control during the test and the applied potential of 500mV wrt SCE was not maintained. However, the key message here is that 25Cr-F255 could suffer from excessive pitting corrosion and is susceptible to brittle fracture in the presence of nitrite when excessively polarised.

Figure 91 shows a very brittle shear fracture with the crack front. The primary crack initiated from the pit. There was significant reduction in the diameter of the gauge. There was no evidence of secondary cracks either on the gauge section or the fractured surface. Figure 93, Figure 94, and Figure 95 show different magnification of the fractured surface. The figures reveal intergranular pitting corrosion in the fractured surface.

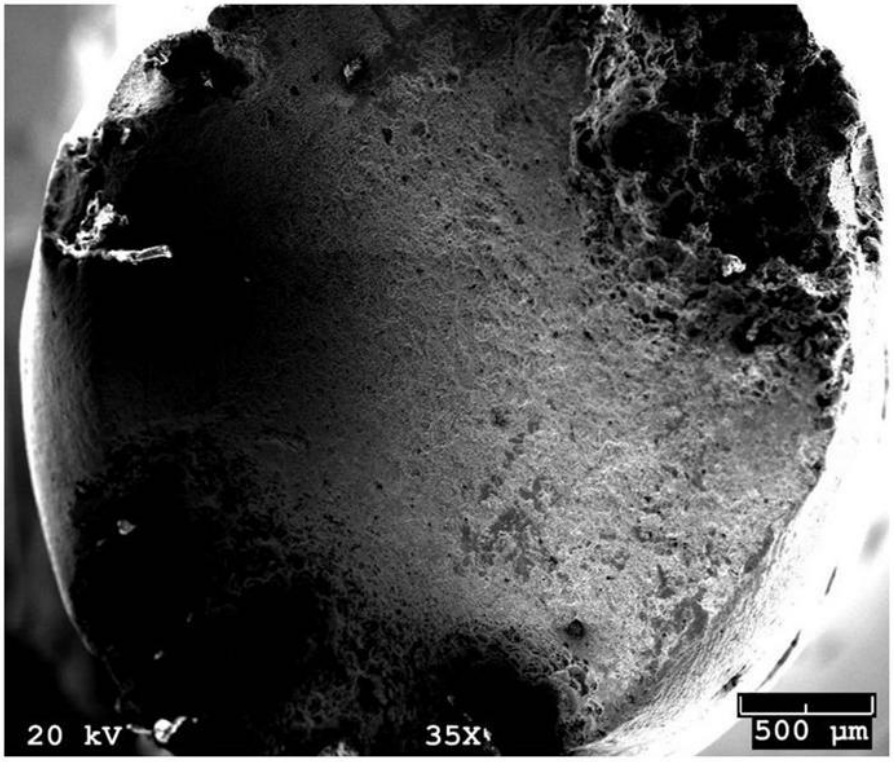

Figure 93: Fractured surface of 25Cr-F255 in deoxygenated seawater with 1000ppm sodium nitrite with an applied potential of 500mV (SCE) at magnification of 35X

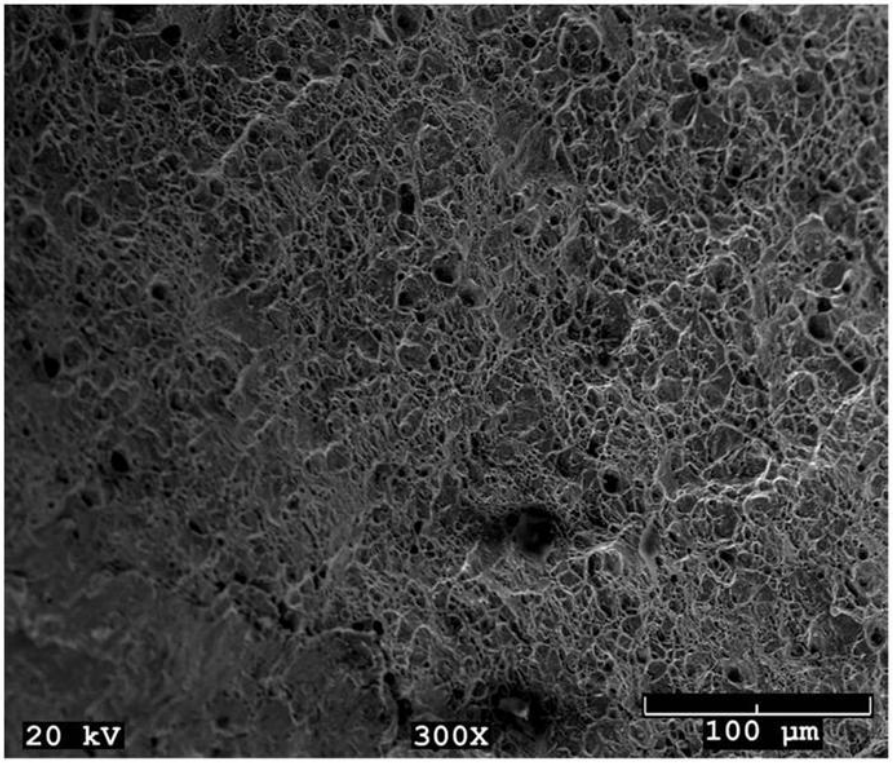

Figure 94: Fractured surface of 25Cr-F255 in deoxygenated seawater with 1000ppm sodium nitrite with an applied potential of 500mV (SCE) at magnification of 300X

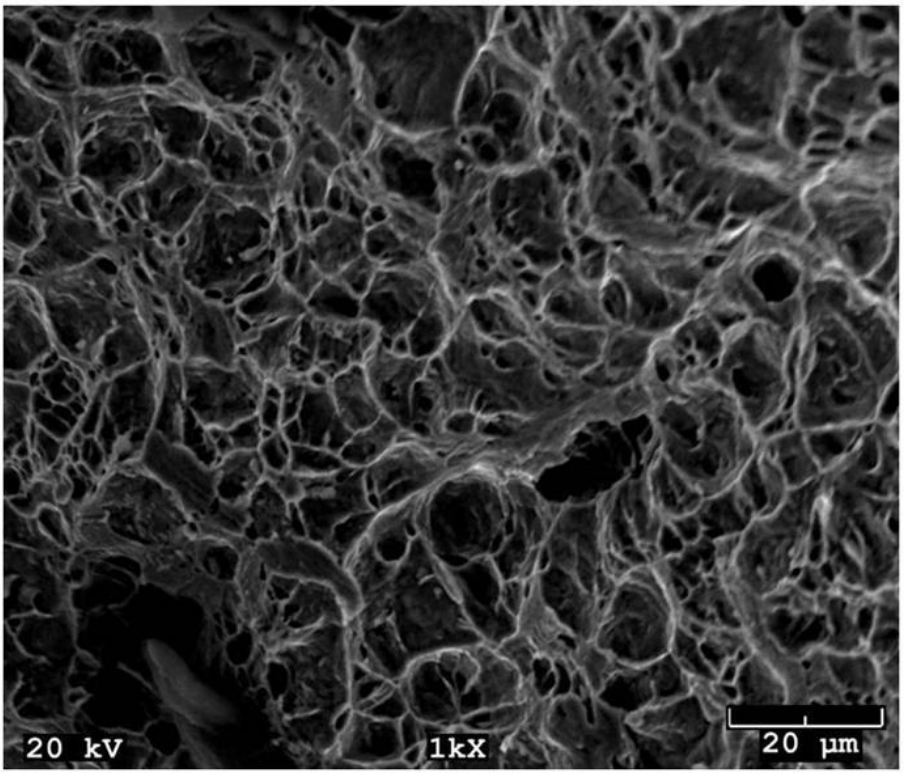

Figure 95: Fractured surface of 25Cr-F255 in deoxygenated seawater with 1000ppm sodium nitrite with an applied potential of 500mV (SCE) at magnification of 1000X

Based on work done by Scott et al, intergranular cracks are characteristics of stress corrosion cracking in nitrate/nitrite solution[268]. Intergranular crack was observed on 25Cr-F225 C-rings after 30 days exposure test in deoxygenated seawater with 1000ppm sodium nitrite at 80^{o}C, but not in the C-rings tested in deoxygenated blank seawater solution at the same temperature. Also, stress corrosion cracking was observed on failed gauge sections of 25Cr-F255 after SSR test in deoxygenated seawater with 1000ppm of sodium nitrite under potentiostatic charge of 500mV with respect to SCE. Based on these test results, it was inferred that 25Cr is susceptible to pitting and stress corrosion cracking in the presence of 1000ppm sodium nitrite in seawater provided breakdown of the passive protective film occurs as a result of aggressive conditions such as tensile stress and excessive polarisation.

The stress-strain plot was used to further analyse the deformation characteristics of the material and also to examine the influence of nitrite on the test material. There are two generally accepted forms, the engineering stress-strain and the true stress-stain.

The engineering stress, σ_{eng}, and engineering strain, ϵ_{eng}, are used extensively in engineering practice and are defined as:

$$\boldsymbol{\sigma_{eng}} = \frac{\boldsymbol{Load,(P)}}{\boldsymbol{Initial\ cross\ sectional\ area,(A_o)}} \tag{88}$$

$$\in_{\boldsymbol{eng}} = \frac{\boldsymbol{change\ in\ lenght,(l_f - l_o)}}{\boldsymbol{initial\ lenght,(l_o)}} \tag{89}$$

While the true stress, σ_{true}, and true strain, ϵ_{true}, are defined as;

$$\boldsymbol{\sigma_{true}} = \frac{\boldsymbol{Load,(P)}}{\boldsymbol{instantaneous\ cross\ sectional\ area,(A_i)}} \tag{90}$$

$$\in_{\boldsymbol{true}} = \boldsymbol{ln}\left\{\frac{\boldsymbol{final\ lenght,(l_f)}}{\boldsymbol{initial\ lenght,(l_o)}}\right\} \tag{91}$$

The fundamental distinction between the engineering stress and true stress, and engineering strain and true strain is that the true stress and strain recognise the interrelation between gauge length and diameter changes associated with plastic deformation. Assuming constant volume, i.e. any

extension of the original length would produce a corresponding contraction of the gauge diameter. Then:

$$\boldsymbol{A_i l_i = A_0 l_o} \tag{92}$$

If:

$$\boldsymbol{\sigma_{true} = \frac{P}{A_i}} \tag{93}$$

Substituting expression for A_i in equation 92 into equation 93, then

$$\boldsymbol{\sigma_{true} = \frac{P}{A_o}(l_i/l_o)} \tag{94}$$

Substituting equation 88 into equation 94 gives the correlation between engineering stress and true stress;

$$\boldsymbol{\sigma_{true} = \sigma_{eng}(l_i/l_o)} \tag{95}$$

From equation 89;

$$\boldsymbol{\frac{l_i}{l_o} = (1 + \epsilon_{eng})} \tag{96}$$

Therefore, substituting equation 96 into equation 95 and equation 91 gives:

$$\boldsymbol{\sigma_{true} = \sigma_{eng}(1 + \epsilon_{eng})} \tag{97}$$

and;

$$\boldsymbol{\epsilon_{true} = In(1 + \epsilon_{eng})} \tag{98}$$

For the purpose of this analysis, engineering stress, σ_{eng}, and engineering strain, ϵ_{eng}, were used.

The stress versus strain curves and the stress versus time to failure for the 13Cr-L80 specimens are shown in Figure 96 and Figure 97 respectively.

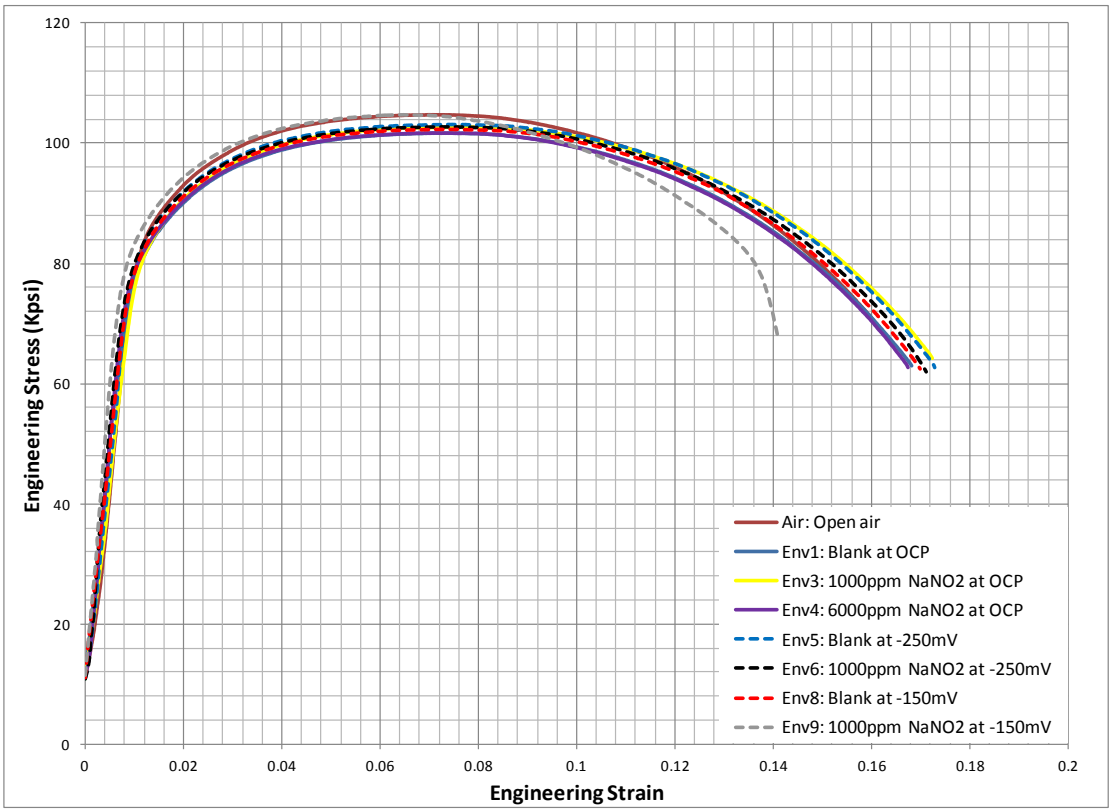

Figure 96: Stress – Strain curves for 13Cr-L80 from SSR test at strain rate of 4 x 10^{-6} /s

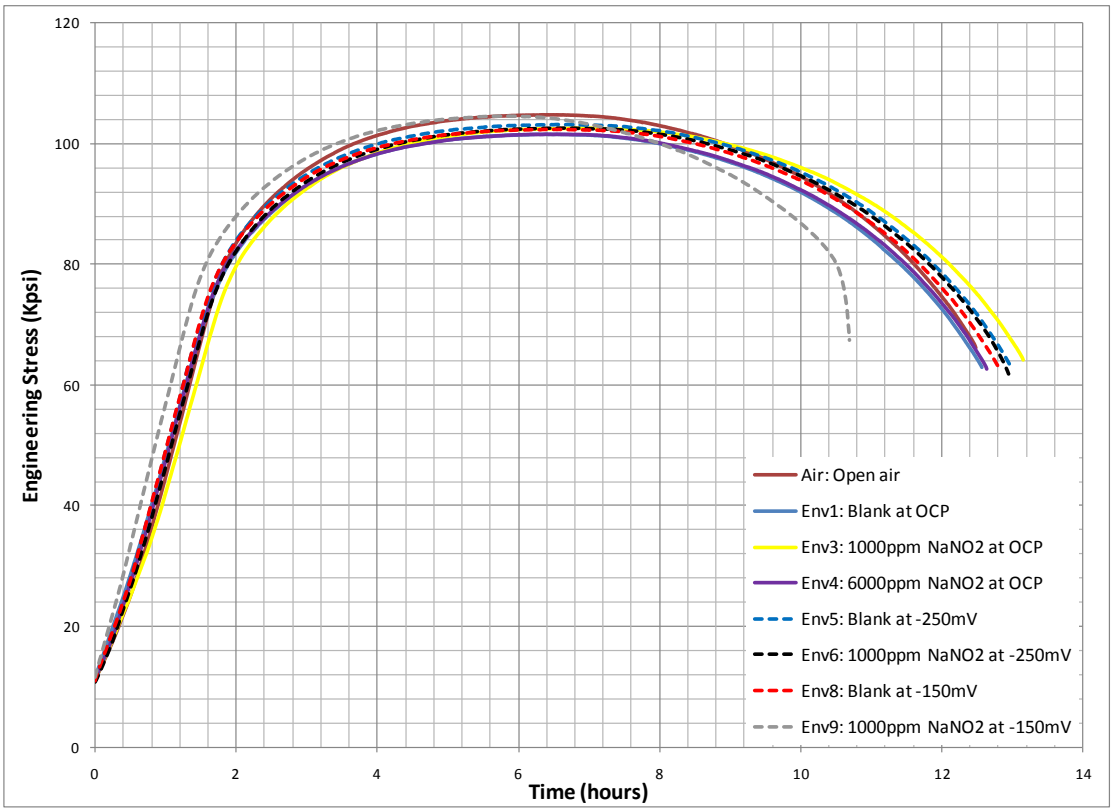

Figure 97: Stress – Time to failure curves for 13Cr-L80 from SSR test at strain rate of 4 x 10^{-6} /s

The two figures show that all the curves had similar characteristics with the exception of the curve for 13Cr in deoxygenated seawater with 1000ppm sodium nitrite polarised at -150mV with respect to the SCE that failed. They all exhibited a linear elastic region in which case the applied force is directly proportional to the displacement associated with the load, provided the elastic limit was not reached, according to Hooke's law i.e.

$$\boldsymbol{F = Kx} \tag{99}$$

where F is the applied force, x is associated displacement and K is the proportionality constant for the material. The elastic region is the linear portion of the curves. When the force acts on a cross sectional area, A and the displacement, x, related to gauge length, l, can be rewritten in the form of stress and strain as follows:

$$\boldsymbol{\sigma = E\epsilon} \tag{100}$$

Where the stress, $\sigma = F/A$, the strain, $\epsilon = x/l$ and E is the proportionality constant know as the Young's modulus which is material specific. Within the linear elasticity zone, the process is fully reversible. Once the elastic limit is reached, plastic deformation begins and the process is no longer reversible. In the plastic deformation zone, a small increment in the applied stress leads to high strain, this region is the parabolic portion of the curves.

Plastic deformation leads to reduction in cross sectional area hence high stress. The stress continues to rise with strain, reflecting increased resistance on the part of the material to further deformation (the process is known as strain hardening) until a maximum stress is reached at which point further elongation leads to decrease in stress. The maximum stress is known as the ultimate tensile strength (UTS) of the material. Beyond the UTS the materials continue to yield until fracture occurs.

At ambient temperature, the API 5CT/ISO 11960[269] technical specification for 13Cr-L80 production casing and tubular specifies minimum yield strength of 80Kpsi (552MPa), minimum tensile strength of 95kpsi (655MPa) and Young modulus of 31290Kpsi (215700MPa). From the SSR test data, the yield strength (σ_{ys}) and Young's Modulus (E) of 13Cr-L80 determined at 80^{o}C were

76Kpsi (524MPa) and 29.5Mpsi (203,395MPa) respectively. These figures are in agreement with the technical specification. The difference in value was due to the fact that the test was carried out at higher temperatures and not ambient temperature. The yield strength decreases with increasing temperature; this has been attributed to increased mobility of dislocations at higher temperatures.

As shown in Figure 96, 13Cr SSR test in air has the highest UTS of about 105kpsi (724MPa). Exposing the specimen to a deoxygenated seawater solution with various sodium nitrite concentrations dropped the UTS by 2-4kpsi with the specimen exposed to deoxygenated seawater with 6000ppm sodium nitrite solution tested at open circuit potential having the least UTS of 102kpsi.

Time to failure was similar for all the curves with the exception of 13Cr in deoxygenated seawater with 1000ppm sodium nitrite polarised at -150mV with respect to SCE which fractured about 2 hours before the rest. It also attained similar UTS as the sample tested in air, confirming additional strain hardening earlier inferred. The rapid drop in stress at a strain of about 0.136 is an indication of excessive yielding which led to necking observed in the specimen. As shown in Figure 97, the stress versus time curve, exhibits similar characteristics as the stress-strain curve.

The material toughness is another important characteristic of the material. It indicates the resistance of the material to fracture, and is defined as the amount of energy absorbed before fracture. Its value can be easily estimated from the area under a stress strain curve.

The stress versus strain curves and the stress versus time to failure for the 25Cr-F255 specimens are shown in Figure 98 and Figure 99 respectively.

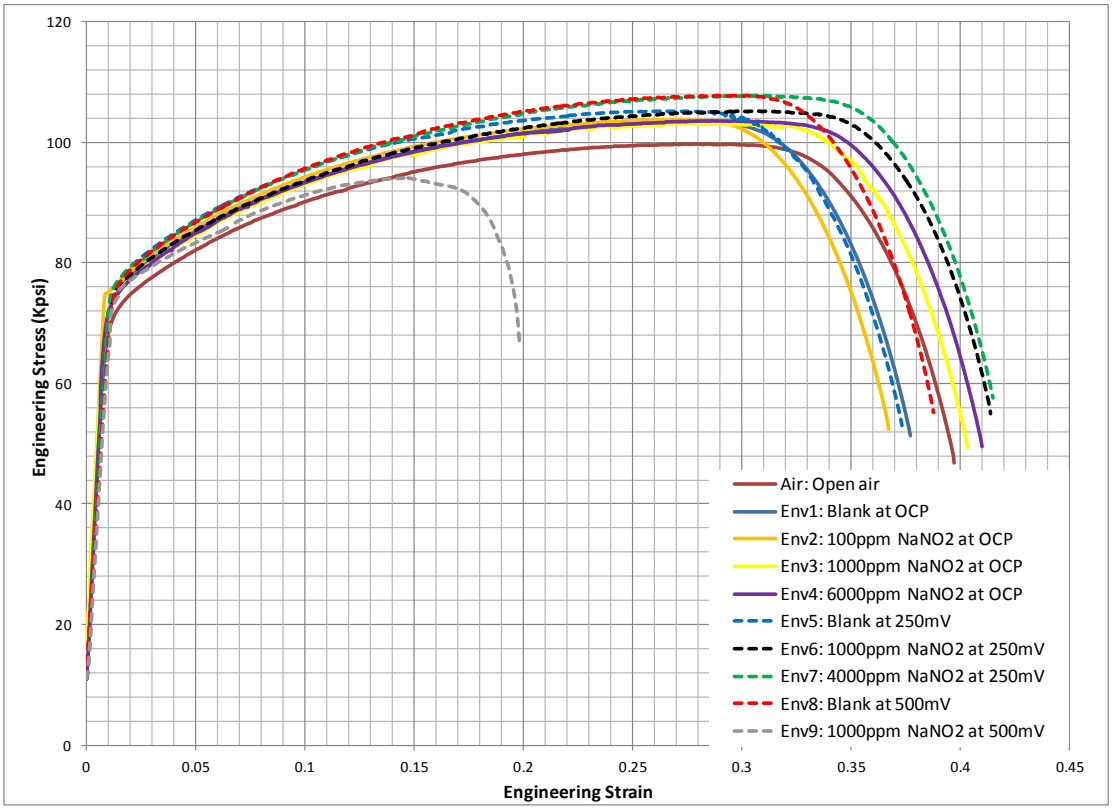

Figure 98: Stress – Strain curves for 25Cr-F255 from SSR test data at strain rate of 4 x 10^{-6} /s

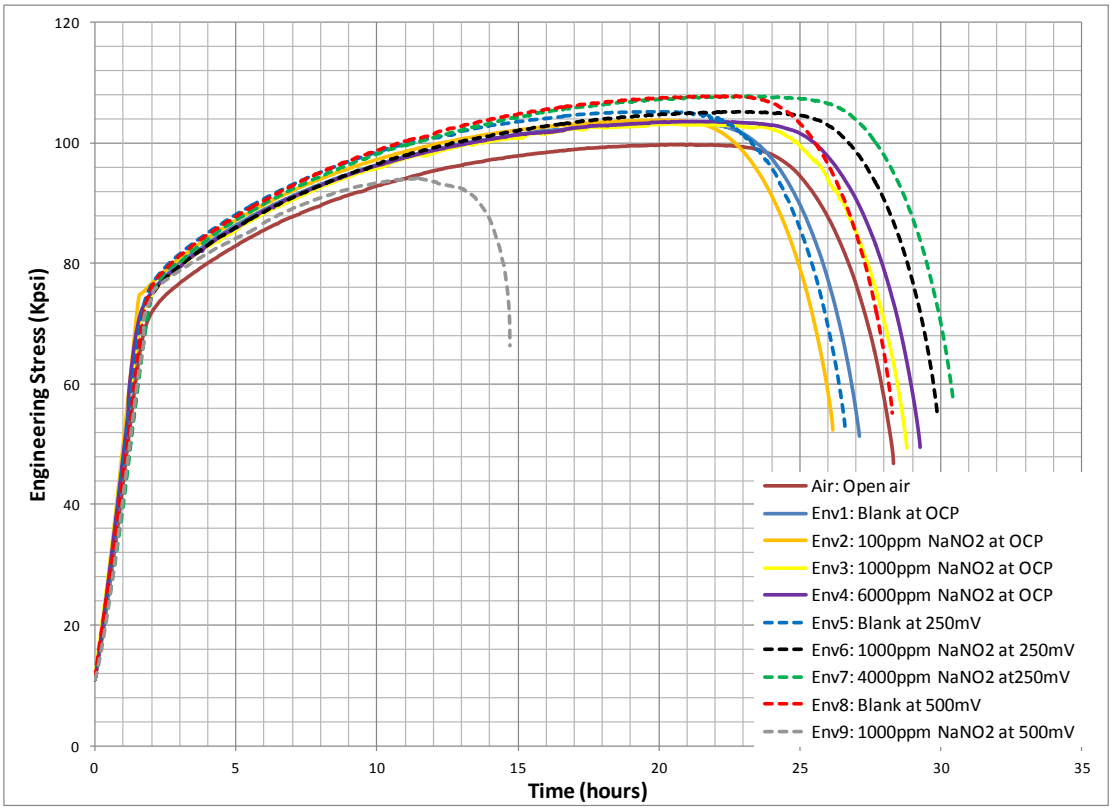

Figure 99: Stress – Time to failure curves for 25Cr-F255 from SSR test data at strain rate of 4 x 10^{-6} /s

The stress-strain curves shown in Figure 98 and the stress-time curves shown in Figure 99 have similar characteristics with those observed for 13Cr exhibiting the linear elastic region. However, the homogeneous plastic deformation of 25Cr is a lot higher than that of 13Cr. The strain prior to fracture for 25Cr is about double strain for 13Cr. This is probably attributed to the mobility of dislocations. 25Cr is a super duplex alloy with a mixture of ferrite and austenite. The austenitic structure is a face centred cubic (fcc) crystal structure while the ferritic structure is a body centred cubic (bcc) crystal structure. On the other hand, 13Cr-L80 is a martensitic structure, super saturated with carbon and has a body centred cubic (bcc) crystal structure. In the fcc lattice, the perfect dislocations of burgers vector; a/2 <110> (where a is the lattice parameter) are dissociated in their {111} slip planes. The well-known split configuration consists of two a/6 <112> Shockley partials separated by a stacking fault ribbon[270].

As a result of the dissociation mode, the fcc lattice opposes a very small resistance to the motion of the dislocations. Actually, the main obstacle to dislocation motion is the interaction with other dislocations. This interaction is both long and short- ranged. The long-range interaction stems from the elastic field of the dislocation lines, while the short-range interactions occur when two dislocations come in contact. The one that plays the major role occurs when two dislocations gliding in non-parallel slip planes intersect each other and locally react to form a sessile product. Such junctions locally pin the moving dislocations and their density increases with increasing strain. The stability of junctions determines the stress level in fcc crystals in multi-slip conditions. In schematic terms, the low yield stress of fcc crystals, their excellent work hardening properties and ductility result from the dislocation–dislocation interaction.

Whereas, in the bcc crystals, the mobility of the a/2 <111> screw dislocations is severely restricted by the particular structure of their core. Along the <111> direction, the bcc structure has a threefold symmetry; three {110} and three {112} planes which are potential dissociation and slip planes in the bcc structure. The screw dislocation has stable positions of low energy at the

centre of gravity of the <111> atomic rows, where the displacements of neighbouring atoms are minimised. Around these sites, the nearest-neighbouring atoms are located on a helix that winds up in a clockwise or counter-clockwise manner. Also, the screw dislocation tends to transform the {111} planes into spiral surfaces. Two different types of core configurations can be obtained depending on the sign of the burgers vector; the first one has high energy which is isotropic while the other has lower energy which exhibits a threefold spreading and degenerate even more[271]. To glide from one site to the other, the extended core structure has to overcome energy barriers, which requires high stress levels at low temperature. Therefore, the resistance opposed by the lattice to this motion is periodic with a periodicity of the order of the lattice spacing. Hence, it is not surprising that 25Cr exhibits higher plastic deformation compared to 13Cr.

Unlike what was observed in the case of 13Cr, the curve for the SSR test of 25Cr performed in air has the least resistance to plastic deformation and the lowest UTS. Increase in the nitrite concentration had no effect on the UTS of both 13Cr and 25Cr however, polarising the specimen slightly increased the UTS of 25Cr. This could be as a result of inherent statistical variability of the measured data. The slow strain rate test is an operation which involves people, machines, machined specimens, environment and measuring equipments. The slow strain rate machine has rotating equipments which wear out over a period of time hence the efficiency and accuracy of the machine are not constant, they gradually deteriorate over time. To reduce variation in mechanical properties of the slow strain rate test specimens as much as possible, the specimens were made from the same piece of metal but then, the machining process of the specimens brought some variability into the picture. Other factors such as operator errors, power surges, fluctuation of process parameters such as temperature and pressure result in statistical variation. These factors can adversely affect the authenticity of the test data hence a process control method had to be put in place to bring the process into a state of statistical control. For the slow strain rate test, the dimensions of the specimen were well defined as shown in Figure 42. The process parameter such as ambient temperature in the autoclave was controlled using a

temperature controller, while regulators were used to control the inlet and outlet gas flow and the pressure was monitored using pressure gauges.

The approach of one variable at a time (OVAT) was adopted in the test methodology; hence only one variable was changed at a time with all the other variables kept constant. As much as possible, the same equipments were utilised. The machines were periodically recalibrated and recertified. Also the tests were carried out in duplicates to confirm adequate replication. Slow strain rate (SSR) tests were conducted, per NACE TM0198-2004[253] and ASTM G129[254] and a constant strain rate of $4x10^{-6}$ /s was used for all the tests.

Even though sufficient controls were put in place, the measuring equipments have error margin and the slow strain rate test specimens have tolerance limits. The gauge diameter and length have tolerance limits of ±0.002 and ±0.005 inches respectively while the radius of curvature of the shoulder section at the ends of the gauge sections and the entire specimen length have tolerance limit of ±0.02 and ±0.005 inches respectively. Fluctuations in temperature and pressure were ±0.5^{o}C and 0.375psi respectively. It is however more important to know the interactive effect of these errors. Understanding the synergistic effect of all these parameters require construction of complex coded design matrix. The practical approach typically adopted is to have sufficient number of replicate tests. That way, satisfactory inference of the interactive effect is made.

Statistical confidence interval is typically used in engineering projects with P90, P50 and P10 being the probability of occurrence of an event having confidence limits of 90%, 50% and 10% respectively. According to Anthony[272], the statistical confidence interval (at 99% confidence limit) for the mean response can be computed using the following equation:

$$\boldsymbol{CI = \bar{x} \pm 3\left\{\frac{\delta_N}{\sqrt{n}}\right\}} \quad (101)$$

Where $\bar{x}$ is the mean response obtained from replica tests, δ_N is the Standard Deviation of response obtained from replica tests, and n is the number of replica tests performed. Standard Deviation is the square root of statistical variance and is given as:

$$\boldsymbol{\delta_N = \sqrt{\frac{1}{n}\sum_{i=1}^{n}(x_i - \bar{x})^2}} \quad (102)$$

Where (x_1, x_2, x_3 .....x_n) are individual responses obtained from replica tests. Substituting equation 102 into equation 101 gives the expression for the confidence index as:

$$\boldsymbol{CI = \bar{x} \pm \frac{3}{n}\sqrt{\sum_{i=1}^{n}(x_i - \bar{x})^2}} \quad (103)$$

Considering the test data for the 13Cr-L80 SSR tests conducted in air and the tests conducted in deoxygenated seawater with 1000ppm sodium nitrite polarised at -250mV with respect to SCE, using equation 103, the UTS calculations with confidence index of 99% are given as 103.2±3.44Kpsi (711.5±23.72Mpa) and 102.6±0.22Kpsi (707.4±1.52Mpa) respectively. While the UTS calculations with confidence index of 99% from test data for the 25Cr-F255 SSR tests conducted in air and the tests conducted in deoxygenated seawater with 1000ppm sodium nitrite polarised at +250mV with respect to SCE, are given as 100.9±4.98Kpsi (711.5±34.33Mpa) and 106.12±2.36Kpsi (731.7±16.27Mpa) respectively.

This analysis shows a possible overlap in the UTS calculations for 25Cr-F255 SSR tests that were conducted in air and the polarised specimen between 103.81Kpsi (715.8MPa) and 106.37Kpsi (733.4MPa). This confirms the postulation that the observed increase in UTS could actually be as a result of inherent statistical variability of the measured data. Therefore, the observed increase in UTS was not considered significant.

As shown in Figure 99, the time to failure was significantly increased with increase in nitrite concentration and electrical polarisation except for the 25Cr sample in Environment 9, (deoxygenated seawater with 1000ppm sodium nitrite polarised at 0.5V with respect to SCE) that exhibits susceptibility to pitting and stress corrosion cracking in the presence of nitrite and failed way before others. For 25Cr that failed in Environment 9, the stress continued to increase gradually just like the other curves, but reached its UTS at a lower stress compared to others after which the stress level rapidly decreased prior to fracture. Rapid decrease in stress just after the UTS, prior to fracture was

observed in all the curves for 25Cr. This illustrates a major mechanical property difference between 13Cr and 25Cr. All the curves for 13Cr showed gradual decrease in stress after the UTS prior to fracture except for 13Cr in the susceptible environment (deoxygenated seawater with 1000ppm sodium nitrite polarised at -150mV with respect to SCE) where a rapid decrease in stress after the UTS was observed. However, the rapid decrease in stress observed was only about 12Kpsi compared to 25Cr where the rapid decrease in stress was in the range of 50Kpsi. It is worth noting that the rapid decrease in stress observed immediately after UTS in curves for 25Cr did not happen immediately after UTS in the case of 13Cr. There was gradual decrease in stress after UTS before the rapid decrease that led to fracture. Similar gradual decrease in stress after UTS before the rapid decrease that led to fracture was also observed in the 25Cr exposed to the susceptible environment (deoxygenated seawater with 1000ppm sodium nitrite polarised at 500mV with respect to SCE) compared to the other curves.

The point defect model attributes passive breakdown to condensation of vacancies on the passive breakdown site hence it is postulated that the presence of nitrite in a deoxygenated seawater solution with 25Cr polarised at 500mV wrt SCE facilitated the condensation of vacancies on the locations where passivity broke down and invariably pitted, the vacancies interacted with lattice dislocations and the vacancies were able to diffuse quickly enough to re-trap the mobile dislocations hence leading to higher stress for plastic deformation to continue i.e. strain hardening which eventually led to untimely brittle fracture of 25Cr.

5 CONCLUSIONS

Susceptibility of CRA to pitting and stress corrosion crack in the presence of nitrite was identified as a gap that would be a good addition to knowledge. Clear objectives and pragmatic methodology were proposed to ensure the objectives of this research work are achieved.

The following hypotheses were made:

a. Typical of anodic inhibitors, nitrite requires a critical concentration for effective inhibition.
b. Although nitrite acts as anodic inhibitor however, below the critical dosage or in excessive concentrations (above 8,000ppm):
    i. Nitrite increases the corrosion rate of corrosion resistant alloys.
    ii. Nitrite makes corrosion resistant alloys specifically (13Cr, 22Cr and 25Cr) susceptible to pitting and stress corrosion cracking. The susceptibility increases with temperature but decreases with increasing alloying of Cr, Mo, N and Ni.

Cyclic Potentiodynamic Polarisation technique (CPP) was used to evaluate the pitting corrosion resistance of 13Cr-L80, 22Cr and 25Cr-F225. The results showed that 13Cr-L80, 22Cr and 25Cr-F225 were susceptible to pitting corrosion in the presence of insufficient amounts of nitrite in deoxygenated seawater at 25^{o}C and 80^{o}C. Their susceptibility to pitting increased with increase in temperature. While 22Cr and 25Cr exhibited a protection margin of about 200mV (difference of the repassivation potential and corrosion potential), 13Cr did not, hence long-term potentiostatic polarisation tests were conducted to further evaluate pitting resistance of 13Cr. Test results further validated the susceptibility of 13Cr to pitting in the presence of nitrite. Although 22Cr and 25Cr exhibited the protection margin, pitting corrosion was still observed on some of the test specimens. It was inferred that pitting occurred because the specimens were polarised to their transpassivity region.

Graphs of the open circuit potential and the corresponding current density (in logarithmic scale) as a function of the nitrite concentration in deoxygenated seawater solution shows asymptotic curves for both 13Cr and 25Cr. Once the critical nitrite concentration was attained, the corrosion rate drastically reduced and further increase in sodium nitrite concentration did not reduce

the corrosion rate any further. Also there was corresponding increase in potential to more noble potentials validating the hypotheses that nitrite is an anodic inhibitor and requires a critical concentration for effective inhibition. It also demonstrates that nitrite, just like most anodic inhibitors increases the corrosion potential in the anodic direction (more-noble) and shifted the anodic polarisation curve to lower currents resulting in a net reduction in the corrosion rate.

The effect of increased sodium nitrite (as an anodic inhibitor) concentration from 0-6000ppm in seawater solution on the cathodic curves varied from metal to metal. In some cases, the effect of increased sodium nitrite concentration on the cathodic curve was not significant while in others it was quite significant. This indicates that the surface activity of the metal has some effect on the cathodic curves.

Graphs of critical pitting potential against the logarithm of the nitrite concentration for both 13Cr and 25Cr generated curves that were similar to those previously reported by Macdonald[43] and Dahan[180] for nitrate on Type 316 stainless steel and further validates the point defect model. The critical breakdown potential increases slightly with increasing nitrite concentration at low nitrite concentrations, until the critical nitrite concentration of 400ppm was reached. At higher concentrations, the pitting potential increased very quickly as shown in Figure 56 and Figure 70. These results indicate 400ppm as the critical nitrite concentration required for sodium nitrite to act as an anodic inhibit on 13Cr-L80 and 25Cr-F255. However, if pitting had occurred, the critical sodium nitrite concentration required for repassivation would be a lot higher. For 13Cr-L80 and 25Cr-F255, the critical sodium nitrite concentrations required for repassivation are 4700ppm and 5500ppm respectively.

These observations confirmed the hypothesis that nitrite is indeed an anodic inhibitor and requires a critical concentration for inhibition. Above the critical concentration, nitrite successfully acts as an anodic corrosion inhibitor for CRA at pH of 8.

25Cr-F255 suffered pitting and intergranular corrosion during 30 days C-ring exposure tests in deoxygenated seawater with 0ppm and 1000ppm sodium

nitrite solution. Intergranular corrosion propagated into intergranular stress corrosion cracking in the C-rings exposed to deoxygenated seawater with 1000ppm sodium nitrite solution but the C-rings exposed to deoxygenated seawater with 0ppm sodium nitrite solution did not. 13Cr-L80 C-rings exposed to both the deoxygenated seawater with 0ppm sodium nitrite and 1000ppm sodium nitrite did not suffer pitting, intergranular corrosion or stress corrosion cracking. This indicates that 25Cr is susceptible to pitting, intergranular corrosion and intergranular stress corrosion cracking in deoxygenated seawater with 1000ppm sodium nitrite.

Injection of up to 6000ppm of sodium nitrite to deoxygenated seawater made neither 13Cr-L80 nor 25Cr-F255 susceptible when the SSR tests were carried out at open circuit potential. Test results of CPP tests carried out in 4.2 confirmed that nitrite actually inhibits corrosion by shifting the open circuit potential to more positive level and shifting the anodic polarisation curve to lower currents with a net reduction in the corrosion rate. However, upon application of potentials close to the pitting potential of 13Cr-L80 and 25Cr-F225, the oxidising power of the test solution was greatly increased and nitrite induced localised pitting. It is postulated that the increase in oxidising power as a result of the increased potential and/or nitrite concentration led to nitrite reduction and dissolution of iron thereby causing localised corrosion.

SSR test samples of both 13Cr-L80 and 25Cr-F255 tested at open circuit potential did not pit or crack in deoxygenated seawater with sodium nitrite concentrations in the range of 0-6000ppm. Also, neither pits nor cracks were observed in 13Cr-L80 and 25Cr-F255 test samples exposed to blank deoxygenated seawater under potentiostatic potential of -150mV (SCE) for 13Cr-L80 and 500mV (SCE) for 25Cr-F255. However specimens tested under the same conditions, but with the addition of 1000ppm sodium nitrite pitted and cracked inferring that 13Cr-L80 and 25Cr-F255 are susceptible to pitting and stress corrosion cracking in the presence of 1000ppm sodium nitrite.

Based on the results of this research work it was concluded that injection of 1000ppm sodium nitrite makes 13Cr-L80 and 25Cr-F255 susceptible to pitting and stress corrosion cracking, provided the passive protective film is broken under aggressive conditions such as applied potential to pitting susceptibility

range or excessive tensile stress. The fact that 13Cr did not crack in the C-ring tests but cracked in the SSR tests further confirms the postulation that the passive layer must be destroyed and the bare metal exposed to nitrite before the material become susceptible.

In conclusion, the observed response of 13Cr and 25Cr confirmed the hypotheses for this research work.

6 RECOMMENDATIONS

The following recommendations were made for further research work;

1. Further investigate the effect of temperature on the critical nitrite concentration required for inhibiting corrosion.
2. Further investigate the correlation between the critical nitrite concentration prior to pitting and repassivation.
3. Further investigate the sensitive of nitrite to aggressive species e.g. Cl^- NO_3^-, SO_4^{2-}
4. Further expand the scope of the SSR test to include several nitrite concentrations below the critical nitrite concentration both at open circuit potentials and under potentiostatic potential. Also investigate the limiting applied potential required for 25Cr to fail in the SSR test.
5. Further expand the point defect model to incorporate the susceptibility effect of nitrite to Type 13Cr stainless steel and Type 25Cr duplex stainless steel.
6. Further investigate that sodium nitrite as an anodic inhibitor is metal specific by carrying out similar tests using different metals such as copper, and aluminium.
7. Further investigate the effect of sodium nitrite as an anodic inhibitor on the cathodic curves using inert working electrodes such as gold or platinum
8. Further investigate the anodic inhibition of sodium nitrite at a wider pH range, to verify the inhibiting effect observed at pH 8 is applicable to other pH.

7 REFERENCE

1. K. Berg Flatval, Sekhar Sathyamoorthy, Cor Kuijvenhoven and Dick Ligthelm, “Building the Case for Raw Seawater Injection Scheme in Barton”, SPE 88568, SPE Asia Pacific Oil and Gas Conference and Exhibition, 18-20 October, Perth, Australia, 2004.
2. W.C. Lee, “Corrosion of mild steel under an anaerobic biofilm”, Ph.D. Dissertation, Montana State University, Bozeman, Montana, 1990
3. Tony Rizk, and Jim Stott, “Effect of pH and Nutritional Variation on Nitrite Generation with Nitrate Treatment”, Reservoir Microbiology Forum 9, Energy Institute workshop on the Use of Nitrate to Control Bacterial Problems, Energy Institute, London, UK, 2003.
4. Tony Rizk, IP Research Report, “The Effect of Nitrate Anti-Souring Treatment on Corrosion of Mild Steel”, Microbiology Committee, The Energy Institute, London, UK, 2006.
5. Y. Chen, M. Gonuguntla and W.D. Grimes, “Sand Screen Materials Selection for Seawater Injection Wells”, GS.08.50993, Shell Global Solution, Texas USA, 2008.
6. S.S Shademan, L.L Wheaton and L.A Skogsberg, “Corrosion Assessment of Carbon Steel and modified 13Cr-110ksi during Nitrate Anti-souring Reservoir Treatment”, EP2006-3014 Shell International Exploration and Production, Inc., Houston, 2006
7. ASTM D1141, “Standard Practice for the Preparation of Substitute Ocean Water”, ASTM International, Pennsylvania, United States, 1998.
8. OSPAR, “OSPAR convention for the protection of the marine environment of the North East Atlantic. Luxembourg 3-7 May 1999”, OSPAR list of substances/ preparations used and discharged offshore which are considered to Pose Little or No Risk to the Environment (PLONOR), Reference number: 199-9, 1999.
9. T. Thorstenson, G. Bødtker, B-L. P. Lillebo, E. Sunde J. Beeder and T. Torsvik, “Biocide Replacement by Nitrate in Seawater Injection Systems”, NACE Corrosion 2002 Paper 02033, NACE International, Houston, Texas USA, 2002.
10. S. Myhr, B-L.P., Lillebo, J. Beeder, E. Sunde and T. Torsvik, “Inhibition of microbial H_2S production in an oil reservoir model Column by nitrate injection”, Applied Microbiology Biotechnology, Volume 58, pp. 400-408, 2002.
11. M.A. Reinsel, J.T. Sears, P.S. Stewart and M.J. McInerney, “Control of microbial souring by nitrate, nitrite or glutaraldehyde injection in a sandstone column”. Journal of Industrial Microbiology and Biotechnology, Volume 17, No. 2, pp. 128-136, Springer Berlin, 1996.
12. J. Larsen, M.H. Rod and S. Zwolle, “Prevention of Reservoir Souring in Halfdan Field by Nitrate Injection”, NACE Corrosion 2004 Paper 04761, NACE International, Houston, Texas USA, 2004.

13. B.C. Dunsmore, T.B. Whitfield, P. A. Lawson and M.D. Collins, “Corrosion by Sulphate-Reducing Bacteria that utilise Nitrate”, NACE Corrosion 2004, Paper 04763, NACE International, Houston, Texas USA, 2004.

14. Z. Dzierzewicz, B. Cwalina, E. Chodurek and L. Bulas, “Differences in hydrogenase and APS-Reductase activity between Desulfovibrio desulfuricans strains growing on sulphate or nitrate”, Acta biologica cracoviensa series botanica, Volume 39, pp. 9-15, 1997.

15. H.J. Seitz and H. Cypionka, “Chemolithotrophic growth of Desulfovibrio desulfuricans with hydrogen coupled to ammonification of nitrate or nitrite”, Archives of microbiology, 1465, pp. 63-67, 1986.

16. R.G.L. McCready, W.D. Gould and F.D. Cook, “Respiratory Nitrate Reduction by Desulfovibrio sp.”, Archives of Microbiology, Volume 135, pp. 182-185, 1983.

17. T. Dalsgaard and F. Bak, “Nitrate reduction in sulphate-reducing bacterium, Desulfovibrio desulfuricans, isolated from a rice paddy soil”, sulphide inhibition, kinetics and regulation. Applied and Environmental Microbiology, pp. 291, 1994.

18. R.F. Mueller, "Microbial Dynamics in Souring Oil Reservoirs", Ph.D. Dissertation, Montana State University, Bozeman, Montana, pp. 155-159, 1994.

19. M.A. Reinsel, "Control of Microbial Souring of Oil in a Porous Media Column", Ph.D. Dissertation, Montana State University, Bozeman, Montana, pp. 108-134, 1995.

20. R.L. Mancinelli and C.P. McKay, “Effects of nitric oxide and nitrogen dioxide on bacterial growth. Applied and Environmental Microbiology, Volume 46, pp. 198-202, 1983.

21. S.R. Thom and R. E. Marquis, “Microbial growth modification by compressed gases and hydrostatic pressure”, Applied and Environmental Microbiology, Volume 47, pp. 780-787, 1984.

22. A. Teske, P. Sigalevich, Y. Cohen and G. Muyzer, “Molecular identification of bacteria from co-culture by denaturing gradient gel electrophoresis of 16S ribosomal DNA fragments as a tool for isolation in pure cultures”, Applied and Environmental Microbiology Volume 62, pp. 4210-4215, 1996

23. A. Greene, C.R. Hubert, S. Haveman, M. Nemati, G.E. Jenneman and G. Voordouw, “Is Oilfield Souring More Efficiently Reduced by Nitrate or Nitrite?” Proceedings of the Reservoir Microbiology Forum 9/, Energy Institute, London, 2003.

24. A.J. Telang, S. Ebert, J.M. Foght, D.W.S. Westlake, G.E. Jenneman, D. Gevertz and G. Voordouw, "Effect of Nitrate Injection on the Microbial Community in an Oil Field as Monitored by Reverse sample Genome Probing", Applied and Environmental Microbiology 63 pp. 1785-1793, 1997.

25. J. Larsen, “Down hole Nitrate Applications to Control Sulphate Reducing Bacteria Activity and Reservoir Souring”, NACE Corrosion 2002 Paper 02025, NACE International, Houston, Texas USA, 2002.

26. G. Voordouw, M. Nemati and G.E. Jenneman, "Use of Nitrate-Reducing, Sulphide-Oxidizing Bacteria to reduce Souring in Oil Fields: Interactions with SRB and Effects on Corrosion", NACE Corrosion 2002, Paper 02034, NACE International, Houston, Texas USA, 2002.

27. J. Larsen, P. F. Sanders and R.E. Talbot, "Experience with the Use of Tetrakishydroxymethylphosphonium Sulphate (THPS) for the Control of Downhole Hydrogen Sulphide", NACE Corrosion 2000, Paper 00123, NACE International, Houston, Texas USA, 2000.

28. T. Haack, R. Diaz and R. E. Talbot, "TetrakisHydroxymethyl-Phosphonium Sulphate (THPS): A New Oilfield Bactericide Providing Iron Sulphide Dissolution and Environmental Benefits", Exitep 98, Mexico City, 15-16 November 1998.

29. D. Gevertz, A.J. Telang, G. Voordouw and G.E. Jenneman, "Isolation and Characterization of Strains CVO and FWKO B, Two Novel Nitrate-Reducing, Sulphide-Oxidizing Bacteria isolated from Oil Field Brine", Applied and Environmental Microbiology, Volume 66, pp. 2491-2501, 2000.

30. E.A. Greene, C. Hubert, M. Nemati, G.E. Jenneman and G. Voordouw, "Nitrite reductase activity of sulphate-reducing bacteria prevents their inhibition by nitrate-reducing, sulphide-oxidizing bacteria", Environmental Microbiology, Volume 5, pp. 607- 617, 2003.

31. S. Dannenberg, S.M. Kroder, W. Dilling and H. Cypionka, "Oxidation of H_2, organic compounds and inorganic sulphur compounds coupled to reduction of O_2 or nitrate by sulphate-reducing bacteria", Archives of Microbiology, Volume 158 pp. 93-99, 1992.

32. G.E. Jenneman, D. Gevertz, “Identification, characterisation and application of sulphide oxidising bacteria in oilfields”, Proceedings of the 8th International Symposium on Microbial Ecology, C.R. Bell, M Brylinski, P. Johnson-Green, Atlantic Canada Society of Microbial Ecology, Halifax, Canada, 1999.

33. Energy Institute, “The simulation of Nitrate Reducing Bacteria in oilfield to control Sulphate Reducing Bacteria, Microbiologically Influenced Corrosion and reservoir souring”, An introduction review, ISBN 085293 394 0, The Energy Institute, London, UK, 2003.

34. E. Sunde, B-L. P. Lillebo and T. Thorstenson, “H_2S Inhibition by Nitrate Injection on the Gullfaks Field”, NACE Corrosion 2004, Paper 04760, NACE International, Houston, Texas USA, 2004.

35. M.J. Mclnerney, K.L. Sublette, V.K. Bhupathiraju, J.D. Coates and R.M Knapp, “Causes and Control of Microbially Induced Souring”, Developments in Petroleum Science 39, Microbial Enhancement of Oil Recovery – Recent Advances, proceedings of the 1992 International Conference on Microbial Enhanced Oil recovery, Editors, E. Premuzic and A. Woodhead, Elsevier, Amsterdam, pp. 363-371, 1993.

36. M. Wright, G.E. Jenneman and D. Gevertz, “Effect of Nitrate on Sulphide Bioscavenging by Indigenous Bacteria in produced Brines from West Texas Oil Fields”, 4th International Petroleum Environmental Conference, San Antonio, Texas, September 9-12, 1997.

37. R.A. Hutson, D.E. Thompson and M. D. Collins, “Genetic interrelationships of saccharolytic Clostridium botulinum types B, E and F and related Clostridia by small-subunit rRNA gene sequences”, FEMS Microbiology Letter 108, pp. 103-110, 1993.

38. Madigan, Martinko and Parker, “Brock Biology of Microorganisms”, Prentice Hall, London, pp. 637-743, 2000.

39. F. Widdel, “Microbial ecology of sulphate and sulphur-reducing bacteria”, edited by A.J.B. Zehnder, Biology of anaerobic microorganisms, John Wiley and Sons Inc., New York USA, pp. 469-585, 1988.

40. Tony Rizk, Jim Stott and Judith Robertson, Concept Document, “An Independent Evaluation of Nitrate Anti-Souring Reservoir Treatment and Its Effect on Corrosion Processes”, CAPCIS Ltd 2003.

41. T. Andersen, Internal Report # 96Q, E10.Doc, June 1996.

42. J.F.D Stott, G. Dicken, T. Rizk, G. Gamble, S. Saul, T. Granli and T. Haegh, “Corrosion Inhibition in PWRI Systems that use Nitrate treatment to control SRB activity and reservoir souring”, NACE Corrosion 2008, Paper 08507, NACE International, Houston, Texas USA, 2008.

43. D.D. Macdonald and S Yang, “Oxyanion Inhibition of Passivity Breakdown and the Nucleation of Pits on Type 316L Stainless Steel”, NACE Corrosion 2007, Paper No. 07589, NACE International, Houston, Texas USA, 2007.

44. A.D. Mercer, I.R. Jenkins and J.E. Rhoades-Brown, “Comparative Study of Factors Influencing the Action of Corrosion Inhibitors for Mild Steel in Neutral Solution –III Sodium Nitrite”, British Corrosion Journal, Volume 3, pp. 136-143, 1968.

45. J.G.N. Thomas, “The Mechanism of Corrosion Prevention by Inhibitors”, in Corrosion: Corrosion control; third edition, Edited by L.L. Shreir, R.A. Jarman and G.T. Burstein, Volume 2, Chapter 17, Butterworth-Heineman, Oxford, UK, 1994.

46. D.M. Brasher, D. Reichenberg and A.D. Mercer, “Comparative Study of Factors Influencing the Action of Corrosion Inhibitors for Mild Steel in Neutral Solution –IV Mechanism of Action of Mixed Inhibitive and Aggressive Anions”, British Corrosion Journal, Volume 3, pp. 144-150, 1968.

47. J.G.N. Thomas and T.J. Nurse, “The Anodic Passivation of Iron in Solutions of Inhibitive Anions”, British Corrosion Journal, Volume 2, pp. 13-20, 1967.

48. D.M. Brasher, “Stability of Oxide Film on Metals in Relation to Inhibition of Corrosion – I Dual Role of the Anion in the Inhibition of the Corrosion of Mild Steel”, British Corrosion Journal, Volume 4, pp. 122-128, 1969.

49. D.M. Brasher, C.P. De and A.D. Mercer, “Film Growth on Mild Steel in Inhibitive Solutions”, British Corrosion Journal, Volume 1, pp. 188-191, 1966.

50. A.D. Mercer, “Some Views on the Corrosion Mechanisms of Inhibitors in Neutral Solutions”, Materials Performance, Volume 29, pp. 45-49, NACE International, Houston, Texas USA, 1990.

51. L. Espada, X.R. Novoa and G. Pena, “Influence of pollutants (Nitrate Anions) on the Corrosivity of Sea Water”, Environmental Technology letters, Volume 10, pp. 237-240, 1989.

52. L. Espada, X.R. Novoa and P. Merino, “Determination of pollution Levels of Sea Waters by Means of their Corrosivity”, Proceedings of Corrosion and Environment 2, University of Barcelona, Spain, 1986.

53. L. Espada, X.R. Novoa, A.M. Bouza and P. Merino, “Corrosivity of Marine Waters Close to Centres of Population: Conditioning Factors”, Rev. Iberoamerican Corrosion protection, Volume 18, pp. 127-130, 1987.

54. Handbook of Chemistry and Physics Rubber, 60th edition, Edited by R.C. Weast and M.J. Astle, CRC press, ISBN 0 8493 0460 8, 1979.

55. E.A. Vik and Co., “Nitrate-Based Souring Mitigation of Produced water – Side effects and challenges from the Draugen Produced water Re-injection Pilot”, SPE 106178, 2007.

56. C. Hubert, M. Nemati, G. Jenneman and G. Voordouw, “Corrosion risk associated with microbial souring control using nitrate or nitrite”, Applied Microbial Biotechnology, Volume 68, pp. 272, 2005.

57. Tony Rizk, “Nitrate Corrosion in PWRI Applications. An Independent Laboratory Study Sponsored by the Energy Institute. Presented on the 11th Energy Institute Reservoir Microbiology Forum (EI/RMF11) workshop on the Use of Nitrate to Control Bacterial Problems, London, UK, November 17-18 2005.

58. C.L. Rempel, R.W. Evitts and M. Nemati, “Dynamics of Corrosion rates associated with Nitrite or Nitrate mediated control of souring under biological conditions simulating an oil reservoir”, Journal of Industrial Microbiology and Biotechnology, Volume 33, No. 10, pp. 878, 2006.

59. C. Kuijvenhoven, “Produced Water Re-injection in the Rotterdam Field”, Reservoir Microbiology Forum 10, Energy Institute workshop on PWRI and Oilfield Microbiology, Energy Institute, London, pp. 29-30, November 2004.

60. P. Ernst and J. Stott, “Laboratory Evaluation of the Effects of Nitrate Injection on the Corrosion for SEIC-Sakhalin”, CAPCIS Ref BA5654 Rev. 1, CAPCIS Ltd, 2009.

61. J. Beeder, “Microbial Activity in a Mixture of Aquifer and Produced Water”, Reservoir Microbiology Forum 10/ Energy Institute Joint Meeting, PWRI and Oilfield Microbiology, Energy Institute, London, pp. 29-30 November 2004.

62. C.M.A. Brett and P.L.C. Melo, “Influence of anions on the corrosion of high speed steel”, Applied Electrochemistry Journal, Volume 27, pp. 959-964, 1997.

63. P.J. Sturman, D.M. Goeres and M.A. Winters, “Control of Hydrogen Sulphide in Oil and Gas Cells with Nitrite Injection”, SPE 56772, Proceedings of Annual SPE Technical Conference, Houston, Texas, Part 2, pp. 357-363, 1999.

64. J. Mc Inerney, A.D. Montgomery and K.L. Sublette, “Microbial Control of the Production of Sulphide”, Proceedings of 3rd US DOE Conference on Microbial Enhancement of Oil Recovery (Norman, Oklahoma, 1990), Elsevier Development in Petroleum Science Series 31, pp. 441-449, 1991.

65. F.Gui, C.S. Brossia, J.A. Beavers and C. Mendez, “The Anodic Polarisation of Carbon Steel in Hanford Nuclear Wastes”, NACE Corrosion 2007, Paper 07593, NACE International, Houston, Texas USA, 2007.

66. K. Suramanian and J. Mickalonis, Anodic Polarisation Behaviour of Low-Carbon Steel in Concentrated Sodium Hydroxide and Sodium Nitrate Solutions”, Electrochemica Acta, Volume 50, pp. 2685, Elsevier Ltd, 2005.

67. A.M. Rosenberg and J. Gaidis, “The Mechanism of Nitrite Inhibition of Chloride Attack on Reinforcing Steel Alkaline Aqueous Environments”, Corrosion Volume 11, pp. 45, 1979.

68. P. Doig and P.E.J. Flewitt, “Electrochemical Dissolution Behaviour of Iron in Dilute Sodium Hydroxide Solution”, Corrosion Science, Volume 17, pp. 369, 1977.

69. R.C. Newman, M.A.A. Ajjawi, H. Ezuber, et. al., “An Experimental Confirmation of the Pitting Potential Model of Galvele”, Corrosion Science, 28, NACE International, Houston, Texas USA, pp. 471, 1988.

70. R.M. Carranza, C.M. Giordano, E. Saenz, and et. al., “Corrosion of Steel Tanks in Liquid Nuclear Wastes”, NACE Corrosion 2006, Paper 06635, NACE International, Houston, Texas USA, 2006.

71. P.E. Zapp and D.T. Hobbs, “Inhibiting Pitting Corrosion in Carbon Steel Exposed to Dilute Radioactive Waste Slurries”, NACE Corrosion 1992, Paper 98, NACE International, Houston, Texas USA, 1992.

72. Encyclopaedia of Electrochemistry of the Elements, Volume 8, “Nitrogen”, pp. 321-479, Marcel-Dekker, 1978.

73. F. Gui et al, “A Study of Localised Corrosion of Carbon Steel in Hanford Nuclear Waste”, NACE Corrosion 2008, Paper no. 08589, NACE International, Houston, Texas USA, 2008.

74. S. Yang and D.D. Macdonald, “Theoretical and experimental studies of the pitting of type 316L stainless steel in borate buffer solution containing nitrate ion”, Electrochimica Acta, Volume 52, No. 5, pp. 1871-1879, Elsevier Ltd, 2007.

75. S.A.M. Refaey, “Inhibition of Chloride Pitting Corrosion of Mild Steel by Sodium Gluconate”, Applied Surface Science, Volume 157, pp. 199, 2000.

76. G. Sussek and M. Kesten, “Effect of Cl- Concentration on the Characteristic Pitting Potential”, Corrosion Science, Volume 15, pp. 225, NACE International, Houston, Texas USA, 1975.

77. F. Wormwell and H.C.K. Ison, Chem. And Ind. London, pp. 293, 1951.

78. M.J. Pryor and Cohen, “The inhibition of the corrosion of iron by some anodic inhibitors”, Journal of the Electrochemical Society, Volume 100, pp. 203-15, ECS Pennington, New Jersey USA,1953

79. U. R. Evans, the corrosion and oxidation of metals: scientific principles and practical applications, St Martin’s Press Inc., New York USA, 1960.

80. J.E.O. Mayne and J.W. Menter, “The mechanism of inhibition of the corrosion of iron by sodium hydroxide solution. Part II”, Journal of the Chemical Society, pp. 103, 1954.

81. M.J. Pryor. and Cohen, “The mechanism of the inhibition of the corrosion of iron by solutions of sodium orthophosphate”, Journal of the Electrochemical Society, Volume 98, pp. 263-72, ECS Pennington, New Jersey USA,1951.

82. R.B. Mears and U.R. Evans, “The Velocity of Corrosion from the Electrochemical Standpoint. Part III”, Proceedings of the Royal Society A: Mathematical, Physical and Engineering Sciences, Volume 146, pp. 153-165, August 1, 1934.

83. W.D. Robertson, "Molybdate and Tungstate as Corrosion Inhibitors and the Mechanism of Inhibition", Journal of Electrochemical Society Volume 98, No. 3, pp. 94-100, ECS Pennington, New Jersey USA,1951.

84. P.W. Sherwood, “Prevention of Corrosion by Water in Oil Refineries”, Anti-Corrosion Methods and Materials Volume 1, Issue: 4, pp. 113 – 120, 1954.

85. U.R. Evans, metallic Corrosion passivity and protection, 2nd Edition, pp. 543, Edward Arnold and Co, London, 1946.

86. N.D. Tomashov, “The theory of corrosion and protection of metals, the science of corrosion”, pp. 168, The Macmillan Company, New York USA, 1966.

87. C.S. Brossia et al, “Inhibition of Stress Corrosion Cracking of Carbon Steel Storage Tanks at Hanford”, NACE Corrosion 2007, Paper no. 07606, NACE International, Houston, Texas USA, 2007

88. C.S. Brossia et al, “Stress Corrosion Cracking of Carbon Steel in Nitrate and Carbonate Wastes at hanford”, NACE Corrosion 2008, Paper no. 08599, NACE International, Houston, TX, 2008.

89. C.S. Brossia et al, Hanford Tanks AY102 and AP101: “Effect of Chemistry and Other Variables on Corrosion and Stress Corrosion Cracking”, Report RPP-RPT-33284, Rev. 0, CH2M, Hill Hanford Group, Richland, WA, USA, 2007.

90. R.S. Ondrejcin, “Stress Corrosion Cracking – The Slow Strain Rate Technique”, ASTM STP 665, pp. 203, ASTM International, West Conshohocken, Pennsylvania USA, 1979.

91. J.J. Krupowicz et al, “Slow Strain Rate Testing of C-Mn Steels in 4 N Sodium Nitrate”, Scripta Metallurgica et Materialia, Volume 25, pp. 1501, 1991.

92. R.N. Parkins, “Stress Corrosion Cracking and Hydrogen Embrittlement of Iron Base Alloys”, NACE Corrosion 5, Paper No. 601, NACE International, Houston, Texas USA, 1977.

93. M.L. Holzworth, R.M. Girdler, L.P. Costas, and W.C. Rion, “How to prevent Stress-Corrosion Cracking of Radioactive Waste Storage Tanks,” Materials Protection, Volume 7, pp. 36-38, NACE International, Houston, Texas USA, 1968.

94. H.H. Le and E. Ghali, “The Electrochemical Behaviour of Pressure Vessel Steel in Hot Bayer Solutions as Related to the SCC Phenomenon”, Corrosion Science, Volume 30, NACE International, Houston, Texas USA, pp. 117, NACE International, Houston, Texas USA, 1990.

95. H.H. Le and E. Ghali, “Stress Corrosion Cracking of Carbon Steel in Caustic Aluminate Solutions of the Bayer Process”, Corrosion Science, Volume 35, pp. 435, NACE International, Houston, Texas USA, 1993.

96. D.D. Macdonald, “Passivity-the key to our metals-based civilization”, Pure and Applied Physical Sciences, Volume 71, No. 6, pp. 951-978, IUPAC, Great Britain, 1999.

97. H.H. Uhlig, “Passivity of Metals” (R. P. Frankenthal, J. Kruger, eds), pp. 1, The Electrochemical Society, Princeton, New Jersey USA, 1978.

98. M. Pourbaix, “Atlas of Electrochemical Equlibria”, NACE-International, Houston, Texas USA 1973.

99. N. Sato, “Passivity of Metals” (R. P. Frankenthal, J. Kruger, eds), pp. 29, The Electrochemical Society, Princeton, New Jersey USA, 1978.

100. M.G. Fontana, Corrosion Engineering Third Edition, McGraw-Hill International Editions, Materials Science and Engineering Series, Singapore 1987.

101. D.D. Macdonald, “The Point Defect Model for the Passive State”, Journal of the Electrochemical Society, Volume 139, Issue 8, pp. 3434-3449, 1992.

102. S. Glasstone, “An Introduction to Electrochemistry”, Van Nostrand, New York, New York USA, pp. 491, 1942.

103. D.E. Williams, J. Stewart, P.H. Balkwill, “The nucleation, growth and stability of micropits in stainless-steel”, Corrosion Science, Volume 36, pp. 1213-1235, NACE International, Houston, Texas USA, 1994.

104. P.C. Pistorius, G.T. Burstein, “Metastable Pitting Corrosion of Stainless Steel and the Transition to Stability”, Philosophical Transactions of the Royal Society, A 341, pp. 531-559, 1992.

105. G.S. Frankel, L. Stockert, F. Hunkeler, H. Bohni, “Metastable Pitting of Stainless Steel”, Corrosion 43, pp. 429-436, NACE International, Houston, Texas USA, 1987.

106. N. Cabrera, N.F. Mott, “Theory of the oxidation of metals”, Report Progress in Physics. Volume 12, pp. No. 1, 163, 1948.

107. F.P. Fehlner, and N.F. Mott, “Low-temperature oxidation”, Oxidation of Metals, Volume 2, No. 1, pp. 59-99, 1970.

108. N. Sato, and M. Cohen, “The Kinetics of Anodic Oxidation of Iron in Neutral Solution – I. Steady Growth Region” Journal of Electrochemical Society, Volume 111, No. 5, pp. 512-519, ECS Pennington, New Jersey USA, 1964.

109. N. Sato, and T. Notoya, “Measurement of the Anodic Oxide Film Growth on Iron for Hours” Journal of Electrochemical Society, Volume 114, No. 6, pp. 585-586, ECS Pennington, New Jersey USA, 1967.

110. A.T. Fromhold, “Nonsimultaneous Place Exchange: A Microscopic High Field Transport Mechanism in Solids” Journal of Electrochemical Society, Volume 127, No. 2, pp. 411-425, ECS Pennington, New Jersey USA, 1980.

111. K.-S. Lei, D.D. Macdonald, B.G. Pound, B.E. Wilde, “Breakdown of the Passive Film on Polycrystal and Single Crystal (100) Nickel by Chloride”, Journal of Electrochemical Society, Volume 135, No. 7, pp. 1625-1632, ECS Pennington, New Jersey USA, 1988.

112. I. Milosev, M. Metokos-Hukovic, M. Drogowska, H. Menard, L. Brossard, “Breakdown of Passive Film on Copper in Bicarbonate Solutions Containing Sulfate Ions”, Journal of Electrochemical Society, Volume 139, No. 9, pp. 2409-2418, ECS Pennington, New Jersey USA, 1992.

113. L.F. Lin, C.Y. Chao, and D.D. Macdonald, “A Point Defect Model for Anodic Passive Film – Chemical Breakdown and Pitting Initiation”, Journal of Electrochemical Society, Volume 128, No. 6, pp.1194-1198, ECS Pennington, New Jersey USA, 1981.

114. D. Ellerbrock, D.D. Macdonald, “Concerning passivity breakdown on solid and liquid gallium and titanium in halide solutions”, Materials Science Forum Volume 185-188, pp. 927-936, 1995.

115. T. Okada, “Halide Nuclei Theory of Pit Initiation in Passive Metals”, Journal of Electrochemical Society, Volume 131, No. 2, pp. 241-247, ECS Pennington, New Jersey USA, 1984.

116. K. Sugimoto, S. Matsuda, Y. Ogiwara, K. Kitamura, “Microscopic Ellipsometric Observation of the Change in Passive Film on 18Cr-8Ni Stainless Steel with the Initiation and Growth of Pit”, Journal of Electrochemical Society, Volume 132, No. 8, pp. 1791-1795, ECS Pennington, New Jersey USA, 1985.

117. N.J. Laycock, S.P. White, J.S. Noh, P.T. Wilson, R.C. Newman, “Perforated Covers for Propagating Pits”, Journal of Electrochemical Society, Volume 45, No. 4, pp. 1101-1108, ECS Pennington, New Jersey USA, 1998.

118. C.B. Bargeron and R.B. Givens, “Source of Oscillations in the Anode Current during the Potentiostatic Pitting of Aluminum”, Journal of the Electrochemical Society, Volume 124, Issue 8, pp. 1230-1232, ECS Pennington, New Jersey USA, 1977.

119. C.B. Bargeron and R.B. Givens, “Precursive blistering in the localised corrosion of aluminum”, Corrosion 36, pp. 618-625, NACE International, Houston, Texas USA, 1980.

120. T. Shibata, T. Takeyama, “Stochastic theory of pitting corrosion”, Corrosion Volume 33, No. 7, NACE-International, Houston, Texas US, pp. 243-251, 1977.

121. U.R. Evans, Corrosion, “while oxygen reduction takes place on the adjacent surfaces”, Volume 7, pp. 238, NACE-International, Houston, Texas USA, 1951.

122. N. Casillas, S. Charlebois, W.H. Smyrl, H.S. White, “Scanning Electrochemical Microscopy of Precursor Sites for Pitting Corrosion on Titanium”, Journal of Electrochemical Society, Volume 140, No. 9, pp. L142-L145, ECS Pennington, New Jersey USA, 1993.

123. N. Casillas, S. Charlebois, W.H. Smyrl, H.S. White, “Pitting Corrosion on Titanium”, Journal of Electrochemical Society, Volume 141, No. 3, pp. 636-642, ECS Pennington, New Jersey USA, 1994.

124. D.D. Mcdonald, S.R. Biaggio, H. Song, “Steady-State Passive Films”, Journal of Electrochemical Society, Volume 139, No. 1, pp. 170-177, ECS Pennington, New Jersey USA, 1992.

125. K.-S. Lei, D. D. Macdonald, B. G. Pound, B. E. Wilde, “Breakdown of the Passive Film on Polycrystal and Single Crystal (100) Nickel by Chloride”, Journal of Electrochemical Society, Volume 135, No. 7, pp. 1625-1632, ECS Pennington, New Jersey USA, 1988.

126. T. Haruna and D.D. Macdonald, “Theoretical Prediction of the Scan Rate Dependencies of the Pitting Potential and the Probability Distribution in the Induction Time”, Journal of the Electrochemical Society, Volume 144, Issue 5, pp. 1574-1581, ECS Pennington, New Jersey USA, 1997.

127. D.E. Williams, C. Westcott, M. Fleischmann, “Stochastic Models of Pitting Corrosion of Stainless Steels”, Journal of Electrochemical Society, Volume 132, No. 8, pp. 1796-1804, ECS Pennington, New Jersey USA, 1985.

128. B. Wu, J. R. Scully, J.L. Hudson, A.S. Mikailov”, Cooperative Stochastic Behavior in Localised Corrosion”, Journal of Electrochemical Society, Volume 144 No. 5, pp. 1614-1620, ECS Pennington, New Jersey USA, 1997.

129. T.T. Lunt, S.T. Pride, J.R. Scully, J.L. Hudson and A.S. Mikailov”, Cooperative Stochastic Behavior in Localised Corrosion”, Journal of Electrochemical Society, Volume 144, No. 5, pp. 1620-1629, ECS Pennington, New Jersey USA, 1997.

130. D.D. Macdonald and M. Urquidi-Macdonald, “Distribution functions for the breakdown of passive films”, Electrochimica Acta, Volume 31, Issue 8, pp. 1079-1086, Elsevier Ltd, 1986.

131. M. Urquidi-Macdonald, D.D. Macdonald, “Theoretical Distribution Functions for the Breakdown of Passive Films”, Journal of Electrochemical Society, Volume 134, No. 1, pp. 41-46, ECS Pennington, New Jersey USA, 1987.

132. D.D. Macdonald, M. Urquidi, “Solute-Vacancy Interaction Model and the Effect of Minor Alloying Elements on the Initiation of Pitting Corrosion”, Journal of Electrochemical Society, Volume 132, No. 3, pp. 555-558, ECS Pennington, New Jersey USA, ECS Pennington, New Jersey USA, 1985.

133. S. Lenhart, M. Urquidi-Macdonald, D.D. Macdonald, “Photo-inhibition of passivity breakdown on nickel”, Electrochimica Acta, Volume 32, No. 12, pp. 1739-1741, Elsevier Ltd, 1987.

134. P. Schmuki, H. Bohni, “Illumination Effects on the Stability of Passive Films", Electrochimica Acta, Volume 40, No. 6, pp. 775-783, Elsevier Ltd, 1995.

135. D. Heaney, D. D. Macdonald, “On the Photoinhibition of Passivity Breakdown on Iron in Chloride-Containing Solutions”, Journal of Electrochemical Society, Volume 146, No. 5, pp. 1773-1776, ECS Pennington, New Jersey USA, 1999.

136. D. D. Macdonald, E. Sikora, M. W. Balmas, R. C. Alkire, “The photo-inhibition of localised corrosion on stainless steel in neutral chloride solution”, Corrosion Science, Volume 38, No. 1, pp. 97-103, NACE-International, Houston, Texas USA, 1996.

137. C.B. Breslin, D.D. Macdonald, E. Sikora, J. Sikora, “Influence of UV light on the passive behaviour of SS316 - effect of prior illumination”, Electrochimica Acta, Volume 42, No. 1, pp. 127-136, Elsevier Ltd, 1997.

138. C.B. Breslin, D.D. Macdonald, E. Sikora, J. Sikora, “Photo-inhibition of pitting corrosion on types 304 and 316 stainless steels in chloride-

containing solutions", Electrochimica Acta, Volume 42, No. 1,pp. 137-144, Elsevier Ltd, 1997.

139. D.D. Macdonald, H. Brookes, M. Urquidi-Macdonald, and M. Vazquez, "Photoinhibition of Pitting on Nickel and Alloy CDA 715 in Buffered Chloride-Containing Solutions", Corrosion 55, No. 4, pp. 343-355, NACE-International, Houston, Texas USA, 1999.

140. S. Fugimoto, T. Yamada, T. Shibata, "Improvement of Pitting Corrosion Resistance of Type 304 Stainless Steel by Modification of Passive Film with Ultraviolet Light Irradiation" Journal of Electrochemical Society, Volume 145, No. 5, pp. L79-L81, ECS Pennington, New Jersey USA, 1998.

141. T.P. Hoar, D.C. Mears and G.P. Rothwell, "The relationships between anodic passivity, brightening and pitting"' Corrosion Science, Volume 5, Issue 4, pp. 279-289, NACE-International, Houston, Texas USA, 1965.

142. J. Stewart and D.E. Williams, "The initiation of pitting corrosion on austenitic stainless steel: on the role and importance of sulphide inclusions Corrosion Science, Volume 33, Issue 3, , pp. 457-463, 465-474, NACE-International, Houston, Texas USA, 1992.

143. R. Ke, and Alkire "Surface Analysis of Corrosion Pits Initiated at MnS Inclusions in 304 Stainless Steel", Journal of Electrochemical Society, Volume 139, No. 6, pp.1573-1580, ECS Pennington, New Jersey USA, 1992.

144. J.R. Galvele, Corrosion - Aqueous Processes and Passive Films, Vol. 23 of Treatise on Materials Science and Technology (J.R. Scully, ed.), pp. 1, Academic Press, New York, 1983.

145. J.R. Galvele, "Transport Processes and the Mechanism of Pitting of Metals", Journal of Electrochemical Society, Volume 123, No. 4, pp. 464-474, ECS Pennington, New Jersey USA, 1976.

146. J.R. Galvele;"Transport Processes in Passivation Breakdown-II. Full Hydrolysis of the Metal Ions", Corrosion Science, Volume 21 Issue 8, pp.551-579, NACE-International, Houston, Texas USA, 1981.

147. P.C. Pistorius, G.T. Burnstein, "Growth of corrosion pits on stainless steel in chloride solution containing dilute sulphate," Corrosion Science, Volume 33, No.12, pp. 1885-1892, NACE-International, Houston, Texas USA, 1992.

148. G.S. Frankel, "Pitting Corrosion of Metals", Journal of Electrochemical Society, Volume 145, No. 6, pp. 2186-2198, ECS Pennington, New Jersey USA, 1998.

149. H. Ezuber, R.C. Newman, "Critical Factors in Localised Corrosion," (G. S. Frankel, R.C. Newman, eds), PV92-9, pp. 12, Electrochemical Society, Princeton, New Jersey, 1992.

150. D.D. Macdonald, C. English, S.J. Lenhart. Report to DOE/BES, SRI International, Menlo Park, Califonia USA, 1985.

151. C. Liu, D.D. Macdonald, “Modeling the failures of low pressure steam turbine disks,” In Proc. 5th International Conference on Nuclear Energy, ICONES, 25-29 May, Nice, France/ASME, New York, 1997.

152. H.H. Strehblow and B. Titze, “Pitting potentials and inhibition potentials of iron and nickel for different aggressive and inhibiting anions”, Corrosion Science Volume 17, No 6, pp. 461-472, NACE International, Houston, Texas USA, 1977.

153. E. McCafferty, “A Competitive Adsorption Model for the Inhibition of Crevice Corrosion and Pitting”, Journal of the Electrochemical Society, Volume 137, Issue 12, pp. 3731-3737, ECS Pennington, New Jersey USA, 1990.

154. C. Lemaitre, B. Baroux, and G. Beranger, Key Engineering Materials, 20-28, pp. 2841, 1987.

155. V.S. Muralidharan, “Role of Anions in the Dissolution, Passivation and Pitting of Metals. A Review” Corrosion, Volume 21, No. 4, pp. 327, NACE International, Houston, Texas USA, 2003.

156. S.B. Basame and H.S. White, “Pitting Corrosion of Titanium The Relationship Between Pitting Potential and Competitive Anion Adsorption at the Oxide Film/Electrolyte Interface”, Journal of the Electrochemical Society, Volume 147, Issue 4, pp. 1376-1381, ECS Pennington, New Jersey USA, 2000.

157. N.G. Thompson and J.H. Payer, “DC Electrochemical Test Methods”, Corrosion Testing Made Easy Volume 6, NACE International, Houston, Texas USA, 1998.

158. M. Stern and A. L. Geary, “Electrochemical Polarization - I. A Theoretical Analysis of the Shape of Polarization Curves”, Journal of the Electrochemical Society, volume 104, Issue 1, pp. 56-63, ECS Pennington, New Jersey USA, 1957.

159. K.B. Oldham, and F. Mansfeld, “On the so-called Linear Polarization Method for Measurements of Corrosion Rates”, Corrosion, volume 27, pp. 434, NACE International, Houston, Texas USA, 1971.

160. F. Mansfeld, “Technical note: some errors in linear polarization measurements and their correction”, Corrosion, volume 30, No. 3, pp. 92, NACE International, Houston, Texas USA, 1974.

161. F. Mansfeld, “Tafel slopes and corrosion rates obtained in the pre-Tafel region of polarization curves”, Corrosion Science, volume 47, pp. 3178–3186, NACE International, Houston, Texas USA, 2005.

162. B.E. Wilde and E. Williams, “The Relevance of Accelerated Electrochemical Pitting Tests to the Long-Term Pitting and Crevice Corrosion Behavior of Stainless Steels in Marine Environments”, Journal of the Electrochemical Society, volume 118, Issue 7, pp. 1057-1062, ECS Pennington, New Jersey USA, 1971.

163. B.E. Wilde, “On Pitting and Protection Potentials: Their Uses and Possible Misuse for Predicting Localized Corrosion Resistance of Stainless Alloys in Halide Media” Localized Corrosion, edited by R.W.

Staehle, B.F. Brown, J. Kruger, and A. Agarwal, pp. 342-352, NACE International, Houston, Texas USA, 1974.

164. A. Anderko, N. Sridhar, and D.S. Dunn, “A general model for the repassivation potential as a function of multiple aqueous solution species”, Corrosion Science, volume 46, pp. 1583-1612, NACE-International, Houston, Texas USA, 2004.

165. N. Sridhar, and G.A. Cragnolino, “Applicability of Repassivation Potential for Long-Term Prediction of Localized Corrosion of Alloy 825 and Type 316L Stainless Steel”, Corrosion, volume 49, pp. 885-894, NACE-International, Houston, Texas USA, 1993.

166. D.S. Dunn, N. Sridhar, and G.A. Cragnolino, “Effect of Surface conditions on localized corrosion of a candidate high-level nuclear waste container material”, 12th International Corrosion Congress, pp. 4021, NACE International, Houston, Texas USA, 1993.

167. K. Sugimoto, and K. Asano, “Analysis of localized corrosion on stainless steel by microcomplex pH-pCl electrode”, edited by H. Isaacs, V. Bertocci, J. Kruger, S. Smialowska, Advances in Localized Corrosion, pp. 375, NACE International, Houston, Texas USA, 1990.

168. T. Nakayama, and K. Sasa, “Critical pitting potential and protection potentials were measured potentiodynamically in 0.IN NaCl solution vibrated by a 200 kHz ultrasonic wave”, Corrosion, volume 32, No. 7, pp. 283-285, NACE International, Houston, Texas USA, 1976.

169. G.R. Engelhardt and D.D. Macdonald, “Deterministic Prediction of Pit Depth Distribution”, Corrosion, Volume 54, pp. 469, NACE International, Houston, Texas USA, 1998.

170. C. Liu, D.D. Macdonald, “Prediction of Failures of Low-Pressure Steam Turbine Disks,” Journal of Pressure Vessel Technology, Volume 119, Issue 4, pp. 393-401, 1997.

171. G. Englehardt, D.D. Macdonald, “Unification of the deterministic and statistical approaches for predicting localised corrosion damage. I. Theoretical foundation,” Corrosion Science, Volume 46, No.11, pp. 2755-2780, NACE-International, Houston, Texas USA, 2004.

172. D.D. Macdonald, C. Liu, M. Urquidi-Macdonald, G. Stickford, B. Hindin, A.K. Agrawal and K. Krist, “Corrosion Science, Volume 50, No.10, pp. 94100761, NACE-International, Houston, Texas USA, 1994.

173. I.T.E. Fonseca, N. Lima, J.A. Rodrigues, M.I.S. Pereira, J.C.S. Salvador, and M.G.S. Ferreira, “Passivity breakdown of Al 2024-T3 alloy in chloride solutions: a test of the point defect model”, Electrochemistry Communications Volume 4, No. 5, pp. 353-357, 2002.

174. Y. Zhang, “Determination of damage functions for the pitting of AISI type 403 blade alloy and ASTM A470/471 disk alloy”, PhD Thesis, Pennsylvania State University, Pennsylvania USA, 2005.

175. Y. Zhang, D.D. Macdonald, M. Urquidi-Macdonald, G. Engelhardt, and R.B. Dooley, “Passivity breakdown on AISI Type 403 stainless steel in chloride-containing borate buffer solution” Corrosion Science, Volume

48, No.11, pp. 3812-3823, NACE-International, Houston, Texas USA, 2006.

176. Z. Szklarska-Smialowska, “Pitting Corrosion of Metals”, NACE International, Houston, Texas USA, 1986.

177. D.D. Macdonald and M. Urquidi-Macdonald, “Theory of Steady-State Passive Films”, Journal of the Electrochemical Society, Volume 137, Issue 8, pp. 2395-2402, ECS Pennington, New Jersey USA, 1990.

178. E. Sikora, and D.D. Macdonald, “Nature of the Passive Film on Nickel”, Electrochimica Acta, Volume 48, No. 1, pp. 69-77, Elsevier Ltd, 2002.

179. D.D. Macdonald, “On the Existence of Our Metals-Based Civilization - Phase-Space Analysis”, Journal of the Electrochemical Society, Volume 153, Issue 7, pp. B213-B224, ECS Pennington, New Jersey USA, 2006.

180. H.A El Dahan, “Pitting corrosion inhibition of 316 stainless steel in phosphoric acid-chloride solutions Part I Potentiodynamic and potentiostatic polarization studies”, Journal of Materials Science, Volume 34, No. 4, pp. 851-857, 1999.

181. ASTM G150, “Standard Test Method for Electrochemical Critical Pitting Temperature Testing of Stainless Steels”, ASTM International, Pennsylvania, USA, 2010.

182. ASTM G48, “Standard Test Methods for Pitting and Crevice Corrosion Resistance of Stainless Steels and Related Alloys by Use of Ferric Chloride Solution”, ASTM International, Pennsylvania, USA, 2009.

183. Technical Data blue sheet, lean duplex stainless steel ATI2102TM Alloy, ATI Allegheny Ludlum, Allegheny Technologies, Pittsburgh USA, 2009.

184. R.C. Newman and R.P. Procter, "Stress corrosion cracking:" 1965-1990. British Corrosion Journal, Volume 25, No. 4, pp 259-269, 1990.

185. D.R. Clarke and K.T. Faber, “Fracture of Ceramics and Glasses,” Journal of Physics and Chemistry of Solids, volume 48, No 11, pp. 1115- 1157, Elsevier Ltd, 1987.

186. T. Magnin and J. Lepinoux, “Metallurgical aspects of the brittle SCC in austenitic stainless steels” Parkins Symposium, TMS, Cincinnati, Ohio USA, pp. 323, 1992.

187. S.P. Lynch, “Environmentally assisted cracking: Overview of evidence for an adsorption-induced localised-slip process”, Acta Metallurgica, volume 36, No 10, Overview No. 74, pp 2639-2661, Elsevier Ltd, 1988.

188. J.R. Galvele, “A stress corrosion cracking mechanism based on surface mobility”, Corrosion Science, volume 27, No 1, pp. 1-33, NACE International, Houston, Texas USA, 1987.

189. P. Marcus, “Corrosion Mechanisms in Theory and Practice” 2nd Edition, Revised and Expanded, Marcel Dekker, Inc, New York, USA, 2002.

190. C. Vichytil, G. Mori, R. Sonnleitner, M. Panzenböck, and R. Fluch, “Corrosion Fatigue Investigations of CrNiMoN Austenitic Stainless

Steels", NACE Corrosion 2011, Paper 11297, pp. 1-17, NACE International, Houston, Texas USA, 2011.

191. R. Sonnleitner, G. Mori, M. Panzenböck, R. Fluch, S. Eglsäer, "Corrosion fatigue and cold deformation of a CrMnN stainless steel", 17th International Corrosion Congress, Las Vegas, paper no. 03822, pp. 1-21, NACE International, Houston, Texas USA, 2008.
192. T. Magnin, "Recent advances for corrosion fatigue mechanisms", ISIJ International, Vol. 35, no. 3, pp. 224-225, 231-232. 1995
193. T. Magnin, "Advances in corrosion deformation interactions", Trans Tech Publications Ltd, Switzerland, p.11-15, 69, 80, 87, 88, 1996.
194. R. Sonnleitner, G. Mori, M. Panzenböck, and R. Fluch, "The effect of cold working on the corrosion fatigue behaviour of a CrNiMoN austenitic stainless steel", NACE Corrosion 2009, paper no 09303 pp 1-20, NACE International, Houston, Texas USA, 2009.
195. T. Magnin, D. Desjardins, and M. Puiggali, "The influence of the mechanical test conditions on the corrosion fatigue behaviour of austenitic stainless steels in chloride solutions", Corrosion Science, Vol. 29, no. 5, pp. 567-576, NACE International, Houston, Texas USA, 1989.
196. R.N. Parkins, "Factors influencing Stress Corrosion Crack Growth Kinetics", Corrosion Science, volume 43, pp. 130-139, NACE International, Houston, Texas USA, 1987.
197. R.N. Parkins and P.M. Singh, "Stress corrosion crack coalescence", Corrosion, volume 46, No 6, pp. 485–499, NACE International, Houston, Texas USA, 1990.
198. P.L. Andersen and I.P. Vasatis, and F.P. Ford, "Behavior of Short Cracks in Stainless Steel at 288^{o}C", NACE Corrosion 1990, Paper no. 495, NACE International, Houston, Texas USA, 1990.
199. F.P. Ford, "Mechanisms of environmental cracking peculiar to power generation industry", Report NP2589, EPRI, Palo Alto, 1982.
200. F.P. Ford, "Stress Corrosion Cracking", Corrosion Processes, edited by R.N. Parkins, pp. 271-309, Applied Publishers, London, 1982.
201. R.N. Parkins, N.J.H. Holroyd, and R.R. Fessler, "Stress corrosion cracking of C-Mn steel in phosphate solutions", Corrosion, Volume 34, No 8, pp. 253-262, NACE International, Houston, Texas USA, 1978.
202. F.P. Ford, "BWR environmental cracking margins in carbon steel piping"', Final Report RP1248-1, EPRI, Palo Alto, 1981.
203. A.R.C. Westwood, and N.S. Stoloff, editors, "Environment-sensitive Mechanical Behavior of Materials", Gordon and Breach, Baltimore, USA, 1965.
204. R.W. Staehle, A.J. Forty and D. Van Rooyen, editors, "Fundamental Aspects of Stress Corrosion Cracking", NACE 1, NACE International, Houston, Texas USA, 1967.

205. J.C. Scully, editor, “Theory of Stress Corrosion Cracking”, Ericera, Portugal, NATO, Brussels, 1971.

206. O. Devereaux, A.J. McEvily, and R.W. Staehle, editors, “Corrosion Fatigue Chemistry, Mechanics and Microstructur, NACE 2, NACE International, Houston, Texas USA, 1972.

207. K. Sieradzki and F.J. Friedersdorf, “Note on the surface mobility mechanism of stress corrosion cracking”, Corrosion Science, volume 36, No 4, pp. 669--675, NACE International, Houston, Texas USA, 1994.

208. R.N. Parkins, “Environment Sensitive Fracture-controlling parameters”, Proceedings of 3rd International Conference on mechanical Behavior of materials, Cambridge, August 20-24, 1979, edited by K.J. Miller and R.F. Smith, pp. 139-139, Pergamon, New York, USA, 1980.

209. D.A. Vermilyea, “Stress Corrosion Cracking and Hydrogen Embrittlement of Iron Base Alloys”, Editted by R.W. Staehle, J. Hochmann, R.D. McCright, and J.E. Slater, pp. 208-217, NACE International, Houston, Texas USA, 1973.

210. R.W. Staehle, “Stress Corrosion Cracking and Hydrogen Embrittlement of Iron Base Alloys, NACE 5, pp. 180, NACE-International, Houston, Texas USA, 1977.

211. P.L. Andresen, “Cracking of Nickel-Base Alloys in High Temperature Water,” Corrosion 47, No 12, pp. 917-938, NACE-International, Houston, Texas USA, 1991.

212. R.C. Newman and M. Satio, “Anodic stress corrosion cracking: Slip dissolution and film induced cleavage”, Corrosion 12, pp. 3, NACE-International, Houston, Texas USA, 1993

213. R.N Parkins, “Predictive approaches to stress corrosion cracking failure”, Corrosion Science, Volume 20, No 2, pp. 147-166, NACE International, Houston, Texas USA, 1980.

214. F.P. Ford, “The crack tip system and its relevance to the prediction of environmentally assisted cracking”, Proceedings of 1st international Conference on Environment Induced Cracking of Metals, Kohler, Wisconsin, NACE, pp. 139-166, 1988.

215. J. Hickling, “Strain induced corrosion cracking; relationship to stress corrosion cracking/corrosion fatigue and importance for nuclear plant service life”, 3rd IAEA Specialists Meeting on Subcritical Crack Growth, Moscow, 1990.

216. K. Sieradzki; R. C. Newman, “Brittle behavior of ductile metals during stress-corrosion cracking”, Philosophical Magazine A, Volume 51, Issue 1, pp. 95 – 132, 1985.

217. J.A. Beavers and E.N. Pugh, “The Propagation of Transgranular Stress Corrosion Cracks in Admiralty Metals”, Metall. Trans. A. Volume 11, pp. 809, 1980.

218. K. Sieradzki; “Atomic and micromechanical aspects of environment induced cracking of metals”, Proceedings of 1st international Conference on Environment Induced Cracking of Metals, Kohler, Wisconsin, NACE, pp. 125-138, 1988.

219. R.C. Newman, “Stress corrosion of austenitic steels”, Proceedings of 1st international Conference on Environment Induced Cracking of Metals, Kohler, Wisconsin, NACE, pp. 489-510, 1988.

220. C. Edeleanu and A.J. Forty, “Some Observations on the Stress Corrosion Cracking of α–Brass and Similar Alloys”, Philosophical Magazine, vol. 46, pp. 521 1960.

221. E.N. Pugh, “Atomistics of Fracture”, edited by R.M Latanision and J.R. Pickens, pp. 997 -999, Plenum, New York USA, 1983.

222. M.T Hahn and EN Pugh, Corrosion, Vol. 36, pp. 380-382, NACE-International, Houston, Texas USA, 1980.

223. D.V Beggs, M.T. Hahn and E.N. Pugh, Proceedings of the A.R. Troiano Honorary Symposium on Hydrogen Embrittlement and Stress Corrosion Cracking, edited by R. Gibala and R.F. Hehemann,. ASTM Metals Park, Ohio USA, 1984

224. E.N. Pugh, “Progress Toward Understanding the Stress Corrosion Problem”, Corrosion, volume 41, No 9, pp. 517-526, NACE-International, Houston, Texas USA, 1985.

225. R.C. Newman, T. Shahrabi, K. Sieradzki, “Film-Induced Cleavage of Alpha-Brass,” Scripta Metallurgica et Materialia volume 23, pp. 71-74, 1989.

226. R.G. Kelly, J. Frost, T. Shahrabi, R.C. Newman “Brittle Fracture of an Au/Ag alloy induced by a Surface film”, Metallurgical Transaction A, No. 22A, pp. 531-541, 1991.

227. R.G. Kelly, A.J. Young and R.C. Newman, “Electrochemical Impedance Spectroscopy”, ASTM STP 1188, edited by J.R. Scully, D.C. Silverman, and M.W. Kendig, ASTM, Philadelphia, 1991, pp. 94, 1991.

228. M. Saito, G.S. Smith and R.C. Newman, "Testing the Film-Induced Cleavage Model of SCC", Corrosion Science, volume 35, Issues 1-4, pp. 411-417, NACE International, Houston, Texas USA, 1993.

229. J.S. Chen, M. Salmeron and T.M. Devine, “Intergranular vs. Transgranular Stress Corrosion Cracking of Cu 30-Au”, Scripta Metallurgica et Materialia, volume 26, No 5, pp. 739, 1992.

230. J.S. Chen, T.M. Devine and M. Salmeron, “Brittle Fracture of Cu-30 Au Induced by a Surface Layer”, Journal of the Electrochemical Society, Volume 139, No 6, pp. L55 ECS Pennington, New Jersey USA, 1992.

231. A. Barnes, A. Nicholas Sr., and R.C. Newman, “Film-Induced Cleavage of Ag-Au Alloys”, Metallurgical and Materials Transactions A, volume 40, No 1, pp. 58-68, 2009.

232. A.W. Thompson and I.M. Bernstein, “The role of metallurgical variables in Hydrogen Assited Environmental Fracture”, Rockwell Science Center Report SCPP-75-63, 1975.

233. M. Billingham and G John, “Determining the Compatibility of High Strength Steels to Cathodic Protection”, NACE Corrosion 2008, Paper 08066, pp. 1-14, NACE International, Houston, Texas USA, 2008.

234. J.H. Chuang, L.W. Tsay, C. Chen, “Crack growth behaviour of heat-treated 4140 steel in air and gaseous hydrogen”, International Journal of Fatigue, Volume 20, No. 7, pp. 531–536, Elsevier Science Ltd, 1998.

235. T.L. Chang, L.W. Tsay, C. Chen, “Influence of gaseous hydrogen on the notched tensile strength of D6ac steel”, Materials Science and Engineering A, Volume 316, Issues 1-2, pp. 153–160, Elsevier Science B.V., 2001.

236. L.W. Tsay, W.C. Lee, R.K. Shiue, J.K. Wu, “Notch tensile properties of laser-surface-annealed 17-4 PH stainless steel in hydrogen-related environments” Corrosion Science, volume 44, No. 9, pp. 2101-2118, NACE International, Houston, Texas USA, 2002.

237. S. Serna et al, “Hydrogen Permeability Behaviour of a High Strength Microalloyed Steel Developed for Sour Service”, NACE Corrosion 2008, Paper 08405, pp. 1-12, NACE International, Houston, Texas USA, 2008.

238. G.E. Kerns, M.T. Wang and R.W. Staehle, “Stress Corrosion Cracking and Hydrogen Embrittlement of Iron Base Alloys”, Stress Corrosion Cracking and Hydrogen Embrittlement of Iron Base Alloys, NACE 5, pp. 700, NACE-International, Houston, Texas USA, 1973.

239. C.S. Carter and M.V. Hyatt, “Review of Stress Corrosion Cracking in Low Alloy Steels with Yield Strengths Below 150 KSI,” Stress Corrosion Cracking and Hydrogen Embrittlement of Iron Base Alloys, NACE-5, pp. 524, NACE-International, Houston, Texas USA, 1977.

240. F.P. Ford, “Quantitative examination of slip-dissolution and hydrogen-embrittlement theories of cracking in aluminium alloys”, Metal Science, Volume 12, N0 7, pp. 326-334, Maney Publishing, UK, 1978.

241. R. Raj and V.K. Varadan, “The kinetics of hydrogen assisted crack growth” Mechanisms of Environment Sensitive Cracking of Materials University of Surrey, UK, edited by P.R. Swann, F.P. Ford, and A.R.C. Westwood, The Metals Society, pp. 426, 1977.

242. R.A. Cottis, “Guides to Good Practise in Corrosion Control – Stress Corrosion Cracking”, The National Physical Laboratory for the Department of Trade and Industry, NPL Management Limited, Middlesex, UK, 2000.

243. A.J. Bursle, and E.N. Pugh, "Environment-Sensitive Fracture of Engineering Materials", The Metallurgical Society, American Institute of Mining, Metallurgical, and Petroleum Engineer, New York USA, pp. 18-47, 1979.

244. R.W. Staehle, “The Theory of Stress Corrosion Cracking in Alloys”, NATO Scientific Affairs Division, Brussels, (Edited by J. C. SCULLY), pp. 223, 1971.

245. E.E. Gdoutos, “Fracture Mechanics: An Introduction”, Solid Mechanics and its Applications, Vol. 123, pp. 153-192, Springer, 2004.

246. F.P. Yang and Z.B. Kuang, “Stress intensity factors for surface fatigue crack in a round bar under cyclic axial loading”, Fatigue and Fracture of Engineering Materials and Structures, Vol. 30, No. 7, pp. 621- 628, 2007.

247. N. Couroneau and J. Royer, “Simplified model for the fatigue growth analysis of surface cracks in round bars under mode I”, International Journal of Fatigue, Vol. 20, No. 10, pp. 711 – 718, 1998.

248. A. Venkatesh, and R.D. Kane “Fracture Analysis of Slow Strain Rate Test for Stress Corrosion Cracking”, NACE Corrosion 2009, Paper 09296, pp. 1-18, NACE International, Houston, Texas USA, 2009.

249. J.I. Dickson, A.J. Russell and D. Tromans, “Stress Corrosion Crack Propagation in Annealed and Cold Worked 310 and 316 Austenitic Stainless Steels in Boiling (154^{o}C) Aqueous $MgCl_2$ Solution”, Canadian Metallurgical Quarterly, Volume 19, pp. 161-167, 1980.

250. ASTM G61, “Standard Test Method for Conducting Cyclic Potentiodynamic Polarisation Measurements for Localised Corrosion Susceptibility of Iron-, Nickel-, or Cobalt-Based Alloys”, ASTM International, Pennsylvania, United States, 1986.

251. NACE Standard TM0177-2005, Standard Test method, “Laboratory Testing of Metals for resistance to Sulphide Stress cracking and stress Corrosion cracking in H_2S Environment”, Item No. 21212, NACE International, Houston, Texas USA, 2005.

252. S.O. Fernandex, and G.F. Tisinai, “Stress Analysis of Unnotched C-Rings Used for Stress Cracking Studies,” Journal of Engineering for Industry, Volume 90, pp. 147–152, 1968.

253. NACE Standard TM0198-2004, Standard Test method, “Slow Strain Rate Test Method for Screening Corrosion Resistance Alloys (CRAs) for Stress Corrosion Cracking in Sour Oilfield Service”, Item No. 21232, NACE International, Houston, Texas USA, 2004

254. ASTM G129, “Standard Practice for Slow Strain Rate Testing to Evaluate the Susceptibility of Metallic Materials to Environmentally Assisted Cracking”, ASTM International, Pennsylvania, United States, 2006.

255. R.C. Weast, Handbook of Chemistry and Physics, 60th Edition, pp. D 155 –160, CRC Press Inc., Florida 1980.

256. ASTM G5, “Standard Reference Test Method for Making Potentiostatic and Potentiodynamic Anodic Polarisation Measurements”, ASTM International, Pennsylvania, USA, 2004.

257. S. Boudin et al, “Analytical and electrochemical study of passive films formed on nickel—chromium alloys: Influence of the chromium bulk concentration”, Surface and Interface Analysis, Volume 22, Issue 1-12, pp. 462–466, 1994.

258. M.J. Graham et al, “The growth and stability of passive films” Advances in Corrosion and Protection, Corrosion Science Volume 35, Issues 1-4, pp. 13-18, NACE International, Houston, Texas USA, 1993.

259. R.W. Revie and, H. H Uhlig, “Corrosion and corrosion control: An Introduction to Corrosion Science and Engineering”, 4th Edition, pp. 100-101, John Wiley & Sons, Inc., Hoboken New Jersey USA, 2008.

260. W. Whitman, and E. Chappell, “Corrosion of Steels in the Atmosphere Corrosion” Industrial & Engineering Chemistry Volume 18, No 5, pp. 533-535, 1926.

261. H. Uhlig, N. Carr, and P. Scneider, “The potentials of Iron-Chromium Alloys Containing Hydrogen” Trans. Electrochem. Soc. Volume 79, pp 111, 1941.

262. R. Olivier, “The Passivity of Fe-Cr Alloys” Proceedings, 6th Meeting, International Committee on Electrochemistry, Thermodynamics, and Kinetics, Poitiers, pp. 314, Butterworths, London UK, 1955.

263. G. Okamoto, “Passive film of 18-8 stainless steel structure and its function”, Corrosion Science Volume 13, pp. 471–489, NACE International, Houston, Texas USA, 1973.

264. B. Baroux, Proceedings, 5th International Symposium on Passivity, Bombannes, France (M. Froment edition), pp. 531, Elsevier, Amsterdam, 1983.

265. Ferralium® 255 Brochure, pp. 10-13, Langley Alloys, A Division of Meighs Ltd, Staffordshire England, 2003.

266. J.R. Vera, D. Shirah, F. Song, “Laboratory Evaluation of Galvanic CO2 Corrosion and Inhibition of Carbon Steel Piping Partially Clad With Alloy 625”, NACE Corrosion 2009, Paper no. 09566, NACE International, Houston, Texas USA, 2009.

267. T.P. Hoar, and U.R. Evans, “The passivity of metals. Part VII. The specific function of chromates” Journal of the Chemical Society. pp 2476-2481, 1932.

268. C.S. Scott et al, “A study of Stress Corrosion Cracking and Localised Corrosion of Carbon Steel in Nitrate Based Nuclear Waste”, NACE Corrosion 2009, Paper no. 09434, NACE International, Houston, Texas USA, 2009.

269. API 5CT/ISO 11960, “Specification for Casing and Tubing”, Petroleum and natural gas industries-Steel pipes for use as casing or tubing for wells, 8th Edition, American Petroleum Institute, 2005.

270. L.P. Kubin, B. Devincre, and M. Tang, “Mesoscopic modelling and simulation of plasticity in fcc and bcc crystals: Dislocation intersections

and mobility", Journal of Computer-Aided Materials Design, volume 5: pp. 31–54, Kluwer Academic Publishers, Netherlands, 1998.

271. M.S. Duesbery, "The dislocation core and plasticity", Dislocations in Solids, volume 8, edited by F. R. N. Nabarro, pp. 67-173, Elsevier, Amsterdam, 1989.

272. J. Antony, "Design of Experiments for Engineers and Scientists", pp. 41, Butterworth-Heinemann an imprint of Elsevier, Oxford, UK, 2003.

273. H.H. Johnson, "Calibrating the Electric Potential Method for Studying Slow Crack Growth," Materials Research and Standards, Volume 5, No 9, pp 442-445, September 1965.

274. J.A. Donovan, "Resistance of Type A537 Class I Steel to Nitrate Stress Corrosion Cracking", DPST- 81-687, Savannah River National Lab, Aiken, SC, 1981.

275. J.A. Beavers et al, "Standard Test Procedure for Stress Corrosion Cracking Threshold Stress Determination", Materials Performance Volume 25, No. 6, NACE International, Houston, Texas USA, 1986.

276. X. Li and L. Chen, "Effect of Mechanical factors on SCC behaviour of Welten 60 Pipeline Steel", Acta Metallurgica Sinica, Volume 29, No. 2, 1993.

277. R.N. Parkins and R. Usher, "The Effect of Nitrate Solutions in Producing Stress Corrosion Cracking in Mild Steel", Proceedings First International Congress on Metallic Corrosion London UK, pp 296-302, Butterworths, 1962.

278. R.N. Parkins, "Development of Strain-Rate Testing and Its Implications." Stress Corrosion Cracking: The Slow Rate technique, ASTM STP 665, G.M. Ugiansky and J.H. Payer, Eds, pp 5-25, American Society for Testing and Materials, Philadelphia USA, 1979.

279. R.N. Parkins, P.W. Slattery, and B.S. Poulson, "The Effects of Alloying Additions to Ferritic Steels upon Stress Corrosion Cracking Resistance", Corrosion, Volume 37, No. 11 Pp. 650-664, NACE International, Houston, Texas USA, 1981.

280. L. Hermann and J.R. Rice, "Comparison of Theory and Experiment for Elastic-Plastic Plane Strain Crack Growth", Metal Science, Volume 14, pp. 285-291, 1980.

281. H. Eriksson, and S. Bernhardsson, "The Applicability of Duplex Stainless Steels in Sour Environments, Corrosion, Volume 47, No 8, pp. 719-727, NACE International, Houston, Texas USA, 1991.

282. R.N. Parkins, "The Controlling Parameters in Stress Corrosion Cracking," Fifth Symposium on Line Pipe Research, Catalog No. L30174 pp. U1-40, American Gas Association, Arlington, VA, 1979.

283. K. Bohnenkamp, "Caustic Cracking of Mild Steel," Proceedings, Conference on Fundamental Aspects of Stress Corrosion Cracking, R.W. Staehle, A.J. Forty, and D van Rooyen, Eds., pp. 374-383, NACE International, Houston, Texas USA, 1969.

284. J.A. Beavers and H. K. Gerhardus, “Limitations of the Slow Strain Rate Test Technique, “ Slow Strain Rate Testing for the Evaluation of Environmentally Induced Cracking: Research and Engineering Applications, ASTM STP 1210, R.D. Kane, Ed., pp. 22-39, American Society for Testing Materials, Philadelphia USA, 1993.

285. G. Mori, S. Sutthiruangwong, M. Czerny and T. Partlic, “Metallurgical and Surface Influence on the Corrosion Resistance of Ni-Cr-Mo Alloys According to ASTM G28”, Corrosion, Volume 60, No 11, pp. 1082, NACE International, Houston, Texas USA, 2004.

286. S.D. Day, M.T. Whalen, K.J. King, G.A. Hust, L.L. Wong, J.C. Estill, and R.B. Rebak, “Corrosion Behavior of Alloy 22 in Oxalic Acid and Sodium Chloride Solutions”, Corrosion, Volume 60, No.9, pp. 804-814, NACE International, Houston, Texas USA, 2004.

287. A.C. Lloyd, J.J. Noel, S. McIntyre, D.W. Shoesmith, “The Open-Circuit Ennoblement of Alloy C-22 and other Ni-Cr-Mo Alloys”, Electrochimica Acta, Volume 49, Issue 17-18, pp.3015, Elsevier Ltd, 2004.

288. N. Priyantha, P. Jayaweera, D.D. Macdonald, A. Sun, “An electrochemical impedance study of Alloy 22 in NaCl brine at elevated temperature. I. Corrosion behaviour”, Journal of Electroanalytical Chemistry, Volume 572, Issue 2, pp.409-419, 2004.

289. D.D. Macdonald, and A. Sun, “An electrochemical impedance spectroscopic study of the passive state on Alloy-22” Electrochimica Acta, Volume 51, Issues 8-9, pp. 1767-1779, Elsevier Ltd, 2006.

290. L.G. McMillion, A. Sun, D.D. Macdonald, D.A. Jones, “General corrosion of alloy 22: Experimental determination of model parameters from electrochemical impedance spectroscopy data”, Metallurgical and Materials Transactions A, Volume 36A, pp. 1129, 2005.

291. C.Y. Chao, L.F. Lin, and D.D. Macdonald, “A Point Defect Model for Anodic Passive Film – Impedance Response”, Journal of Electrochemical Society, Volume 129, No. 9, pp.1874-1879, ECS Pennington, New Jersey USA, 1982.

292. C.Y. Chao, L.F. Lin, and D.D. Macdonald, “A Point Defect Model for Anodic Passive Film – Film Growth Kinetics”, Journal of Electrochemical Society, Volume 128, No. 6, pp. 1187-1194, ECS Pennington, New Jersey USA, 1981.

293. N. Sato, and M. Cohen, “The Kinetics of Anodic Oxidation of Iron in Neutral Solution – II. Initial Stage” Journal of Electrochemical Society, Volume 111, No. 5, pp. 519-522, ECS Pennington, New Jersey USA, 1964.

294. R.W. Hertzberg, “Deformation and Fracture Mechanics of Engineering Materials”, 4th Edition, John Wiley & Sons, Inc, New York USA, 1996.